Understanding The Role Of Metabolite/Growth Factor Mediated Bioenergetic And Metabolic Alterations In Tumor Cell That Facilitate Cancer Progression And Chemoresistance

Thesis Submitted For The Degree Of Doctor Of Philosophy (Science) In Biochemistry

By

Sampurna Ghosh

DEPARTEMENT OF BIOCHEMISTRY

UNIVERSITY OF CALCUTTA

2021

Dedicated

To My

Family

Acknowledgement

This thesis is the cumulative result of my research work for last 5 years. I have been supported and accompanied by several people without them I would not have completed this long journey. I would like to express my heartfelt gratitude to all of them who hold a special place in my heart.

Firstly, I take this opportunity to confer my sincere thanks and respect to the Almighty God who is the creator of all the initial and final mode of destiny.

I would like to express my sincere gratitude towards my Ph.D. supervisor Prof. Sib Sankar Roy, Senior Principal Scientist, CSIR-IICB, Kolkata for providing me the opportunity of carrying out my research work in his laboratory under his able guidance. He gave me full independence to implement new ideas in the research projects and his critical approach to the problems made me perform better. This journey would not have been successful without his mentorship.

It is impossible to extend enough thanks to my family who gave me encouragement and motivation throughout this process. No words are enough to describe the contribution of my parents in my life. My parents always believed in my capabilities and gave me my wings to fly to follow my dream. They always supported to take every decision in my life and tolerated my untimely routines and frustration. I am very much lucky to have parents like them. I would like to express my gratitude towards them to instill the good values in me, for all the blessings and their throughout encouragement to pursue my interests. I would like to thank Boudi who have always supported me like elder sister that helped me achieve my goals. The innocent and rejuvenating smile of Roddur always helped me in overcoming all the frustration.

I am thankful to have lab-mates Prosenjit Da, Parash, Eshani Di, Shreya, Priti, Deepshikha, Suman, Eshayan and Debarati for providing me with a vivacious environment. I would like to thank my seniors Nabanita di, Shreya di, Upasana di, Tulika di, Ashok Da, Rahul Da for their kind help. It is from them that I learnt the most of the techniques that I have used in my research work.

I like to acknowledge technical assistance from Mr. Prabir Kumar Dey who helped me in every possible ways. I would like to extend my gratitude towards Tanmoy da, Debaleena di (Flow cytometry) and Sounak da (confocal microscopy) for their technical assistance .

I would like to extend my sincere thanks to all my relatives and well wishers who have helped and encouraged me in several ways. I am lucky to have few friends who have always given their love, support and inspiration.

I would like to express my sincere thanks to all the professor of Department of Chemistry and Biochemistry, Presidency College who have encouraged me and inspired me to pursue research work.

I would like to express my deep respect to the professors of Department of Biochemistry, University of Calcutta for encouraging me to join this field of research and for proper guidance.

I gratefully thank all the respected faculties, co-researchers and all others associated at CSIR-IICB. I am thankful to the staff members of Central instrument facility (CIF), library, animal house, P&I, R&C, Bill and Account Sections for their generous help and co-operation.

I am also thankful to the ex-Director, Prof. Samit Chattopadhyay and the present Director, Prof. Arun Bandopadhyay (CSIR-IICB) for giving me this opportunity.

I would like to thank UGC, Govt. of India for providing me the research fellowship to accomplish the dissertation work of my thesis. Lastly, I gratefully acknowledge CSIR-Indian Institute of Chemical Biology, Kolkata for providing me all the facilities and a friendly atmosphere to carry out my work.

Sampurna Ghosh
Dated: 3/12/21
Cell Biology and Physiology Division,
CSIR-Indian Institute of Chemical Biology,
4, Raja S. C. Mullick Road,
Kolkata- 700032, India.

Table of Contents

Chapter 1: Stemness and chemoresistance properties are imparted through TGFβ1- PITX2 signaling in OC cells

Chapter 2: DRP1 regulates stemness and chemoresistance upon glutamine deprivation in cancer

ACRONYMS

ABC Transporter	**ATP- Binding cassette transporter**
ALDH	**Aldehyde dehydrogenase**
ATP	**Adenosine tri-phosphate**
BSA	**Bovine serum albumin**
CAF	**Cancer associated fibroblast**
CSC	**Cancer stem cells**
2-DG	**2-Deoxy glucose**
DAPI	**4’,6-diamidino-2-phenylindole**
DCFDA	**2',7'-dichlorodihydrofluorescein diacetate**
DEAB	**N,N-diethylaminobenzaldehyde**
DMEM	**Dulbecco’s modified eagle media**
DNA	**Deoxy-ribonucleic acid**
DRP1	**Dynamin related protein 1**
ECAR	**Extracellular acidification rate**
ECM	**Extracellular matrix**
EMT	**Epithelial messenchymal transition**
ETC	**Electron transport chain**
FBS	**Fetal bovine serum**
GDH	**Glutamate dehydrogenase**
GLS	**Glutaminase**

GSH	**Reduced glutathione esters**
HCC	**Hepatocellular carcinoma**
HIF1α	**Hypoxia inducible factor 1α**
HK2	**Hexokinase 2**
HRP	**Horse raddish peroxidase**
IB	**Immunoblot**
ICA	**Intensity co-relation analysis**
IHC	**Immuno-histochemistry**
IMM	**Inner mitochondrial membrane**
IP	**Immunoprecipitaton**
α-KG	**α-Ketoglutarate**
LDH	**Lactate dehydrogenase**
L-DON	**6-diazo-5-oxo-L-norleucine**
MEM	**Minimal essential media**
MFN	**Mitofusin**
NAC	**N-Acetyl cysteine**
NAD	**Nicotinamide adenine dinucleotide**
NOCO	**Nocodazole**
OC	**Ovarian cancer**
OCR	**Oxygen consumption rate**
OMM	**Outer mitochondrial membrane**
OXPHOS	**Oxdative phosphorylation**

PBS	**Phosphate buffer saline**
PDH	**Pyruvate dehydrogenase**
PDK	**Pyruvate dehydrogenase Kinase**
PI	**Propidium iodide**
PITX2	**Pituitary homeobox 2**
PVDF	**Polyvinylidene difluoride**
q-PCR	**Quantitative polymerase chain reaction**
Rh123	**Rhodamine 123**
RIPA buffer	**Radio-immuno precipita tion assay buffer**
ROS	**Reactive oxygen species**
RPMI-1640	**Roswell Park Memorial Institute media- 1640**
RTK	**Receptor tyrosine kinase**
RNase	**Ribonuclease**
SDH	**Succinate dehydrogenase**
SIRT	**Sirtuin**
SSZ	**Sulphasalazine**
SDS	**Sodium dodecyl sulfate**
SEM	**Standard error of mean**
TF	**Transcription factor**
TGFβ1	**Transforming growth factor β1**
TME	**Tumor microenvironment**
TBS-T	**Tris-buffered saline containing 0.1% Tween-20**

REVIEW OF LITERATURE

1. Overview of Cancer

- **1. A. About cancer:**

Cancer is a combination of 100 or more diseases where the abnormal cells divide rapidly and migrate to the secondary site from the origin and they form the tumor.

- **1. B. History of Cancer:**

The earliest evidence of cancer (although the term "cancer" was not used) was found in the textbook of Egyptian trauma surgery in early 3000 BC where they mentioned about 8 cases of tumors or ulcers in the breast. They removed these tumors using a fire drill and mentioned that there was no treatment.

The term cancer was originated by Greek physician Hippocrates (460-370 BC). He was known as the 'Father of Medicine'. He described non-ulcer and ulcer forming tumors as carcinos and carcinoma. These terms are referred to as crab in Greek. The roman physician Celsus (28-50 BC) translated and coined the term cancer, which is the Latin term of crab.

In Padua Giovanni Morgagni first established the base for cancer study by doing an autopsy to discover the clinical pathology of the disease in a dead body in 1761. In the nineteenth century, Rudolf Virchow called as founder of cellular pathology, linked microscopic pathology in the autopsied body to find out the illness (Faguet, 2015).

- **1. C. Statistics of cancer:**

Cancer is the deadliest disease in the world. The number of new cancer cases is 19.3 million whereas 10.0 million cancer deaths occurred in 2020. In Asian countries, there is the highest cancer incidence with death rate and prevalence **(Fig. 1)**.

The most common cancer incidence are breast, lung, colon and rectum, prostate, skin (non-melanoma) with the cases of 2.26 million, 2.21 million, 1.93 million, 1.41 million, 1.2 million respectively **(Fig. 2)**.

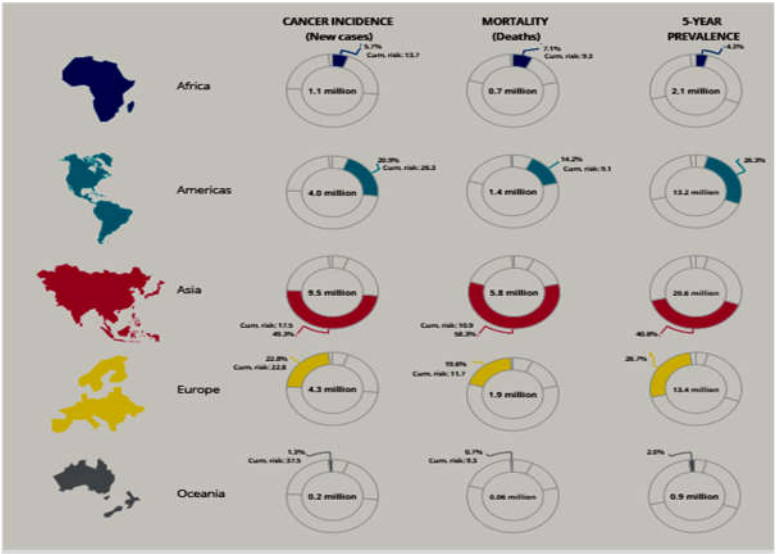

Figure 1: Worldwide cancer incidence, death rate, and prevalence in different continents (Globocon 2020, WHO)

Among these, the most common cancer deaths are lung, colon and rectum, liver, stomach, and breast with the death cases of 1.80 million, 935 000, 830 000, 769 000, and 685 000 respectively (Sung et al., 2021) **(Fig. 2)**.

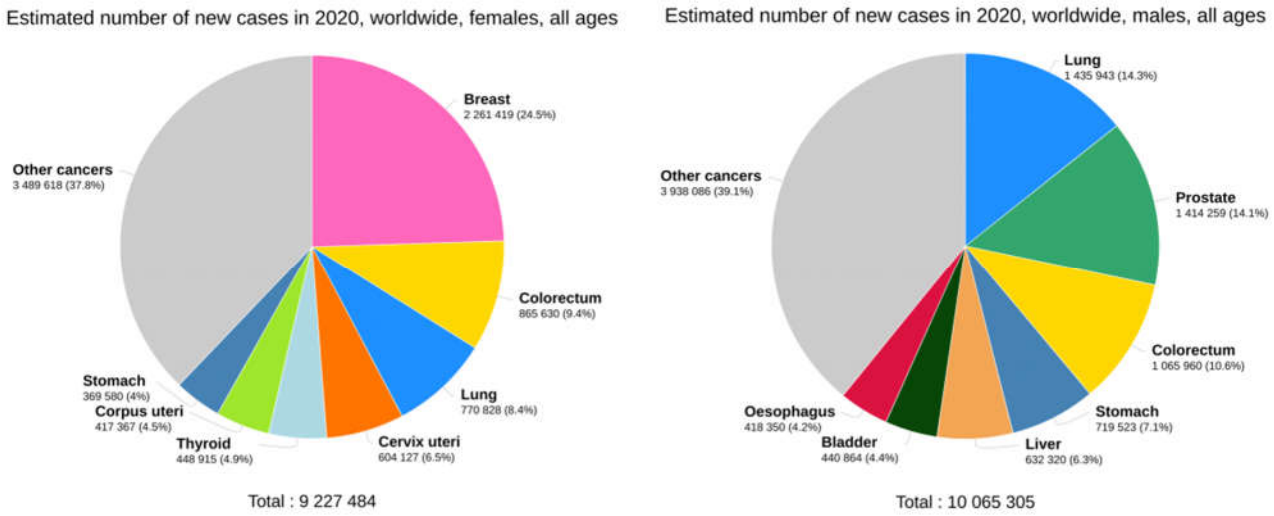

Figure 2: Worldwide cancer incidence (%) in both females and males (Globocon 2020, WHO)

- **1.D. Type of Cancer:**

There are 5 major types of cancer: carcinoma, sarcoma, myeloma, lymphoma, and leukemia.

i) Carcinoma: In this type of cancer, originate from epithelial tissue that covers the surface of the organ**.** It includes melanoma, basal cell carcinoma, squamous cell skin cancer, Merkel cell carcinoma.

ii) Sarcoma: In sarcoma, cancer originates from connective tissue. There are a few types of sarcoma, including soft tissue sarcoma, osteosarcoma, Ewing's sarcoma, chondrosarcoma.

iii) Lymphoma: In this cancer, cells are proliferating in the lymph gland or node. The types of lymphomas are Hodgkin's lymphoma, Non-Hodgkin's lymphoma, and cutaneous lymphoma.

iv) Leukemia: It is also called blood cancer and it originates in the bone marrow. It includes acute lymphocytic leukemia, agnogenic myeloid leukemia, acute myeloid leukemia, chronic myeloid leukemia, chronic lymphocytic leukemia, essential thrombocythemia, myelodysplastic syndromes (MDS), hairy cell leukemia.

v) Myeloma: It arises in plasma cells of bone marrow (https://stanfordhealthcare.org/medical-conditions/cancer/cancer/cancer-types.html).

- **1.E. Stages of cancer:**

The stage of cancer is determined using the TNM staging system in most cancer.

a)"T" denotes the size, location, or migration status.

TX:- No indication of tumor or it cannot be measurable.

T0:- No evidence of tumor.

Tis:- Tumor is 'in situ" i.e it is located in the primary site and does not migrate to peripheral tissue.

T1-4:- It indicates the size and location of the tumor. When the tumor migrates to the deeper side of the tissue, the number will increase.

b) Node (N): N indicates whether the tumor affected the lymph node.

N0:- No lymph node with cancer.

N1-3:- More lymph nodes with cancer, the number will larger.

c) Metastases (M):

M0:- If cancer does not spread to the other part of the body.

M1: when tumor metastasizes to other parts of the body.

Cancer stage classification:

Depending upon the TNM staging system, the stage of cancer is classified into 4 groups:

Stage 0: In this stage, the cancer is located in the primary site where they arise, but does not spread to adjacent tissue.

Stage 1: In this stage, the tumor does not enter deeper into the adjacent tissue and is not found in the lymph node also. This is referred to as the early stage of cancer.

Stage 2 and Stage 3: In these two stages, tumors migrate deeper into the nearby tissue and also metastasize to the lymph node.

Stage 4: In this stage, tumors are migrated not only to the lymph node, and also to other secondary sites of the body. This is called advanced or metastatic cancer (https://www.cancer.net/navigating-cancer-care/diagnosing-cancer/stages-cancer, 2021).

2. Cancer stem Cells and chemoresistance

- **2. A. About cancer stem cells (CSCs):**

The first experimental evidence of CSCs was appeared in 1997 in acute myeloid leukemia by the identification of CD34+ CD38- leukemic cells which have self-renewal and differentiation properties. After the injection of these cells in severe combined immunodeficient mice (SCID), they act like stem-like cells and generate acute myeloid leukemia (Yadav and Desai, 2019a).

Stemness is a phenotype associated with the self-renewal property and dedifferentiation capability of a cell. Stem cells (SC) can dedifferentiate into various types of other cells in response to multiple environmental factors and stimuli. However, they need a specific niche with specific factors and cytokines to survive. In contrast, cancer stem cells (CSC) can sustain in the tumor microenvironment (low oxygen, nutrient) to maintain tumor progression **(Fig. 3)**.

It is known that CSCs are a tiny set of cells within the tumor, generated due to mutation of somatic stem cells during malignancy. These CSCs have self-renewal and dedifferentiation capacity and they also interact with the tumor microenvironment to maintain the tumor heterogeneity, proliferation, and metastasis (Aponte and Caicedo, 2017).

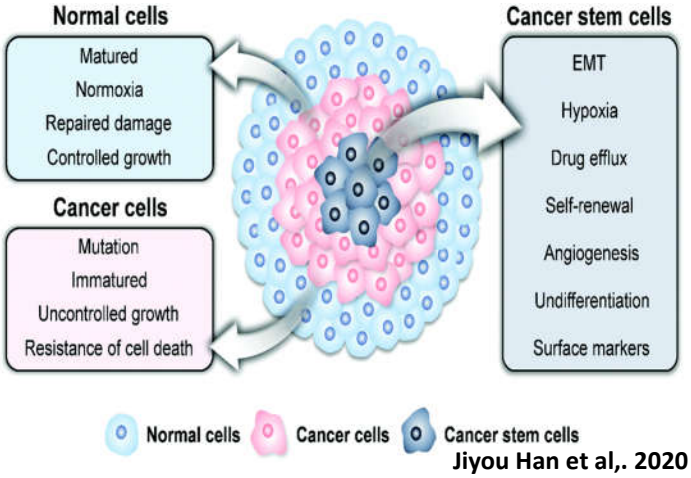

Figure 3: Comparison of characteristics among normal cell, cancer cells, and cancer stem cells

- **2. B. Origin of CSCs in tumors:**

(a) Alteration in stem cells microenvironment in tissue,

(b) Due to mutation or epigenetic alteration leads to change the cellular metabolism, signaling pathway, and cell cycle progression,

(c) Proliferation of cells with changed molecular phenotypes leads to generating heterogeneous primary tumors and metastases (Klonisch et al., 2008).

- **2. C. Features of Cancer stem cells:**

1. A small number of CSCs can initiate new tumors which indicates that they have tumorigenic

properties.

2. They have the self-renewal and dedifferentiation capability through which they generate multiple cancer lineages by symmetric and asymmetric cell division. Due to the high expression of SOX2, OCT4, NANOG, these cells gained the property of self-renewal and dedifferentiating.

3. They have specific surface markers which are membrane proteins. These markers are used to isolate the CSCs population through fluorescence-activated cell sorting (FACS). CD44, CD45, CD31, CD117 are surface markers for CSCs observed in ovarian cancer and colorectal cancer (Yadav and Desai, 2019a).

CD44: It is a transmembrane glycoprotein, known as P- glycoprotein. In the cell membrane, CD44 acts as a receptor molecule to hyaluronic acid (HA), osteopontin, collagen, and matrix metalloprotease (MMP). The binding of CD44 with ligands facilitates cancer progression and metastasis. Due to alternative splicing, CD44 has different variants or isoforms and they present in various cancer subtypes. The elevated level of cleaved and soluble CD44 acts as the marker in gastric and colorectal cancer. Expression of CD44 acts as a marker for CSCs in colorectal, ovarian, breast, pancreatic, prostate, and head /neck squamous carcinoma (Burgos-ojeda et al., 2012; Senbanjo and Chellaiah, 2017).

CD117: CD117 is phosphorylated by binding of stem cell factors. It plays key roles in cancer proliferation, apoptosis, migration, and dedifferentiation. It acts as a marker for CSC in gastric, prostate, non-small lung, and ovarian cancer. $CD44^{+}$ $CD117^{+}$ were chemoresistant and have the potential to initiate new tumors (Harris et al., 2021)

CD31 and CD45: Erythroid-myeloid progenitor cells expressed CD31 and CD45 markers. They are specific for endothelial cell differentiation.

4. CSCs have high aldehyde dehydrogenase activity (ALDH). ALDH regulates retinol metabolism and signaling which have a great role in embryonic development. Retinal is converted to retinoic acid (RA). This RA enters the nucleus and activates the heterodimers of RA receptors (RAR) and retinoic X receptors (RXR). These heterodimers act as a transcription factor to regulate the downstream effectors. ALDH enhances chemoresistance by

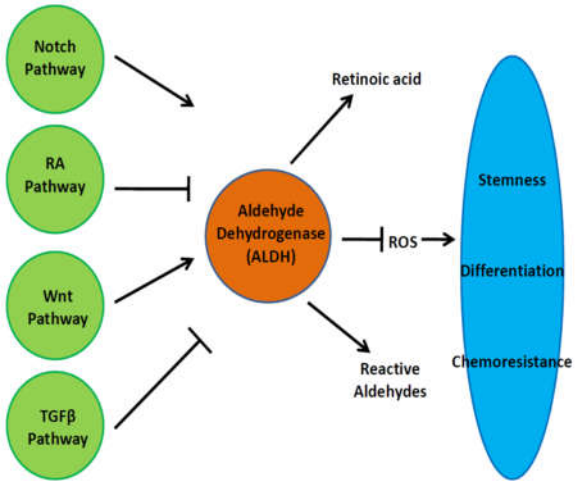

Figure 4: Regulation and role of ALDH in cancer

oxidizing cytotoxic chemotherapy into

non-toxic forms. Chemotherapy and radiotherapy induce oxidative stress which can be scavenged by ALDH and thereby protects tumor cells from an oxidative stress injury. They have the potential for spheroid formation. ALDH also promotes chemoresistance through regulating the RA-mediated signaling pathway **(Fig. 4)** (Xu et al., 2015).

5. The cells have drug resistance or drug effluxing capability. They have enhanced expression of active transmembrane ATP–binding cassette (ABC) transporters which pump out various cytotoxic drugs and dye at expense of ATP. ABC- family transporters include MRCP, MDR1/ ABCB1), BCRP/ABCG2 which helped the cell to efflux DNA –binding dye Hoechst 33342, which are depicted as 'side population' (Chen et al., 2013; Klonisch et al., 2008).

6. The cells have deregulated signaling in three embryonic pathways: Wnt/β-catenin, Notch, and Hedgehog (Hh) pathways.

7. CSCs have the spheroid forming ability in non-adherent conditions with serum-free media, containing growth factors. They are characterized by round in shape with enriched CSCs population **(Fig. 5)** (Shaheen et al., 2016; Yadav and Desai, 2019b).

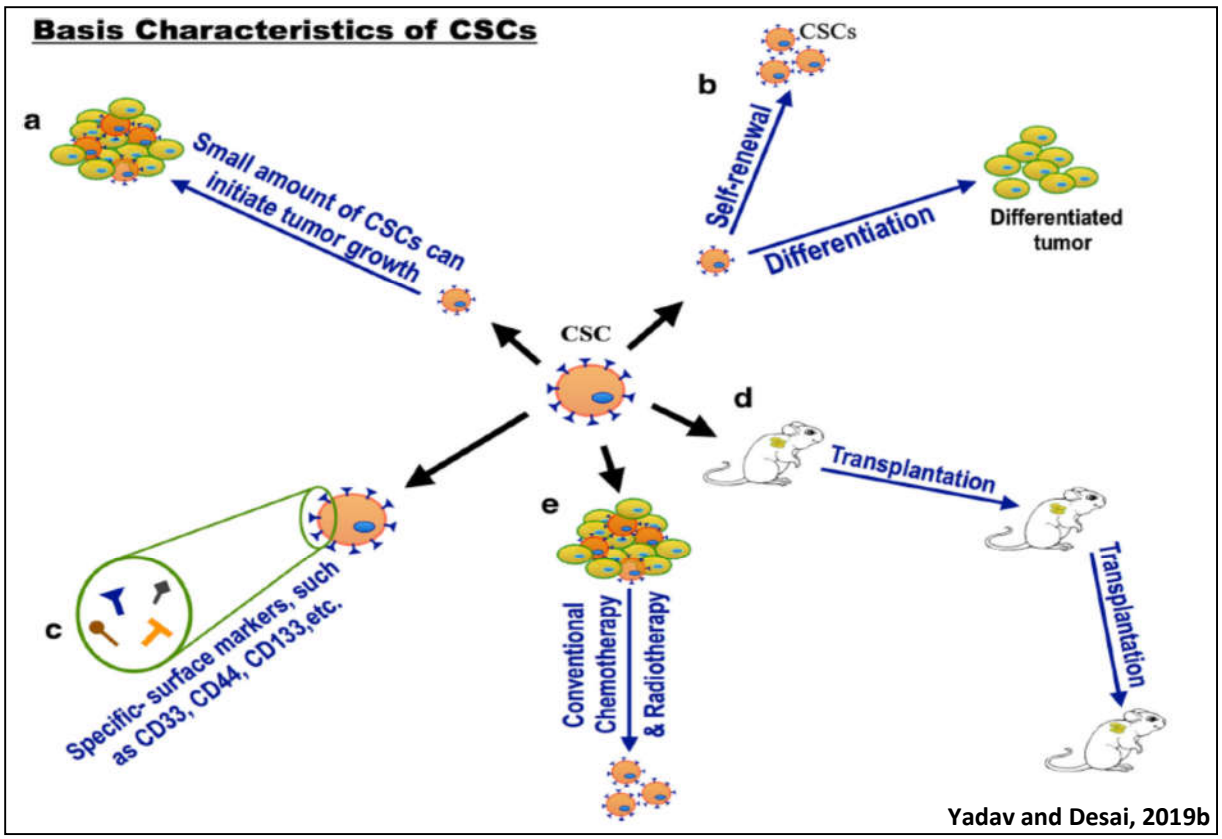

Figure 5: Basic characteristics of cancer stem cells (CSCs)

- **2.D. Interaction between tumor microenvironment (TME) and CSC**:

Tumor microenvironment formed with extracellular matrix (ECM), stromal cells (including fibroblasts, adipocyte, mesenchymal, endothelial, and immune cells) (Bighetti-Trevisan et al., 2019). ECM is a dynamic structure, comprised of fibrous proteins (collagens), glycoproteins (fibronectins, laminins), proteoglycans, and polysaccharides (hyaluronic acid, HA). The components of ECM acts as a physical hurdle for the transport of solute, water, and chemotherapeutic drug.

It also acts as a site for the adhesion of CSCs in the TME, for example, CD44 on the CSCs bind to HA in the ECM and enhances the expression of stemness markers such as SOX2, NANOG, MDR1 in breast and ovarian cancer. Linear orientation and distribution of collagen fiber in TME facilitated migration and metastasis of CSCs. Tumor ECM is much stiffer than the normal ECM due to overexpression of ECM components and ECM-modifying enzymes. ECM stiffness regulates CSC's self-renewal and differentiation properties and also mediates the mechanotransduction signaling pathway to increase the stemness features (Nallanthighal et al., 2019).

3. EMT and metastasis in cancer:

- **3.A. Epithelial-mesenchymal transition (EMT):**

EMT is a multifaceted process through which epithelial cells are converted into the mesenchymal type and these phenomena occur in three biological processes as; a) during embryonic development, b) adult tissue regeneration and c) cancer progression. Epithelial cells have apical-basal polarity and the adjacent cells are connected through gap junction, tight junction, and desmosomes whereas mesenchymal cells lose their connection between adjacent cells and they separated by extracellular matrix (Ribatti et al., 2020).

- **3.B. Transcription factors involved in EMT:**

EMT is occurred by some EMT-activating transcription factors (EMT-TF) such as Snail, Twist, and Zeb. These EMT-TFs regulate all the steps of cancer progression. These transcription factors repress the expression of the epithelial marker, E-cadherin, and promote mesenchymal phenotype.

The TFs included in the SNAIL family are Snail1, Snail2 (also known as Slug), and Snail3 which are transcriptional repressors. Snail1, Snail2 binds to the E-cadherin promoter and downregulates its activity. TGFβ regulates Snail expression in embryonic development and cancer progression. The functionality and localization of Snail1 are regulated by its phosphorylation. Glycogen Synthase Kinase-3 (GSK3) phosphorylates Snail and promotes its

export from the nucleus and degradation. Therefore, GSK3 represses EMT processes in multiple cancer cells. In contrast, phosphorylation of Snail1 by p21-activated kinase (PAK1) induces nuclear import and activates EMT (Georgakopoulos-Soares et al., 2020).

TWIST family included Twist1 and Twist2 which act as both transcriptional activators and repressors. They directly regulate cancer invasion by repressing E-cadherin expression whereas simultaneously they enhance the expression of mesenchymal markers such as Fibronectin, N-cadherin, Vimentin. The Twist is also involved in the regulation of stemness features in cancer. Akt and MAPK can phosphorylate Twist to promote cancer invasion. On contrary, phosphorylation by IKKβ induces degradation of Twist.

ZEB family is comprised of Zeb1 and Zeb2 which are regulated by various signaling molecules. TGFβ and wnt-β-catenin pathways regulate Zeb1 expression. Additionally, Snail and Twist also regulate their expression. Post-transcriptional modification such as phosphorylation and sumoylation modulates the function of Zeb **(Fig 6)** (Georgakopoulos-Soares et al., 2020).

- **3. C. The biomarkers OF EMT in cancer:**

Cell Surface markers of EMT:

Switching between cadherin i.e from E-cadherin to N-cadherin promotes EMT. Epithelial cells express E-cadherin and therefore loss of E-cadherin is a feature of mesenchymal cells. Integrin signaling promotes EMT and various integrin molecules are present both in epithelial and mesenchymal cells. Therefore, integrin is a general marker for EMT. Another EMT marker that expressed EMT-associated ECM alteration is DDR2 (discoidin domain receptor tyrosine kinase 2) **(Fig. 6)** (Morandi et al., 2017).

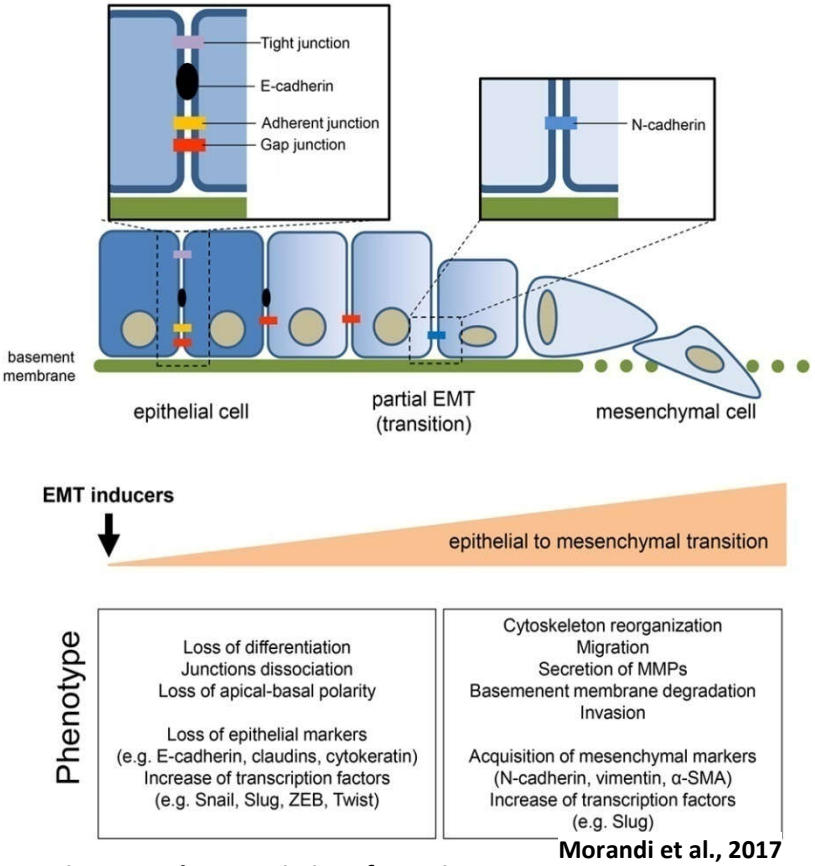

Morandi et al., 2017

Figure 6: Characteristics of EMT in cancer

Cytoskeletal marker of EMT:

One of the members of the Ca^{2+}-binding S100 proteins family, FSP1 is one of the cytoskeletal makers for EMT. Intermediate filament protein, Vimentin is another EMT marker and its

expression enhances cancer progression. α-SMA (α-Smooth muscle actin) is observed in EMT in the breast cancer cell. Localization of β-catenin depicts functional activity. In a normal cell or non-invasive tumor cell, β-catenin is localized in the cell membrane, however, during EMT progression it is either localized in cytosol or nucleus **(Fig. 6)** (Georgakopoulos-Soares et al., 2020).

Extracellular matrix protein (ECM) in EMT:

Fibronectin, Collagen 1 and 3, Laminin 5 are ECM proteins involved in EMT progression.

- **3.D. EMT and metastasis:**

In the metastasis process, cancer cells migrate from their site of origin to the secondary sites through the bloodstream and lymphatic nodes. EMT is an initial step for migration where the mesenchymal cells acquire the features for mobility. Metastasis is a complex process with the involvement of 5 steps.

Step 1: Invasion where the cancers cells migrate to the surrounding stroma from the initial site.

Step 2: Intravasation where the cancer cells cross the wall of the vessels and enter into the circulatory system.

Step 3: Survival of the cancer cells in the circulatory system.

Step 4: Extravasation where the cancer cells exit from the blood vessels and enter into the secondary organ.

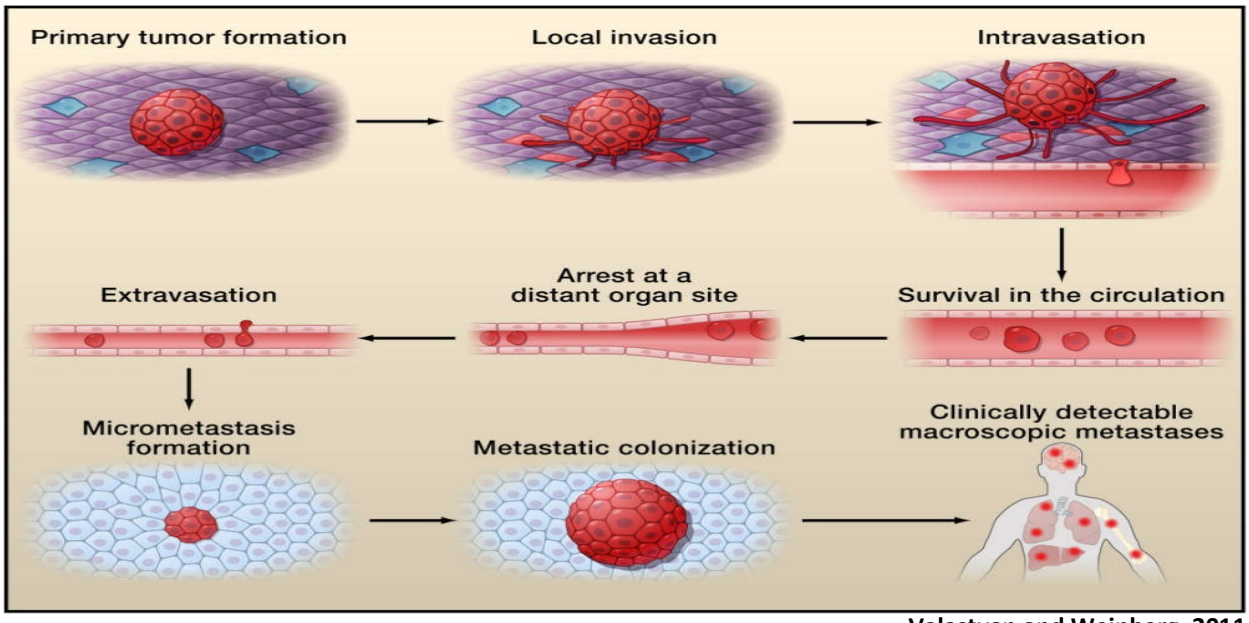

Valastyan and Weinberg, 2011

Figure 7: Steps of metastasis in cancer

Step 5: After colonization, the cancer cells develop tumors at the secondary site (Valastyan and Weinberg, 2011) **(Fig. 7).**

4. TGFβ signaling in cancer

TGFβ is a polypeptide secreted by tumor cells and stromal cells, act as a signaling molecule in normal and malignant cells. It plays a dual role in cancer progression and in regulating stemness. TGFβ is a ligand for TGFβ type I and type II receptors, and activates downstream signaling pathways.

- **4. A. Canonical SMAD dependent TGFβ signaling pathway:**

TGFβ is produced as a big latent TGFβ complex, comprised of latency-associated peptides and a latent TGF binding protein. Upon activation, they bind to the heterodimeric complex of type I and type II receptors.

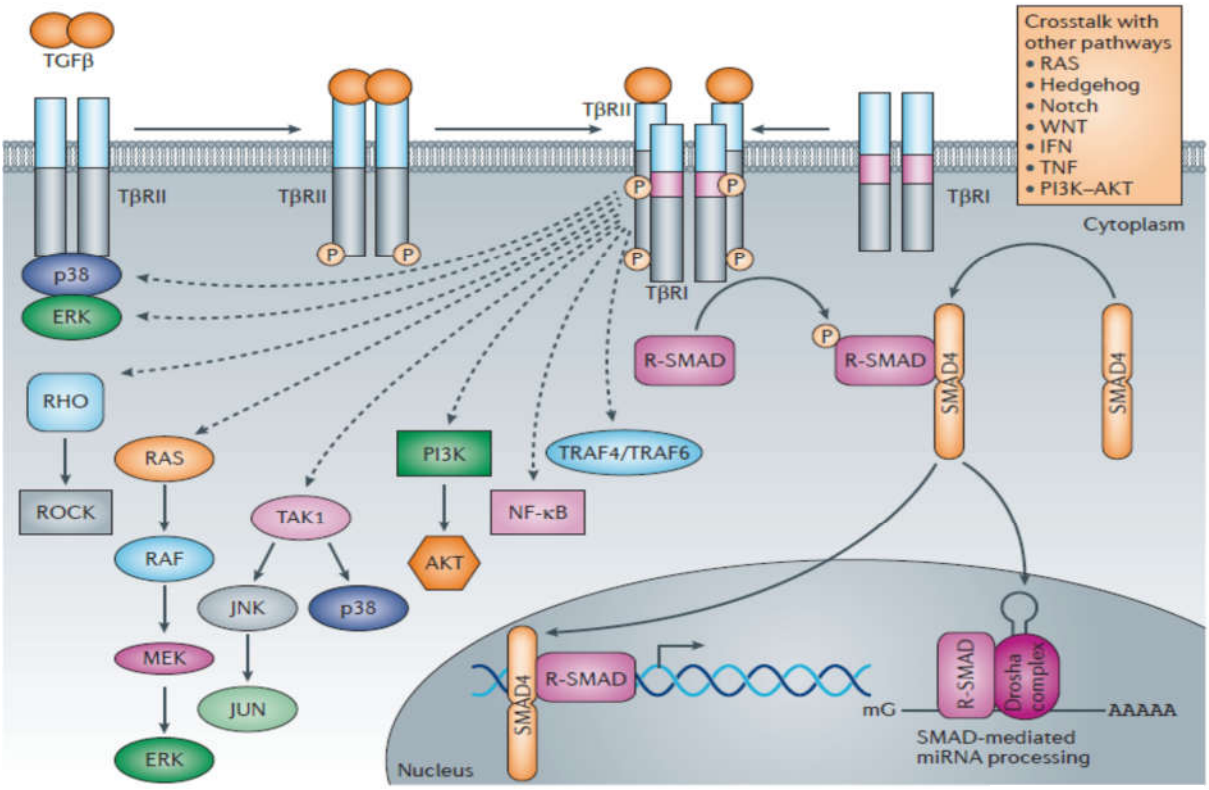

Akhurst & Hata, 2012

Figure 8: Canonical and non-canonical SMAD dependent TGFβ signaling

Then Type II receptor trans-phosphorylate Type I receptor through its cytoplasmic Ser/Thr kinase activity and this signal are propagated through recruitment of TGFβ receptor-specific SMAD (SMAD2 and SMAD3). This heteromeric complex interacts with co-SMAD (SMAD4) and they translocate to the nucleus. This complex is associated with DNA- interacting transcription factor to regulate then downstream events, depending upon the type of this transcription

factor. Additionally, SMAD2 regulates miRNA processing in the nucleus **(Fig. 8)** (Akhurst and Hata, 2012).

- **4.B. Non-canonical TGFβ signaling pathway:**

TGFβ receptor complex can propagate the signaling through the activity of various signaling molecules, other than SMAD. These signaling molecules include p38 Mitogen-activated protein kinases (p38MAPK), Extracellular signal-regulated kinase (ERK), Phosphoinositide 3-kinase (PI3K)–AKT, TNF receptor-associated factor 4 (TRAF4), TRAF6, TGFβ-activated kinase 1 (TAK1), and nuclear factor-κβ (NF-κβ). TGFβ signaling can be modulated by other signaling pathways such as Hedgehog, Wnt, interferon (IFN), Notch, tumor necrosis factor (TNF), and RAS pathways **(Fig. 8)** (Akhurst and Hata, 2012).

- **4.C. Role of TGFβ-SMAD complex in tumor suppression and inhibiting stemness:**

In normal and premalignant epithelial cells, TGFβ attenuates cell proliferation, cell cycle and promotes apoptosis by upregulating the expression of cyclin-dependent kinase (CDK) inhibitors (1A 2B), apoptosis inducer death-associated protein kinase (DAPK). In addition, it suppresses one of the key transcriptional activators c-Myc to inhibit tumor progression. Cancer cells avoid this pathway by inactivation of the major component of TGFβ signaling. However, various cancer types have activated the TGFβ signaling pathway which does not confer tumor-suppressive effect, rather it drives the non-canonical oncogenic signaling (Yeh et al., 2019a, 2019b).

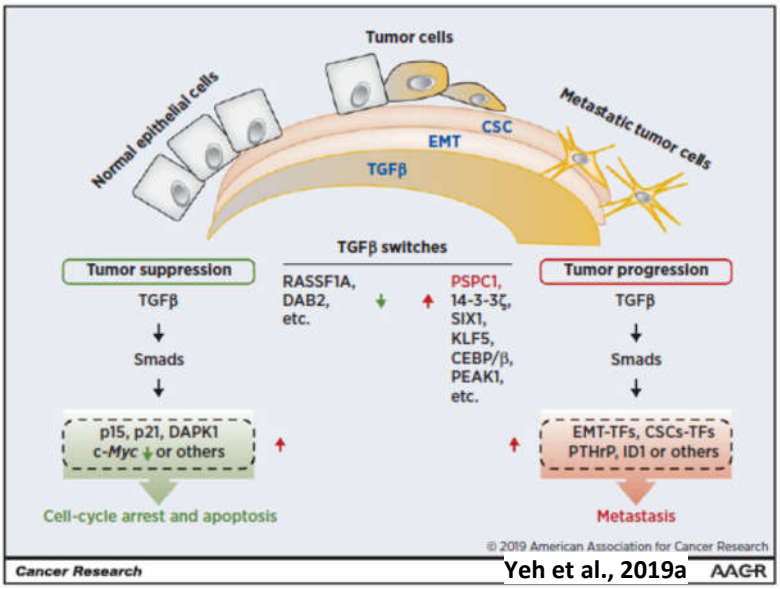

Figure 9: Negative regulation of TGFβ in cancer progression

TGFβ represses breast cancer progression through two independent pathways: (i) by downregulating the early progenitor or CSC pool, (ii) inducing differentiation of committed cells or facilitating the transformation of highly proliferative to less proliferative and differentiated form. Therefore, CSCs have lost their self-renewal potential and reduced their population in breast cancer. By negative regulation of ABCG2, TGFβ reduces CSCs population in gastric cancer also **(Fig. 9)** (Bellomo et al., 2016).

D. Positive regulation of TGFβ in stemness and metastasis in cancer:

In glioblastoma, the autocrine signaling of TGFβ acts on SOX4 and thereby enhances the expression of stemness marker SOX2 and OCT4. It also induces self-renewal of glioma initiating cells via SMAD-dependent signaling of leukemia inhibitory factor (LIF) to activate the LIF-Janus kinase-STAT pathway (Bellomo et al., 2016). In hepatocellular carcinoma (HCC), SMAD-dependent transcriptional regulation promotes demethylation of CD133 promoter and thereby enhances tumorigenic potential of $CD133^{+}$ population. In ovarian cancer (OC), TGFβ promotes stemness and chemoresistance by enhancing the expression of ZEB1 (Mitra et al., 2018). In non-small lung cancer, TGFβ treatment promotes EMT and stemness through methylation of CD87 and Slug promoter region (Kim et al., 2020). It also promotes epirubicin drug resistance through regulating EMT, stemness, and apoptosis in triple-negative breast cancer (TNBC) (Xu et al., 2018).

5. PITX2 (Pituitary homeobox 2)

- **5. A. About PITX2:**

PITX2 is a bicoid-like homeodomain transcription factor that regulates the proliferation of cells in a tissue-dependent manner and play important role in the development of the embryo. This gene is localized in chromosome 4 and it contains 6 exons that encode isoforms by alternative splicing. There are four isoforms: PITX2A, PITX2B, PITX2C, and PITX2D. Three new isoforms have been identified i.e PITX2E, PITX2F, and PITX2G, which have 2 new exons upstream of known PITX2 exons. These isoforms contain identical C-terminal parts and homeodomain but they have different N-terminal domains **(Fig. 10)** (Bosenko and Semina, 2005; Muncke et al., 2005).

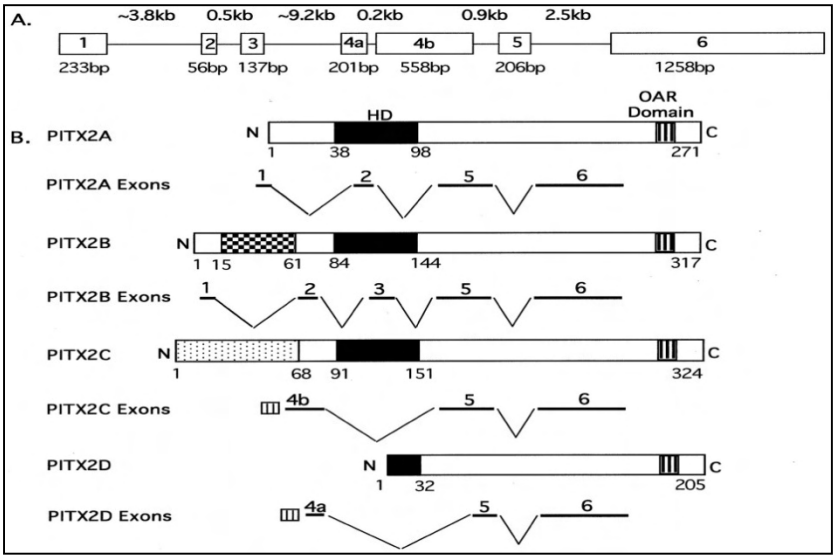

Muncke et al., 2005

Figure 10: Different splicing isoforms of PITX2 gene

- **5. B. Developmental role of PITX2:**

PITX2 plays a great role in left-right asymmetry in embryonic development. It acts as a mediator between asymmetric organ morphogenesis and the left lateral plate mesoderm (l-LPM) formation (Schweickert et al., 2000). It involves asymmetrical development of the tooth, eye,

and abdominal organs such as the gut, stomach, spleen, and heart also (Essner et al., 2000). It also has a role in limb myogenesis. It acts as an intermediate between Pax3 and MyoD gene and binds to MyoD enhancers for enact limb myogenesis (Honoré et al., 2010). PITX2 also binds the enhancer of cVg1, which is TGFβ like a signal for polarity development in twins (Weeks and Melton, 1987). PITX2 has also a role in gonad development in a sexually dimorphic manner (Nandi et al., 2011).

- **5.C. Role of PITX2 in cancer:**

PITX2 orchestrates Wnt/ β-catenin pathway and TGFβ signaling to enhance cell proliferation and migration respectively in OC (Basu and Roy, 2013; Basu et al., 2015). It also enhances cancer progression through Wnt/ β-catenin pathway in lung adenocarcinoma (Luo et al., 2019). Wnt/Dvl/CTNNB1 and Hedgehog/TGFβ pathways regulate the progression in colorectal cancer (Hirose et al., 2011). It is also enhanced in thyroid cancer and promotes cell proliferation (Huang and Zhu, 2008). PITX2 DNA methylation is a prognostic marker for breast cancer progression (Aubele et al., 2017). Hypermethylation of the PITX2 promoter decreased its expression and was associated with a poor prognosis in prostate cancer (Vinarskaja et al., 2013). In renal cancer cells, PITX2 promotes doxorubicin resistance through transcriptional activation of ABCB1 (Lee and Chakraborty, 2013). IFNα signaling promotes PITX2 expression through which it induces resistance to letrozole in the breast cancer cell (Xu et al., 2019). In esophageal squamous cell carcinoma, miR-644a suppressed PITX2 expression by binding to its promoter, and downregulation of this miRNA promotes stem-like features through enhancing PITX2-Wnt/β-catenin pathway (Zhang et al., 2017). Paired-related homeobox transcription factor 1 (PRRX1) downregulates PITX2-miR-200a and PITX2-miR-200b/429 and deficiency of PRRX1 promotes EMT through PITX2 mediated pathway in HCC (Chen et al., 2021). Through Wnt/β-catenin pathway, PITX2 promotes chemoresistance in the colorectal cancer cell. In addition, it regulates the expression of ABC drug transporters in colon and kidney cancer cells (Lee and Thévenod, 2019).

6. Metabolic reprogramming in cancer

Cancer cells alter their metabolic pathway depending upon the environmental condition, the requirement of energy, survival strategy to support their proliferation and growth. During the progression of cancer, metabolic reprogramming occurs by the interaction of internal and external factors (Brandon Faubert, Ashley Solmonson, 2020). Therefore, metabolic reprogramming or alteration is an emerging hallmark of cancer cells (**Fig. 11)** (Hanahan and Weinberg, 2011).

6.A. Altered glucose metabolism in cancer:

In contrast to normal cells, cancer cells utilize glucose very rapidly to produce energy through glycolysis. The pyruvate produced in this pathway synthesizes lactate in aerobic conditions , which is known as the Warburg effect. Glucose metabolism is regulated both positively and negatively at three rate-limiting steps in cancer. Hexokinase (HK1, HK2) is the first rate-limiting enzyme that produces glucose-6-phosphate (G6P). HK2 binds to mitochondria through a voltage-dependent anion channel (VDAC). G6P allosterically inhibits HK2 and causes its dissociation from mitochondria.

In proliferating cancer cells, this inhibition is not abundant as G6P is rapidly converted into glucose-1, 6-bisphosphate. Oncogenic KRAS, oncogenic BRAF, hypoxia-inducible factor (HIF1α), Akt are enhances the expression and translocation of glucose transporters in the membrane and therefore glucose uptake is enhanced in cancer cells. HK2 expression and activity are increased by oncogene Myc, HIF1α, and Akt. Phosphorylation by Akt induces its association with mitochondria and intracellular activity.

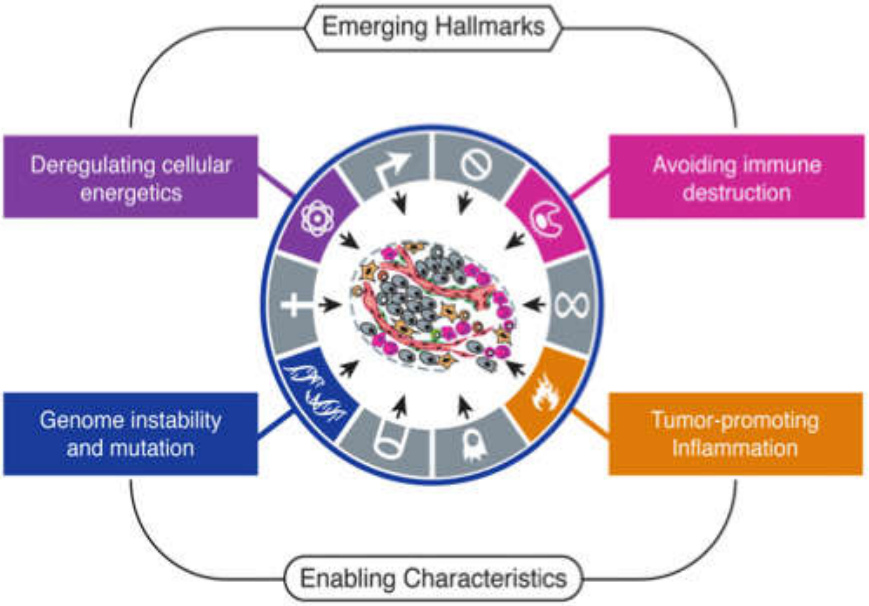

Hanahan and Weinberg et al, 2000

Figure 11: The emerging hallmarks of cancer

The second committed step, phosphofructokinase (PFK1) converts fructose-6-phosphate (F6P) to fructose-1, 6- bisphosphate (F-1,6-BP). This enzyme is allosterically activated by fructose-2, 6-bisphosphate (F-2,6-BP) which is produced by 6-phosphofructo 2-kinase/fructose-2, 6-bisphosphatase (PFK2/F2,6-BPase or PFKFB). Various downstream products of glycolysis such as lactate, PEP, citrate, palmitoyl Co-A, and ATP can inhibit PFK1. HIF1α regulate PFKFB3 which is enhanced in cancer cells in normoxic condition. Akt also phosphorylates and activates PFKFB3 followed by upregulation of PFK. Under the oxidative stressed condition, the activity of PFK is inhibited to divert them in the pentose phosphate pathway (PPP) which synthesizes NADPH and regulates redox homeostasis. Excess palmitoyl-CoA and citrate attenuated PFK and therefore flow back F6P to the PPP and produce NADPH for lipogenesis. Therefore, high PFK activity is not

essential for cancer cells. Glycosylation at Ser 529 is also inhibited PFK activity by F-2,6-BP.

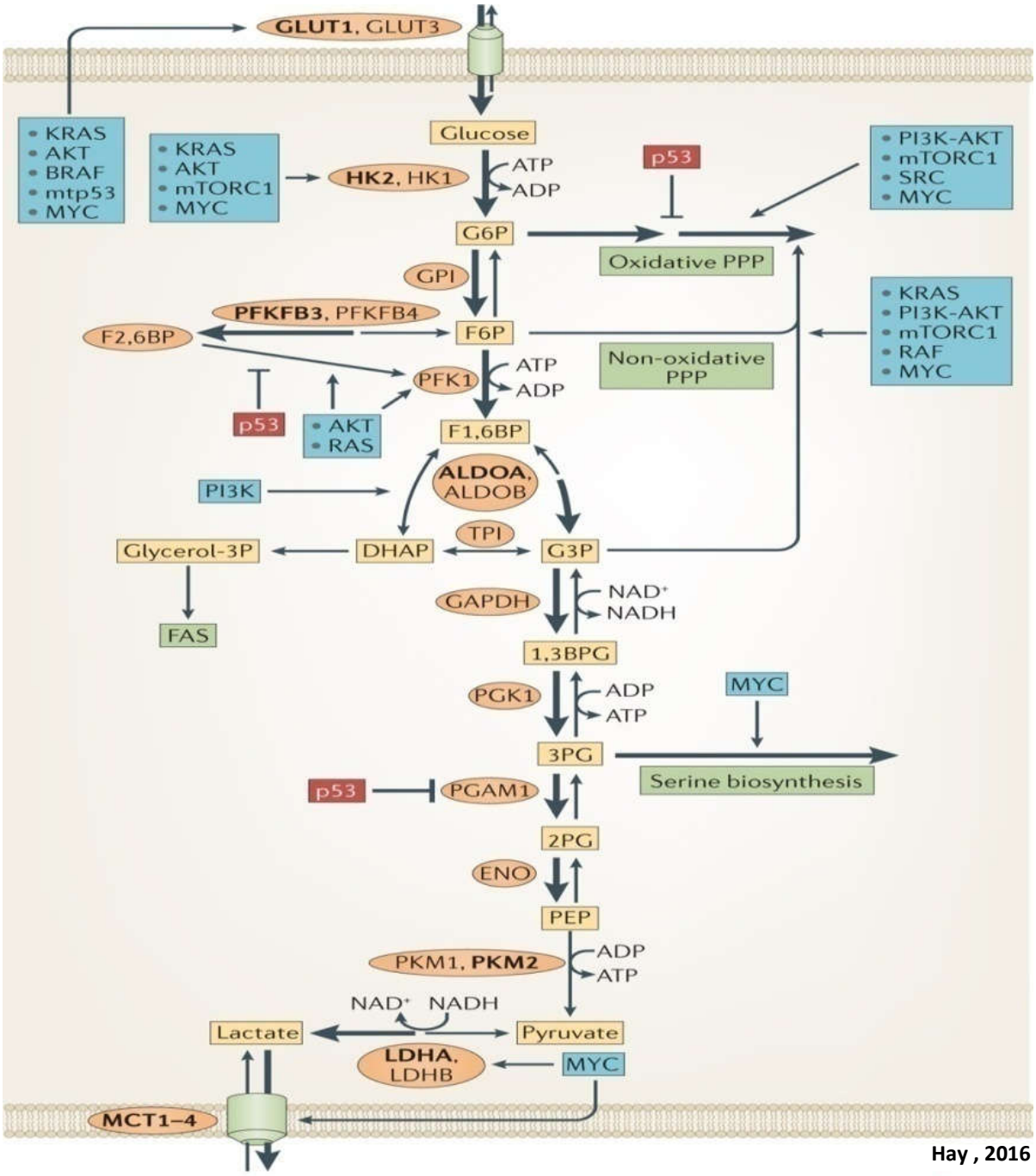

Figure 12: Regulation of glucose metabolism in cancer

The third committed step of glycolysis was driven by pyruvate kinase 2 (PKM2) which was positively regulated by F-1,6-BP, and serine. A high level of these metabolites drives the glycolytic pathway in the forward direction and synthesizes ATP. Independently phosphorylation and oxidation of PKM2 at tyrosine 105 and cysteine 358 respectively inhibit its activity and thereby channelize substrate to the serine biosynthesis pathway and one-carbon

metabolism pathway. In addition, enhances the flow of metabolites towards oxidative PPP and maintains the redox balance.

HIF1α and MYC regulate the expression of LDHA, MCT1 and therefore enhance lactate synthesis and its transport from the cancer cell. Tumor suppressor p53 also regulate the expression of a glycolysis and apoptosis regulator, TIGAR, which binds to HK2 and enhances its activity under hypoxic condition. Gain of function mutation of p53 enhances GLUT1 translocation to the membrane (Hay, 2016) **(Fig. 12)**.

6.B. Alteration in glutamine metabolism in cancer:

Among the non-essential amino acids, glutamine is most predominant in human blood. Its average concentration ranges from 0.4mM to 0.7mM under normal physiologic conditions (Bhutia and Ganapathy, 2016). As it is a non-essential amino acid, the body can synthesize glutamine as per its glutamine is taken up by the liver and the liver can itself synthesize it, although the liver has more regulatory capability than synthesis glutamine (John, 2003). Although glutamine is synthesized endogenously, some of the cells required it to meet their normal demand. The most willing accepter of glutamine are intestinal epithelial cells, tubular epithelial cells in the kidney, activated immune cells, and proliferating cancer cells (John, 2003; Newsholme, 2001; Newsholme et al., 2003; Wise and Thompson, 2010). Therefore, glutamine is important to drive to the TCA cycle and produce substrate to synthesize nucleotides, fatty acids, and hexosamine (Pavlova and Thompson, 2016).

- **Transport of glutamine in cancer cells:**

a) Cytosolic transport of glutamine in cancer: As glutamine is a neutral charge, polar amino acid, it cannot cross the plasma membrane of the cell directly. Therefore, it is transported into the cell via various transporters. The most abundant and well-studied glutamine transporter in the cancer cell is ASCT2/SLC1A5. Apart from ASCT2, other transporters such as LAT1, $ATB^{0,+}$, SNAT and xCT are responsible for glutamine transport in the cancer cell **(Fig. 13)**.

b) Mitochondrial transport of glutamine in cancer: Mitochondrial glutamine transport is an area that is still under darkness. Recently it is investigated that a novel variant of SLC1A5 has an N-terminal mitochondrial localization signal used to transport cytosolic glutamine to mitochondria. Hypoxia induces the localization of the SLC1A5 variant to mitochondria by HIF2α (Yoo et al., 2020). Some reports also suggested that another transporter GLAST (Glutamate aspartate transporter), widely present in the neuronal cell, has transport glutamate in mitochondria (Magi et al., 2019). According to the protein atlas database, GLAST is absent in normal ovarian cells but it is low expressive in the ovarian cancer cell (Https://www.proteinatlas.org/ENSG00000079215-SLC1A3/pathology). SLC25 may have a role

in transporting glutamine into mitochondria, though it is not well established yet (Matés et al., 2020).

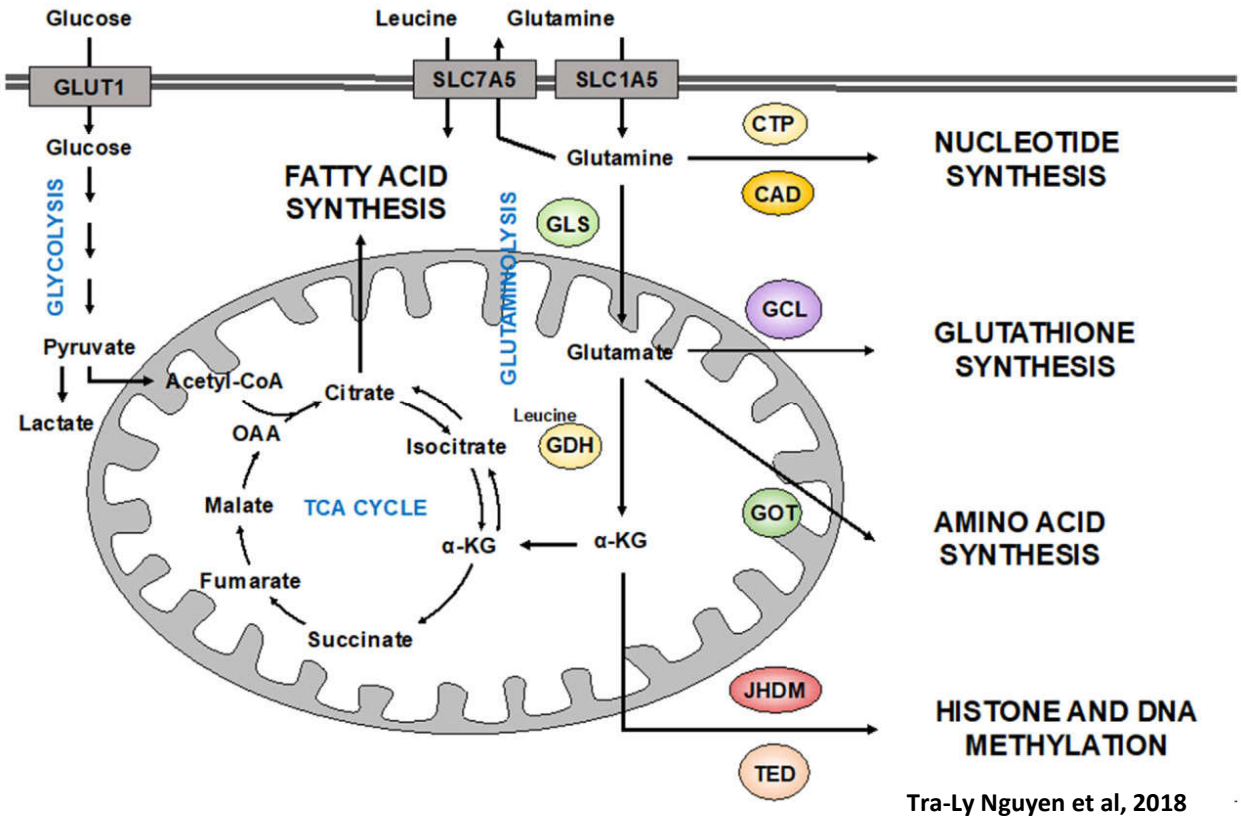

Figure 13: Transport and utilization of glutamine in various metabolic pathways in cancer cell

- **(ii) Glutamine metabolism or glutaminolysis:**

The crucial role of glutamine is to fuel the TCA cycle and produce ATP. In the canonical pathway, Glutamine is metabolized into glutamate by glutaminase (GLS). Glutaminase is produced from two types of genes: (1) GLS1 or kidney type glutaminase which is expressed ubiquitously, (2) GLS2 or liver type glutaminase which is specifically localized to the liver. Alternative splicing of GLS1 produced two isoforms: one is full isoform (GLS1) and a truncated form known as glutaminase C (GAC). GLS2 transcript produced from the GLS2 gene. Therefore, three types of GLSs such as GLS1, GLS2, and GAC have been identified and all of them are localized to the mitochondria. GLS1 and GAC are overexpressed in various cancer and they have a great role to promote glutamine addiction in cancer cells whereas GLS2 acts as a tumor suppressor in some contexts. Recently some reports indicate that GLS2 is pro-tumorigenic and it is upregulated in breast cancer (Altman et al., 2016).

Three types of enzymes can catalyze the conversion of glutamate to a-KG: (1) glutamate dehydrogenases (GDH), (2) glutamate pyruvate transaminases (GPTs), and (3) glutamate oxaloacetate transaminases (GOTs). GDH produces a-KG and ammonia from glutamate. GPT has

two isoforms, one is cytosolic (GPT1) and another is mitochondrial (GPT2) which produces a-KG and alanine. Glutamate oxaloacetate transaminases (GOTs), or aspartate aminotransferase (ASP) also has two isoforms: GOT1 (Cytoplasmic isoform) and GOT2 (mitochondrial isoform). It also produces α-KG and aspartate (Altman et al., 2016).

α-KG is a substrate for the TCA cycle and therefore glutamine act as an anaplerotic substrate to fuel TCA Cycle. Five carbon of glutamine enter into the TCA cycle as α-KG and it releases from the cycle as malate which has four carbon. Therefore, the conversion of α-KG to malate produces one CO_2, ATP, NADH, and $FADH_2$ also.

- **(iii) Glutamine and redox homeostasis:**

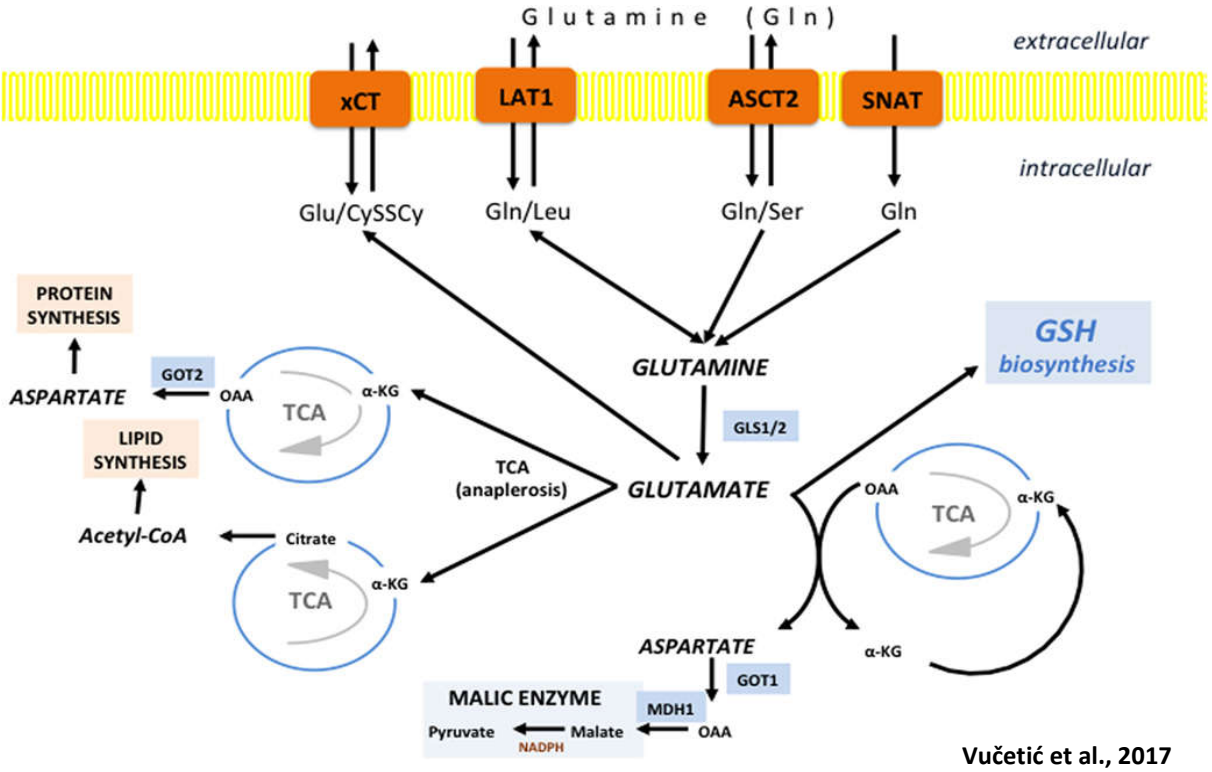

Vučetić et al., 2017

Figure 14: Role of glutamine to maintain redox balance

ROS can act as a signaling molecule to induce pro-tumorigenic action at its physiological concentration, but at higher concentrations, it can damage the cellular machinery and promote apoptosis. Mitochondrial ROS can produce from electron leaking in the ETC chain. Enhancement of glutamine oxidation produces more ROS. Glutamine can scavenge intracellular ROS.

There are three ways by which glutamine can maintain cellular ROS:

a) Firstly, glutamine can produce glutathione which is an antioxidant that can neutralize cellular ROS and superoxide. It is a tripeptide consisting of glycine-glutamate-cysteine. Glutathione is

synthesized by two steps reaction: In the first step glutamate and cystine are condensed by glutamate-cysteine ligase (GCL) and in the second step glycine is added by glutathione synthetase (GSS), producing tripeptide glutathione.

b) Secondly, glutamine-derived glutamate regulates the uptake of cysteine coupled with glutamate efflux through xCT. xCT functioned to maintain the cellular ROS by transferring cysteine to glutathione synthesis.

c) Thirdly, glutamine-derived NADPH is involved to maintain cellular redox homeostasis. Reducing the form of NADPH is involved not only in fatty acid and nucleotide biosynthesis but also to oxidize the reduced form of glutathione (GSSG) and thioredoxin. Therefore, the oxidized form of GSH and thioredoxin can again scavenge cellular ROS **(Fig. 14)** (Vučetić et al., 2017).

- **(iv) Regulation of glutamine metabolism in cancer cells:**

c-Myc: Myc is the third most prevalent oncogene overexpressed in cancer. Oncogenic signaling pathways such as mTORC1 activates Myc and Myc-transformed cells become glutamine dependent by upregulation of glutamine transporter and induce expression of GLS1, GDH, and aminotransferase. It also has a role in the production of an oncometabolite, 2-hydroxyglutarate, and also synthesizes glutathione in hypoxia conditions. This oncogene enhanced the expression of pyrroline5-carboxylate reductase 1 (PYCR1) and pyrroline-5-carboxylate synthetase (ALDH18A1) to drive proline production from glutamine and therefore glu-pro axis confers prognosis in luminal breast cancers **(Fig. 15)** (Craze et al., 2018).

KRAS: In Pancreatic ductal adenocarcinoma (PDAC), upon knockdown of KRAS, the protein and gene expression of GDH increase with the reduction of GOT1 which suggests that KRAS is an important player for coordinating non-canonical glutamine metabolism to sustain cell growth and proliferation (Son et al., 2013). KRAS is responsible for decoupling between glucose and glutamine metabolism which in turn leads to channel carbon and nitrogen from glutamine to other building blocks of the cell (Gaglio et al., 2011). KRAS mutation and oxidative stress blocked this malate dehydrogenase 1 (MDH1) methylation and promote proliferation in pancreatic cancer **(Fig. 15)** (Wang et al., 2016).

Hypoxia: In the oxidative cancer cell, glutamine uptake is promoted through lactate signaling (Pérez-Escuredo et al., 2016). Along with two glutamine transporter such as SLC7A5 (LAT1) and SLC1A1, hypoxia upregulated the expression of SLC38A2 (SNAT2) in a broad range of breast cancer cell lines. SNAT2 is induced by ERα but predominantly HIF1α is responsible for its induction and its regulation generates endocrine resistance in breast cancer (Morotti et al., 2019). HIF1α directly regulates GLS1 and thus promotes tumor proliferation, invasion, and metastatic colonization in colorectal cancer (Xiang et al., 2019).

mTORC1: Amino acid availability activates mTORC1 and thereby it regulates the biosynthetic pathway for the synthesis of amino acid, fatty acid in the proliferating cell and suppresses the degradative pathway like autophagy. Arginine and leucine can together activate mTORC1 via RAS-related GTPase (RAG) complex on the lysosome. Glutamine can regulate mTORC1 through exchange with leucine via LAT1. Lysosomal Transporter SNAT9 which transports glutamine, arginine, leucine can also regulate RAG-dependent mTORC1 activation. Glutamine also promotes RAG independent mTORC1 lysosomal localization through ADP-ribosylation factor 1 (ARF1). Glutamine-derived α-KG may also regulate RAGb activity and mTORC1 Activation. Following these pathways, mTORC1 can be activated and regulate the downstream effector molecules **(Fig. 15)** (Altman et al., 2016).

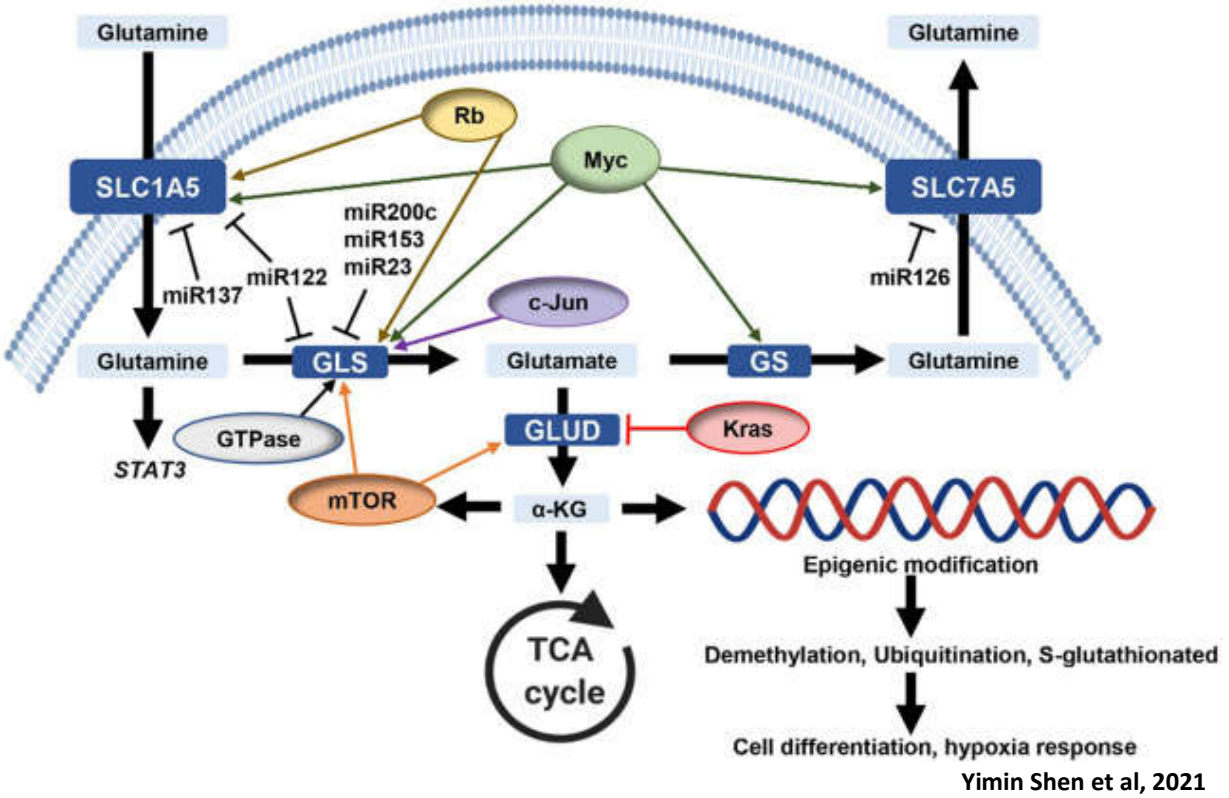

Yimin Shen et al, 2021

Figure 15: Regulator of glutamine metabolism in cancer

- **(v) Role of glutamine metabolism in cancer invasion, metastasis, and progression:**

Glutamine is signaled through mTORC1 which in turn regulates the growth of advanced estrogen receptor-positive breast cancer cells in glutamine dependent manner (Demas et al., 2019). In ovarian cancer (OC), glutamine-dependent mtORC1 regulates cell invasion and metastasis (Yuan et al., 2015). The glutamate produced in the cytosol is transported to the microenvironment using xCT transporter and thereby it binds to the GRM3 receptor which in turn facilitates GRM3 driven MT1-MMP trafficking to promote invasiveness in breast cancer

(Dornier et al., 2017). Glutamine deprivation-induced p53 activation which in turn activates p53 dependent genes. SLC7A3 is an arginine transporter that is induced by p53. Arginine itself cannot maintain all the metabolic pathways in the absence of glutamine. However, it can activate mTORC1 which regulates cell growth in the absence of glutamine (Lowman et al., 2019). Various growth factors also regulate glutamine metabolism and promote EMT. TGFβ and Wnt can regulate GLS1 expression by regulating a transcription factor DLX2. DLX2/GLS1/Glutamine metabolism axis promotes EMT by suppressing the expression of p53 dependent miRNA (Lee et al., 2016).

In the absence of glutamine, exogenous asparagine can also rescue cell survival and proliferation by facilitating the expression of glutamine synthetase (GLUL) and maintaining protein synthesis (Pavlova et al., 2018). In glutamine-deprived conditions, sarcoma cells are adapted to upregulate the expression of glutamine synthetase (GLUL). Therefore GLUL maintains the intracellular level of glutamine and thereby they can proliferate (Issaq et al., 2019).

Immature myeloid cells (IMC) are generated from hematopoietic stem cells (HPC). This IMC is the major contributor to the TME of a solid tumor with high immunosuppressive capacity. Differentiated IMC has high glycolytic capacity but they depend upon glutaminolysis in absence of glucose. Through the binding of glutamate to glutamate receptor NMDR, T cells are activated and proliferated. Therefore, glutamine derived α-KG and glutamate-NMDA receptor axis is responsible for the final activation of activated immunosuppressive IMC in the tumor microenvironment (Wu et al., 2019).

In a highly invasive OC cell, glutamine catabolism is higher compared to their anabolism. Therefore, highly aggressive cells are glutamine dependent and they utilize it for their proliferation, invasion, and maintaining redox balance. Signal transducer and activator of transcription 3 (STAT3) is a cytoplasmic transcription factor that promotes malignant transformation and chemoresistance of cancer cells in response to various growth factors and cytokines. Glutamine promotes tyrosine 705 phosphorylation on STAT3 in invasive OC which regulates its invasiveness by regulating the gene related to invasions such as THBS1, SERPINE1/2, COL5A1, THBD, and PLAU (Yang et al., 2014). Extracellular glutamine acts as a signaling molecule to activate STAT3 (phosphorylation on Y705) in cervical and breast cancer and promote proliferation by maintaining metabolic activities. This glutamine-dependent STAT3 activation is independent of its metabolism (Cacace et al., 2017).

- **(vi) Role of glutamine metabolism in promotion of cancer stemness and chemoresistance:**

PDAC cells have a non-canonical glutamine metabolism pathway and pancreatic cancer stem cells (PCSC) are also dependent on it. Under glutamine-deprived conditions, PCSC lost their stemness characteristic, self-renewal capability, and amount of ROS increased which leads to apoptosis. These PCSC cells can survive in glutamine-deprived conditions with the addition of oxaloacetate but not with the addition of α-KG. Therefore, it suggests that Therapeutic targeting of non-canonical glutamine metabolism pathway can enhance the radiosensitivity of PCSC (Li et al., 2015). ROS can act as a signaling molecule to phosphorylate β-catenin and thereby diminish β-catenin activity and stemness character. Therefore, it can regulate stemness in glutamine-dependent non-small lung carcinoma and pancreatic cancer cell (Liao et al., 2017).

High expression of GLS1 is correlated with the stemness property of hepatocellular carcinoma (HCC). GLS1 can regulate the redox balance by producing glutathione. Thioredoxin-related protein, nucleoredoxin also inhibits the Wnt/β-catenin pathway in response to ROS. ROS inhibits the expression of both β-catenin and stemness marker and therefore, GLS1 regulates stemness property through ROS/Wnt/β-catenin pathway and thereby targeting GLS1 Can eradicate the stem population in HCC (Li et al., 2019). GLS1 also regulates aldehyde dehydrogenase (ALDH) expression in head and neck cancer and glutaminolysis-ALDH axis promotes the generation of cell population with high stemness phenotype (Kamarajan et al., 2017).

Glutamic pyruvate transaminase (GPT) is a cytosolic biomarker that maintains glutamine homeostasis within the cell. This enzyme drives the reversible transamination reaction between alanine and a-KG to synthesize glutamate and pyruvate. It is reported that GPT2 is overexpressed in breast cancer which in turn reduces α-KG level. In contrast, GPT2 overexpression leads to enhance the amount of α-KG in cancer-associated fibroblasts (CAF). Highly proliferating cancer cells consume α- KG rapidly for anabolic pathway but CAF might not need for its anabolic process. The high amount of α-KG can stabilize HIF1α which in turn activates the sonic hedgehog signaling pathway leads to stemness. Therefore, GPT2 can be a potential target for breast cancer treatment (Cao et al., 2017).

Again in cholangiocarcinoma, cisplatin treatment in hypoxic conditions drives the cell towards chemoresistance through upregulation of c-Myc. However, in the core of the tumor where the cells are both nutrient and oxygen-deprived, they can rescue the cells from cisplatin resistance. We can conclude that the chemoresistance generated through hypoxia can be counteracted by glutamine deficiency (Wappler et al., 2020). Platinum-resistant OC cells show higher dependency on glutamine through enhanced expression of glutamine transporter (ASCT2) and

glutaminase. Here, also cisplatin treatment increases glutamine metabolism which in turn upregulates c-Myc and thereby the cells become resistant to cisplatin (Hudson et al., 2016).

Glutamine deprivation stimulates Wnt signaling in APC-mutant intestinal organoids derived from colorectal cancer through decreasing α-ketoglutarate levels and promoting stemness. Supplementation of α-ketoglutarate induces hypomethylation of DNA and histone H3K4me3 which enhances the expression of differentiation-associated genes and reduces the Wnt signaling pathway respectively (Tran et al., 2020). Similarly patient-derived ^{V600E}BRAF melanoma cells, low glutamine concentration promotes hypermethylation on H3K27 which leads to stimulating dedifferentiation of cancer cells. In the intratumoral core region, glutamine deficiency creates a low α-ketoglutarate level which is utilized by Jumonji domain-containing (JmjC) histone demethylase (HDMs) for their activity. Therefore, glutamine deprivation promotes cell dedifferentiation and chemoresistance through attenuated histone demethylation (Pan et al., 2016).

Myeloid-derived suppressor cells (MDSC) promote cancer stemness by inducing the expression of miRNA101 in OC. CtBP2 is a co-repressor that has a miRNA101 binding site at its 3'UTR. Therefore, suppression of CtBP2 via miRNA101 leads to enhancing the expression of stem markers such as SOX2, OCT4, NANOG due to their incapability of CtBP2 to bind to their promoter and thereby enhances stemness in OC by MDSC (Cui et al., 2013). Therefore, it can be suggested that glutamine availability can promote cancer stem cells via the interaction between tumor microenvironment, immunosuppressive IMCs, and cancer cells.

7. Mitochondrial dynamics in cancer

Mitochondria are known as the "powerhouse" of the cell as they produce ATP through the electron transport chain (ETC). It is a major player regulating cell proliferation, redox balance, apoptosis, calcium ion storage, immunity, and inflammation. Due to their highly dynamic nature, they undergo fission and fusion rapidly under a metabolic or extracellular stressed condition, which drives cancer progression.

- **7. A. Mitochondrial Fission proteins:**

The mitochondrial outer membrane is fragmented by dynamin-related protein 1 (DRP1). The site of mitochondrial fragmentation is guided by the endoplasmic reticulum (ER). This ER-contact site is marked by replicating mtDNA. Several outer membrane protein receptors such as Mff, Fis1, Mid49, and Mid51 are involved in the binding of DRP1 and they assemble as an oligomeric complex. Oligomeric DRP1 accumulates at the ER marked site and there is a constant equilibrium is maintained between cytosol and mitochondria. Constriction of the outer and

inner membrane is driven by the GTP hydrolysis of DRP1. Mitochondrial constriction is facilitated by actin nucleation and polymerization which is regulated by ER-bound INF2 and mitochondrial Spire1C. Post-translational modification such as phosphorylation, sumoylation, ubiquitination, S-Nitrosylation, and O-Gluc-N-Acylation regulates DRP1 activity and mitochondrial fission. Phosphorylation of DRP1 occurs at 3 major sites: — Ser616, Ser637, and Ser693. DRP1 Phosphorylation at Ser616 promotes mitochondrial fission, however, phosphorylation Ser637 and Ser693 induce the opposite effect. Additionally, phosphorylation of DRP1 receptor, Mff increased binding of DRP1 and mitochondrial fission. Sumoylation of DRP1 occurs at the non-consensus sequence of the B-domain. This sumoylation facilitates the signaling crosstalk between mitochondria and ER to induce apoptosis. E3 ubiquitin ligase MARCH5/MITOL and parkin are involved in the ubiquitination of DRP1 and these ubiquitin ligases also promote proteasomal degradation of Mid49 (Maycotte et al., 2017; Tilokani et al., 2018).

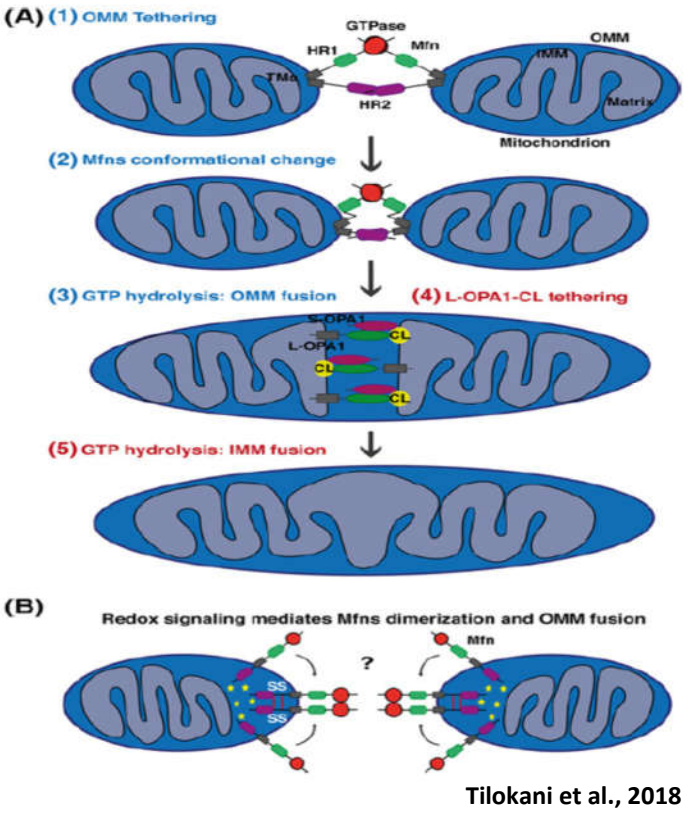

Tilokani et al., 2018

Figure 16: Mechanism of mitochondrial fission

In absence of DRP1, FIS1 regulates mitochondrial fission. It regulates fission by binding to the fusion machinery such as Mfn1, Mfn2, Opa1 and inhibiting their GTPase activity.

Other proteins involved in mitochondrial fission are ganglioside-induced differentiation-associated protein 1 (GDAP1) and SLC25A46 **(Fig. 16)** (Ma et al., 2020).

- **7. B. Mitochondrial Fusion proteins:**

The fusion proteins involved in the outer mitochondrial membrane and inner mitochondrial membrane are Mitofusin (MFN1 and MFN2) and optic atrophy protein 1 (OPA1) respectively.

Mitochondrial fusion occurred in three steps: the mitochondria are anchored in transposition and the membrane is in close contact. Due to the GTP hydrolysis, the conformation changes occur which in turn regulates the fusion of two outer mitochondrial membranes.

MFNs are transmembrane proteins in OMM. These transmembrane domains are separated by the N-terminal heptad repeat 1 (HR1) domain and C-terminal heptad repeat 2 (HR2) domain. During mitochondrial fusion, two mitochondria in anti-parallel position interact through the HR2 domain of MFN which leads to the fusion of two mitochondrial membranes via GTP hydrolysis.

After fusion of the OMM, IMM fusion was mediated by another protein OPA1, and one component of a phospholipid, cardiolipin. There are two isoforms of OPA: L-OPA and S-OPA, however, only L-OPA is sufficient for the fusion of IMM. MFN1 is involved in OPA- dependent mitochondrial fusion (Maycotte et al., 2017).

- **7. C. Role of mitochondrial dynamics in cancer:**

i) Apoptosis and autophagy:

During apoptosis, there is permeabilization of the mitochondrial outer membrane (MOMP) and mitochondrial fission is observed at this time. At the site of fission, DRP1, MFN1, and OPA1 co-localize during apoptosis, and also knock-down of these proteins or overexpression of fusion proteins leads to decrease apoptosis. Mutant OPA1 can form oligomeric forms and block cytochrome C release and apoptosis. Sumoylation of mitochondria is necessary for cristae remodeling and apoptosis. However, mitochondrial fission not always leads to apoptosis, sometimes MFN1 and MFN2 regulate apoptosis by interacting with Bax and inducing Ca^{+2} influx.

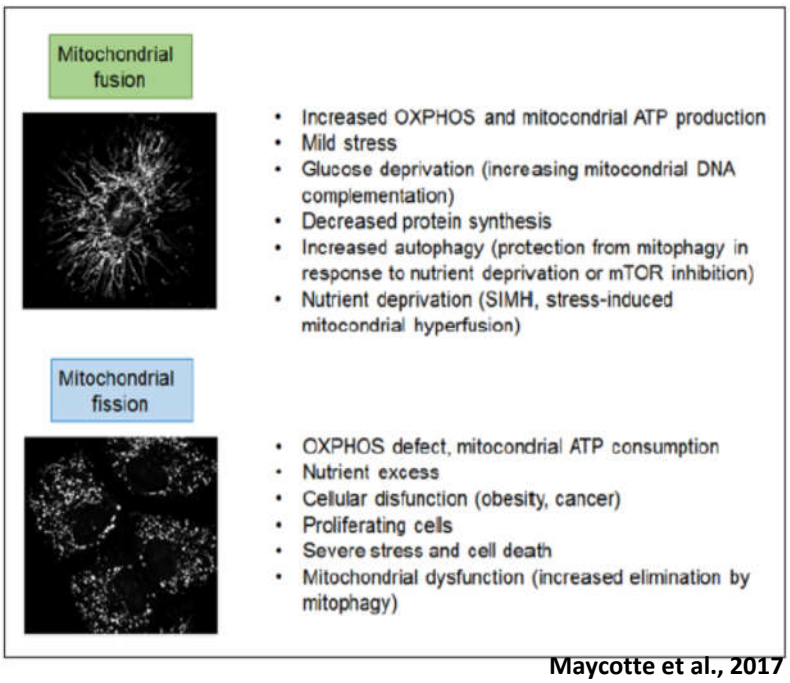

Maycotte et al., 2017

Figure 17: Mitochondrial dynamics and cellular function

Mitochondrial fission proteins such as FIS1 regulate the accumulation of the SNARE Protein Syntaxin 17 (STX17) and promotes mitophagy. In addition, DRP1 and OPA1 interact with mammalian mitophagy receptor FUNDC1 and are involved in mitophagy **(Fig. 17)** (Maycotte et al., 2017).

ii) Migration:

Migration is a crucial step for cancer progression and metastasis. Overexpression of DRP1 and low expression of MFN1 promotes metastasis in the breast cancer cell. Inhibition of DRP1 suppresses the invasive property of glioma cells. During metastases, mitochondria localize at the end of the microtubule and provide energy to the migrating cancer cells. Alteration of mitochondrial dynamics in fission/fusion attenuates lymphocyte polarization and migration (Ma et al., 2020).

iii) ROS generation:

Several reports suggested that overexpression of DRP1 or silencing of MFN1 leads to producing a high amount of ROS in various cancer cells. Mutation in MFN1 and MFN2 produces elevated ROS and therefore enhanced fission-induced ROS production.

ROS has a great role in regulating mitochondrial dynamics. It promotes post-translational modification of DRP1 which in turn enhances mitochondrial fission. ROS drive various signaling pathways such as, PI3K/ Akt, Ras/MAPK/ERK, and NF-κβ pathways which lead to promote cancer proliferation, metastasis, and stemness/chemoresistance **(Fig. 17)** (Ma et al., 2020).

iv) Metabolism:

Mitochondrial dynamics regulate the metabolic alteration in cancer cells. It is reported that fusion enhances oxidative phosphorylation. By shifting the metabolism towards oxidative phosphorylation, MFN1 promotes metastasis in hepatocellular carcinoma. However, DRP1 upregulates the expression of mitochondrial pyruvate carrier in prostate cancer and thereby enhances oxidative phosphorylation. In addition, nutrient deprivation also facilitates mitochondrial dynamics. It is reported that Serine deprivation attenuates colorectal cancer cell proliferation through downregulating ceramide metabolism and mitochondrial fusion. In glucose starved conditions, reduction in MFN2 promotes breast cancer cell survival **(Fig. 17)** (Ma et al., 2020).

8. Sirtuin 4 (SIRT4)

- **8.A. About Sirtuins:**

Sirtuins are a class of signaling proteins involved in metabolic regulation. They are evolutionarily conserved with various functional characteristics and acquire new functions throughout the evolution (Vaquero, 2011). Although they have both histone and non-histone protein target, some of them have specific histone deacetylase activity whereas few of them has other non-

histone substrates. They belong to the family of class III histone deacetylase and there are 7 types of SIRTs included in the mammalian SIRT family.

SIRTs can be classified into three groups depending on their localization in the cell, i.e (1) Nuclear Sirtuins: SIRT1, SIRT6, and SIRT7 are mainly localized in the nucleus, (2) Cytoplasmic Sirtuins: SIRT2 is cytoplasmic whereas (3) Mitochondrial Sirtuins: SIRT3, SIRT4 and SIRT5 located in the mitochondria. Although SIRT can re-localize within the cell to modulate different signaling pathways under various conditions (developmental stage, cell cycle phase, metabolic status, tissue type, etc.). Moreover, SIRT1, SIRT2, and SIRT7 are located in both the cytoplasm and nucleus (Carafa et al., 2019).

Sirtuins are involved in major cellular pathways (DNA damage repair, metabolism, transcriptional regulation, aging) which are involved in cancer progression. SIRT has a dual role as a tumor suppressor and tumor promoter (Oncogenes) depending on the (a) expression level in tissue, (b) effect on other tumor suppressors or proto-oncogenes, and (c) effect on the cell cycle, cell growth, and cell death (Carafa et al., 2019).

- **8.B. Role of SIRT4 in metabolism:**

SIRT4 is a mitochondrial protein and acts as a linker between mitochondrial metabolism and cancer progression. It has several enzymatic activities which are functional in a context-dependent manner. Like the most sirtuin family protein, SIRT4 has deacetylase activity and it inhibits malonyl CoA decarboxylase (MCD). Therefore, SIRT4 deficient mice show the high activity of MCD and it leads to deregulated lipid metabolism with tolerance in exercise and diet-induced obesity (Chen et al., 2019). MTPα is a mitochondrial protein, involved in fatty acid oxidation (FAO). SIRT4 deacetylase MTPα and therefore promotes its ubiquitination and proteasomal degradation which leads to inhibit FAO and lipid accumulation in non-alcoholic fatty liver disease (Tomaselli et al., 2020). It is responsible for maintaining NAD^+/ NADH ratio within mitochondria. Through its deacetylation activity, SIRT4 regulates leucine metabolism and deficiency of SIRT4 leads to deregulated leucine metabolism and increased insulin secretion.

Another unique enzymatic activity of SIRT4 is lipoylation. Pyruvate dehydrogenase (PDH) enzyme act as a bridge between glycolysis and the TCA cycle and SIRT4 removes the lipoyl moiety from the PDH subunit and thereby inhibits its function. In this way, SIRT4 is directly involved in regulating glycolysis.

It is known that through its ADP –ribosylation activity, SIRT4 inhibits glutamate dehydrogenase (GDH) in pancreatic β cells. Therefore, by inhibiting GDH, ATP production hampers which leads to reduce insulin production (Wang et al., 2020). SIRT4 regulates ATP production by deacylation of an uncoupler protein ANT2. Therefore, SIRT4 is involved in regulating oxygen consumption

and decreases ATP production through ANT2 –dependent manner (Wang et al., 2020).

- **8.C. Role of SIRT4 in regulating mitochondrial dynamics and ROS:**

Being a mitochondrial resident protein, SIRT4 is also involved in the regulation of mitochondrial ROS. SIRT3 deacetylates and activates a ROS scavenging enzyme stearoyl Co-A desaturase (MnSOD) and thereby maintains mitochondrial ROS. SIRT4 competes with SIRT3 for the binding with MnSOD and therefore inhibits SIRT3 dependent MnSOD activation.

In the obese patient with non-alcoholic fatty liver disease, SIRT4 expression was low which leads to enhance fatty acid oxidation in the liver and skeletal muscle. A high rate of fatty acid oxidation produces mitochondrial ROS (Han et al., 2019). High expression of SIRT4 promotes mtROS production through its enzymatic activity and also reduces mitophagy by reducing the expression of Parkin in HEK293. Upon interaction with OPA-1, SIRT4 reduces mitophagy and enhances fusion (Han et al., 2019). SIRT4 inhibits DRP1 phosphorylation and interaction with Fis1 in lung cancer

- **8.D. SIRT4 and cancer:**

Most of the studies indicated that SIRT4 is a tumor suppressor, however, in some of the cases it acts as an oncoprotein. Low gene expression of SIRT4 is observed in colorectal, lung, ovarian, endometrial, breast, gastric, prostate, renal, liver, and hematological cancer. Their reduced expression is correlated with a poor prognosis of the disease.

Besides, mTORC1 can regulate glutamine metabolism in a cell-specific manner. SIRT4 is also regulated by mTORC1 in response to nutrient uptake and metabolism. A transcriptional co-repressor, C-terminal binding protein (CtBP) acts as a sensor for intracellular metabolites such as glucose and glutamine. CtBP regulates glutaminolysis by increasing GDH activity through repression of SIRT4 at the high level of intracellular glucose concentration. In pancreatic β cells, SIRT4 represses GDH activity by ADP-ribosylation (Haigis et al., 2006). In glucose starved conditions, CtBP cannot dimerize and therefore it is unable to repress SIRT4 through binding to its promoter which leads to decreased GDH activity (Wang et al., 2018). loss of CtBP increased intracellular acidification and decreased glutamine consumption, in turn, promotes apoptosis in breast cancer (Wang et al., 2015). Therefore, CtBP couples between glucose and glutamine metabolism in cancer. Activation of mTORC1 leads to degrading CREB2 (cAMP response element) which in turn represses SIRT4. Therefore, mTORC1 regulates glutamine metabolism and proliferation via SIRT4 (Csibi et al., 2013).

The cross-talk between SIRT4 and SIRT1 suppresses tumorigenesis in the breast cancer cell. SIRT4 suppresses SIRT1 activity by regulating glutamine metabolism. Low SIRT4 enhances high

SIRT1 activity and therefore SIRT1 promotes deacetylation of H4K16ac and BRACA1 to promote self-renewal properties in breast cancer (Du et al., 2020).

UHRF1 is known as ubiquitin-like with plant homeodomain and ring finger domains 1, which is an upstream regulator of SIRT4. It binds to the SIRT4 promoter and represses its transcription. SIRT4 regulates HIF1α and negatively modulates aerobic glycolysis. Therefore, UHRF1 promotes aerobic glycolysis by suppressing SIRT4 expression in pancreatic cancer (Hu et al., 2019).

SIRT4 can regulate the cell cycle, apoptosis, migration, and metastasis. DNA damage can increase SIRT4 expression and thereby prevent cell cycle progression. In colorectal cancer, SIRT4 has anti-proliferative activity and also inhibits EMT progression. SIRT4 induces mitochondrial fission and therefore, inhibits apoptosis and induces cell proliferation in lung cancer (Tomaselli et al., 2020). Also in HCC, SIRT4 promotes cell survival by inhibiting apoptosis.

INTRODUCTION TO THE PRESENT WORK

Cancer is the second foremost reason for mortality worldwide after heart disease. The major trait of cancer is the fast proliferation of atypical cells that develop beyond their usual boundaries and migrate to the new destination of the body after EMT. After completion of treatment procedures such as surgical removal of the tumor and systemic chemo/radiotherapy, a subset of cancer cells gain the ability to efflux the drug often and therefore they become chemoresistant. To survive in a stressful environment, they often become quiescent and migrate to the other organs to reinitiate malignancy. Therefore, the main complications associated with these diseases due to aggressiveness metastasis, and resistance to therapeutics. To combat the scenarios, we have focused and shed a light on the molecular mechanism behind these problems in this thesis with proper scientific studies, models, and experimental strategies.

Based on the background studies, we have three objectives which are discussed below:

Objective 1:

In the tumor microenvironment (TME), various growth factors promote proliferation, epithelial-mesenchymal transition (EMT), and metastasis of cancer cells by activating different signaling pathways (Witsch et al., 2010). In ovarian cancer cells, TGFβ1 promotes stemness and chemoresistance through EMT (Mitra et al., 2018). There are few reports which suggested that multiple homeobox transcription factors are also associated with stemness/chemoresistance. One of the homeobox transcription factors PITX2 activates the SMAD2/3 dependent TGFβ signaling pathway to promote invasion in ovarian cancer (Basu et al., 2015). In addition, PITX2 promotes chemoresistance by regulating the expression of efflux transporter ABCB1 and ABCG2 in the colon, kidney cancer (Lee and Thévenod, 2019).

Therefore, in Chapter 1, our main objective was: To decipher the signaling cross-talk between TGFβ and homeobox transcription factor to induce chemoresistance in ovarian cancer cells. In our reports, we firstly wanted to elucidate whether TGFβ1 promotes PITX2 expression and the mechanism associated with PITX2-induced stemness/chemoresistance and metabolic alteration in ovarian cancer.

Objective 2:

Different nutrients and metabolites also have a role in regulating stem-like properties and chemoresistance. Metabolic reprogramming is an emerging hallmark of cancer cells for their survival in nutrient or oxygen-depleted conditions. In this condition, glutamine acts a major role to drive the TCA cycle and producing energy. Additionally, it involves the synthesis of other amino acids, nucleotides, fatty acids, and hexosamine (Pavlova and Thompson, 2016). In breast

cancer cells, glutamine deficiency promotes epigenetic alteration to induce the dedifferentiation of cells (Pan et al., 2016). Similarly, the Wnt signaling pathway can be activated by deficiency of α-ketoglutarate (α-KG) in pancreatic ductal adenocarcinoma. Therefore, indirectly glutamine limitation induces stem-like traits (Tran et al., 2020). Mitochondrial morphology and its localization changes to adapt in nutrient limiting conditions and promote drug resistance (Jagust et al., 2019). Dynamin-related protein 1 (DRP1) is involved in mitochondrial fission and mitochondrial fragmentation is associated with the proliferation of cancer stem cells in breast epithelium (De Francesco et al., 2018).

Therefore, in Chapter 2, the objective was: To explore the mechanism by which glutamine deprivation promotes stemness and chemoresistance in cancer. We aimed to focus on the role of glutamine in promoting stem-like characteristics and followed by chemoresistance in ovarian and colorectal cancer. We also tried to link mitochondrial dynamics and localization with glutamine deprivation for induction of stemness.

Objective 3:

Glutaminolysis is regulated through various factors in cancer. In glutaminolysis, glutamine is converted into glutamate by the enzyme glutaminase (GLS) and glutamate dehydrogenase (GDH) catalyzes the conversion of glutamate to α-ketoglutarate. SIRT4, the least characterized protein in the Sirtuin family, which has ADP ribosyltransferase activity is involved in ribosylation of GDH and therefore represses its activity. GDH maintain cellular redox homeostasis in cell and thereby SIRT4 is linked with cellular redox balance (Jin et al., 2015). SIRT4 repress cancer progression by regulating glutamine metabolism in colorectal and breast cancer (Du et al., 2020; Miyo et al., 2015). Being a mitochondrial protein SIRT4 is also a negative controller of glycolysis. In pancreatic cancer, UHRF1 is an upstream regulator of SIRT4, and it promotes proliferation and aerobic glycolysis by repressing SIRT4 (Hu et al., 2019). It also blocks tumor progression by inhibiting the ERK-DRP1 pathway and mitochondrial fusion in non-small lung cancer (Fu et al., 2017). Considering these background studies, we wanted to focus on the role of SIRT4 in ovarian cancer and the associated mechanism linked with cancer progression.

Therefore, in Chapter 3, our objective was: To investigate the role of glutamine metabolism regulatory factor, SIRT4 in the regulation of EMT in ovarian cancer. We want to decipher whether glutaminolysis regulates EMT progression in ovarian cancer and how SIRT4 plays role in EMT by regulating glutaminolysis.

MATERIALS AND METHODS

Materials

- **Cell lines: Table 1**

Serial no.	Name	Make	Catalog Number
1	**PA1**	ATCC	CRL-1572
2	**SKOV3**	ATCC	HTB-77
3	**HCT-116**	ATCC, A kind gift from Dr. Samit Chattopadhyay, CSIR-IICB	CCL-247
4	**IOSE-385**	A kind gift from from N. Aueresperg and C. Salamanca, Vancouver,Canada	
5	**IOSE-364**	A kind gift from N. Aueresperg and C. Salamanca, Vancouver,Canada	
6	**ID8**	MERCK	SCC145

- **Cell Culture Media and serum: Table 2**

Serial no.	Name	Make	Catalog Number
1	**Minimal essential media α (MEM α)**	Himedia	AL080A
2	**Minimal essential media α (MEM α) W/O Gln**	Himedia	AL080
3	**RPMI-1640**	Himedia	AL199A
4	**RPMI-1640 W/O Gln**	Himedia	AL060
5	**Dulbecco's modified Eagle's medium(DMEM)**	Himedia	AL066A
6	**Dulbecco's modified Eagle's medium(DMEM) W/O Gln**	Himedia	AL066
7	**Medium- 199**	Gibco	11150059

Serial no.	Name	Make	Catalog Number
8	**MCDB-105**	Sigma-Aldrich	M6395
6	**Opti-MEM**	Gibco	31985070
7	**Fetal bovine Serum (FBS)**	Gibco	10082139

- **Primary Antibodies: Table 3**

Serial no.	Name	Make	Catalog Number
1	**PITX2**	Santa Cruz Biotechnology	sc-8748
2	**OCT4**	Cell signaling Technology (CST)	2750
3	**SOX2**	Cell signaling Technology (CST)	3579
3	**ABCG2**	Santa Cruz Biotechnology	sc-58222
4	**HK2**	Cell signaling Technology (CST)	2867
5	**SDHA**	Cell signaling Technology (CST)	5839
6	**OXPHOS COMPLEX**	Abcam	ab110411
7	**p-DRP1 (Ser616)**	Cell signaling Technology (CST)	3455
8	**MFN1**	Cell signaling Technology (CST)	14739BC
9	**MFN2**	Cell signaling Technology (CST)	9482
10	**NRF2**	Invitrogen	PA5-27882
11	**xCT /SLC7A11**	Cell signaling Technology (CST)	12691
13	**SIRT4**	Santa Cruz Biotechnology	sc-135797
14	**VIMENTIN**	Cell signaling Technology (CST)	5741T

Serial no.	Name	Make	Catalog Number
15	**N-CADHERIN**	Cell signaling Technology (CST)	13116T
16	**HIF1α**	Santa Cruz Biotechnology	sc-53546
17	**E-cadherin**	Santa Cruz Biotechnology	sc-7870
18	**p-p70s6k (T389)**	Cell signaling Technology (CST)	9205
19	**p-mTORC1 (S2448)**	Cell signaling Technology (CST)	2971
20	**α-TUBULIN**	Cell signaling Technology (CST)	2125
Fluorophore tagged Primary antibodies			
21	**CD44-PE**	BD BIOSCIENCES	550989
22	**CD117-APC**	BD BIOSCIENCES	341096
23	**CD31-FITC**	BD BIOSCIENCES	560984
24	**CD45-PE-Cy7**	BD BIOSCIENCES	557748
HRP- tagged secondary antibodies			
25	**Anti-Rabbit HRP Tagged secondary antibody**	Cell signaling Technology (CST)	7074
26	**Anti-mouse HRP tagged secondary antibody**	Cell signaling Technology (CST)	7076
27	**Anti-goat HRP tagged secondary antibody**	Santa Cruz Biotechnology	sc-2354
Fluorophore-tagged secondary antibodies			
28	**Anti- Rabbit alexa fluor 488**	Invitrogen	A11008
29	**Anti-rabbit alexa fluor 555**	Invitrogen	A48283
30	**Anti-mouse alexa fluor 488**	Invitrogen	A32723
31	**Anti-mouse alexa fluor 633**	Invitrogen	A21052

Serial no.	Name	Make	Catalog Number
32	**Anti-goat alexa fluor 488**	Iinvitrogen	A11055

siRNAs: Table 4

Serial no.	Name	Make	Catalog Number
1	**siPITX2 (h)**	Santa Cruz Biotechnology	sc-44016
2	**siSMAD2 (h)**	Santa Cruz Biotechnology	sc-38374
3	**siNRF2 (h)**	Santa Cruz Biotechnology	sc-37030
4	**siDRP1 (h)**	Santa Cruz Biotechnology	sc-43732
5	**SixCT (h)**	Santa Cruz Biotechnology	sc-76933
6	**siSIRT4 (h)**	Santa Cruz Biotechnology	sc-63024
7	**siSCRAMBELED (h)**	Santa Cruz Biotechnology	sc-37007

Clones: Table 5

Serial no.	Name	Make	Catalog Number
1	**PITX2A**	Gene script	Customised
2	**PITX2B**	Gene script	Customised
3	**SIRT4-FLAG**	Addgene	13815
4	**pRL**	Promega	E2231
6	**pGL3-Luc vector**	Promega	E1751

Reagents and kit: Table 6

Serial no.	Name	Make	Catalog Number
1	**TGFβ1**	Sigma-Aldrich	T7039
2	**U0126**	Calbiochem	662005
3	**SB203580**	Calbiochem	559389
4	**TGFβ receptor kinase inhibitor**	Calbiochem	616451
5	**MDiVi-1**	Sigma-Aldrich	M0199
6	**L-DON (6-Diazo-5-oxo-L-norleucine)**	Sigma-Aldrich	D2141
7	**Sulphasalazine**	Sigma-Aldrich	S0883
8	**Nocodazole**	Merck	487928
9	**glutathione reduced ethyl ester (GSH)**	Sigma-Aldrich	G1404
10	**N-acetyl cysteine (NAC)**	Sigma-Aldrich	A7250
11	**RNAiso Plus reagent**	Takara	9109
12	**iScript cDNA synthesis kit**	Biorad	1708891
13	**Biorad Sybr green**	Biorad	1725120
14	**ECL reagent**	Biorad	1705062
15	**MitoTracker Red CMXRos**	Invitrogen	M7512
16	**Glycostress kit**	Agilent	103344-100
17	**Mitostress kit**	Agilent	103015-100
18	**ALDEFLUOR kit**	Stem cell Technologies	01700
19	**B27 supplement**	Gibco	17504044

Serial no.	Name	Make	Catalog Number
20	**rhEGF**	Sigma-Aldrich	F0291
21	**Insulin**	Sigma-Aldrich	I0320000
22	**Rhodamine123**	Sigma-Aldrich	R302
23	**Propidium Iodide**	Invitrogen	P1304MP
24	**RNase A**	Fermentas	ENO531
25	**Annexin-V-FITC/PI assay Kit**	Invitrogen	V13242
26	**Dual-luciferase assay kit**	Promega	E1910
27	**Mitosox™ red**	Invitrogen	M36008
28	**JC-1 dye**	Invitrogen	T3168
29	**Rhodamine phalloidin**	Invitrogen	R415
30	**Alexa fluor 488 Phalloidin**	Invitrogen	A12379
31	**DAPI**	Sigma-Aldrich	D9542
32	**Hoechst stain**	Sigma-Aldrich	14533
33	**Lysotracker blue**	Invitrogen	L7525
34	**HIF1α inhibitor**	Calbiochem	400089
35	**Rapamycin**	Calbiochem	553210
36	**Glutamine**	Sigma-Aldrich	G7513
37	**L-Glutamic acid dimethyl ester hydrochloride**	Sigma-Aldrich	49560
38	**Dimethyl 2-oxoglutarate (DMKG)**	Sigma-Aldrich	349631

Primer sequence: Table 7

Gene name	Forward primer (5'- 3')	Reverse primer (5'- 3')	Tm (^{0}C)
PITX2A	CGGCGTGTGTGCAATTAGAG	CGCCCACGTCCTCATTCT	60
PITX2B	GGCCGTTGAATGTCTCTTCT	CCTCTTTTCGGCTCTCAGG	60
OCT4	GCAGCTTAGCTTCAAGAACATGTG	TCAGCTTCCTCCACCCACTT	60
SOX2	TGCGAGCGCTGCACAT	GCAGCGTGTACTTATCCTTCTTCA	60
NANOG	GCATCCGACTGTAAAGAATCTTCA	CATCTCAGCAGAAGACATTTGCA	60
ABCG2	GATGTCTAAGCAGGGACGAACAA	GGTGAGGCTATCAAACAACTTGAA	60
ABCB1	GTGTGGTGAGTCAGGCTGTAT	TCTCAATCTCATCCATGGTGA	60
CD44s	TCCAACACCTCCCAGTATGACA	GGCAGGTCTGTGACTGATGTACA	60
CD44 epithelial	GAAAGGAGCAGCACTTCAGG	GAGGTCCTGTCCTGTCCAAA	60
L19	GCGGATTCTCATGGAACACA	GGTCAGCCAGGAGCTTCTTG	59

Primer sequence for cloning ABCB1 Promoter in pGl3 basic vector: Table 8:

Gene name	Forward primer (5'- 3')	Reverse primer (5'- 3')
Promoter cloning of ABCB1	ACCCACCCAATCATTTAAA	CTTAATCCCAGCCACACCTA

Methods

Cell culture:

Human ovarian cancer cell lines PA1 and SKOV3 were grown in Minimal essential media-α (MEM α) and RPMI-1640 respectively. Human colorectal carcinoma cell line HCT116 was cultured in Dulbecco's modified Eagle's medium (DMEM). Human Immortalized Ovarian Surface Epithelial cells (IOSE-364 and IOSE-385) were maintained in a 1:1 ratio of Medium-199 and MCDB-105 supplemented as previously mentioned (Ray et al., 2017). The media were supplemented with 10% FBS and the cells were grown at 37^{o}C in a humidified 5% CO_2 atmosphere. Cells were cultured in a vented T25 flask for maintenance. When the cell confluency reached 70-80%, the media was discarded and 0.25% trypsin-EDTA was added for 2/3 min. Then, the cells are collected in a 15 ml centrifuge tube, containing FBS-supplemented media and pelleted down by centrifugation at 500-1000 g for 5 min. The cell pellet was re-suspended in respective cell culture media and split in T25 flask into 1:3 ratios.

Treatments of cells and transient transfection:

Respective treatments were given when the cells are 60-70% confluent condition. The cells were starved for at least 6 h before the glutamine deprivation study. Similar cell starvation was done in TGFβ-treated experiments, and these treatments were given in respective incomplete media**.** Glutamine deprivation experiments were performed in the glutamine-free medium of respective cells with 10% FBS reconstituted condition. As mentioned, the cells were treated with 5 nM/ml of TGFβ, 14 µM of MDiVi-1, 10 µM of U0126, 10 µM of SB203580, 1 mM of L-DON (6-Diazo-5-oxo-L-norleucine), 250 µM of Sulphasalazine (SSZ), 1µg/ml of nocodazole (NOCO), 2 mM of glutathione reduced ethyl ester (GSH), 10 mM of N-acetyl cysteine (NAC), 20 ng/ml of TGFβ receptor kinase inhibitor (TGFRI), 300 nM of HIF1α inhibitor, 100 ng/ml of rapamycin (Rapa). For the experiments with overexpression or silencing of genes, transfection was done at 70-80% confluent condition of the cells. Overexpression plasmids of PITX2A, PITX2B, SIRT4 were used. 1 µg/ml of plasmid DNA was transfected in the cell with 3 µl of lipofectamine in Opti-MEM media. The siRNA against PITX2, SMAD2, DRP1, NRF2, xCT, SIRT4 (Santa Cruz Biotechnology, Dallas, TX) were used at 20 nM/well-using lipofectamine 2000 (Invitrogen) in the cells.

RNA isolation and quantitative real-time PCR (q-PCR):

The cells were mixed with RNAiso Plus reagent and incubated at room temperature for 15 min for dissolving the nucleoprotein complex. Then chloroform was added and the mixture was shaken vigorously and the mixture was kept at room temperature for 15 min to allow phase

separation. After that, the mixture was centrifuged at 12,000 g for 15 min at 4^{o}C. Then the upper aqueous layer was collected and mixed with 2.5 times Isopropanol. Again the mixture was kept at room temperature for 20 min and then centrifuged at 12000 g for 15 min at 4^{o}C. The supernatant was discarded and the pellet was washed with 75% ethanol. The RNA pellet was air-dried and then re-suspended in DEPC-treated water for further cDNA preparation and q-PCR.

The quality of the isolated RNA was checked by RNA gel electrophoresis and 260 nm/280 nm absorbance ratio. The concentration of the total RNA was calculated from absorbance at 260 nm.

For the cDNA preparation, 0.5 µg RNA was used and cDNA was synthesized using iScript cDNA synthesis kit. For the 20 µl reaction mixture, 4 µl cDNA synthesis buffers and 0.5 µl of reverse transcriptase enzyme were added and volume was made up with nuclease-free water. The thermal cycle was as follows: a) Priming: 5 min at 25^{o} C, b) Reverse transcription: 20 min at 46^{o} C, c) RT inactivation: 1 min at 95^{o}C, d) Hold at 4^{o}C.

Q-PCR was performed with Biorad SYBR green on the ABI 7500 Real-Time PCR system (Applied Biosystems, Foster City, CA). For each well of 96-well PCR plate, the components are added as follows: 0.25 µl of cDNA, 1.25 µl of Biorad SYBR green, 0.5 µl of primer (5 µM), and 3 µl of nuclease-free H_2O. The cycle of PCR is as follows: (a) initial denaturation: 95^{o}C for 5 min, (b) the cycling steps: 94^{o}C for 15 s, annealing for the 30 s at a particular temperature (primer specific), extension at 72^{o}C for 30 s, (c) melting curve stage: 45^{o}C-90^{o}C. For endogenous control, L19 (60 s ribosomal protein) primer was used, and fold change was calculated by the C_T value method. The formula used for fold change calculation is $2^{-[\Delta\Delta CT\ (sample)\ -\ \Delta\Delta CT\ (Treated)]}$.

The primers were designed by using Primer Express 3.0 software and validated by NCBI primer blast. All the primers were obtained from Integrated DNA technology.

Sub-cellular fractionation procedure:

Cells were scraped out from the culture plate with fractionation buffer and incubated in ice for 15 min. For lysed cells, they were passed through a 1 ml syringe containing 27 gauge needles 10 times, and the lysate was kept on ice for 20 min. Then the lysate was centrifuged at 720 g for 5 min at 4^{o}C. The pellet contains nuclei and the supernatant contains cytoplasm, membrane, and mitochondria. The supernatant was transferred to a new tube and kept on ice. The nuclear pellet was re-suspended with fractionation buffer and again passed through a 27 gauge needle 10 times followed by centrifugation at 720 g for 10 min at 4^{o}C. This pellet contains the nucleus and further protein was isolated from this pellet. Similarly, mitochondria were isolated from the previously collected supernatant. The supernatant was centrifuged at 10,000 g for 5 min at 4^{o}C and the pellet contained mitochondria. The cytoplasm was present in this supernatant. Protein was isolated from mitochondria and cytosol by the following procedure.

Protein isolation and western blot analysis:

The cells were scraped out using phosphate buffer saline (PBS) and then pelleted down by centrifugation at 3000 g for 5 min. The cells pellet was lysed using RIPA buffer containing DTT, PMSF, and protease inhibitor cocktail. Then, the mixture was kept on ice for 20 min and then sonicated 5 times with 30 s pulse with 10 s interval. Then the lysate was centrifuged at 10,000 g for 10 min at 4^{o}C and the supernatant was collected. The concentration of protein was estimated by the Lowry-Folin method and the protein sample was prepared for western blot analysis. An equal amount of protein sample was loaded in SDS-PAGE and followed by western blot was performed. After transferring the proteins on the PVDF membrane, blocking was done with 3% BSA in TBST buffer. The primary antibodies used are p-DRP1 (S616), HK2, SDHA, MFN1, MFN2, OCT4, SOX2, total OXPHOS complex, ABCG2, SIRT4, VIimentin, N-cadherin, p-p70S6K (T289), α-Tubulin. HRP-tagged secondary antibody was used for the respective primary antibody. α-Tubulin was used as an endogenous control to normalize the expression of other proteins. ECL detection reagent was used to detect the chemiluminescence band in the blot.

Extracellular flux analysis:

Agilent seahorse extracellular flux analyzer was used to measure extracellular acidification rate (ECAR) and Oxygen consumption rate (OCR) as mentioned previously (Ray et al., 2017). 3000 cells/well were seeded for PA1 and HCT116 cells whereas 6000 cells/well were plated for SKOV3. Each treatment was given in triplicate well. For ECAR measurement, cells were starved with glucose-free basal DMEM media for 1 h. After that, the glycostress kit was used with three consecutive injections of glucose, oligomycin, and 2-DG in each well. In the case of measuring OCR, cells were starved with basal DMEM media containing glucose, glutamine, and pyruvate. Mitostress kit was used with three consecutive injections of oligomycin, FCCP, and antimycin/ Rotenone in each well.
The ECAR and OCR value was normalized by estimating protein concentration in each well. Analysis was done by WAVE (Agilent-Seahorse Bioscience) software.

Immuno-fluorescence Confocal microscopy:

For immunofluorescence microscopy, cells were grown on cover-slip and respective treatment was given on this cover-slip. After completion of the respective treated condition, cells were washed with 1X PBS 2 times. Then, cells were fixed with 4% paraformaldehyde for 20 min at room temperature and again washed with 1X PBS 2 times with 5 min intervals. For permeabilization, 0.1% triton-X was added to cover the surface of the cover-slips and kept for 20 min. After that, the cells were washed again with 1X PBS and then 3% BSA in PBS was added

for blocking for 2 h. Then, the respective primary antibody was given in 1:200 dilutions in blocking buffer overnight at 4^{O}C. The next day, the cells were washed 3 times with PBS at 15 min intervals. Fluorescence-tagged secondary antibody was given in these cells in 1:400 ratios for 2 h at room temperature. Again, the cells were washed with 1X PBS 3 times and then DAPI (0.25 µg/ml) was added to stain the nucleus. Lastly, cells are washed with 1X PBS and mounted on the glass slides with mounting media. The images were captured by Leica confocal microscope (TCS SP8, Buffalo Grove, IL, USA) with x63 oil immersion objective lens.

MitoTracker Red CMXRos staining was performed for visualization of mitochondrial morphology. This stain was added in 50 nM into the cell media and incubated for 20 min at 37^{O}C. After mitochondrial staining, the cells were washed and the next procedure was performed from the fixation step as discussed above.

For phalloidin staining, the cells were prepared up to the addition of a secondary antibody. Then, the stain was added before the addition of DAPI in 1:400 dilution for 20 min at room temperature and then washed with 1X PBS and the next procedures were performed as mentioned above.

Immunohistochemistry (IHC) microscopy:

Human ovarian cancer tissue and normal ovarian tissue samples were obtained from SGCCRI with proper ethical approval. These tissue slides were de-parafinised by incubating in xylene 2 times with 2 min each. Then the samples were hydrated with 100% ethanol by placing twice for 3 min and followed by kept in 90%, 80%, 70%, 50%, and then water for 2 min each. For retrieval of antigen, the slides were kept in sodium citrate (pH=6) in coupling jars and put in a heating chamber for 20 min. After that, cells were blocked with 3% BSA in PBS for 2 h at room temperature. Then the slides were incubated with the primary antibody in a humidified chamber overnight at 4^{0}C. The next day, the cells were washed with PBST 3 times, and the respective secondary antibody was given in those slides for 2 h. Nuclei were stained with DAPI for 5 min and again these slides were washed with PBST. Slides were mounted with mounting media and images were acquired using Leica confocal microscope (TCS SP8, Buffalo Grove, IL, USA) with a 20x oil immersion objective lens.

Intracellular and extracellular antigen staining and measurement by Flow cytometry:

For staining the intracellular protein, firstly cells were scrapped out from a 60 mm dish and washed with 1X PBS. Then the cells were fixed with 4% formaldehyde by adding drop-wise in gentle vortexing condition and incubated at 37^{0}C for 10 min. After that, cells were kept on ice for 1 min and pelleted down. The supernatant was discarded and these cells were then permeabilized by the addition of 90% chilled methanol drop-wise in gentle vortexing

conditions. Cells were kept at -20^{o}C for overnight and on the day of the experiment, cells were pelleted down and washed twice with PBST. After that, the cells were blocked with incubation buffer containing 0.5% BSA in PBS. Then the cells were incubated with the primary antibody in 1:400 dilutions for 1 h at 37^{o}C. Moreover, the cells were washed with PBST and secondary antibody was given in 1:800 dilutions for 30 min at 37^{o}C. The fluorescent intensity was measured through the LSR Fortessa cell analyzer (BD Bioscience).
Live cells were stained for checking extracellular antigen. After scrapping out the cells with PBS, they were pelleted down and incubated with Fluorophore-tagged primary antibody (CD44-PE, CD117-APC, CD31-FITC, CD45-PE-Cy7) in 1:400 dilutions for 30 min at 37^{o}C. After completion of the staining procedure, cells were washed 3 times with PBS and then analyzed using a flow cytometer as mentioned earlier.

Aldehyde dehydrogenase (ALDH) activity assay:

Aldehyde dehydrogenase (ALDH) assay was performed using the ALDEFLUOR kit. For each sample, cells tubes were labeled as 'test' and 'control'. First, ALDEFLUOR DEAB Reagent was added to the empty control tube. Diethylaminobenzaldehyde (DEAB) is a specific inhibitor for ALDH and it was used for correcting background fluorescence. In another 'test' tube substrate BODIPY-amino acetaldehyde was added and then mixed. From this tube, half volume was transferred to the 'control' tube. Both 'control' and 'test' tubes were incubated at 37^{o}C for 1 h. After staining was done, cells were washed with PBS and fluorescence intensity was measured by flow cytometry as previously mentioned using the FACS Diva software (Mitra et al., 2018).

Spheroid formation study:

For the spheroid formation study, 5X10^{3} cells were seeded in a low attachment 6-well plate (Corning) and allowed to grow in the serum-free media (SFM) containing B27 supplement, rhEGF, and insulin for 1-4 days following the previous standard protocol (Mitra et al., 2018). For the secondary generation of the spheroid, previous spheroids were collected and centrifuged at 1000 g for 5 min. Then, the pellet was re-suspended in spheroid growing media and re-plated in another low attachment 6 well plates. Again, the spheroids were allowed to grow for the next 4 days. The spheroids were visualized, counted, and their images were acquired under a phase-contrast microscope (EVOS, Invitrogen) and their size was measured using the ImageJ software.

Rhodamine 123 efflux assay:

After completion of the treatment regiment, Rhodamine 123 (Rh123, 200 ng/ml) was treated in the serum-free media and kept at 37^{o}C for 1 h in a humidified CO_2 incubator. Then the cells

were washed and again replenished with respective media. In this condition, cells were kept at 37^{o}C overnight in a humidified CO_2 incubator. Before performing the assay, these cells were washed with PBS and analyzed through a flow cytometer as mentioned previously (Mitra et al., 2018). The dye effluxing population and retaining population were observed and % population was calculated from flow cytometric data.

Cell cycle analysis:

After trypsinization, the cells were washed with PBS and fixed with 70% ethanol by drop-wise addition in with gentle vortexing condition and then kept overnight at -20^{o}C. After centrifugation, the cells were washed again with PBS and re-suspended the pellet with 1X PBS containing PI (1.5 mM) and RNaseA (1 mg/ml). The cell suspension was incubated for 10-15 min at room temperature and analyzed by flow cytometer.

Annexin-V-FITC/Propidium Iodide (PI) Apoptosis assay:

Annexin-V-FITC/PI Apoptosis assay was performed following manufacturer protocol (Invitrogen). Cells were trypsinized and washed with 1X binding buffer. Then the cell pellet was re-suspended with binding buffer containing FITC-tagged annexin-V and PI followed by incubation at room temperature for 15 min. Flow cytometric analysis was done and the results have been represented in a dot plot.

Estimation of mitochondrial ROS and total cellular ROS:

Mitochondrial ROS generation was determined by using the Mitosox red mitochondrial superoxide indicator. The cells were treated with this indicator for 20 min at 37^{o}C. Then the amount of ROS generation was determined using a flow cytometer.
Similarly, total cellular ROS was measured by DCFDA staining. The cells were treated with DCFDA and incubated for 20 min at 37^{o}C. Then the total cellular ROS has measured through flow cytometric analysis.

Co-immunoprecipitation assay:

Cells were scraped out from the cell plate and pelleted down by centrifugation at 3000 g for 5 mins. This cell pellet was re-suspended with IP lysis buffer and kept for 5 mins in ice. Then the tubes were spun at 13000 g for 10 mins. The supernatant was collected and protein was estimated by the lowry method.

Agarose-A beads were conjugated with one of the primary antibodies by incubating for 1 h at room temperature with a vertical mixing process. This mixture was centrifuged for 2 min at 3000 g at 4^{o}C and the supernatant was discarded. These samples were washed with washing buffer for 2times. In these beads, 200 µg of protein was added and incubated overnight at 4^{o}C. The immunoprecipitated complex was collected by centrifugation at 3000 g for 2 min at 4^{o}C. The supernatant was discarded and the pellet was washed with washing buffer 2 times. By adding sample buffer, a protein sample was prepared for western blot analysis. In western blot, the blot was probed with another primary antibody that interacts with the initial one.

Luciferase promoter activity assay:

Genomic DNA was isolated from ovarian cancer cells and this DNA was used as the template for PCR to clone the 1.6 kb promoter region of ABCB1. This clone was inserted into the pGL3-Luc vector to obtain the ABCB1-pGL3 clone. pRL-CMV clone which expressed Renilla-luciferase was used for normalization.

For this luciferase promoter activity assay, cells were seeded in a 12-well plate. 4 sets of transfection were done such as pRL-CMV, pRL-CMV+ ABCB1-pGL3, pRL-CMV+ ABCB1-pGL3+ PITX2A/B. In another set of experiments, transfected sets were only pRL-CMV, pRL-CMV+ ABCB1-pGL3, pRL-CMV+ ABCB1-pGL3+ siPITX2. Transfection was done with lipofectamine 2000 reagent for 6 h in Opti-MEM. After completion of the transfection period, the transfecting media was changed with respective cell culture media. This assay was performed with a dual-luciferase reporter assay system. After lysing the cells with lysis buffer, firefly and renilla luciferase activity was measured in Glomax 96-well microplate luminometer following manufacturer protocol (Bhattacharya et al., 2018).

Measurement of mitochondrial membrane potential by JC-1 staining:

After harvesting the cells with PBS, JC-1 stain was added into PBS and incubated for 20 min. Then the cells were washed with PBS and analyzed through flow cytometry. The mitochondrial membrane potential was measured by the transition from green (529 nm) monomeric of JC1 to red JC-1 aggregates form (590 nm). A decrease in the red/green fluorescence intensity ratio indicated mitochondrial depolarization.

Animal model:

All animal experiments were performed with proper approval from the Institutional Ethical committee. Tumors were grown in C57BL/6 female mice (3-4 weeks old) by injecting ID8 cells. ID8 cells were grown in DMEM containing 10% FBS *in vitro* condition. C57BL/6 mice were

subcutaneously injected in their lower right quadrant with the mixture of $3X10^7$ cells and Matrigel (19 mg/ml) in a 1:1 ratio. Detectable tumors were observed after 4 days of injection and they were included in the study. These mice were randomly divided into control and treated groups when they reached about 100 mm^3. 125 µl PBS was injected in the control mice and there were three treatment groups which were injected through a tail vein as follows: (i) 125 µl L-DON solution (0.6 mg/kg body weight), (ii) 125 µl MDiVi-1 (5 mg/Kg body weight), (iii) 125 µl MDiVi-1 (5 mg/Kg body weight). This treatment was continued for 4 days. Within this treatment regimen of these mice, weight and tumor size were measured every day. After completion of this period, mice were dissected and tumors were isolated for further experiments. The final weight and volume of the tumor were measured after isolation. For histological analysis, the tumors were fixed with 10% formalin and paraffin blocks were prepared. Hematoxylin and Eosin staining and IHC were performed with these tissue sections.

Image analysis

The distance between mitochondria and nucleus was measured using ImageJ software. First, the red channel (MitoTracker red) images were converted into 8-bit images, and then a straight line is drawn from the center of the nucleus up to the region of mitochondrial fluorescence within the cell boundary. The fluorescent intensity throughout the line was extracted.
The mitochondrial length analysis and co-localization analysis were done with LAS X software (Leica Microsystems) and co-localization was analyzed with ImageJ (NIH) software.

Statistical analysis:

All statistical analyses were performed using Microsoft Excel and GraphPad Prism-5 software. The data were represented as ± SEM. A two-tailed paired t-test was performed when the number of samples was two and the one-way ANOVA (followed by Bonferroni post-test analysis, Dunnet test analysis) was done, where the sample size is >2. P values <0.05 were considered to be statistically significant. All the experiments were performed three times unless otherwise stated.

CHAPTER 1

STEMNESS AND CHEMORESISTANCE PROPERTIES ARE IMPARTED THROUGH TGFβ1- PITX2A/B SIGNALING IN OC CELLS

Introduction:

In recent years, difficulties arise in cancer due to metastasis and recurrence after chemotherapy. Tiny populations of cancer cells can efflux the drug and they are known as cancer stem cells (CSC). Somatic cells are genetically transformed into CSCs during cancer progression. Along with their self-renewal and dedifferentiation capacity, these cells have the adaptability to sustain in a stressful environment and reinitiate malignancy.

In the tumor microenvironment (TME), various growth factors such as transforming growth factor β (TGFβ), epidermal growth factor (EGF), fibroblast growth factor (FGF), vascular endothelial growth factor (VEGF), insulin-like growth factor (IGF) which promote proliferation, epithelial-mesenchymal transition (EMT) and metastasis of cancer cells by activating different signaling pathway (Witsch et al., 2010). In ovarian cancer cells, TGFβ1 promotes stemness and chemoresistance through EMT. Here, it regulates transcription of ZEB1 which is in turn involved in EMT-mediated stemness (Mitra et al., 2018). TGFβ1 is a ligand for TGFβ receptor II (TGFβRII) and activated TGFβRII phosphorylate TGFβ receptor I (TGFβRI). Activated phosphorylated TGFβRI then activate downstream signaling pathway by regulatory SMAD. SMAD-dependent TGFβ1 signaling pathway alters the gene expression of various transcription factors involved in cancer progression (Lu et al., 2017).

DLX2, a bicoid/paired-like homeobox transcription factor is regulated by TGFβ1 and induces EMT through metabolic reprogramming (Lee et al., 2016). TGFβ1 signaling regulates another homeobox transcription factor, PITX2 expression in left-right asymmetry development. There are few reports which suggested that PITX2 activates the SMAD2/3 dependent TGFβ signaling pathway to promote invasion in ovarian cancer (Basu et al., 2015). In addition, PITX2 also promotes ovarian cancer cell proliferation through the Wnt/β-catenin pathway (Basu and Roy, 2013). Contrastingly, TGFβ and Wnt signaling pathways regulate EMT by their co-activation in ovarian cancer (Mitra and Roy, 2017). PITX2 also has a role in the generation of stemness and chemoresistance features in the colon, kidney, and squamous cell carcinoma (Lee and Thévenod, 2019). Therefore, we tried to link between TGFβ1 and PITX2 to decipher the mechanism through which chemoresistance occurs in ovarian cancer.

Results:

TGFβ1 regulates PITX2 expression in ovarian cancer cell line:

Considering the previous background, we have tried to relate TGFβ1 signaling and PITX2 expression in ovarian cancer. We have found that PITX2A/2B gene expression enhances upon both 24 h and 48 h of TGFβ1 treatment in PA1 in both gene and protein levels **(Fig. 1A, B, D, E)**. However, these expressions were enhanced only at 48 h of TGFβ1 treatment in SKOV3 **(Fig. 1C)**. A similar result was obtained in confocal microscopy **(Fig. 1F)**. TGFβ1 cannot restore the expression of PITX2A/B when TGFβ receptor kinase inhibitor (TGFβRKI) was used in both PA1 and SKOV3 **(Fig. 1G, H)**. Based on these results, it indicated that TGFβ1 treatment for a long duration can upregulate the expression of PITX2 isoforms in the ovarian cancer cell.

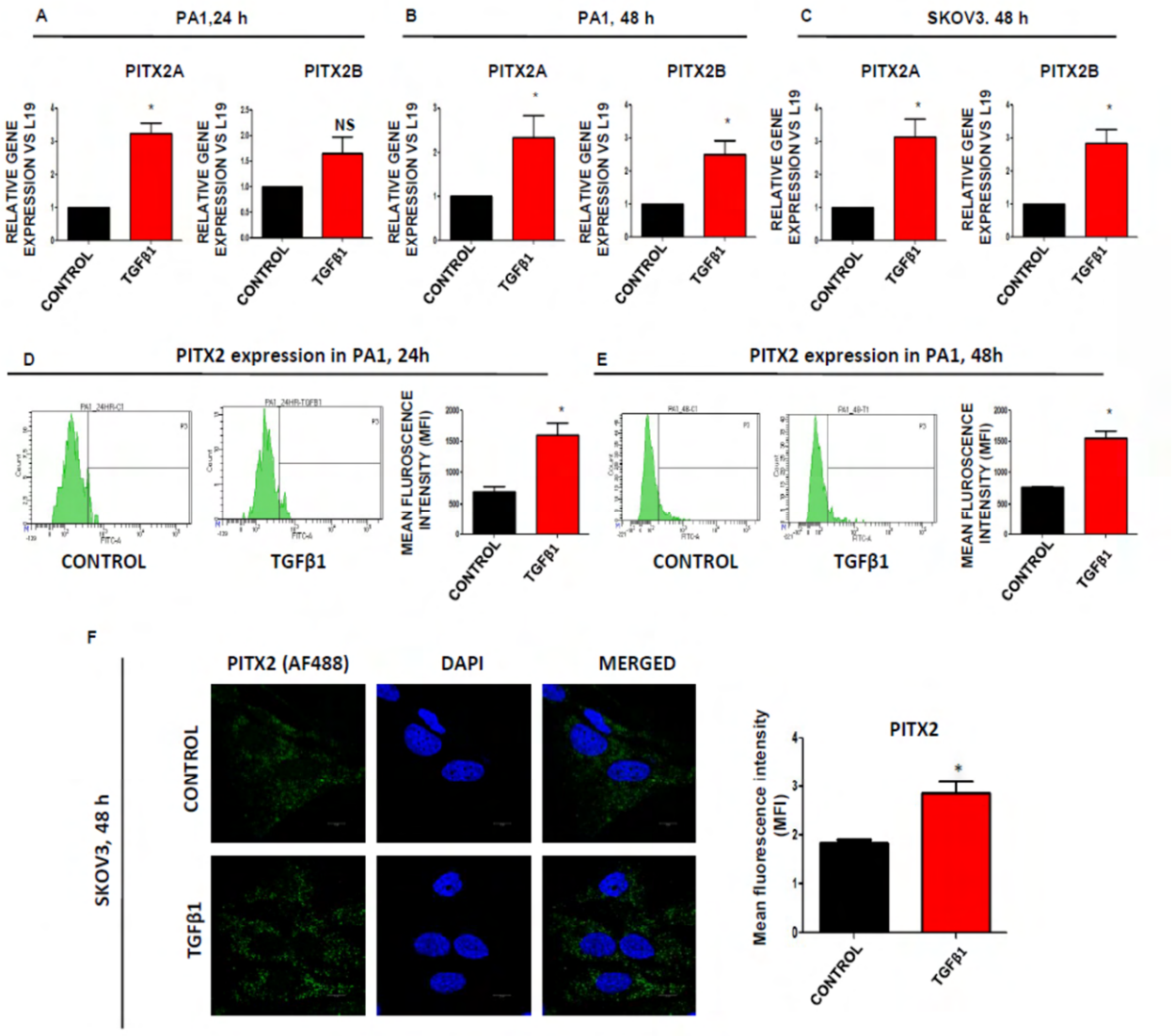

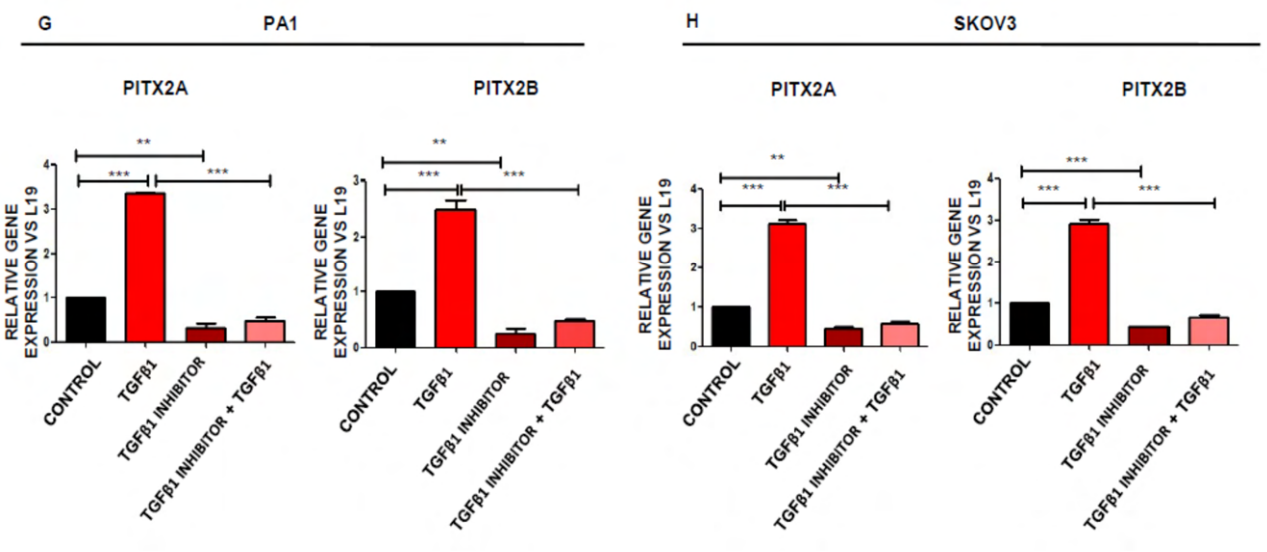

Figure 1: PITX2A/B expression enhanced by TGFβ1 signaling: (A, B) PITX2A/B gene expression was enhanced upon 24 h and 48 h of TGFβ1 treatment in PA1. (C) At 48 h of TGFβ1 treatment upregulates PITX2A/B gene expression in SKOV3. (D, E) PITX2A/B protein expression was checked at both 24 h and 48 h of TGFβ1 treatment in PA1. (F) Microscopic images depicted that PITX2A/B expression enhanced upon TGFβ1 treatment in SKOV3. (G, H) TGFβ1 receptor kinase inhibitor downregulates PITX2A/B gene expression in presence of TGFβ1 in both PA1 and SKOV3. The statistical significance was analysed and represented as NS for non-significant,*p<0.05, **p<0.01, ***p<0.001. Scale bar 10 µm (F).

TGFβ1 mediated PITX2A/B expression orchestrated through both SMAD and ERK-dependent pathway independently in OC:

To check the signaling pathway associated with TGFβ1 induced PITX2A/B expression, we have blocked both the SMAD pathway and non-SMAD pathway. When we blocked the SMAD pathway by silencing, found that PITX2A/B expression was hampered and it was not restored upon TGFβ1 treatment. These results indicate that PITX2A/B expression was SMAD-dependent **(Fig. 2A, C)**. Similar results were obtained in protein expression also through flow cytometry **(Fig. 2E, F)**. For checking the association of the non-SMAD pathway, we have inhibited the MEK-ERK signaling pathway by U0126 and the p38MAPK pathway by SB23580. It has been observed that upon blocking the MEK-ERK pathway, PITX2A/B expression was reduced and it was not increased upon TGFβ1 treatment, though we did not find significant change using SB23580 **(Fig. 2B, D)**. Therefore, we concluded that PITX2 expression was regulated by TGFβ1 through both SMAD-dependent and ERK-dependent pathways.

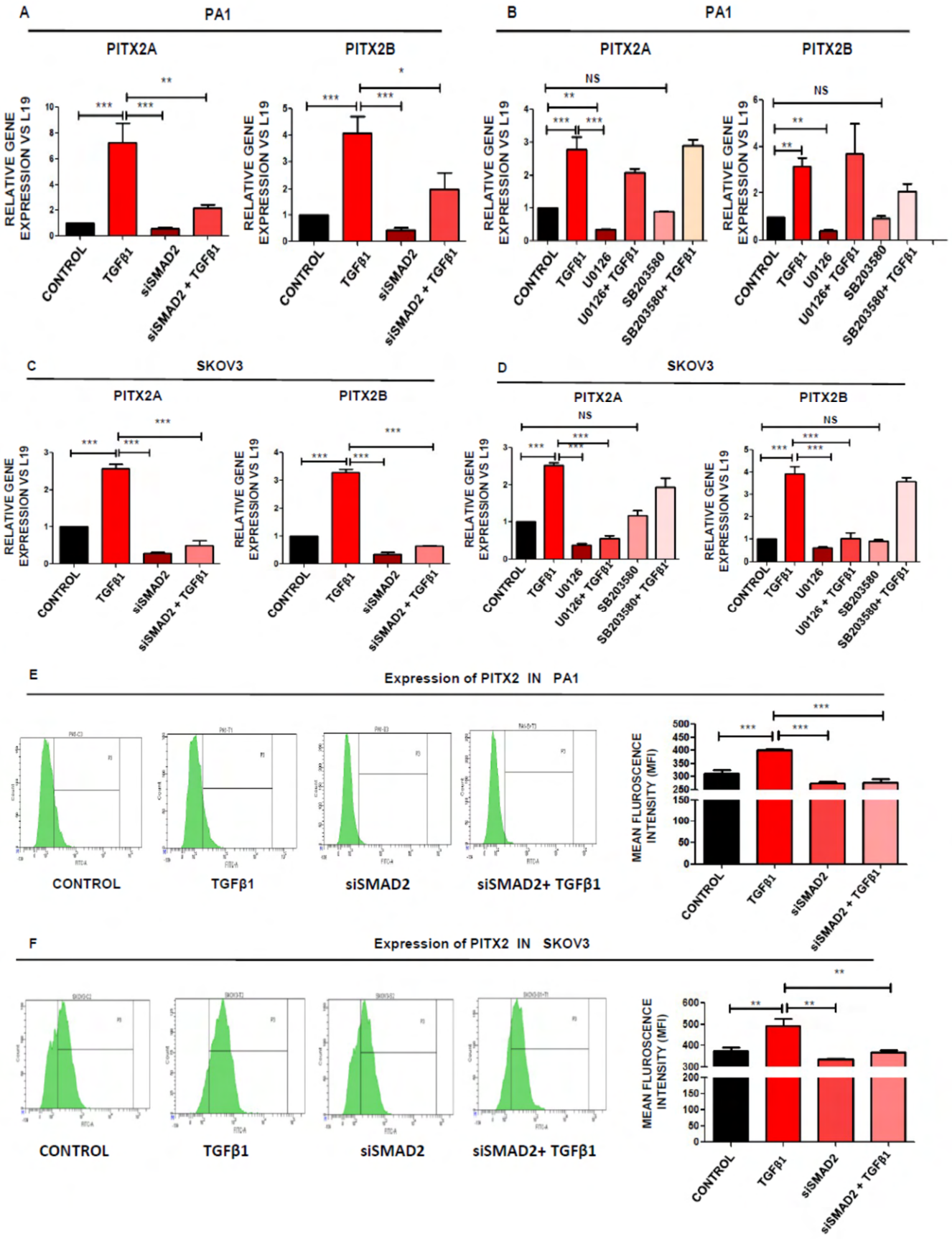
A
PA1
PITX2A
PITX2B
RELATIVE GENE EXPRESSION VS L19
CONTROL
TGFβ1
siSMAD2
siSMAD2 + TGFβ1
B
PA1
PITX2A
PITX2B
NS
U0126
U0126+ TGFβ1
SB203580
SB203580+ TGFβ1
C
SKOV3
PITX2A
PITX2B
D
SKOV3
PITX2A
PITX2B
E
Expression of PITX2 IN PA1
CONTROL
TGFβ1
siSMAD2
siSMAD2+ TGFβ1
MEAN FLUROSCENCE INTENSITY (MFI)
F
Expression of PITX2 IN SKOV3
CONTROL
TGFβ1
siSMAD2
siSMAD2+ TGFβ1
MEAN FLUROSCENCE INTENSITY (MFI)

Figure 2: Both SMAD and ERK signaling pathways were involved in regulating TGFβ1 mediated PITX2 Expression: qPCR analysis was performed using siSMAD, ERK Inhibitor (U0126), and p38MAPK inhibitor (SB203580) treated condition to check the alteration of PITX2A/B gene expression in both PA1 (A, B) and SKOV3 (C, D). Protein expression of PITX2 was checked by silencing SMAD2 in the presence or absence of TGFβ1 in both PA1 (E) and SKOV3 (F) cell lines. The statistical significance was analyzed and represented as NS for non-significant,*p<0.05, **p<0.01, ***p<0.001.

PITX2A/B promotes stem-like characteristics in epithelial ovarian cancer (EOC) cells:

PITX2 can promote EMT and invasion by activating TGFβ1 and activin in ovarian cancer. Again, TGFβ1 signaling can induce stemness followed by EMT. Therefore, we hypothesized that PITX2 may have the ability to promote stem-like characteristics in epithelial ovarian cancer cells. First, we have observed that the transient transfection of PITX2A/B isoforms can enhance the gene expression level of stemness markers such as OCT4a, SOX2, and NANOG with time points. In both SKOV3 and PA1 cell lines, the expression of OCT4a, SOX2 was not significantly enhanced at 24 h of PITX2A/B overexpression **(Fig. 3A-B)**. However, these markers were increased at 48 h of PITX2A/B overexpression in PA1, SKOV3, and IOSE-364 **(Fig. 3C-E).** Similar results were obtained in their protein expression also **(Fig. 3F-G).** Cancer stem cells have the property to form tumor spheroids in non-adherent conditions. It has been found that PITX2A/B can also induce to form of spheroids and increase the size and number with generation and time in PA1 **(Fig. 3H-I)**.

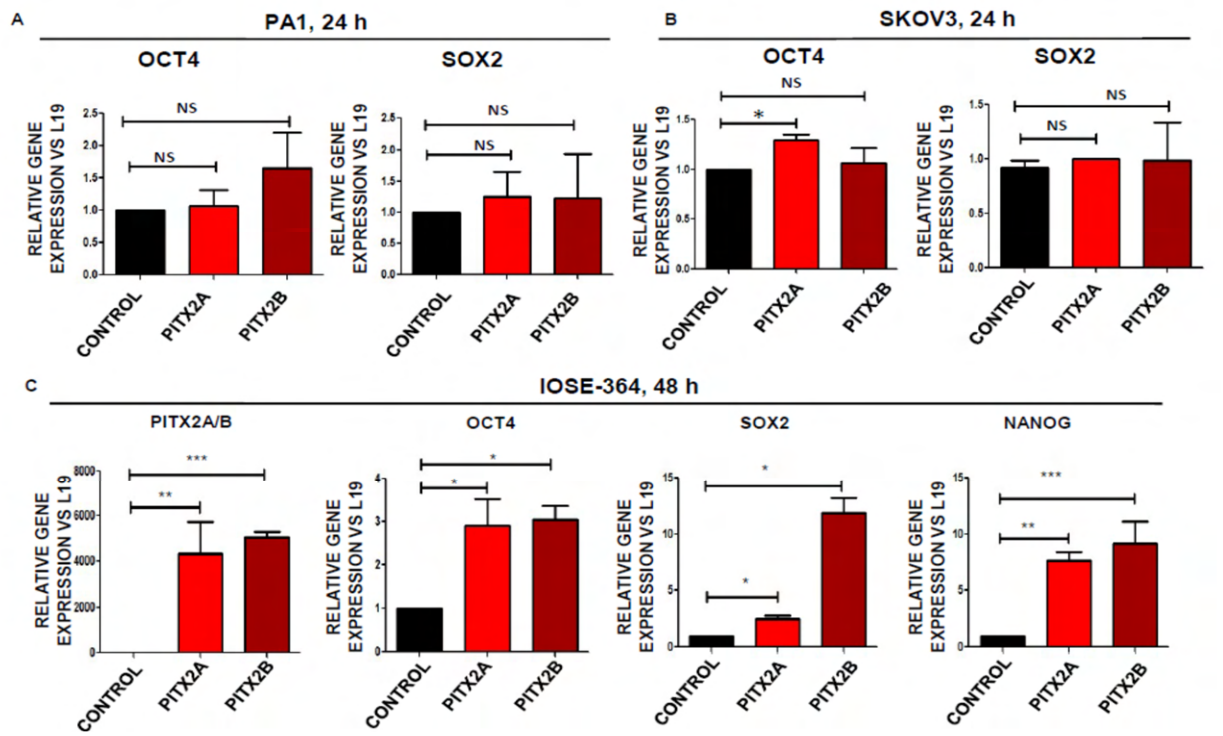

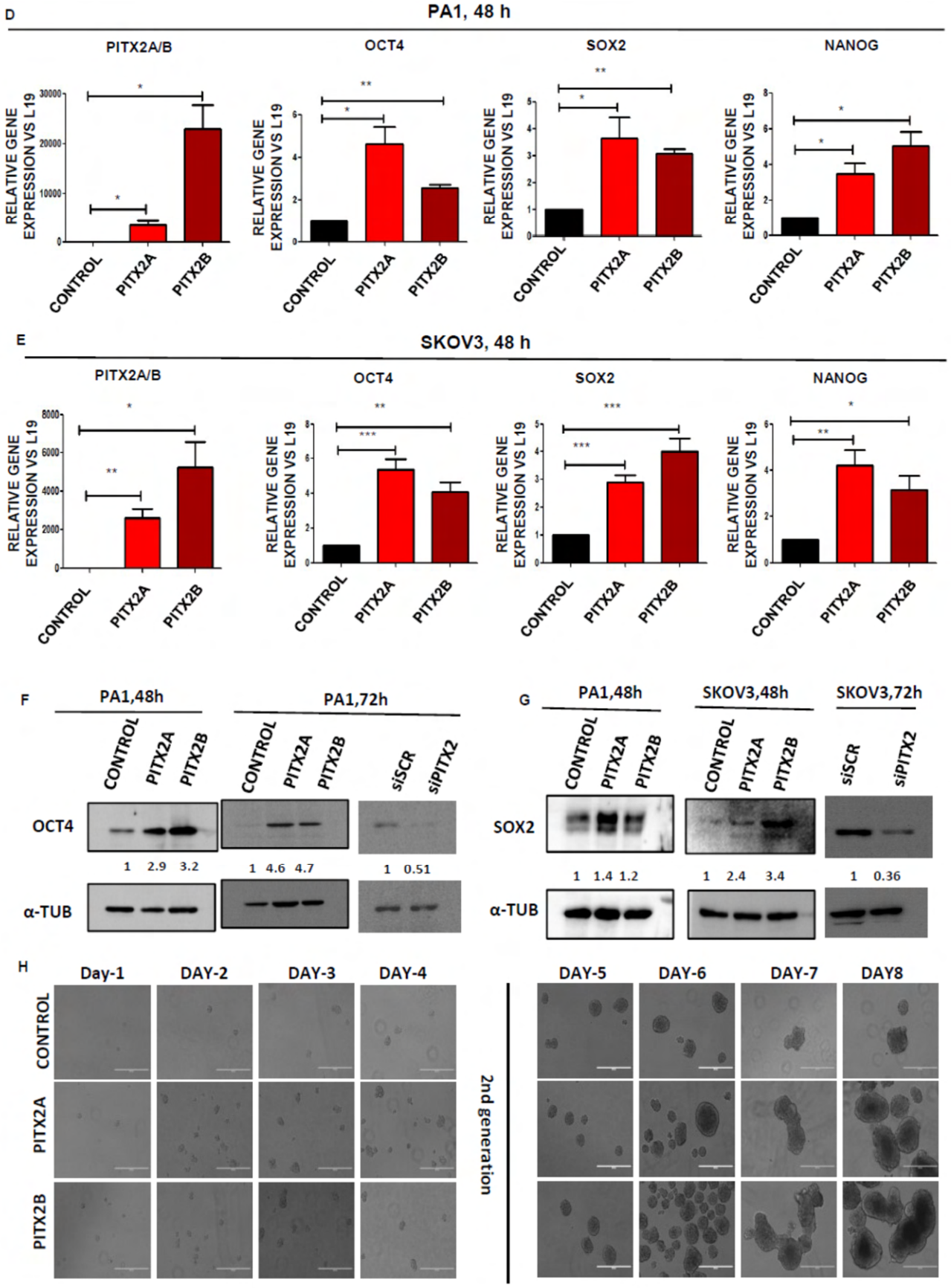
D
PA1, 48 h
PITX2A/B
OCT4
SOX2
NANOG
RELATIVE GENE EXPRESSION VS L19
CONTROL
PITX2A
PITX2B
E
SKOV3, 48 h
F
PA1,48h
PA1,72h
CONTROL
PITX2A
PITX2B
siSCR
siPITX2
OCT4
α-TUB
1 2.9 3.2
1 4.6 4.7
1 0.51
G
PA1,48h
SKOV3,48h
SKOV3,72h
SOX2
1 1.4 1.2
1 2.4 3.4
1 0.36
H
Day-1
DAY-2
DAY-3
DAY-4
DAY-5
DAY-6
DAY-7
DAY8
2nd generation

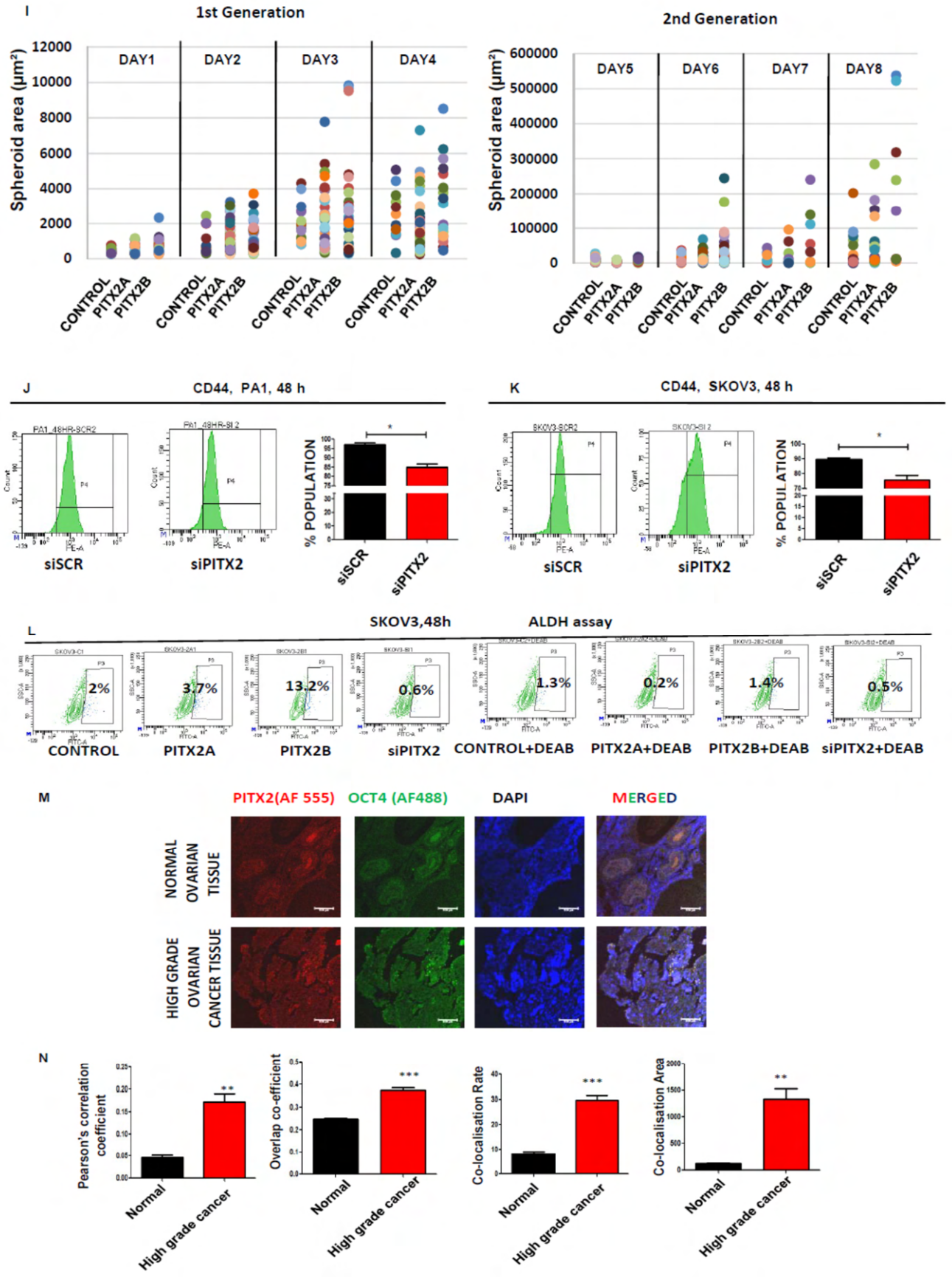
I
1st Generation
2nd Generation
Spheroid area (µm²)
DAY1
DAY2
DAY3
DAY4
DAY5
DAY6
DAY7
DAY8
CONTROL
PITX2A
PITX2B
J
CD44, PA1, 48 h
siSCR
siPITX2
% POPULATION
K
CD44, SKOV3, 48 h
L
SKOV3,48h
ALDH assay
2%
3.7%
13.2%
0.6%
1.3%
0.2%
1.4%
0.5%
CONTROL
PITX2A
PITX2B
siPITX2
CONTROL+DEAB
PITX2A+DEAB
PITX2B+DEAB
siPITX2+DEAB
M
PITX2(AF 555)
OCT4 (AF488)
DAPI
MERGED
NORMAL OVARIAN TISSUE
HIGH GRADE OVARIAN CANCER TISSUE
N
Pearson's correlation coefficient
Overlap co-efficient
Co-localisation Rate
Co-localisation Area
Normal
High grade cancer

Figure 3: PITX2A/B induces stem-like features in ovarian cancer: At 24 h of PITX2A/B overexpression OCT4 and SOX2 were not enhanced in PA1 (A) and SKOV3 (B). At 48 h, PITX2A/B overexpression enhanced the expression of OCT4a, SOX2, and NANOG in IOSE-364 (C), PA1 (D), and SKOV3 (E). Protein expression of OCT4 (F) and SOX2 (G) was enhanced when PITX2A/B was overexpressed. (H, I) Bright-field microscopy of spheroids formed in PA1 and the size was measured and plotted. PITX2 silencing reduces the expression of CD44 in PA1 (J) and SKOV3 (K) and are represented both in histogram and bar diagram. (L) Aldehyde dehydrogenase activity assay depicted that the ALDH-positive population increased in SKOV3. (M-N) protein expression of OCT4 and PITX2 enhanced in high-grade ovarian cancer tissue compared to the normal ovarian tissue and quantitative data represented in bar diagram. The statistical significance was analyzed and represented as NS for non-significant,*p<0.05, **p<0.01, ***p<0.001. Scale bar 400 µm (H), 100 µm (M).

By knocking down PITX2 using siRNA, CD44 was reduced in PA1 and SKOV3 **(Fig. 3J-K)**. In the ALDH activity assay, ALDH-positive cells were enhanced upon PITX2A/B induction, whereas the opposite result was found upon its silencing **(Fig. 3L)**. Expression and co-localization of OCT4 and PITX2 were enhanced in high-grade ovarian cancer tissue as compared to normal ovarian tissue **(Fig. 3M-N)**. Therefore, it is indicated that PITX2A/B has a role in the promotion of stem-like traits in ovarian cancer.

Metabolic phenotype in the cancer stem cells which are induced by PITX2A/B:

We then proceed to determine the metabolic parameters and phenotype of cancer stem cells induced by PITX2. Firstly, we have focused on the glycolytic phenomenon of PITX2 induced stem cells. At 48 h of PITX2 overexpression, enhances extracellular acidification rate, glycolysis, and glycolytic capacity in both PA1 and SKOV3 **(Fig. 4A, C)** whereas ECAR, glycolysis, glycolytic capacity decreases upon 72 h of PITX2 overexpression in PA1 **(Fig. 4B)**. In addition, we did not find any change in the glycolytic phenomenon in SKOV3 at 72 h **(Fig. 4D)**. This indicates that,

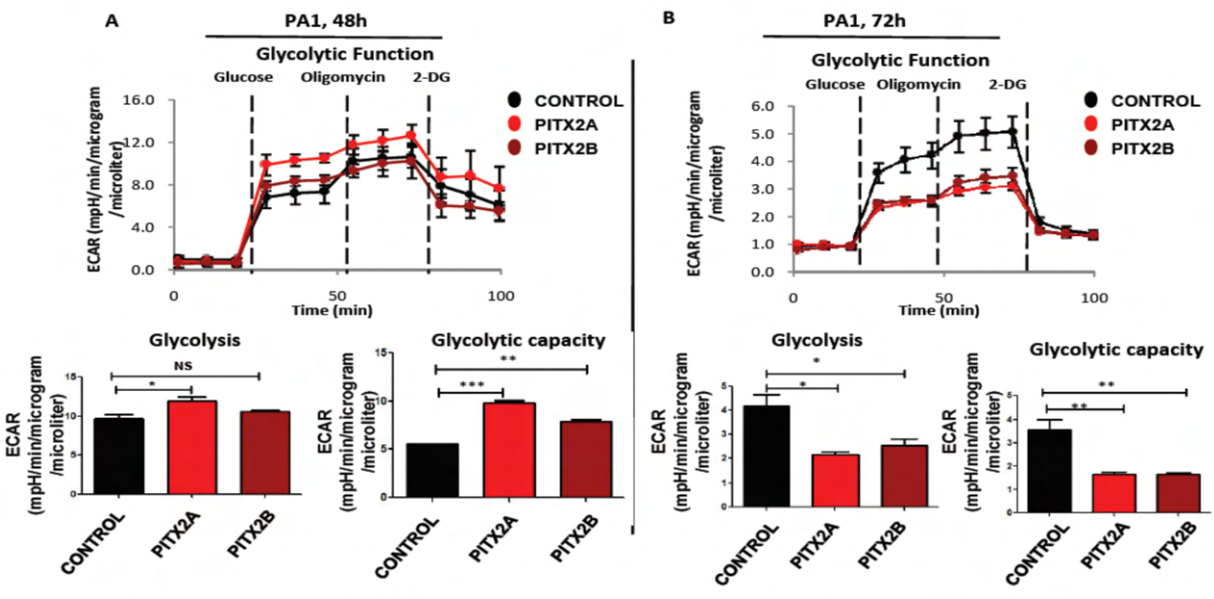

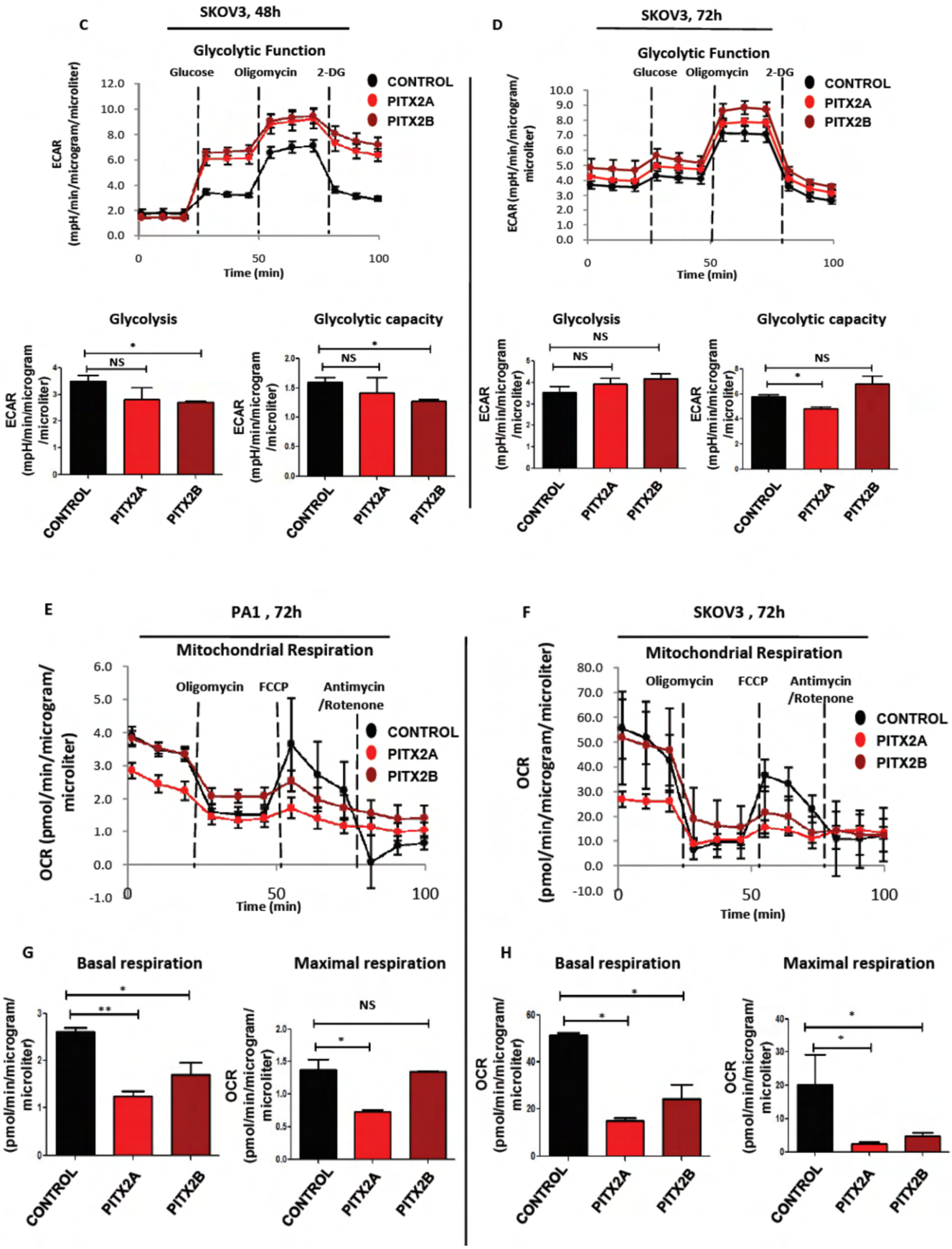
C
SKOV3, 48h
Glycolytic Function
Glucose
Oligomycin
2-DG
CONTROL
PITX2A
PITX2B
ECAR (mpH/min/microgram/microliter)
Time (min)
Glycolysis
Glycolytic capacity
NS
*
ECAR (mpH/min/microgram /microliter)
CONTROL
PITX2A
PITX2B
D
SKOV3, 72h
Glycolytic Function
Glucose
Oligomycin
2-DG
CONTROL
PITX2A
PITX2B
ECAR (mpH/min/microgram/ microliter)
Time (min)
Glycolysis
Glycolytic capacity
NS
*
ECAR (mpH/min/microgram /microliter)
CONTROL
PITX2A
PITX2B
E
PA1 , 72h
Mitochondrial Respiration
Oligomycin
FCCP
Antimycin /Rotenone
CONTROL
PITX2A
PITX2B
OCR (pmol/min/microgram/ microliter)
Time (min)
G
Basal respiration
Maximal respiration
*
**
NS
OCR (pmol/min/microgram/ microliter)
CONTROL
PITX2A
PITX2B
F
SKOV3 , 72h
Mitochondrial Respiration
Oligomycin
FCCP
Antimycin /Rotenone
CONTROL
PITX2A
PITX2B
OCR (pmol/min/microgram/ microliter)
Time (min)
H
Basal respiration
Maximal respiration
*
OCR (pmol/min/microgram/ microliter)
CONTROL
PITX2A
PITX2B

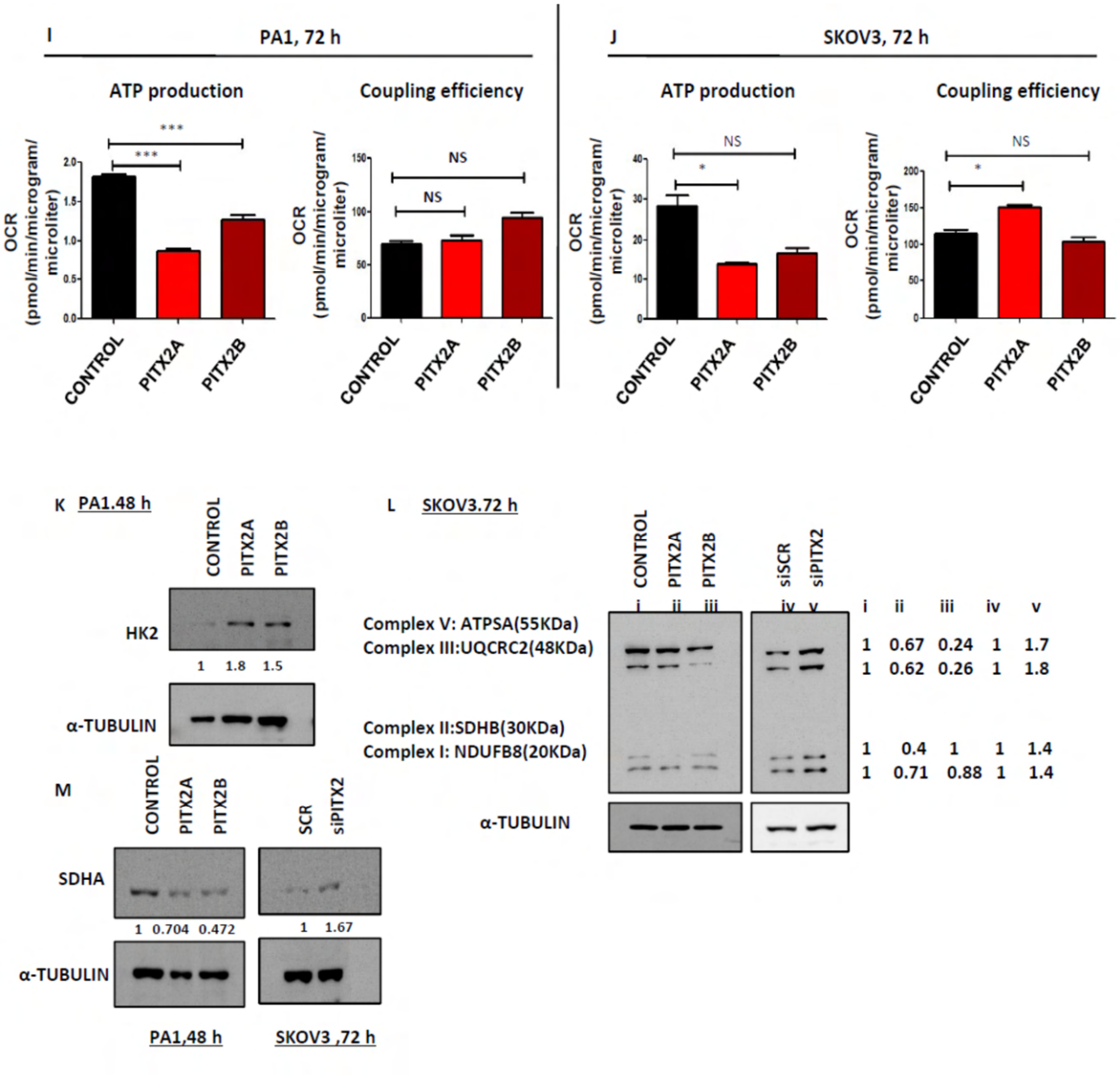

Figure 4: Metabolic reprogramming upon PITX2A/B overexpression in OC cells: ECAR, glycolysis, and glycolytic capacity was measured upon overexpressing PITX2A/B at 48 h and 72 h both in PA1 (A-B) and SKOV3 (C-D). OCR, maximal and basal respiration was decreased upon 72 h of PITX2 overexpression in PA1 (E, G, I) and SKOV3 (F, H, J). (K) Protein level of HK2 increased upon PITX2A/B overexpression in PA1 at 48 h. (L) OXPHOS complex proteins were reduced when PITX2A/B was overexpressed, however, opposite results were obtained due to its silencing in SKOV3. (M) SDHA expression was reduced in PA1 and enhanced upon its silencing in SKOV3. The statistical significance was analysed and represented as NS for non-significant,*p<0.05, **p<0.01, ***p<0.001.

CSCs are less dependent on glycolysis. We then examined the parameters of mitochondrial respiration by extracellular flux analysis and found that PITX2A/B attenuates both basal and maximal oxygen consumption rate and ATP production in both SKOV3 and PA1 at 72 h **(Fig. 4E-**

J). We have also checked the expression of various proteins involved in glycolysis and oxidative phosphorylation. Hexokinase 2 (HK2) was enhanced at 48 h of PITX2A/B overexpression in PA1 whereas OXPHOS complex proteins were reduced in SKOV3 at 72 h. In contrast, these proteins were enhanced upon silencing of PITX2 in SKOV3 **(Fig. 4K, L)**. Another mitochondrial protein Succinate dehydrogenase A (SDHA) was reduced at 48 h of PITX2A/B overexpression in PA1 and increased upon its silencing in SKOV3 at 72 h **(Fig. 4M)**. Altogether, these data highlighted that PITX2A/B induced stem cells become metabolically inactive.

TFGβ1-PITX2A/B signaling also regulates chemoresistance through ABCB1 in ovarian cancer:

We have already observed that PITX2A/B promotes stem-like features in ovarian cancer and chemoresistance is a marker for cancer stem cells. Keeping this in mind, we wanted to decipher the mechanism of PITX2A/B regulated chemoresistance. At first, PITX2A/B upregulates the gene expression of drug efflux transporters such as ABCB1 and ABCG2 in IOSE-364, PA1, and SKOV3 (**Fig. 5A-C)** and found a similar expression pattern of ABCG2 protein **(Fig. 5D-E)**. In rhodamine

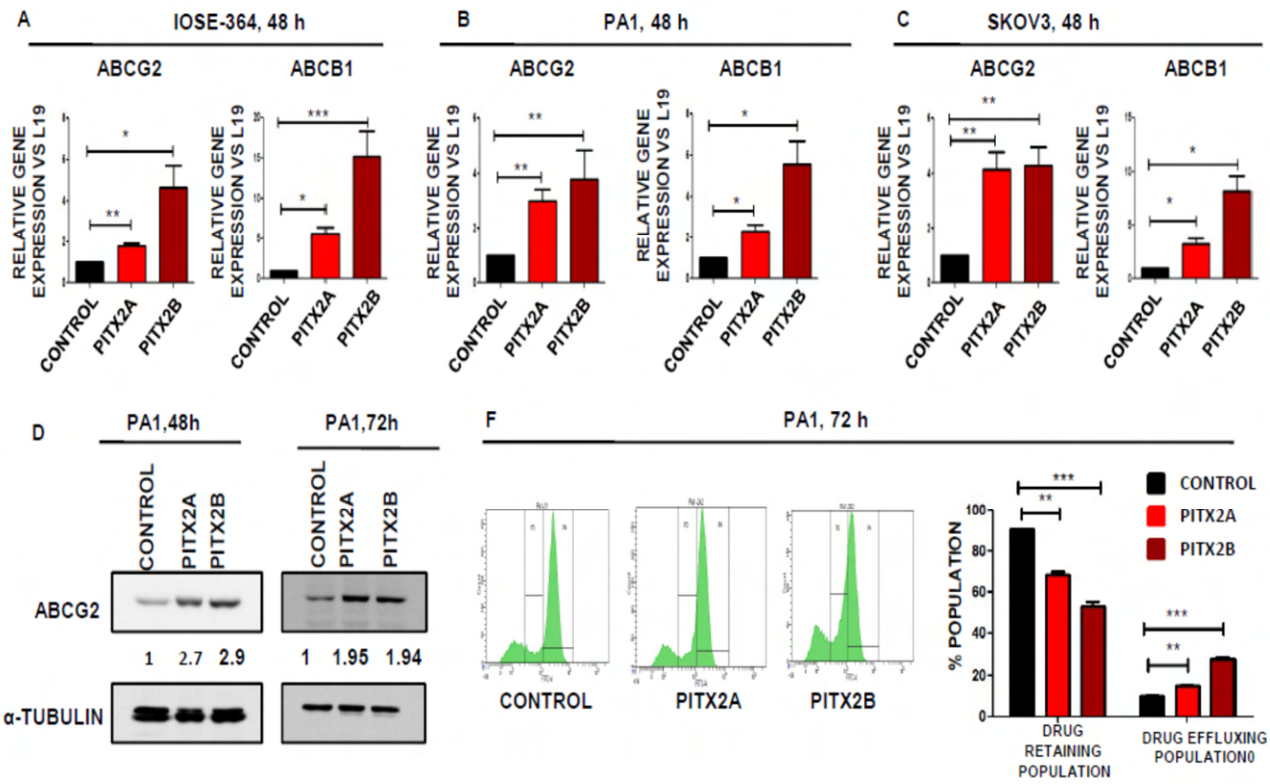

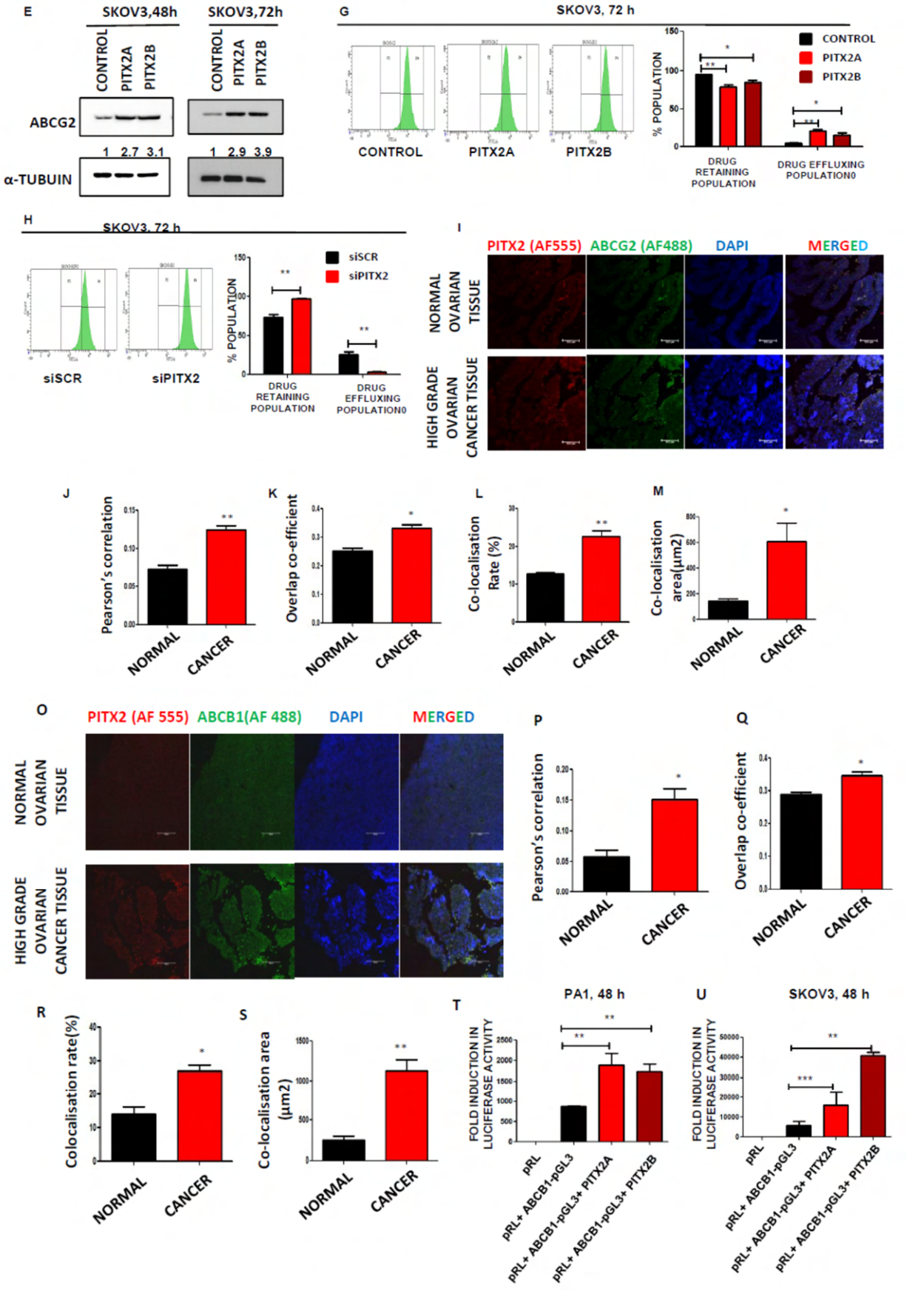
E
SKOV3,48h
SKOV3,72h
CONTROL
PITX2A
PITX2B
ABCG2
1 2.7 3.1
1 2.9 3.9
α-TUBUIN
G
SKOV3, 72 h
CONTROL
PITX2A
PITX2B
% POPULATION
DRUG RETAINING POPULATION
DRUG EFFLUXING POPULATION0
H
SKOV3, 72 h
siSCR
siPITX2
I
PITX2 (AF555)
ABCG2 (AF488)
DAPI
MERGED
NORMAL OVARIAN TISSUE
HIGH GRADE OVARIAN CANCER TISSUE
J
Pearson's correlation
K
Overlap co-efficient
L
Co-localisation Rate (%)
M
Co-localisation area(µm2)
NORMAL
CANCER
O
PITX2 (AF 555)
ABCB1(AF 488)
DAPI
MERGED
P
Pearson's correlation
Q
Overlap co-efficient
R
Colocalisation rate(%)
S
Co-localisation area (µm2)
T
PA1, 48 h
FOLD INDUCTION IN LUCIFERASE ACTIVITY
pRL
pRL+ ABCB1-pGL3
pRL+ ABCB1-pGL3+ PITX2A
pRL+ ABCB1-pGL3+ PITX2B
U
SKOV3, 48 h

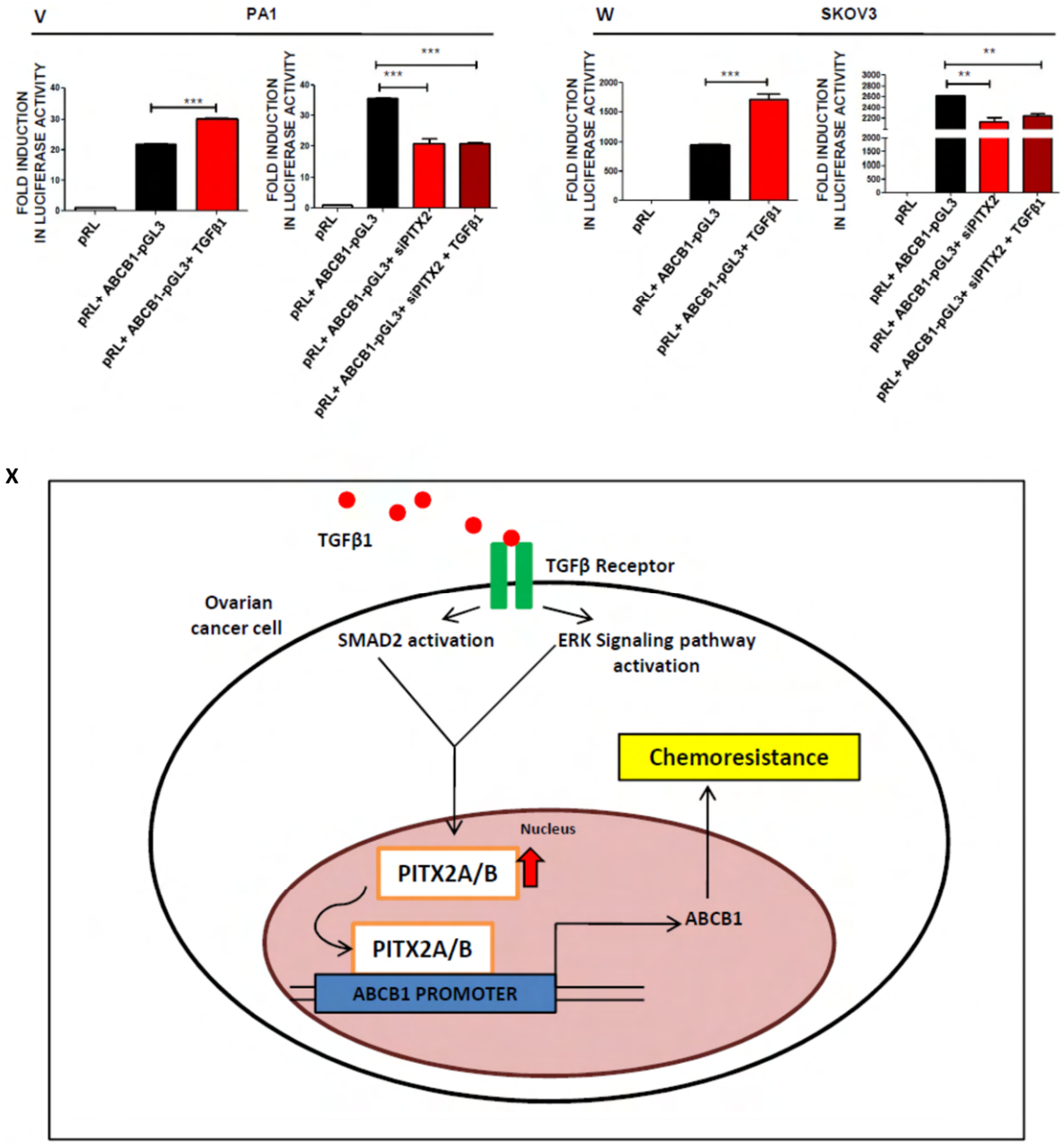

Figure 5: PITX2A/B promotes chemoresistance by enhancing ABCB1 expression in OC: Gene expression of ABCG2 and ABCB1 were represented in bar diagram after overexpressing PITX2A/2B in IOSE-364 (A), PA1 (B), and SKOV3 (C). The protein level of ABCG2 was enhanced after 48 h and 72 h of PITX2A/B overexpression in PA1 (D) and SKOV3 (E). Rhodamine efflux assay was performed and represented in both histogram and bar diagram in PA1 (F) and SKOV3 (G, H). (I) Expression of ABCG2 and PITX2 in human ovarian cancer tissue samples were checked through IHC and (J-M) quantified data was represented in the bar diagram. (O-S) IHC study depicted that ABCB1 expression was enhanced with PITX2 in high-grade ovarian cancer tissue and represented in bar diagram. (T, U) ABCB1 promoter binding assay was depicted in the bar diagram in both SKOV3 and PA1. ABCB1 promoter activity was enhanced upon TGFβ1 treatment whereas it was decreased upon PITX2 silencing in both PA1 (V) and SKOV3 (W). (X) The schematic diagram depicted that TGFβ1- PITX2A/B signaling enhances

chemoresistance in OC cells. The statistical significance was analyzed and represented as NS for non-significant,*p<0.05, **p<0.01, ***p<0.001. Scale bar 100 µm (I, O).

123 efflux assay, the drug effluxing population increases after 72 h of PITX2A/B overexpression **(Fig. 5F-G)**. Contrasting results were observed when PITX2 was silenced in SKOV3 **(Fig. 5H)**. In high-grade ovarian cancer tissue samples, expression of ABCG2 and ABCB1 was enhanced compared to normal ovarian tissue as quantified through intensity correlation analysis (ICA) **(Fig. 5I, O)**. Pearson coefficient, overlap co-efficient, co-localisation rate (%), and co-localisation area for ABCG2 and ABCB1 expression with PITX2 were enhanced in high-grade cancer tissue **(Fig. 5J-M, P-S)**. In an in-silico study, we observed that the ABCB1 promoter has a PITX2 binding site. To confirm this observation, we did a luciferase promoter binding assay and confirmed that PITX2A/B binds to the promoter of the ABCB1 gene and enhances its transcription in both PA1 and SKOV3 **(Fig. 5T, U)**. To establish the TGFβ1-PITX2A/B signaling axis promotes ABCB1 expression, we have treated TGFβ1 in PITX2 silenced condition and found that ABCB1 expression remained less as compared to normal condition **(Fig. 5V, W)**. Altogether, we suggested that TGFβ1- PITX2 signaling axis promotes ABCB1 expression in OC cells.

Discussion

The tumor microenvironment is comprised of various stromal cells, immune cells, and vascular cells which are associated with cancer prognosis by secreting growth factors, cytokines, and chemokines (Yuan et al., 2016). Transforming growth factor (TGFβ) is one of the growth factors, secreted from the stromal cells which promotes cancer invasion, metastasis, and chemoresistance in ovarian cancer (Gao et al., 2014; Mitra and Roy, 2017; Mitra et al., 2018; Yeung TL, Leung CS, Wong KK, 2013). In contrast, in normal cells and early stages of cancer, TGFβ signaling attenuates cancer progression. It is reported that TGFβ1 promotes stem-like characteristics through ZEB1-mediated EMT in ovarian cancer. Cancer upregulated gene (CUG)2 also mediates TGFβ signaling to enhance stem-like phenotype in breast cancer (Kaowinn et al., 2019). Again, TGFβ induces tissue transglutaminase (TG2) expression which in turn promotes EMT and enhances cancer stem cells in ovarian cancer (Cao et al., 2012). TGFβ signaling and sonic hedgehog induces PITX2 expression in embryonic development of left-right asymmetry in vertebrate (Shiratori and Hamada, 2014). We have also found that PITX2A/B is regulated by TGFβ1 in OC. The activated TGFβ receptor activates the downstream signaling pathway by regulatory SMAD. SMAD-dependent TGFβ1 signaling pathway alters the gene expression of various transcription factors involved in cancer progression (Lu et al., 2017). TGFβ also functions through ERK, p38MAPK, JNK, and PI3K-Akt signaling pathways in SMAD independent manner (Zhang, 2017). In our case, TGFβ1 driven PITX2A/B expression occurred through both SMAD-

dependent manner and ERK pathway. Therefore, we indicated that TGFβ1 has driven both SMAD and ERK-dependent signaling promotes PITX2A/B expression in OC cells.

Along with its function in embryonic development, PITX2 has a major role in EMT and cancer progression. PITX2A promotes invasion through activation of activin and TGFβ in ovarian cancer and also mediates progression through the Wnt/β-catenin pathway in lung and ovarian cancer (Basu and Roy, 2013; Basu et al., 2015; Luo et al., 2019). On the contrary, hypermethylation of PITX2 promoter is also linked with poor prognosis in hormone receptor-positive breast cancer patients (Maier et al., 2007). Similarly, Its expression is correlated with survival in colorectal cancer (Hirose et al., 2011). Therefore, we deciphered the importance of PITX2A/B on the promotion of stem-like features and chemoresistance in OC. We found that PITX2A/B enhances the stemness properties. Moreover, PITX2A/B binds on ABCB1 and promotes chemoresistance in OC.

The term ‘metabostemness' indicates that metabolism is involved in the regulation of genes associated with stemness and self-renewal (Menendez and Alarco´n, 2014). Several reports suggested that glycolysis enhances in CSCs of glioblastoma, breast cancer, lung cancer, liver cancer, ovarian cancer, colon cancer, and osteosarcoma whereas some of the reports this CSCs less rely on glycolysis due to their quiescent nature (Chae and Kim, 2018; El Hout et al., 2020). These contradictory results indicate that the metabolic phenotype of the same CSCs varies due to environmental factors, regulating players, and signaling pathways. In our case, glycolysis decreases in PA1 at the late stage of PITX2 overexpression, but it remains high in SKOV3 at 72 h. Then, changes arise in glycolysis due to the enhancement of the stem population with time. Similarly, CSCs in glioma depend upon OXPHOS for their survival and they have high mitochondrial reserve capacity (De Francesco et al., 2018). CSCs in breast cancer produce more ATP compared to the differentiated form. We observed that mitochondrial respiration is hampered due to PITX2 overexpression at 72 h in both PA1 and SKOV3. As both the glycolysis and mitochondrial oxidation attenuated during PITX2A/B overexpression, we concluded that PITX2A/B induced stem cells are metabolically inactive.

Chemoresistance is a trait of CSCs and therefore we wanted to decipher the role of PITX2A/B in promoting chemoresistance in cancer. It is reported that PITX2A/B binds to the promoter of ABCB1, a drug efflux transporter, and thereby cancer cells can survive after chemotherapy in colon cancer and kidney cancer (Lee and Thévenod, 2019). In breast cancer, PITX2 promotes resistance for letrozole via IF1TM1 signaling (Xu et al., 2019). We investigated that PITX2 binds to the ABCB1 promoter and enhances its expression. It has been also found that TGFβ signaling is involved in regulating PITX2 mediated chemoresistance in OC. Besides regulating PITX2 in left-right asymmetry in embryos, TGFβ1-PITX2A/B signaling promotes stemness and chemoresistance by enhancing ABCB1 expression in OC.

CHAPTER 2

DRP1 REGULATES STEMNESS AND CHEMORESISTANCE UPON GLUTAMINE DEPRIVATION IN CANCER

Introduction

Metabolic reprogramming or alteration is an emerging hallmark of cancer cells due to survival in nutrient or oxygen stressed conditions. Therefore, glucose produces energy through glycolysis and then the pyruvate produces lactate instead of entering into the TCA cycle oxygen limiting condition. In this condition, glutamine plays a major role to fuel the TCA cycle and producing energy. Additionally, it involves the synthesis of other amino acids, nucleotides, fatty acids, and hexosamines (Pavlova and Thompson, 2016). The average physiological concentration of glutamine in the blood is 0.6-0.9 mM but it reduces in cancer patients (Jiang et al., 2019; Souba et al.,1993). Most of the cancer cells do not have glutaminase synthetase (GS) for de novo synthesis, therefore they depend upon exogenous glutamine (Cluntun et al., 2017). Some reports suggested that cancer-associated fibroblast (CAF) and adipocyte in the tumor microenvironment can supply glutamine to ovarian cancer and pancreatic ductal carcinoma respectively (Meyer et al., 2016; Yang et al., 2016).

Glutamine enters into the cell through various transporters such ASCT2 (SLC1A5), LAT1 (SLC7A5), SNAT (SLC38), $ATB^{0,+}$ (SLC6A14) which are overexpressed in cancer (Scalise et al., 2017). There are some mitochondrial glutamine transporters for example SLC1A5 variant, GLAST, SLC25 which are involved in the import of glutamine for glutaminolysis (Kandasamy et al., 2018; Scalise et al., 2017; Yoo et al., 2020). Glutaminolysis is a two-step process: in the first step glutamine is converted into glutamate by glutaminase (GLS) and glutamate dehydrogenase (GDH) catalyzes the conversion of glutamate into α-ketoglutarate (α-KG). This α-KG enters into the TCA cycle to produce ATP and therefore glutamine acts as an anaplerotic substrate to drive the TCA cycle (Zhang et al., 2017b). Different oncogenic factors, signaling pathways such as MYC, KRAS, mTORC1 signaling enhances the expression of these enzymes and promotes cancer invasion, migration, and metastasis (Altman et al., 2016).

In contrast, some of the cancer cells survive in a glutamine-deprived environment by their adaptive mechanism. Depending upon specific cell type, origin, oncogenic mutation, and TME, glutamine deprivation also promotes the alteration in their metabolic pathway (Jiang et al., 2019). The cells in the core of a solid tumor survive in nutrient and oxygen limiting conditions. In breast cancer, glutamine deficiency promotes epigenetic alteration to induce the dedifferentiation of cells (Pan et al., 2016). Similarly, the Wnt signaling pathway can be activated by deficiency of α-ketoglutarate (α-KG) in pancreatic ductal adenocarcinoma. Therefore, indirectly glutamine limitation enhances stem-like traits and chemoresistance (Tran et al., 2020).

Cancer stem cells are generated by the genetic alteration or mutation of somatic cells during tumorigenesis. These small populations of cells have self-renewal and differentiation properties and they survive in stressed conditions and maintain their population by interacting with TME

(Aponte and Caicedo, 2017). Most of the CSC are glycolysis dependent and some of them have a high oxygen consumption rate (OCR), though the metabolic phenotype of CSCs are not only dependent upon the origin of cancer but also on other associated factors such as involved signaling pathway and TME (El Hout et al., 2020). Mitochondrial dynamics are also linked with CSCs. Mitochondrial morphology and its localization changes to adapt in nutrient limiting conditions and promote drug resistance (Jagust et al.,2019). Dynamin-related protein 1 (DRP1) is involved in mitochondrial fission and it is overexpressed in tumor-initiating cells in the brain and mitochondrial fragmentation is associated with the propagation of stem-like cells in breast epithelium (De Francesco et al., 2018). It is also reported that perinuclear localization of mitochondria is one of the features of CSCs and it regulates transcription of stemness factors by creating ROS enriched nucleus (Al-Mehdi et al., 2012).

In this study, we aimed to focus on the role of glutamine in promoting stem-like characteristics and followed by chemoresistance in ovarian and colorectal cancer. We also tried to link mitochondrial dynamics and localization with glutamine deprivation for induction of stemness. In addition, we analyzed and examined the fate of stemness to regulate redox balance.

Results:

Cancer stemness markers are enhanced upon glutamine deprivation in cancer cell

Cancer stem cells (CSC) can survive in nutrient and oxygen limiting conditions within the tumor and they have the capability of self-renewal and dedifferentiation (Aponte and Caicedo, 2017). It is already reported that glutamine deprivation promotes stem-like features by attenuation of histone demethylation in breast and colorectal cancer (Pan et al., 2016; Tran et al., 2020). At first, we performed cell cycle analysis by continuously culturing PA1 cells in glutamine depleted condition up to passage 8. Cells were arrested in the G0/G1 phase of the cell cycle upon glutamine deprivation which is independent of passage number **(Fig. 1A-B)**. It suggested that cells underwent a non-proliferating quiescent stage like CSCs in absence of glutamine. To revalidate these results, we checked the expression level of pluripotent stem cell markers like SOX2, OCT4, NANOG and found that their expression was enhanced in both mRNA and protein levels upon glutamine deprivation **(Fig, 1C-D)**. We observed that nuclear localization of OCT4 enhanced in this condition in PA1 **(Fig. 1E)**. Moreover, SOX2 expression also increased upon glutamine deprivation in HCT116 as observed in confocal microscopy **(Fig. 1F)**.

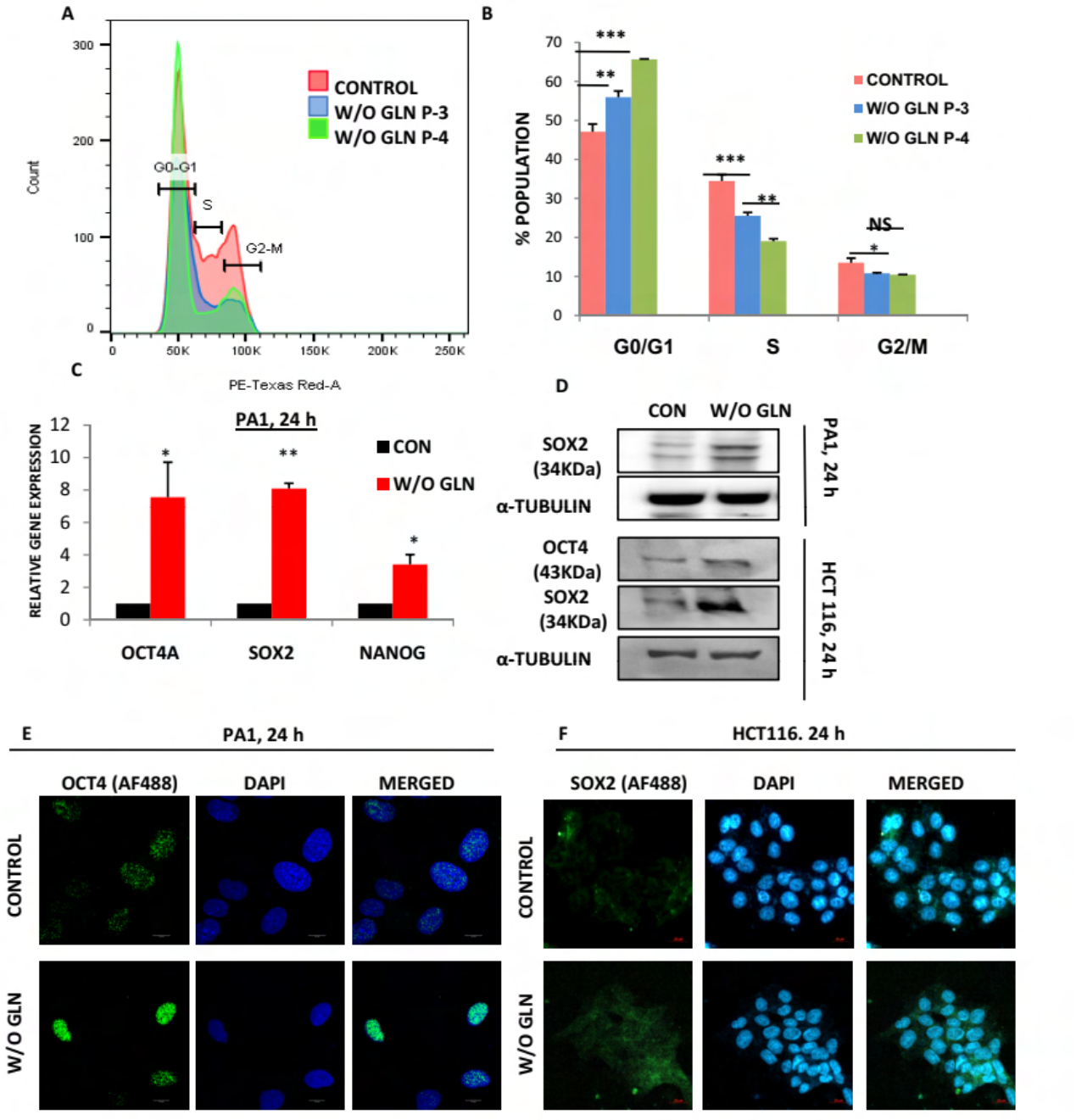

Figure 1: Glutamine deprivation enhanced the stemness associated genes: (A) Upon glutamine deprivation cells were arrested in G0/G1 phase as depicted in the histogram and (B) cell cycle analysis data was represented in the bar diagram in PA1. (C) The gene expression of OCT4, SOX2, and NANOG were elevated in glutamine-deprived conditions in PA1 after 24 h. (D) Protein expression of SOX2 was enhanced upon 24 h of glutamine starvation in both PA1 and HCT116 and OCT4 expression also increased in HCT116. (E) Confocal microscopic images of OCT4 in PA1 and (F) SOX2 in HCT116 upon 24 h of glutamine deprivation. The statistical significance was analyzed and represented as NS for non-significant,*p<0.05, **p<0.01, ***p<0.001. Scale bar 10 µm (E, F).

Cell surface markers of cancer stem cells are upregulated upon glutamine deprivation

In addition, we observed the expression of cell surface antigens of cancer stem cells such as CD44 and CD117 are upregulated after both 24 h and 48 h of glutamine starvation in PA1 whereas expression of CD44 and CD45 were increased in HCT116 at 48 h **(Fig. 2A, C, E, H-J)**. In contrast, we have not found any significant changes in the expression level of CD31 and CD45 after 24 h incubation in glutamine limiting condition, however, at 48 h, CD45 level was increased significantly in PA1 cells **(Fig. 2B, D, F)**. Deregulation in the alternative splicing of CD44 promotes stemness in tumors (Bhattacharya et al., 2018). We have also found that the mRNA level of CD44 standard (CD44s) isoform was upregulated, along with the reduction in the epithelial variant (CD44e) under glutamine limiting conditions in PA1 cells **(Fig. 2K)**.

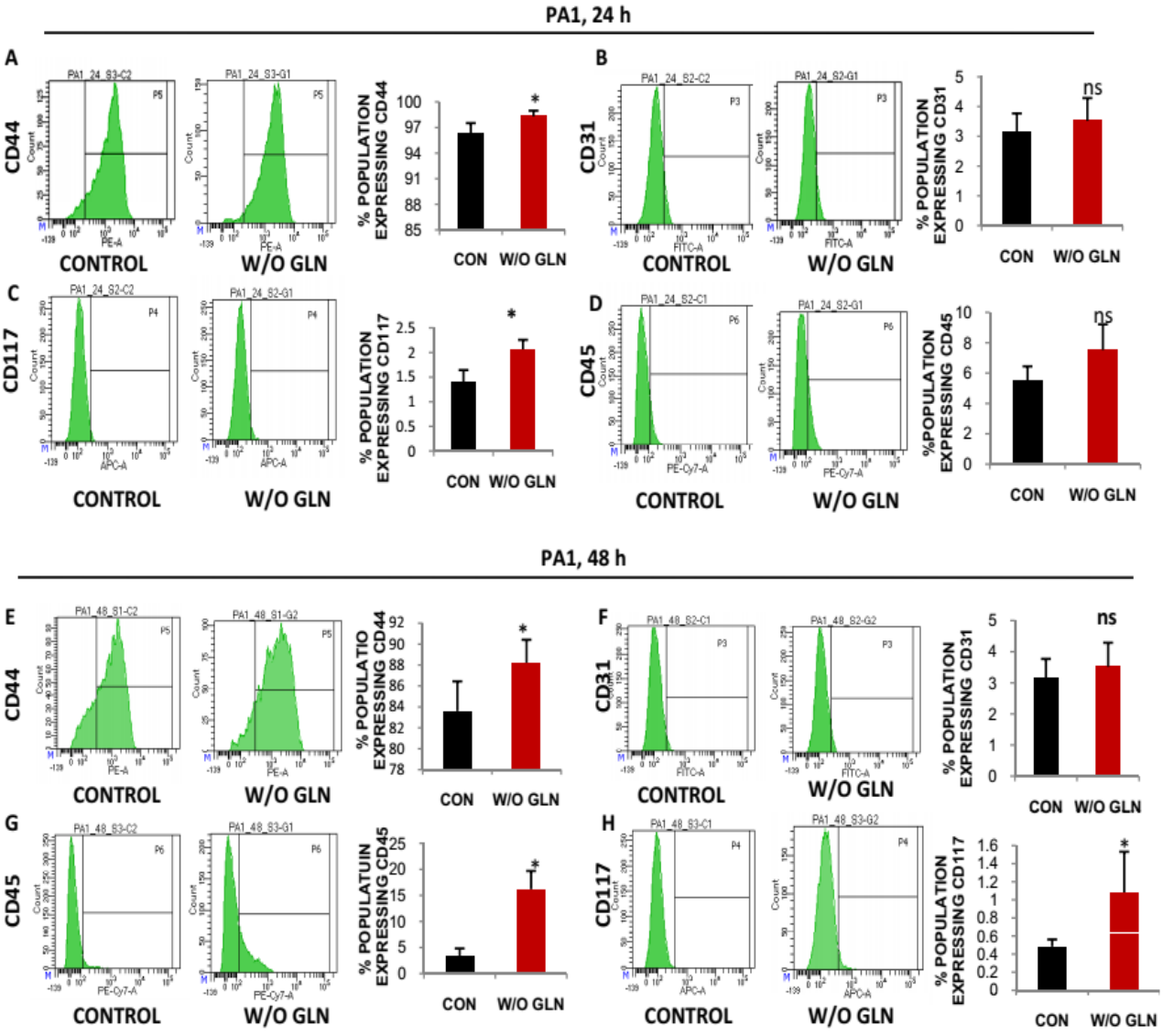

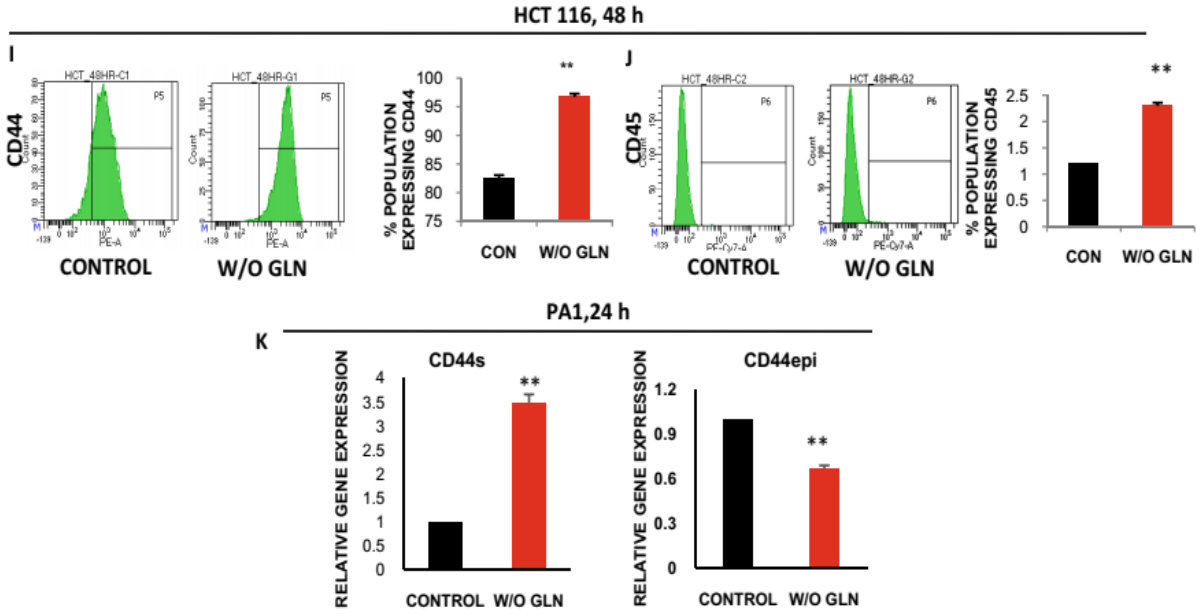

Figure 2: CD markers are enhanced in glutamine deprived condition: (A-H) CD44, CD31, CD117 and, CD45 levels were checked in PA1 upon 24 h and 48 h of glutamine deprivation and represented in bar diagram. (I-J) CD44 and CD45 levels were enhanced upon 48 h of glutamine deprivation in HCT116. (K) Gene expression of CD44s and CD44epi were represented in the bar diagram in glutamine-deprived conditions at 24 h in PA1. The statistical significance was analysed and represented as NS for non-significant,*p<0.05, **p<0.01, ***p<0.001.

Glutamine deprivation is solely responsible for inducing stem-like features and promotes chemoresistance in cancer

To establish the role of glutamine deprivation for promoting stem-like characteristics, we added glutamine after 24 h of glutamine starvation and noticed that glutamine addition normalized the level of SOX2 in PA1 **(Fig. 3A)**. This indicates that glutamine deprivation is exclusively responsible for inducing the expression of stem-markers. In consistent with our prior observation, aldehyde dehydrogenase (ALDH) activity which is a marker of CSC, was also enhanced upon 24 h of glutamine-starvation **(Fig. 3B)**. Collectively these data indicated that glutamine deprivation enhances stem-like features in cancer.

Chemoresistance is associated with stemness and it becomes a character of CSCs. Chemoresistance in CSC is linked with the overexpression of drug efflux pumps which are mainly ATP binding cassette (ABC) family transporters, such as ABCG2, ABCB1. Glutamine deprivation promotes the upregulation of ABCG2 expression in both gene and protein levels **(Fig. 3C-D)**. To examine the drug efflux capability of these cancer cells, we performed Rhodamine 123 (Rh123) efflux assay and it showed that glutamine starved cells exported out Rh123 more effectively compared to control cells in extracellular space. Additionally, flow

cytometric analysis depicted that Rh123 retaining cell population decreases upon glutamine deprivation **(Fig. 3E-F)**.

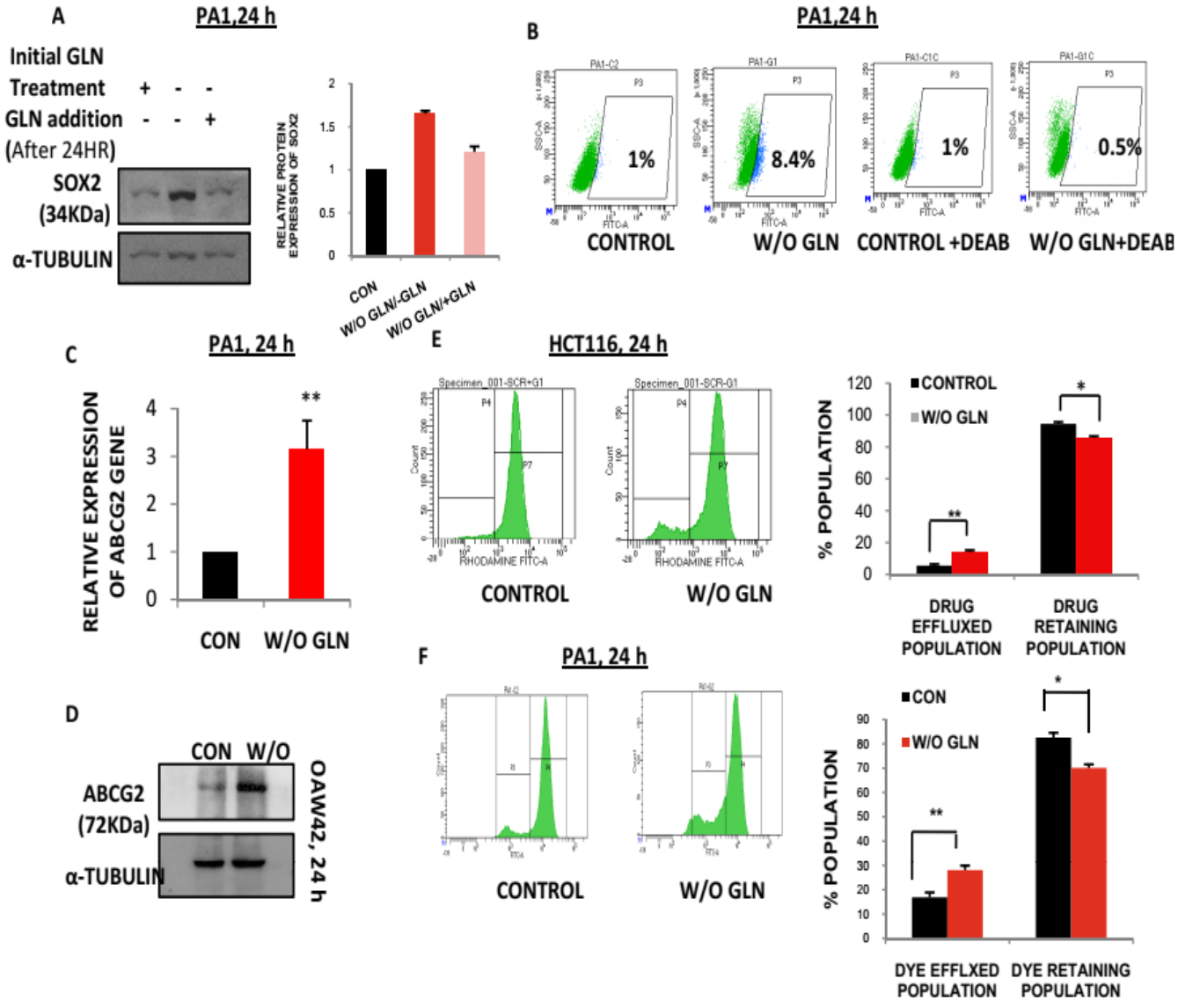

Figure 3: Glutamine deprivation promotes chemoresistance in cancer: (A) Re-supplementation of glutamine after its deprivation restored SOX2 protein expression in PA1. (B) Aldehyde dehydrogenase assay was performed and represented in the dot plot. (C) Gene expression of ABCG2 was represented in the bar diagram. (D) Protein expression of ABCG2 is also enhanced in OAW42 upon glutamine deprivation. Rhodamine 123 dye efflux assay was performed in HCT116 (E) and PA1 (F) upon glutamine deprivation and represented in both histogram and bar diagram. The statistical significance was analyzed and represented as NS for non-significant,*p<0.05, **p<0.01, ***p<0.001.

Glutamine deprivation promotes perinuclear localization of fragmented mitochondria in cancer

In cancer cells, glutamine is the main source for fueling the TCA cycle in mitochondria, and

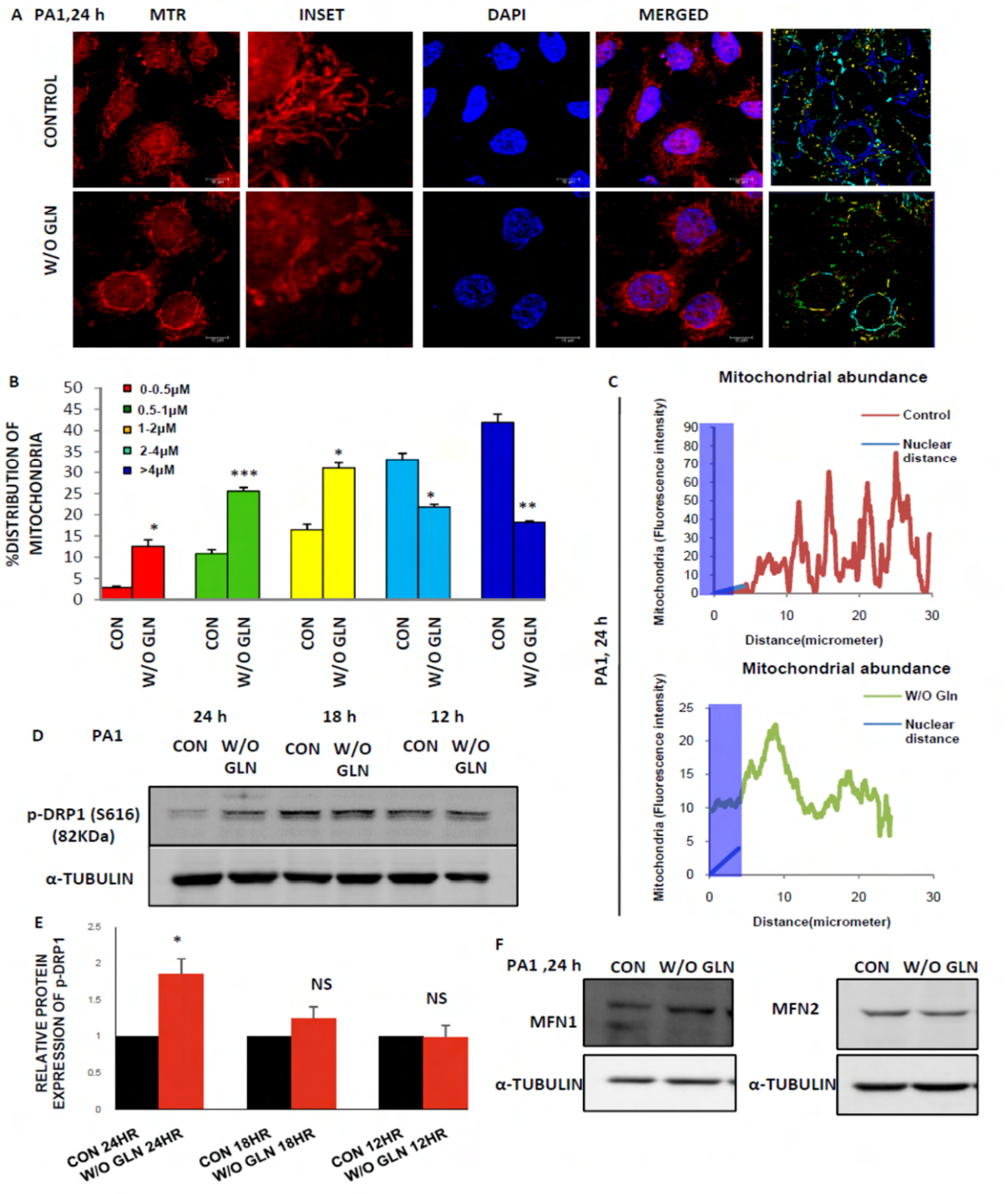

Figure 4: DRP1 promotes mitochondrial fission in glutamine deprived condition: (A-B) Under 24 h of

glutamine deprived condition, confocal microscopy of PA1 have shown fragmented mitochondria and % distribution of fragmented mitochondria is represented bar diagram. (C) The distribution of mitochondria around the nucleus was calculated and represented in line scan graph. (D-E) Expression of p-DRP1 (S616) at 12 h, 18 h, and 24 h of glutamine starvation was determined and quantitative data was represented in the bar diagram. (F) Protein levels of MFN1 and MFN2 remain unaltered after 24 h of glutamine deprivation. The statistical significance was analyzed and represented as NS for non-significant,*p<0.05, **p<0.01, ***p<0.001. Scale bar 10 µm (A).

mitochondrial dynamics regulate the fate of cancer cells. Depending upon these background informations, we hypothesized that mitochondrial dynamics may have a role in promoting In cancer cells, glutamine is the main source for fueling the TCA cycle in mitochondria and stem-like features upon glutamine deprivation. Interestingly, we found that mitochondrial fission occurs due to glutamine deficiency and observed perinuclear localization of fragmented mitochondria which is another feature of CSCs **(Fig. 4A-C)**. The percent of short mitochondria enhanced with a concomitant decrease in elongated one upon glutamine deficiency. To look upon the responsible factors involved in mitochondrial fission, we observed that phosphorylation of DRP1 at S616 is elevated in absence of glutamine **(Fig. 4D-E)**. We did not find any change in the expression of mitochondrial fusion protein MFN1 and MFN2 **(Fig. 4F)**. Therefore, it is suggested that glutamine deprivation may promote mitochondrial fragmentation through phosphorylation of DRP1.

Mitochondrial fission protein, DRP1 is responsible for promoting stem-like traits and chemoresistance in glutamine limiting conditions

Both the DRP1 inhibitor (MDiVi-1) and siDRP1 can reduce the expression level of CD44 in glutamine-free conditions in PA1 and HCT116 respectively **(Fig. 5A-B)**. Stem cells can form 3D spheroids in non-adherent conditions, which is another remarkable feature of CSCs. Glutamine deprivation promotes larger spheroid formation whereas MDiVi-1 treatment rescues the cells from spheroid formation in glutamine-free medium and therefore the size of the spheroid remains the same as control **(Fig. 5C-D)**. In confocal microscopy, fragmented mitochondria were observed in the spheroid formed in glutamine restricted conditions **(Fig. 5E-F)**. Colocalization of CD44 and p-DRP1 elevated in ovarian cancer tissue compared to the normal ovarian tissue section which was presented using intensity correlation analysis (ICA). This ICA data indicated that colocalization rate, Pearson's correlation, colocalization area, and overlap coefficient were enhanced in cancerous tissue **(Fig. 5G-H)**. The above results convincingly depicted that glutamine starvation can increase stem-like traits through DRP1 signaling in cancer.

Following the previous data, we aimed to determine whether this DRP1 signaling is associated with chemoresistance along with stemness. Disrupting the DRP1 phosphorylation using MDiVi-1 and siDRP1 pronouncedly increases Rh123 dye retaining population upon glutamine starvation

in Rh123 efflux assay **(Fig. 5I-J)**. These experiments thus unraveled DRP1 as the potential factor for promoting stem-like traits and chemoresistance in cancer.

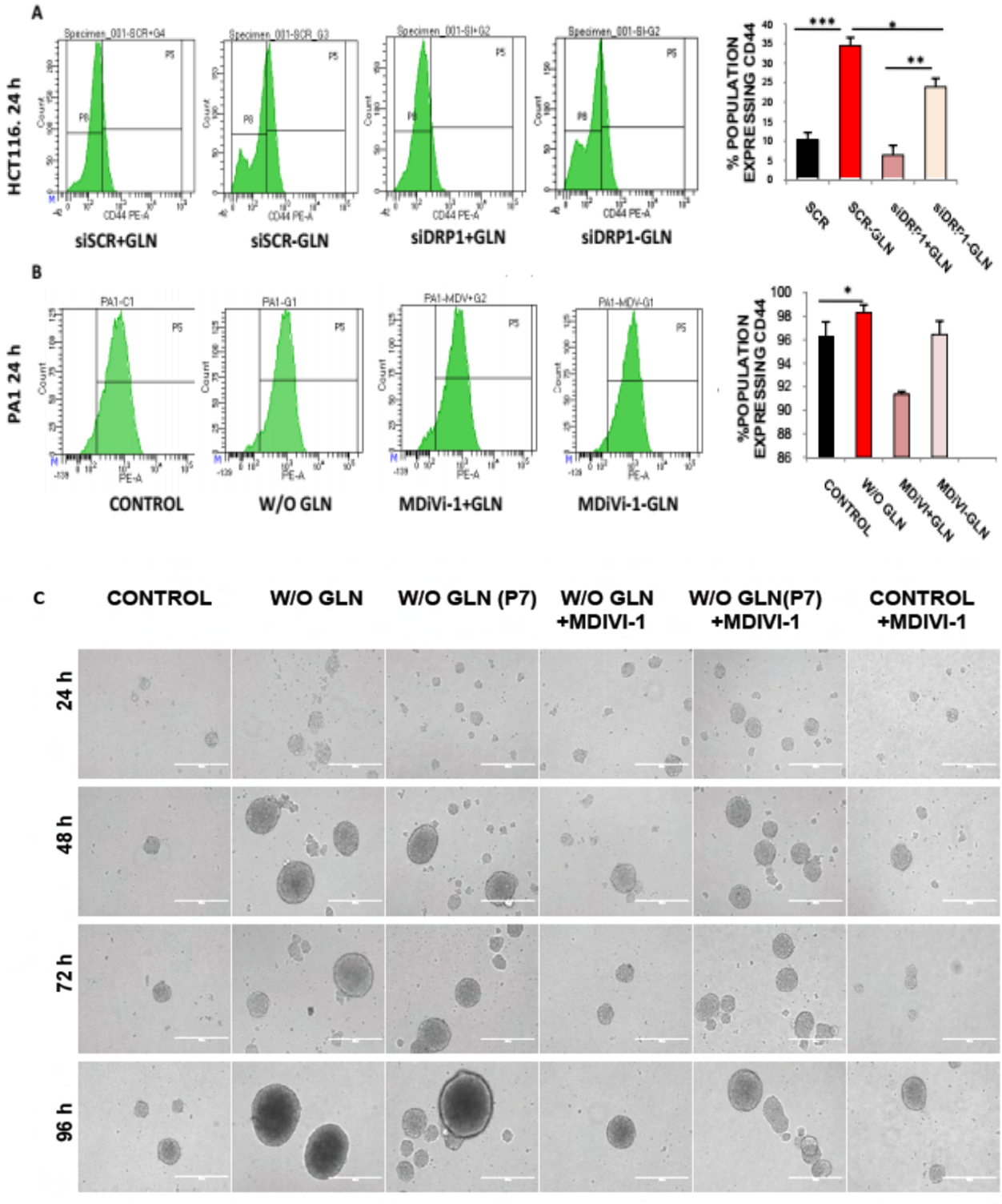

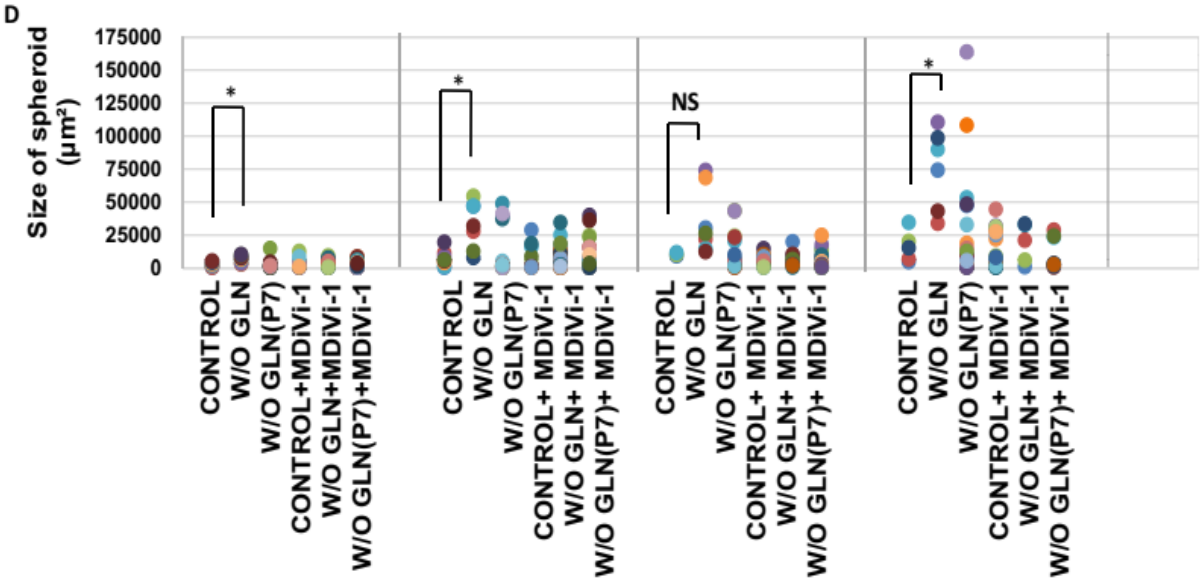
D
Size of spheroid (µm²)
175000
150000
125000
100000
75000
50000
25000
0
*
*
NS
*
CONTROL
W/O GLN
W/O GLN(P7)
CONTROL+MDiVi-1
W/O GLN+MDiVi-1
W/O GLN(P7)+MDiVi-1

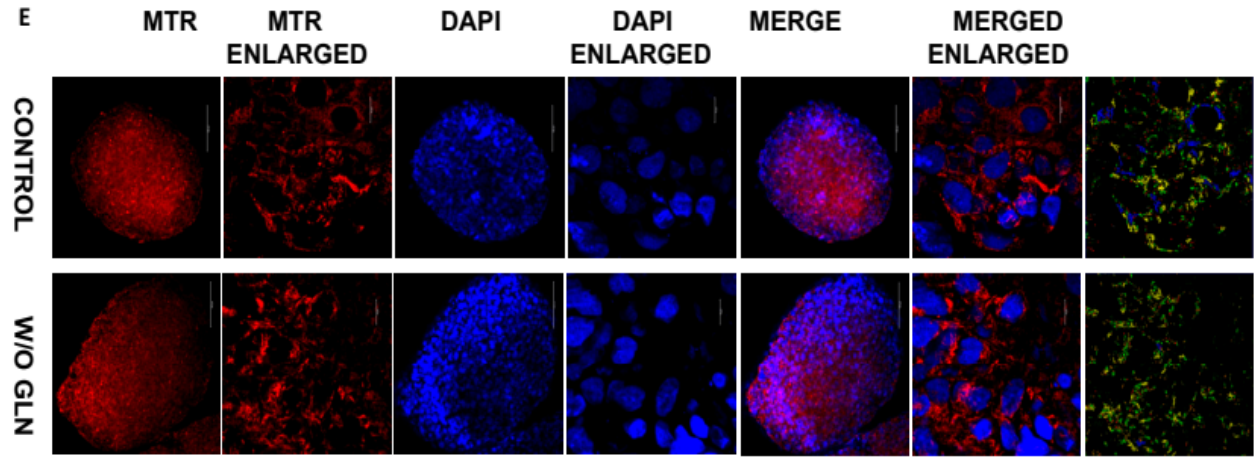
E
MTR
MTR ENLARGED
DAPI
DAPI ENLARGED
MERGE
MERGED ENLARGED
CONTROL
W/O GLN

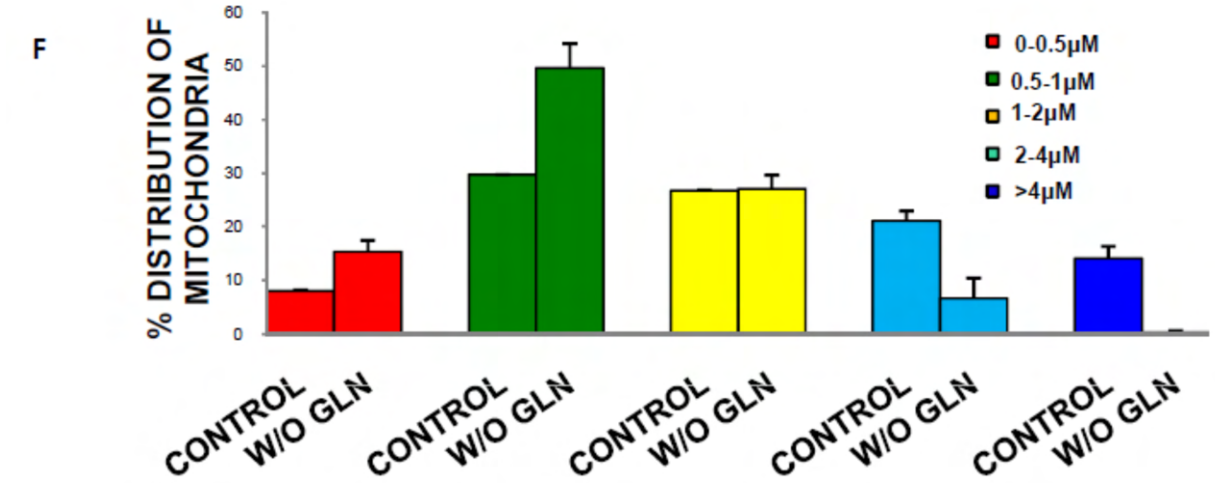
F
% DISTRIBUTION OF MITOCHONDRIA
60
50
40
30
20
10
0
0-0.5µM
0.5-1µM
1-2µM
2-4µM
>4µM
CONTROL
W/O GLN

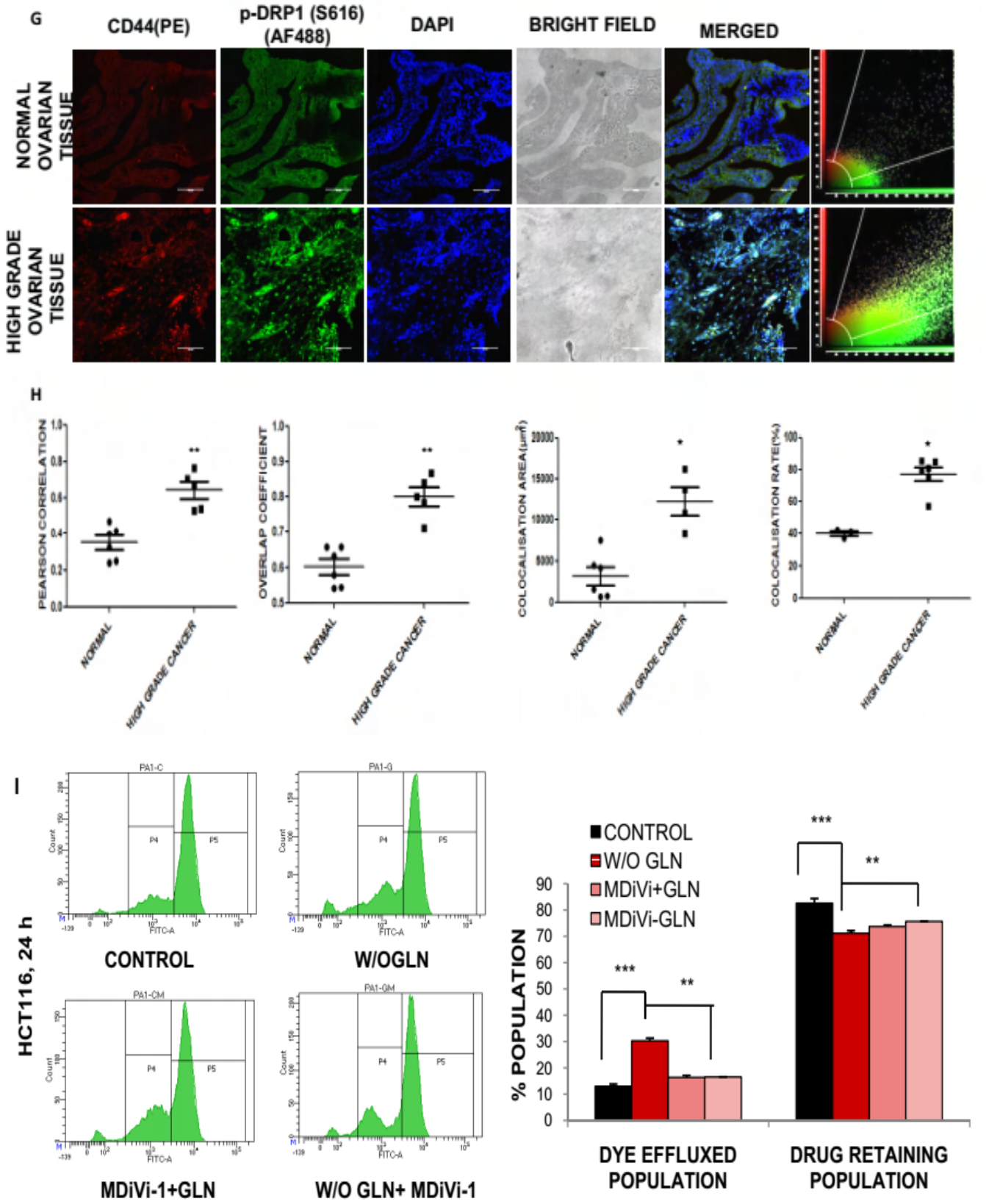
G
CD44(PE)
p-DRP1 (S616) (AF488)
DAPI
BRIGHT FIELD
MERGED
NORMAL OVARIAN TISSUE
HIGH GRADE OVARIAN TISSUE
H
PEARSON CORRELATION
OVERLAP COEFFICIENT
COLOCALISATION AREA(μm²)
COLOCALISATION RATE(%)
NORMAL
HIGH GRADE CANCER
I
HCT116, 24 h
CONTROL
W/OGLN
MDiVi-1+GLN
W/O GLN+ MDiVi-1
CONTROL
W/O GLN
MDiVi+GLN
MDiVi-GLN
% POPULATION
DYE EFFLUXED POPULATION
DRUG RETAINING POPULATION

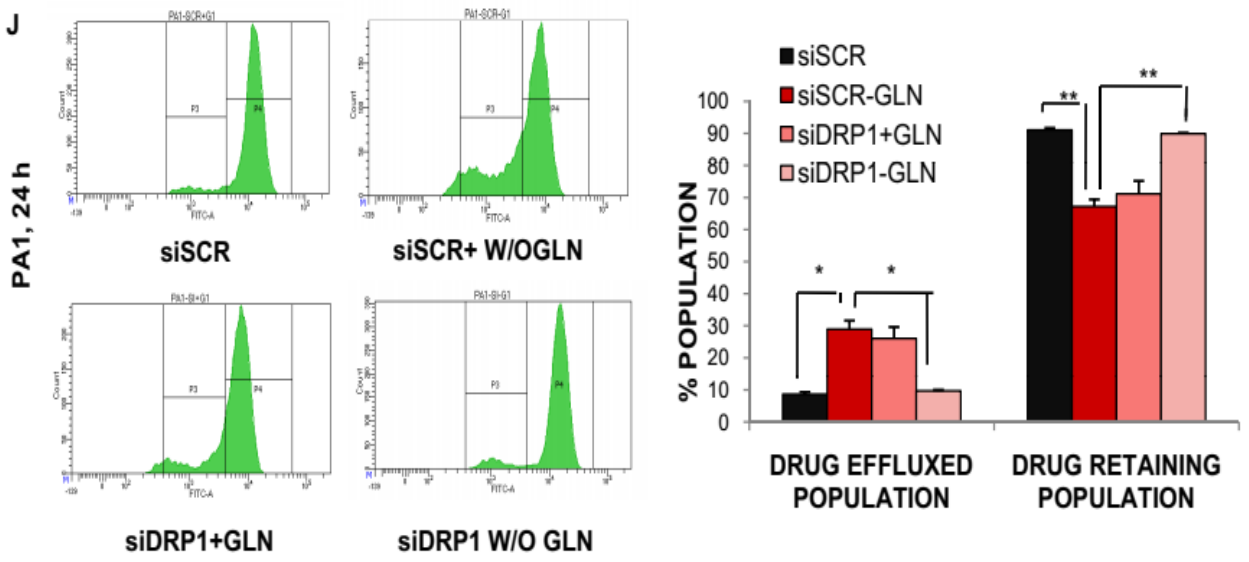

Figure 5: DRP1 promotes stemness and chemoresistance in glutamine limiting condition: (A, B) CD44 expression reduced upon silencing and inhibiting DRP1 in glutamine restricted condition in HCT116 and PA1 respectively. (C-D) Size and the number of spheroids were represented in phase-contrast microscopy and presented in a dot plot. (E-F) Mitochondrial fragmentation was visualized in spheroids formed upon glutamine deprived condition in PA1 and the distribution of mitochondria represented in bar diagram. (G-H) Co-expression of CD44 and DRP1 were enhanced in high-grade ovarian cancer tissue compared to the normal ovary and ICA data represented in the plot. (I-J) Rhodamine 123 efflux assay was performed using inhibitor- and siRNA against DRP1 in glutamine deprived conditions in HCT116 and PA1 cells respectively. The statistical significance was analysed and represented as NS for non-significant,*p<0.05, **p<0.01, ***p<0.001. Scale bar 400 µm (C), 100 µm (D, F), 10 µm (Enlarged images of D).

DRP1 promotes stemness and chemoresistance by redox regulation

Though DRP1 is responsible for promoting stemness and chemoresistance in cancer, the mechanism behind it remains unknown. Therefore, we tried to focus on how mitochondrial fragmentation and their localization promote stem-like characteristics. Previously, we obtained that CD44 is upregulated upon glutamine deprivation and the various report suggested that CD44 localizes with xCT in the cell membrane. xCT is an antiporter that transports glutamate in exchange for cysteine into the cytosol and maintains the redox balance by synthesizing glutathione. We found that xCT expression enhances in glutamine deprived conditions and consistently therefore colocalization with CD44 also increases in cancer **(Fig. 6A-D)**. In contrast, we did not find a significant change in mitochondrial ROS amount in the glutamine limiting condition. In addition, Inhibiting or silencing of xCT, no significant change was observed in ROS amount **(Fig. 6E-G)**. In confocal microscopy using DCFDA, we observed that ROS accumulate in the nucleus in absence of glutamine **(Fig. 6H)**. As mitochondria are localized around the nucleus

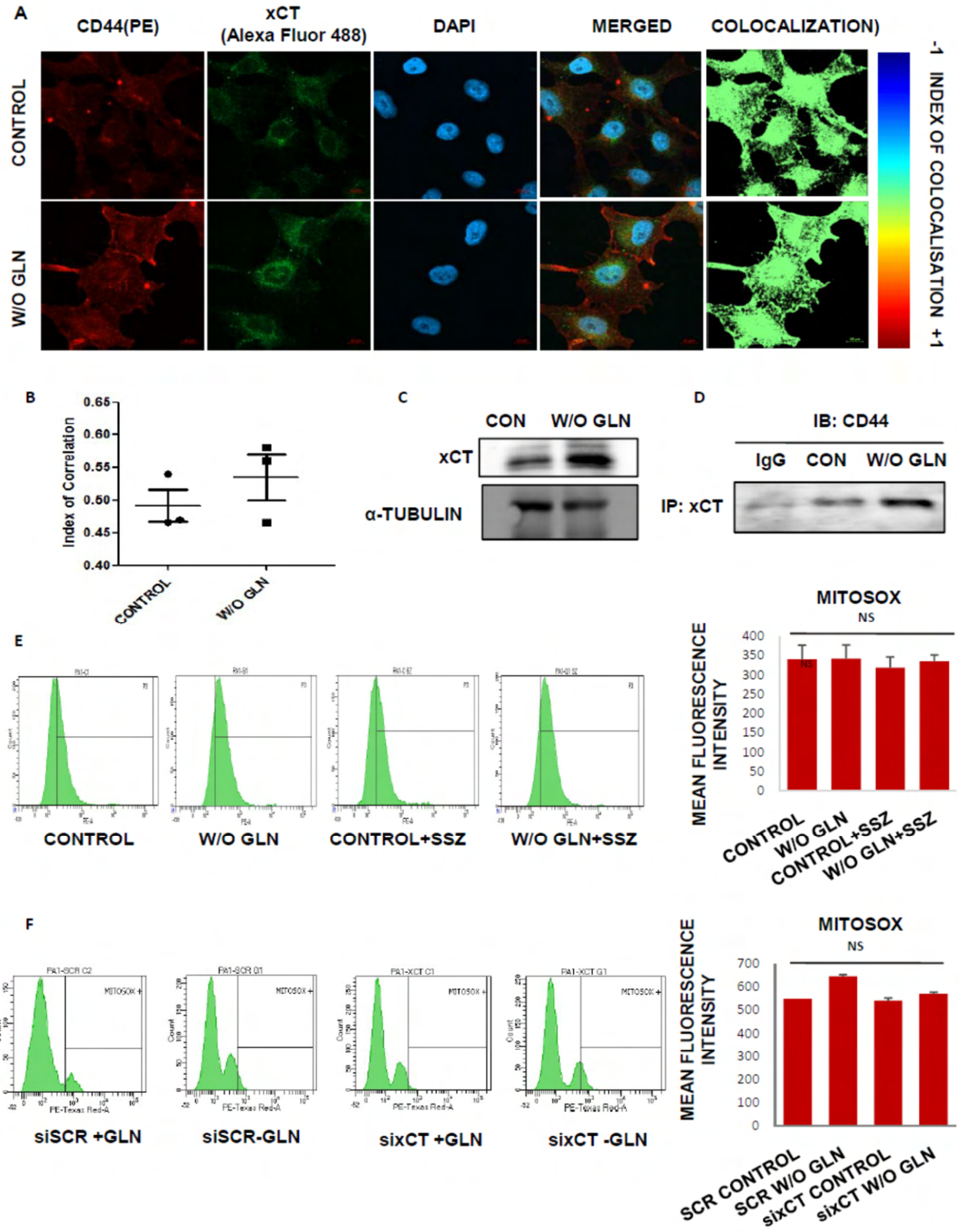
A
CD44(PE)
xCT (Alexa Fluor 488)
DAPI
MERGED
COLOCALIZATION)
CONTROL
W/O GLN
-1
INDEX OF COLOCALISATION
+1
B
Index of Correlation
0.65
0.60
0.55
0.50
0.45
0.40
CONTROL
W/O GLN
C
CON
W/O GLN
xCT
α-TUBULIN
D
IB: CD44
IgG
CON
W/O GLN
IP: xCT
E
CONTROL
W/O GLN
CONTROL+SSZ
W/O GLN+SSZ
MITOSOX
NS
MEAN FLUORESCENCE INTENSITY
400
350
300
250
200
150
100
50
0
CONTROL
W/O GLN
CONTROL+SSZ
W/O GLN+SSZ
F
siSCR +GLN
siSCR-GLN
sixCT +GLN
sixCT -GLN
MITOSOX
NS
MEAN FLUORESCENCE INTENSITY
700
600
500
400
300
200
100
0
SCR CONTROL
SCR W/O GLN
sixCT CONTROL
sixCT W/O GLN

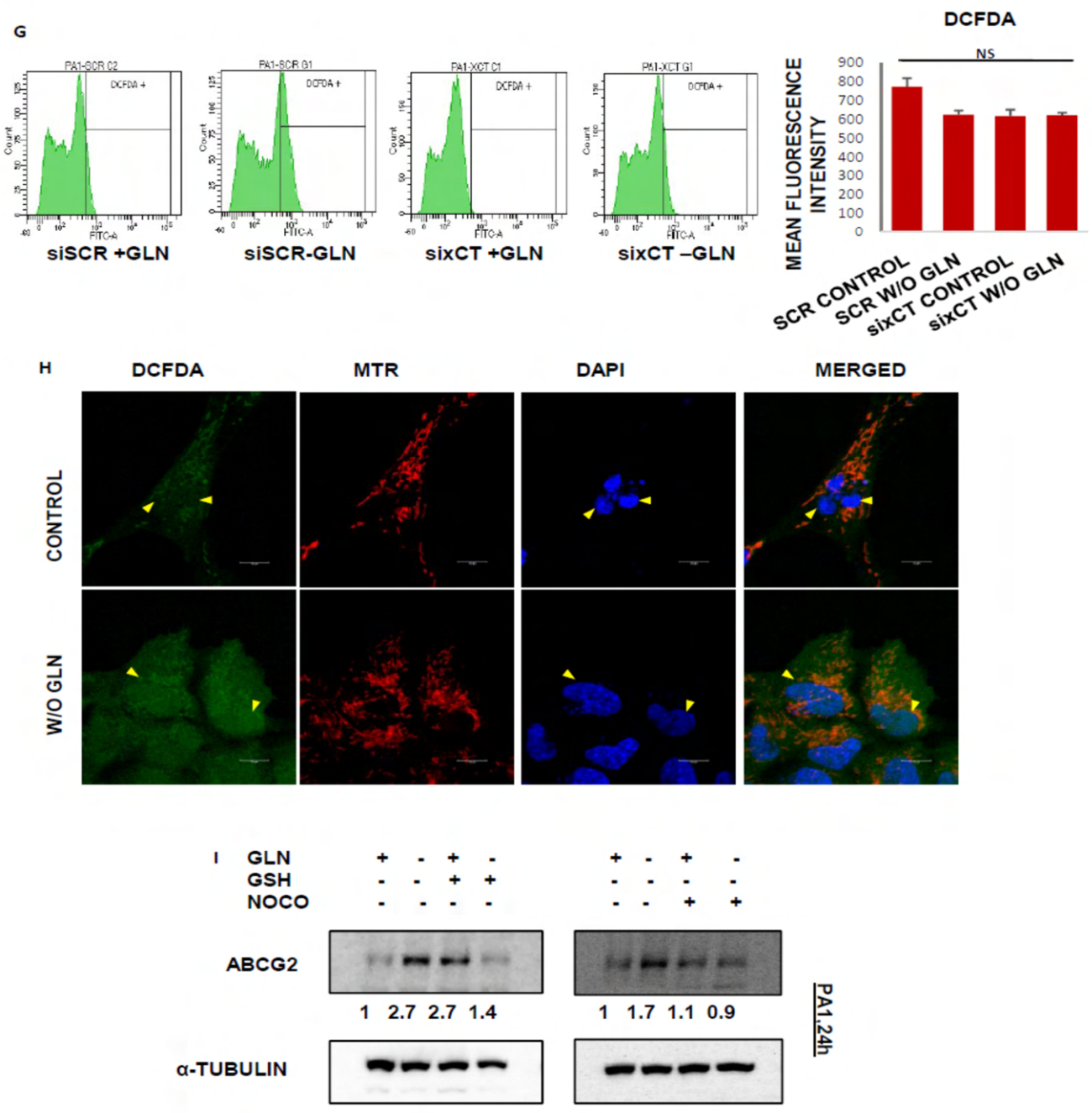

Figure 6: Mitochondrial redox homeostasis regulates chemoresistance in glutamine deprived condition: (A-B) Confocal microscopic images depicted that colocalization of CD44 and xCT enhanced upon glutamine deprivation in PA1 and quantitative data represented in bar diagram. (C-D) Expression of xCT increased and they interact with CD44 upon glutamine limitation in PA1 as observed through co-immunoprecipitation. (E) Sulphasalazine (SSZ) treatment did not reduce mitochondrial ROS in glutamine-deprived conditions in PA1. (F-G) sixCT was unable to control mitochondrial and total cellular ROS in glutamine-deprived conditions in PA1 as evidenced in flow cytometric data and represented in both histogram and bar diagram. (H) Cellular ROS localization was observed through confocal microscopy using DCFDA staining in PA1. (I) GSH and NOCO treatment independently can able to decrease the ABCG2 expression in glutamine limiting conditions in PA1. The statistical significance was

analyzed and represented as NS for non-significant,*p<0.05, **p<0.01, ***p<0.001. Scale bar 10 µm (A, H).

in the CSCs, they may generate ROS in the nucleus. When we have used GSH, found that ABCG2 expression decreased in absence of glutamine **(Fig. 6I).** In addition, blocking mitochondrial mobility using nocodazole (NOCO), attenuated ABCG2 expression in glutamine deficient conditions in PA1 **(Fig. 6I)**. Altogether, these data suggested that mitochondrial ROS may regulate chemoresistance upon glutamine deprivation in cancer.

NRF2 is involved in the induction of chemoresistance in glutamine limiting conditions

Some reports indicate that nuclear ROS can activate various transcription factors such as NRF2 which in turn promote stemness and chemoresistance. In addition, from the interactome study, we found that xCT, ABCG2 interact with NRF2 in string analysis **(Fig. 7A).** Confocal microscopic images depicted that NRF2 bind to DNA in glutamine limiting condition in HCT116 **(Fig. 7B).** Glutamine deprivation promotes nuclear translocation of NRF2 as we found that its expression enhances in nuclear fraction compared to the cytosolic part **(Fig. 7C)**. *In silico* study suggested that the ABCG2 promoter has an NRF2 binding site. Silencing of NRF2, we have found decreased expression of ABCG2 in protein level **(Fig. 7D)** and drug effluxing population in

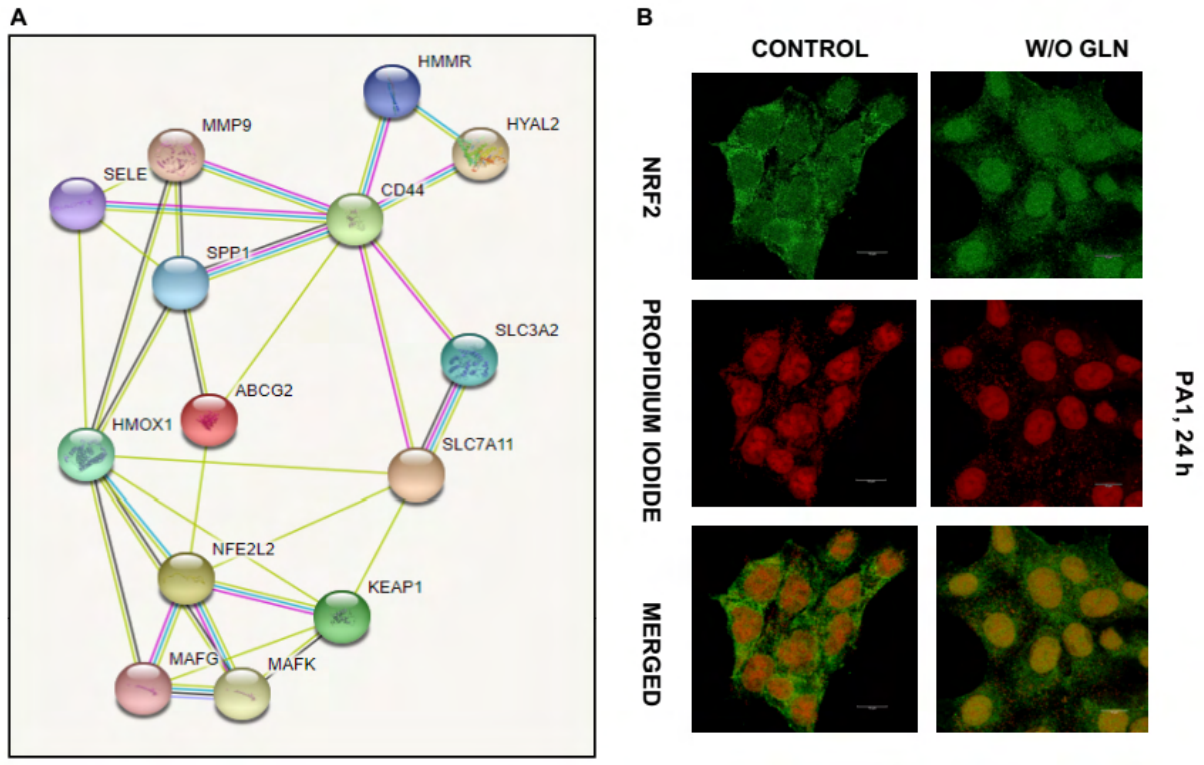

glutamine

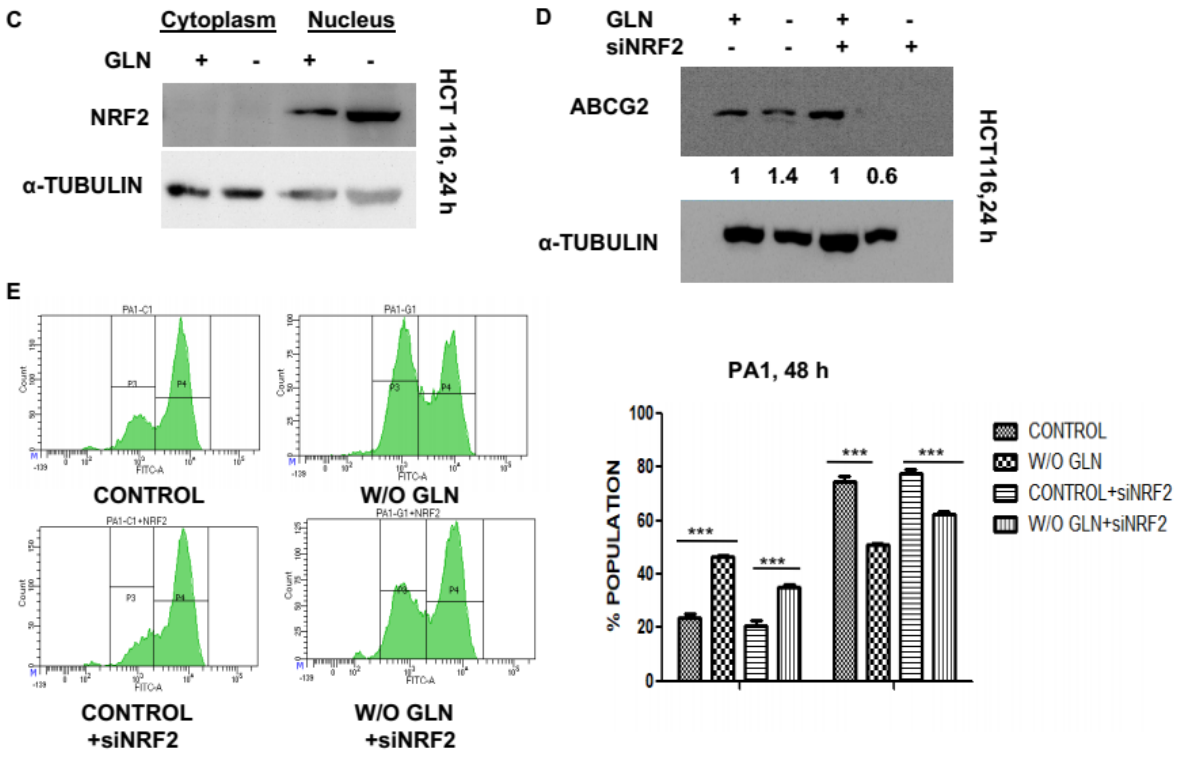

Figure 7: NRF2 mediates chemoresistance in glutamine limiting condition: (A) String analysis revealed the interaction among NRF2, xCT, and ABCG2. (B) Confocal microscopic images depicted the accumulation of NRF2 in the nucleus under glutamine deprivation. (C) NRF2 increased in the nuclear fraction of HCT116 upon glutamine deprivation. (D) siNRF2 prevents the enhancement of ABCG2 expression in glutamine-deprived conditions in PA1. (E) Rhodamine dye efflux assay depicted that siNRF2 reduced drug effluxing population in PA1. The statistical significance was analyzed and represented as NS for non-significant,*p<0.05, **p<0.01, ***p<0.001. Scale bar 10 µm (B).

restricted condition **(Fig. 7E)**. These data suggested that NRF2 is another factor regulating stemness and chemoresistance in glutamine-free conditions.

A small molecule pharmacological inhibitor of glutaminase, L-DON can exert similar effects like glutamine starvation

In the recent era, glutaminase is one of the promising targets to block cancer progression. Various glutaminase inhibitors like L-DON, BPTES, Compound 968, CB-839 are used to inhibit glutamine usage by the cells. Therefore, these inhibitors imitate a situation of glutamine starvation in cancer cells. We found that phosphorylation of DRP1 (S616) was significantly enhanced by L-DON treatment **(Fig. 8A)**. Similarly, it increases mitochondrial fragmentation **(Fig. 8B)**. We have also checked the extracellular acidification rate (ECAR) after L-DON treatment and found that it is elevated like glutamine starved condition **(Fig. 8C-D)**. In addition,

it can also enhance the expression of SOX2 in PA1 **(Fig. 8E)**. Altogether, our study reveals that L-DON promotes a similar effect to glutamine deprivation in cancer.

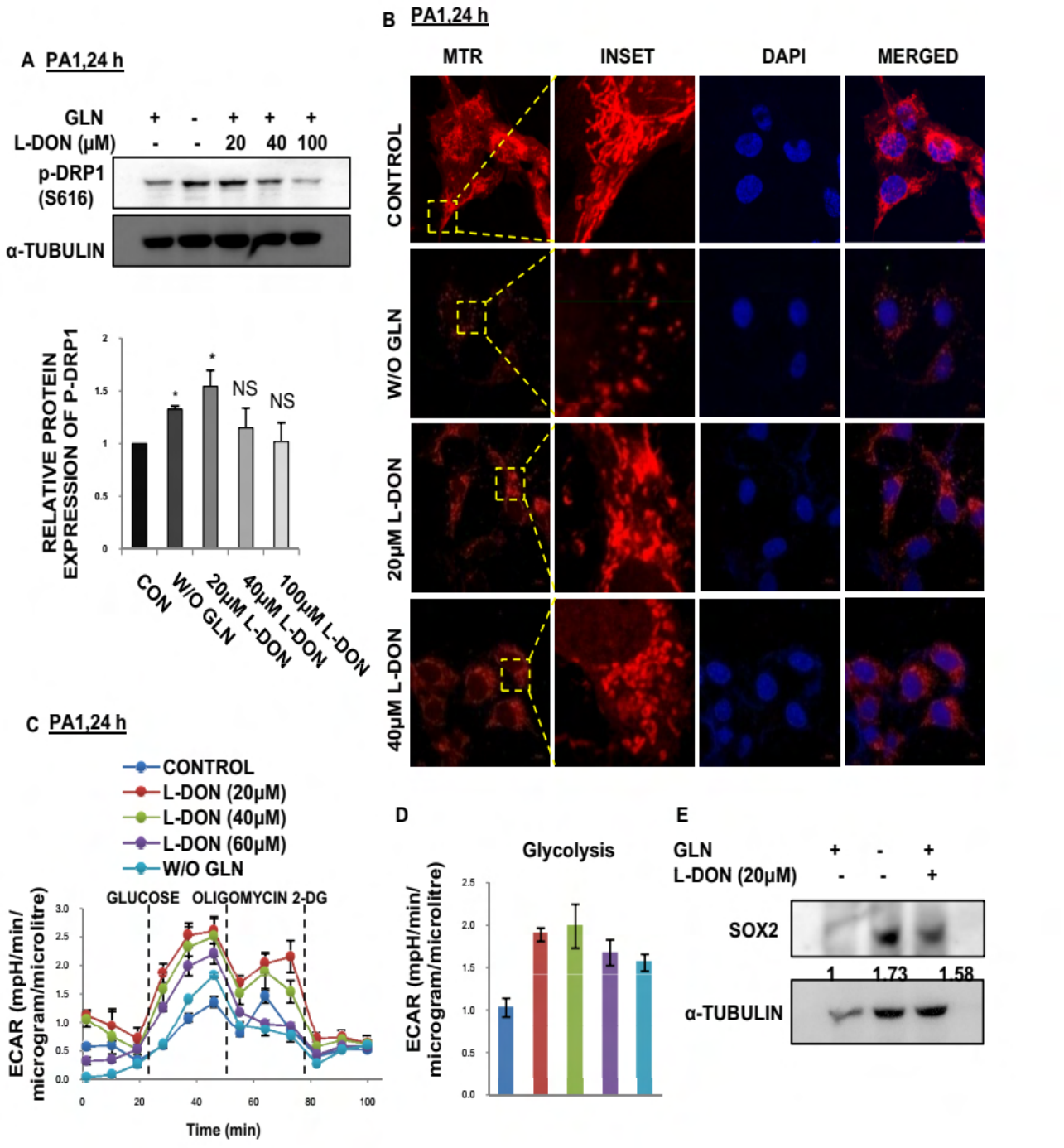

Figure 8: L-DON exerts a similar effect like glutamine deprivation in cancer: (A) p-DRP1 enhanced upon L-DON treatment in control media in PA1. (B) Mitochondrial fragmentation occurred in L-DON treated conditions in PA1. (C-D) ECAR and glycolysis were also enhanced upon L-DON treatment as happened in

glutamine deprivation. (E) L-DON promotes the elevation of SOX2 in PA1. The statistical significance was analyzed and represented as NS for non-significant,*p<0.05, **p<0.01, ***p<0.001. Scale bar 10 µm (B).

Combination therapy of L-DON and MDiVi-1 together can combat stemness and chemoresistance in cancer

As L-DON enhances the CSC population in tumors and MDiVi-1 can reduce this population, therefore, we tried the combination therapy of L-DON and MDiVi-1 to rescue tumor cells from becoming chemoresistant. Most interestingly, we observed that dual treatment of L-DON and MDiVi-1 promotes apoptosis in the cancer cell (PA1), while the minimal effect was found in normal cells (IOSE-385) **(Fig. 9A)**. Further, to establish the results in *in-vivo*, we investigated in syngeneic mice model (C57BL/6) using ID8 (mouse ovarian epithelial cancer cell) cells. To validate the effect of MDiVi-1 in glutamine starved condition, we injected it with or without

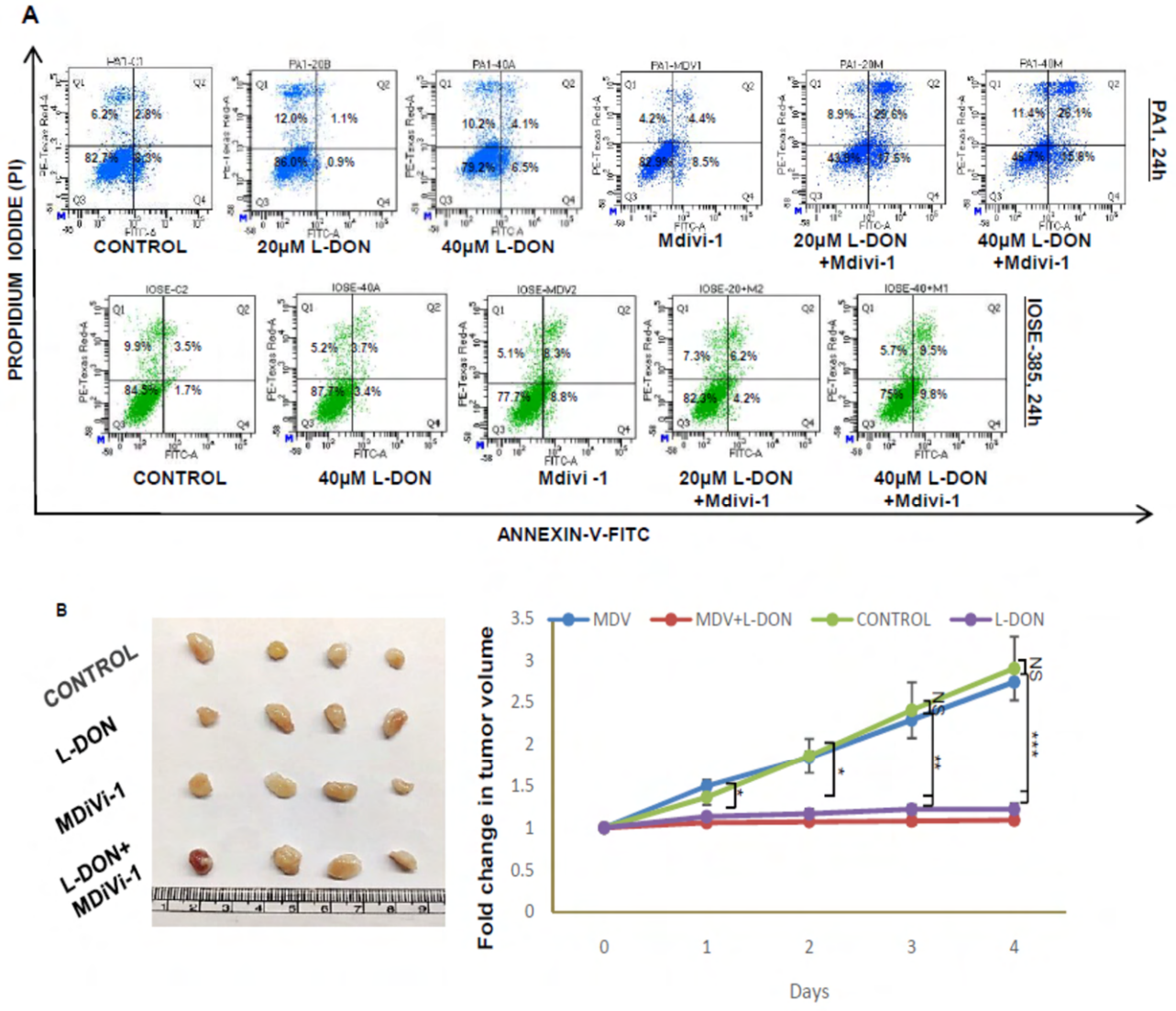

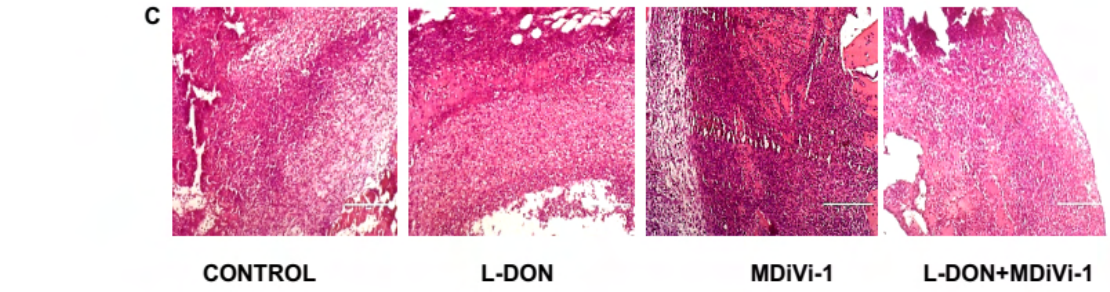
C
CONTROL
L-DON
MDiVi-1
L-DON+MDiVi-1

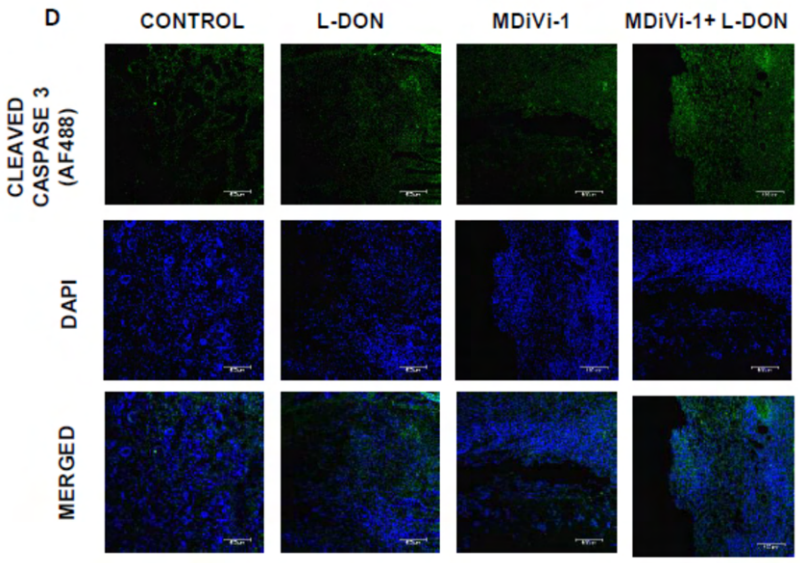
D
CONTROL
L-DON
MDiVi-1
MDiVi-1+ L-DON
CLEAVED CASPASE 3 (AF488)
DAPI
MERGED

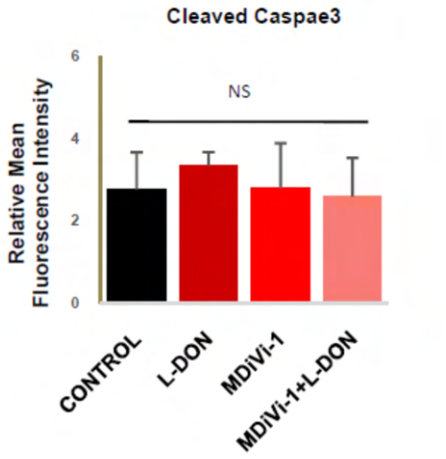
Cleaved Caspae3
Relative Mean Fluorescence Intensity
NS
6
4
2
0
CONTROL
L-DON
MDiVi-1
MDiVi-1+L-DON

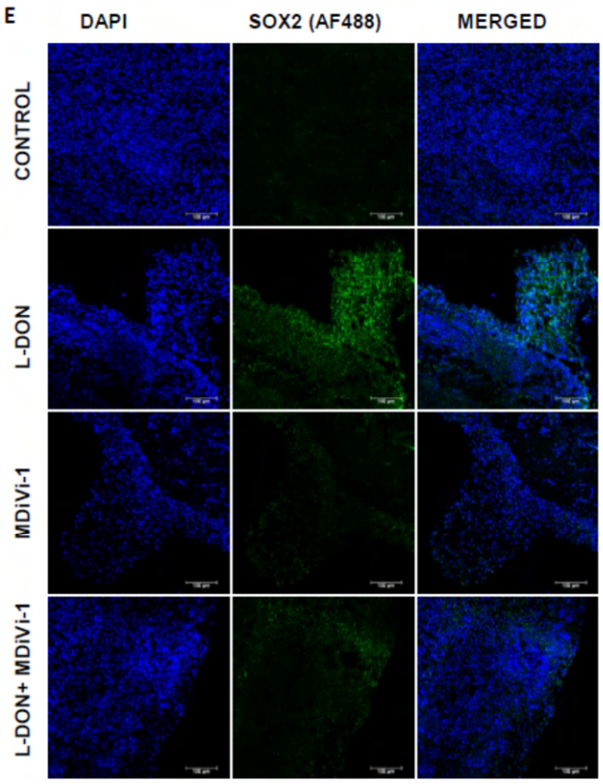
E
DAPI
SOX2 (AF488)
MERGED
CONTROL
L-DON
MDiVi-1
L-DON+ MDiVi-1

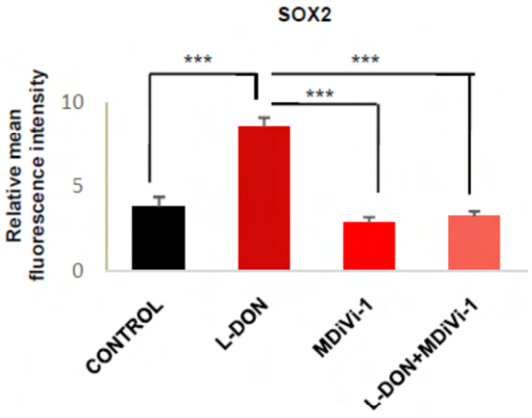
SOX2
Relative mean fluorescence intensity
***
***
***
10
5
0
CONTROL
L-DON
MDiVi-1
L-DON+MDiVi-1

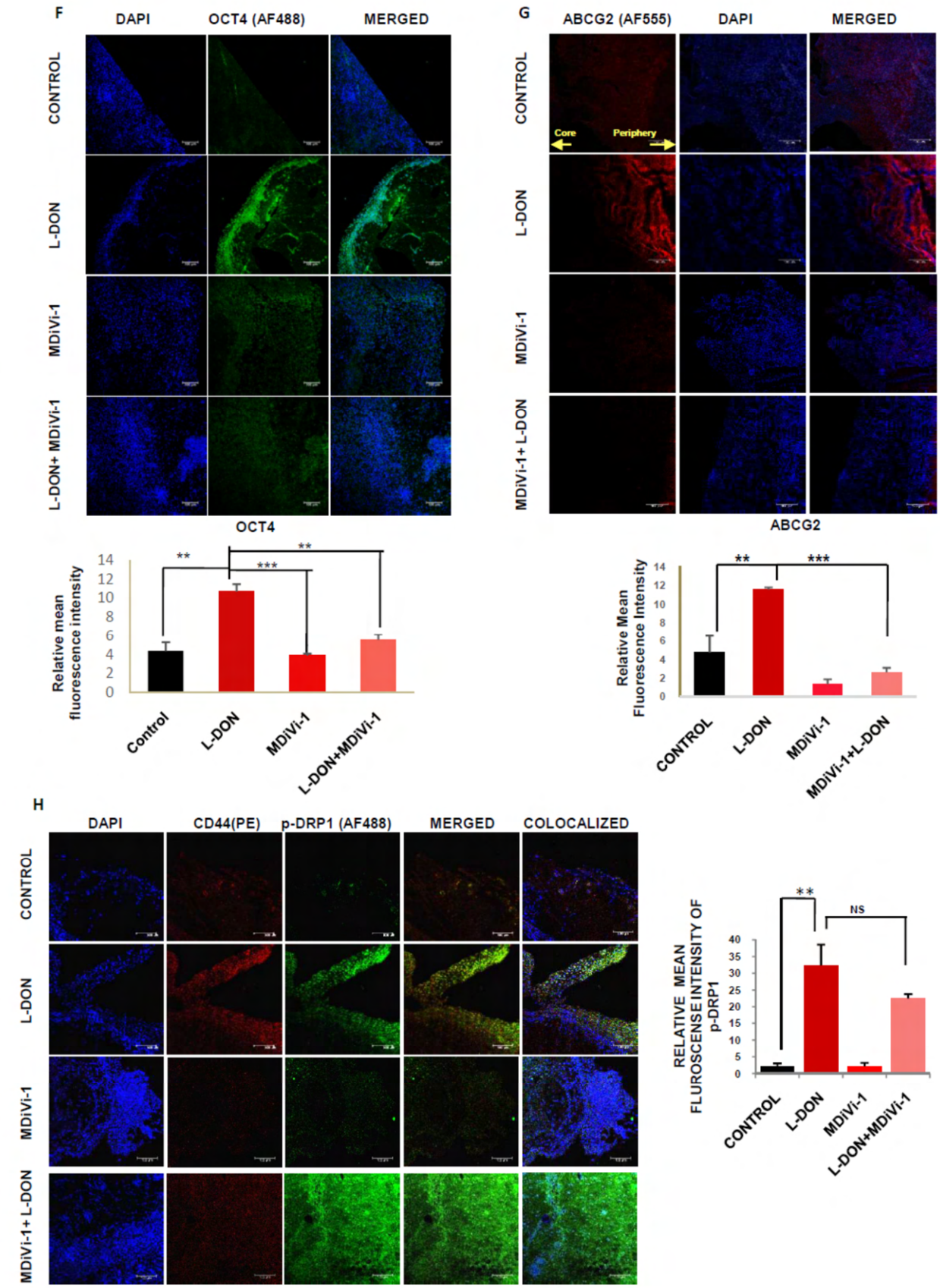
F
DAPI
OCT4 (AF488)
MERGED
CONTROL
L-DON
MDiVi-1
L-DON+ MDiVi-1
OCT4
Relative mean fluorescence intensity
Control
L-DON
MDiVi-1
L-DON+MDiVi-1
G
ABCG2 (AF555)
DAPI
MERGED
Core
Periphery
MDiVi-1+ L-DON
ABCG2
Relative Mean Fluorescence Intensity
CONTROL
MDiVi-1+L-DON
H
CD44(PE)
p-DRP1 (AF488)
COLOCALIZED
RELATIVE MEAN FLUROSCENSE INTENSITY OF p-DRP1
NS
L-DON+MDiVi-1

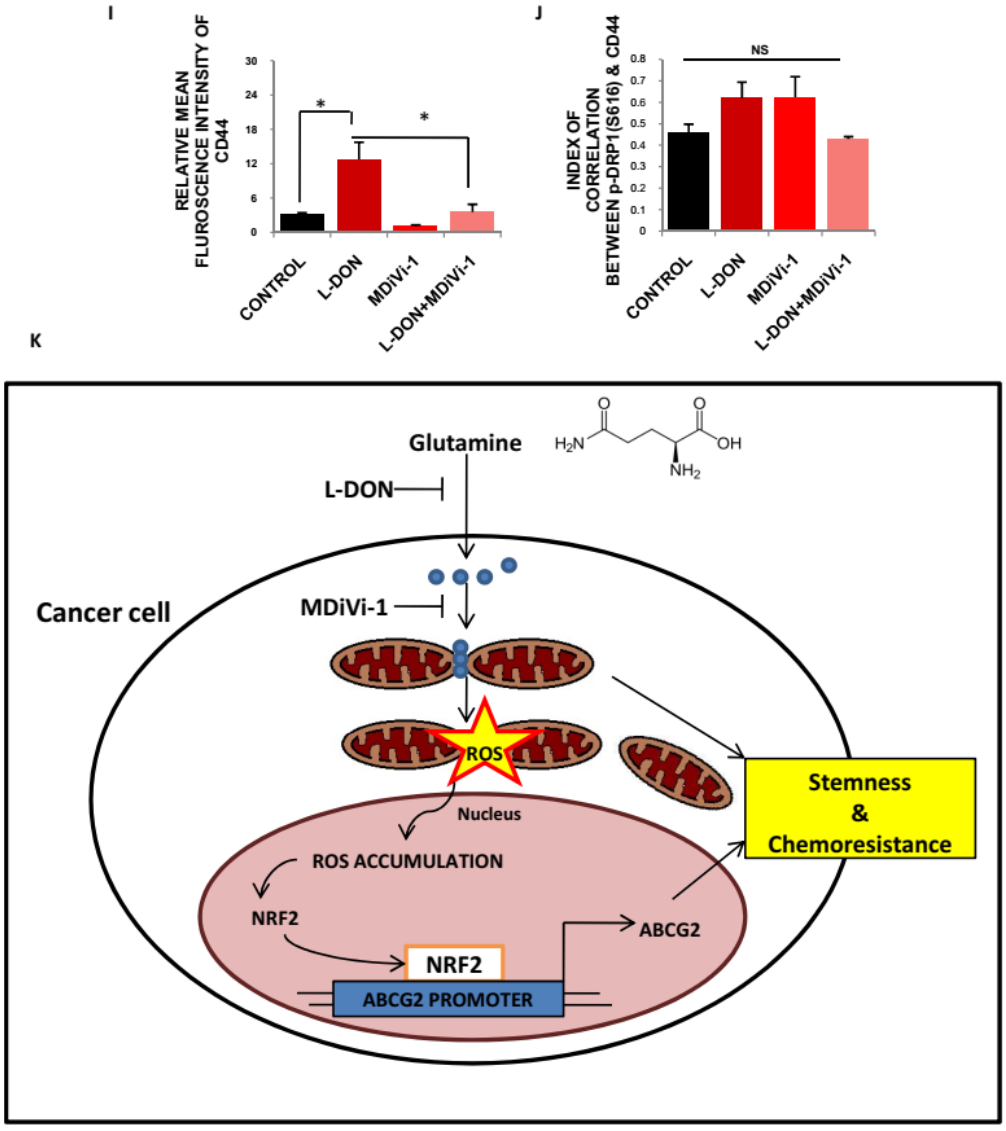

Figure 9: Dual treatment of L-DON and MDiVi-1 reduce the burden of cancer stem cells. (A) Annexin-V/ PI assay depicted that dual treatment of L-DON and MDiVi-1 can kill the cancer cells without affecting normal ovarian cells. (B) Tumor volume remained unchanged in L-DON treated and L-DON+MDiVi-1 treated condition in mice model and represented in the line graph. (C) Hematoxylin and eosin staining was done in tumor sections. (D) Expression of cleaved caspase3 remained unaltered in different treatments and represented in bar diagram. (E-G) SOX2, OCT4, and ABCG2 were enhanced in L-DON treated conditions whereas L-DON+MDiVi-1 reduces those expressions in the tumor. (H-J) p-DRP1 and CD44 expression and colocalization were enhanced upon L-DON treatment with concomitant decrease in L-DON+MDiVi-1 treated condition in the tumor. (K) The schematic diagram depicted that glutamine deprivation promotes stemness and chemoresistance by regulating DRP1 phosphorylation in cancer. The statistical significance was analysed and represented as NS for non-significant,*p<0.05, **p<0.01, ***p<0.001. Scale bar 400 µm (C), 100 µm (D,E, F, G, H).

L-DON in 100 mm^3 tumor-bearing mice consecutively for 3 days, whereas the animals of the control set were injected with an equal volume of PBS **(Fig. 9B)**. L-DON treatment even in presence of MDiVi-1 significantly inhibitor tumor growth, however, MDiVi-1 was alone unable to stall cancer cell proliferation. A similar result was observed in histological sections with hematoxylin and eosin staining, which depicted that lower number of cells are present in tumor core in both L-DON treatment and L-DON +MDiVI-1 treatment **(Fig. 9C)**. We did not observe any change in the expression of caspase-9, which suggested that L-DON+MDiVi-1 treatment cannot promote apoptosis in the mice **(Fig. 9D)**. There was increased expression of OCT4, SOX2, and ABCG2 after L-DON treatment that was significantly reduced by MDiVi-1 in the *in-vivo* model **(Fig. 9E-G).** L-DON-treated tumors showed increased DRP1 phosphorylation (S616) and CD44 expression along with increased co-localization of these proteins, while dual treatment of L-DON and MDiVi-1 significantly reduced the CD44 expression **(Fig. 9H-J)**. These data give us a sneak that pharmacological inhibition of GLS1 and mitochondrial fission simultaneously inhibit tumor growth with a reduction in the CSC population **(Fig. 9K)**.

Discussion

Addiction to glutamine is one of the features of growing tumor cells and this incident is utilized for diagnosis purposes using 18F-Gln in PET scanning (Venneti et al., 2015). It is well reported that tumor core regions are glutamine deficient and glutamine deficiency causes dedifferentiation of tumor cells (Pan et al., 2016; Vaupel et al., 1989). We have depicted that stemness and chemoresistance property imparted through phosphorylation of DRP1 in glutamine deprived conditions in cancer.

Deregulated mitochondrial dynamics is associated with cancer and we found that glutamine deficiency enhances stemness properties along with mitochondrial fragmentation. The level of p-DRP1 (S616) was increased with enrichment of shorter mitochondria (<2µm) upon glutamine deprivation. A similar result was observed in the spheroids formed in glutamine deficiency. DRP1 is responsible for promoting stemness features in various cancer (Cai et al., 2016; Peiris-Pagès et al., 2018). Considering these reports, we have also found that phosphorylation of DRP1 induces mitochondrial fragmentation and stemness property under glutamine deprivation. Fragmented mitochondria are localized around the nucleus and this perinuclear localization is one of the attributes of CSCs. DRP1 inhibition using MDiVi-1 blocked retrograde transport of mitochondria and also inhibits stemness properties. Additionally, we found reduced expression of ABCG2 upon inhibition of mitochondrial movement by microtubule inhibitor, nocodazole in glutamine starvation in cancer. Therefore, we suggested mitochondrial fragmentation and its localization is important to regulate stem-like features in cancer.

ROS is an important factor in mitochondrial fragmentation and the generation of stemness in cancer (Hu et al., 2019). It is designated as a 'double-edged sward' as it promotes tumorigenesis and stemness (Chatterjee and Chatterjee, 2020). xCT is responsible for maintaining ROS in cancer cells and it colocalizes with CD44 (Guo et al., 2011). As we found enhanced expression and colocalization of CD44 and xCT, therefore we hypothesized that xCT may be responsible for regulating ROS, mitochondrial fragmentation, and stemness in glutamine-deprived conditions. However, we did not get any change in total and mitochondrial ROS upon silencing xCT in glutamine starved condition. These results indicated that xCT is not involved in regulating ROS under glutamine-limiting conditions. By confocal microscopy, we observed that ROS accumulation occurs in the nucleus. We suggested that the perinuclear localization of mitochondria is responsible for nuclear ROS accumulation. It is reported that nuclear ROS accumulation triggered the various gene expression of transcription factors through guanidine oxidation (Al-Mehdi et al., 2012). In string analysis, we analyzed that CD44, xCT, ABCG2 has interaction with one of the transcription factor NRF2. Various reports suggested that NRF2 has a role in regulating chemoresistance through ABCG2 (No et al., 2014). We have also found that there is enhanced NRF2 level in nuclease in glutamine deprived condition and upon its silencing, the level of ABCG2 and drug effluxing population decreased. Therefore, we can conclude that DRP1 driven mitochondrial fragmentation and localization promote stemness and chemoresistance through activation of NRF2 in cancer.

Recently, glutaminolysis is targeted therapeutically to reduce tumor growth and combat cancer. Combination therapy of glutaminase inhibitor along with inhibitor for specific signaling pathway reduces tumor proliferation (Jin et al., 2016; Matés et al., 2020). We found that glutaminase inhibitor, L-DON imitated glutamine deprived condition in cancer cell line and mice tumor model. Though it kills cancer cells in *in vitro* cell line , however, it inhibits tumor growth without altering cell survival in mice tumor model. However, L-DON increased the expression of stemness markers SOX2, OCT4, NANOG in tumors which is significantly reduced by combination treatment of L-DON and MDiVi-1. It is already reported that MDiVi-1 has been used to reduce CSCs population (Peiris-Pagès et al., 2018). Therefore, dual treatment of L-DON and MDiVi-1 can reduce CSCs burden and halt tumor growth, which can be a promising approach for diagnostic purposes.

CHAPTER 3

ROLE OF GLUTAMINE METABOLISM REGULATORY FACTOR, SIRT4 IN REPRESSION OF EMT IN OVARIAN CANCER

Introduction:

Besides stemness and chemoresistance, EMT and metastasis are other major problems associated with ovarian cancer progression. Through EMT, epithelial cells lose their apical-basal polarity and they become mesenchymal which facilitates cancer cells migration to the secondary organ (Valastyan and Weinberg, 2011).

Metabolic reprogramming is involved in the regulation of EMT and cancer progression (Sun and Yang, 2020). Glutamine dependency increases with cancer aggressiveness. In contrast, glutamine depletion facilitates EMT in pancreatic cancer cells (Recouvreux et al., 2020). Glutamate is produced through glutaminolysis and it acts as a signaling molecule to promote invasion in the breast cancer cell (Dornier et al., 2017). Glutaminolysis is facilitated by two enzymatic steps: in Step1, glutaminase (GLS) converts glutamine to glutamate and in Step2, glutamate is converted into α-ketoglutarate through glutamate dehydrogenase (GDH). Highly invasive ovarian cancer cells are glutamine-dependent through STAT3 signaling (Yang et al., 2014). Glutamine metabolism is regulated through various factors in cancer. mTORC1 is the master regulator of glutamine metabolism or glutaminolysis. Glutamine can activate mTORC1 whereas it can regulate glutaminolysis. Therefore, its activity depends on the nutrient availability and status of accessory factors. In an exchange with leucine and glutamine, mTORC1 is activated on the lysosome (Altman et al., 2016). On the contrary, mTORC1 regulates glutaminolysis through repressing the activity of SIRT4 (Csibi et al., 2013a).

SIRT4, the least characterized protein in the SIRT family, which has ADP-ribosyltransferase activity is involved in ribosylation of glutamate dehydrogenase (GDH) and therefore represses its activity. GDH maintain cellular redox homeostasis in cell and thereby SIRT4 is linked with cellular redox balance (Jin et al., 2015). SIRT4 represses cancer progression by regulating glutamine metabolism in colorectal and breast cancer (Du et al., 2020; Miyo et al., 2015). Being a mitochondrial protein SIRT4 is also a negative controller of glycolysis. In pancreatic cancer, UHRF1 is an upstream regulator of SIRT4, and its promotes proliferation and aerobic glycolysis by repressing SIRT4 (Hu et al., 2019). It also blocks tumor progression by inhibiting the ERK-DRP1 pathway and mitochondrial fusion in non-small lung cancer (Fu et al., 2017).

Considering these background studies, firstly, we focused on the role of glutaminolysis in regulating EMT in ovarian cancer cells. Secondly, we wanted to decipher the function of the regulator of glutaminolysis such as mTORC1 and SIRT4 in glutamine-deprived conditions. Moreover, we investigated the effect of SIRT4 in the progression of EMT and deciphered the mechanism behind it in OC.

Results:

Glutaminolysis regulates the EMT process in ovarian cancer cells

It is reported that glutamine deprivation regulates EMT and migration in ovarian cancer cells (Prasad and Roy, 2021). We want to decipher whether solely glutamine is responsible for this regulation or the by-product of glutaminolysis may have a role in facilitating EMT in OC. Firstly, we observed that the expression of a mesenchymal marker, N-cadherin was decreased upon glutamine deprivation, however, supplementation of the by-product of glutaminolysis such as glutamate (GLU) and α-ketoglutarate (α-KG) can restore the expression of this protein in PA1 cells **(Fig. 1A)**. The opposite result was observed in the expression level of the epithelial marker, E-cadherin **(Fig. 1B)**. Similarly, in western blot analysis, the expression of vimentin and N-cadherin were downregulated in glutamine starved conditions. Again, the addition of glutamate

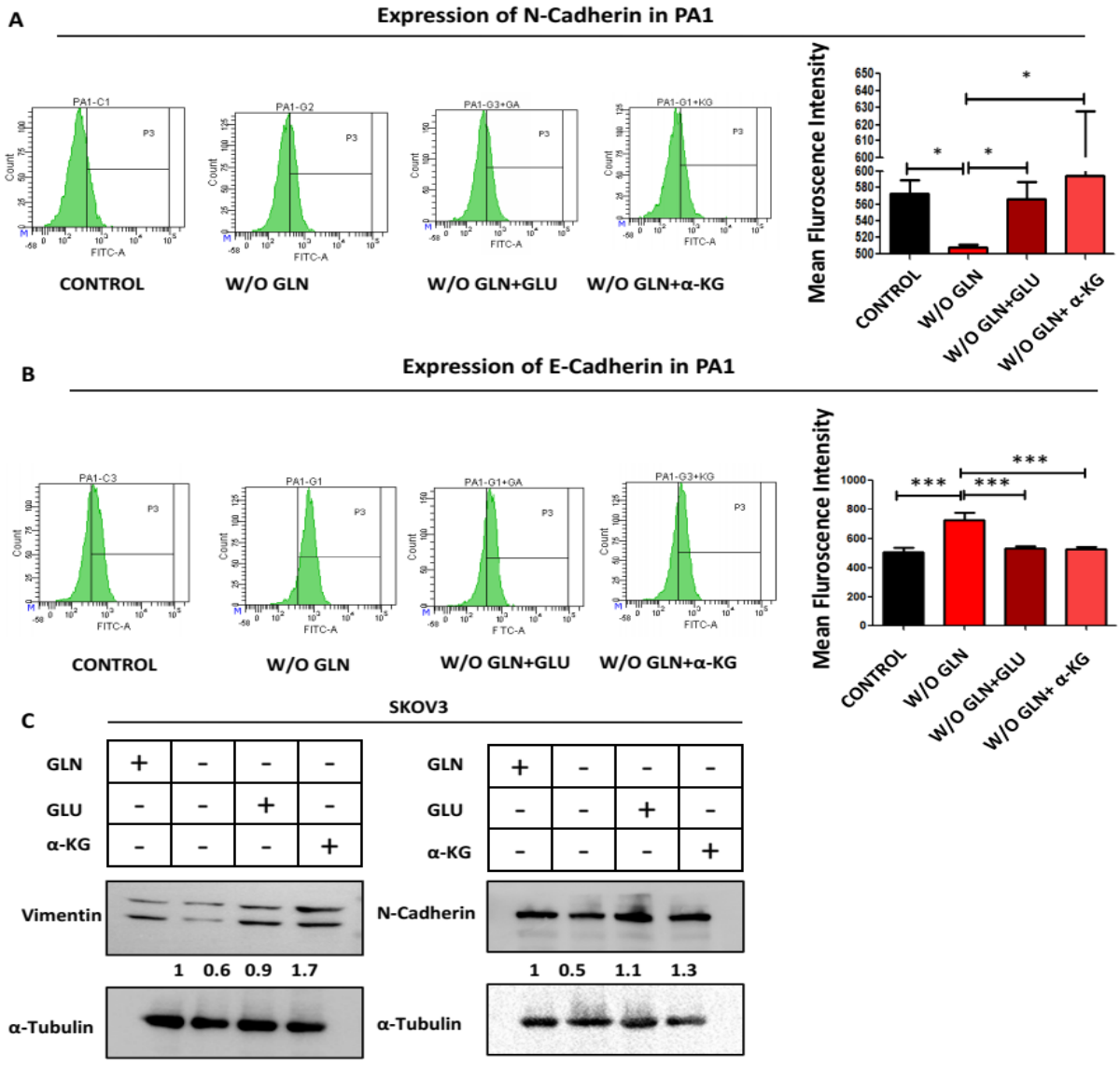

Figure 1: EMT is regulated by glutaminolysis in OC cells. (A, B) Expression of N-cadherin and E-cadherin was checked through flow cytometric analysis and data was represented in both histogram and bar diagram in PA1 cells at 48 h. (C) Expression of vimentin and N-cadherin was decreased upon glutamine deprivation as observed in western blot analysis in SKOV3 at 48 h. The statistical significance was calculated and represented as NS for non-significant,*p<0.05, **p<0.01, ***p<0.001.

and α-ketoglutarate in glutamine-deprived media enhanced those proteins' expression in SKOV3 cells **(Fig. 1C).** These results depicted that not only glutamine but also by-product of glutaminolysis are responsible for promoting EMT in OC cells.

Glutamine deprivation regulates the mTORC1-p70S6K signaling axis in ovarian cancer

The cross-talk between glutamine and mTORC1 is bidirectional. In absence of glutamine, cancer cells depend upon arginine through p53-associated transcriptional regulation and increased cell proliferation by activation of mTORC1 (Lowman et al., 2019). In contrast, it is reported that mTORC1 also regulates glutaminolysis through SIRT4 in cancer (Csibi et al., 2013). Considering these, we focused on the link between glutamine and mTORC1 signaling in OC. In confocal microscopy, upon glutamine deprivation, we did not find a significant change in the expression of p-mTORC1 (S2448) which localizes on the lysosome upon activation in PA1 cells **(Fig. 2A)**. However, the expression of p-p70S6K (T389) was decreased in glutamine starved

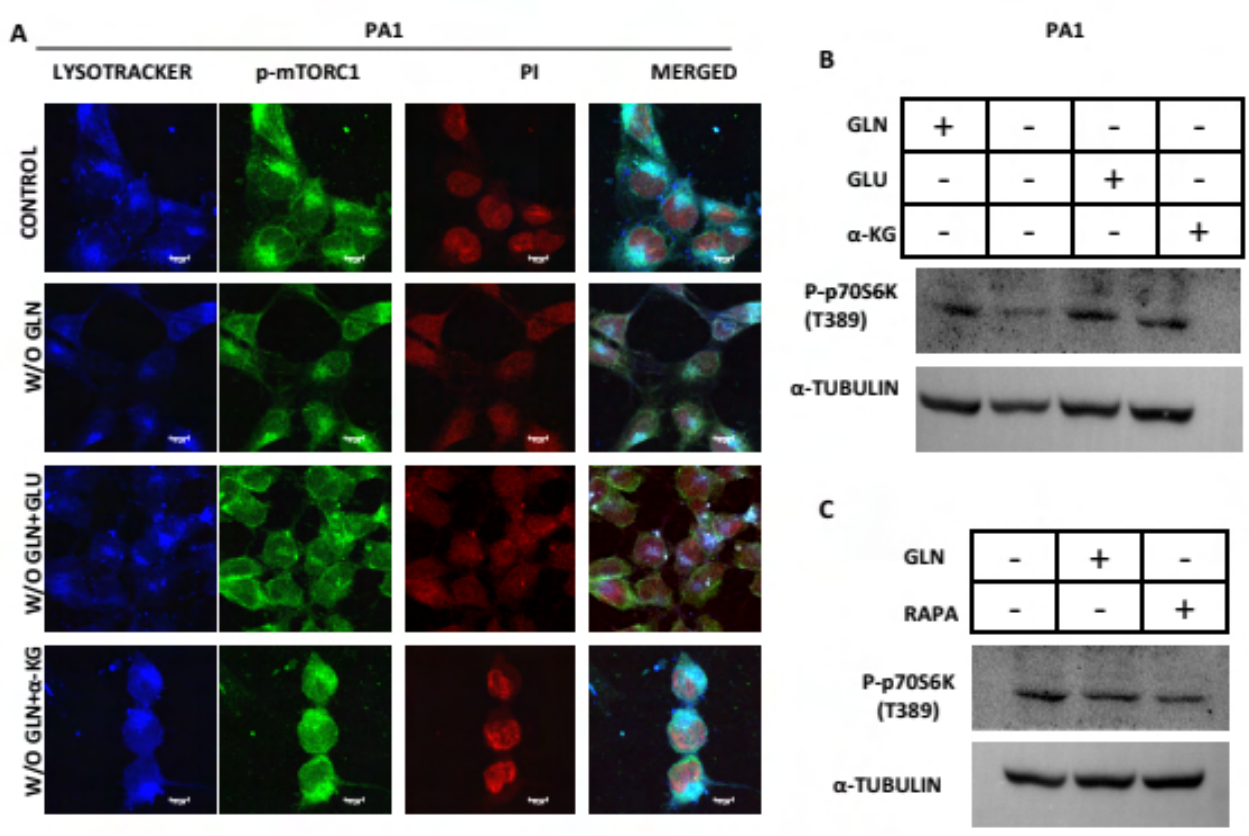

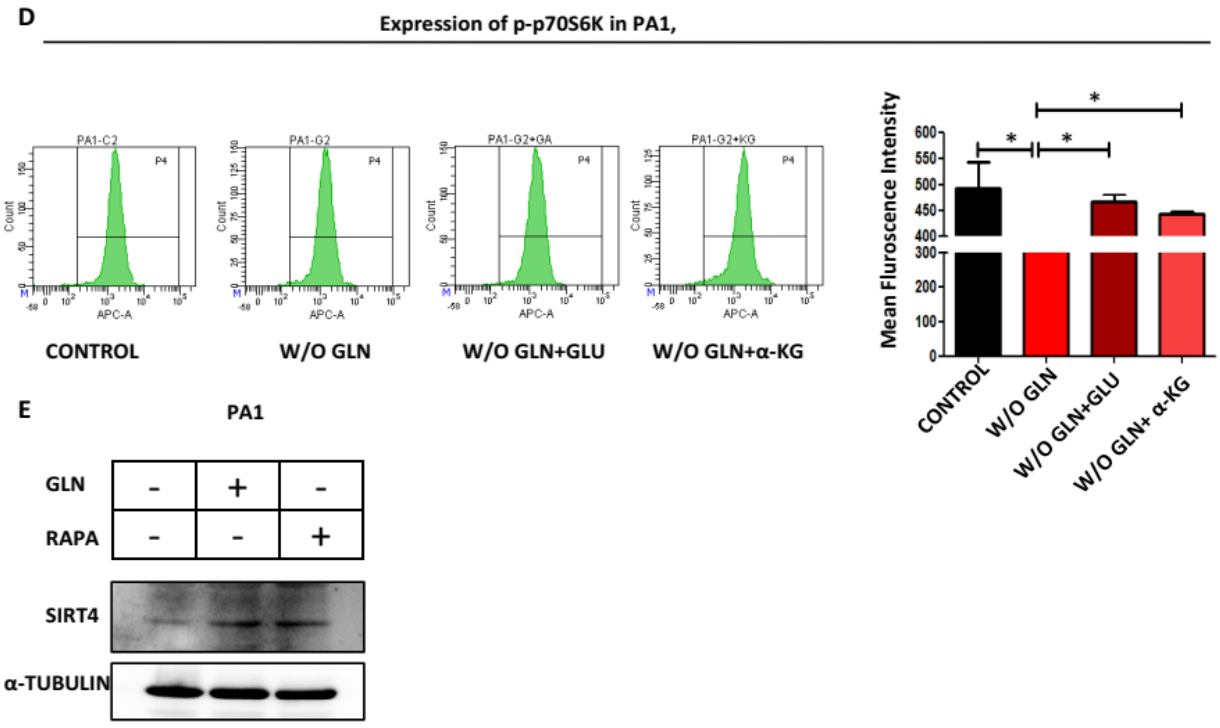

Figure 2: Glutaminolysis regulates mTORC1 and SIRT4 in OC. (A) In immunofluorescence confocal microscopy, expression of p- mTORC1 was checked along with lysosome in PA1 under 48 h of glutamine deprived condition along with the addition of glutamate and α-ketoglutarate. (B) p-p70S6K (T389) was downregulated upon glutamine staved state and the effect was reverted upon supplementation of glutamate and α-ketoglutarate in PA1 at 48 h. (C) Rapamycin (RAPA) treatment in glutamine deprived condition, expression of p-p70S6K (T389) again decreased compared to without Rapa treated condition in PA1. (D) In flow cytometric analysis, also depicted the expression of p-p70S6K (T389) in PA1. (E) Expression of SIRT4 was checked upon glutamine deprived condition along with RAPA in PA1. The statistical significance was calculated and represented as NS for non-significant, *p<0.05, **p<0.01, ***p<0.001. Scale bar 10 µm (A).

condition and this effect was again back to normal upon glutamate and α-ketoglutarate treatment **(Fig. 2B)**. Additionally, rapamycin (RAPA) treatment in glutamine-deprived conditions again downregulates the expression of p-p70S6K (Thr389) compare to only glutamine-deprived cells **(Fig. 2C).** Similar results were observed in flow cytometric analysis **(Fig. 2D).** Therefore, it indicated that glutamine deprivation downregulates mTORC1 signaling and glutaminolysis is responsible for regulating this activation in OC cells. It is already mentioned that mTORC1 regulates glutaminolysis through repressing SIRT4 expression in cancer (Csibi et al., 2013). We checked the expression of SIRT4 and found that it was increased upon glutamine limiting condition in PA1 **(Fig. 2E)**. These results indicated that the by-products of glutaminolysis have role in promoting mTORC1-SIRT4 signaling in OC.

Role of SIRT4 in repressing EMT in ovarian cancer

Glutaminolysis is regulated by SIRT4 as it repressed the activity of GDH by ADP-ribosylation activity (Haigis et al., 2006). It is already reported that SIRT4 acts as a tumor suppressor in pancreatic, colon, and breast cancer (Jeong et al., 2013). Human protein atlas reports also suggested that SIRT4 expression is very low in ovarian cancer. Therefore, we wanted to validate the expression of SIRT4 and focused on the role of glutaminolysis regulating factor to promote EMT in OC. We checked this result through IHC and observed that SIRT4 expression is very less in ovarian cancer tissue compared to normal ovarian tissue **(Fig. 3A)**. SIRT4 is upregulated when it was transiently transfected in PA1 but the expression of vimentin was significantly reduced **(Fig. 3B)**. In both confocal microscopy and flow cytometric analysis, the expression of N-cadherin was decreased in PA1, whereas, the concomitant increase was observed in the expression of E-cadherin upon overexpression of SIRT4 **(Fig. 3C, D)**. A similar result was obtained in the expression of N-cadherin through flow cytometric analysis **(Fig. 3E).** Phalloidin-labeled F-actin was predominantly organized in control cells compared to SIRT4 overexpressed PA1 cells **(Fig. 3F)**. Altogether, it was observed that SIRT4 acts as an antagonist in PA1 cells.

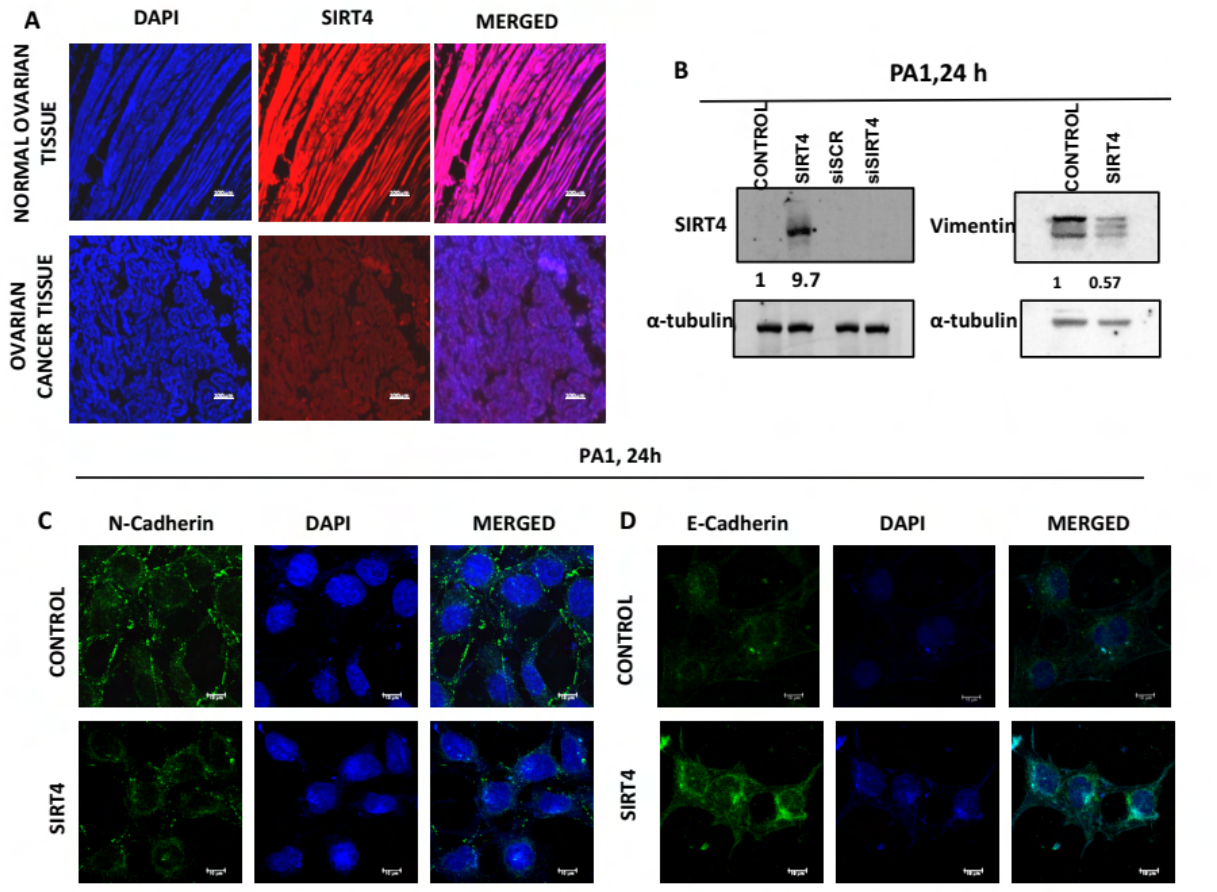

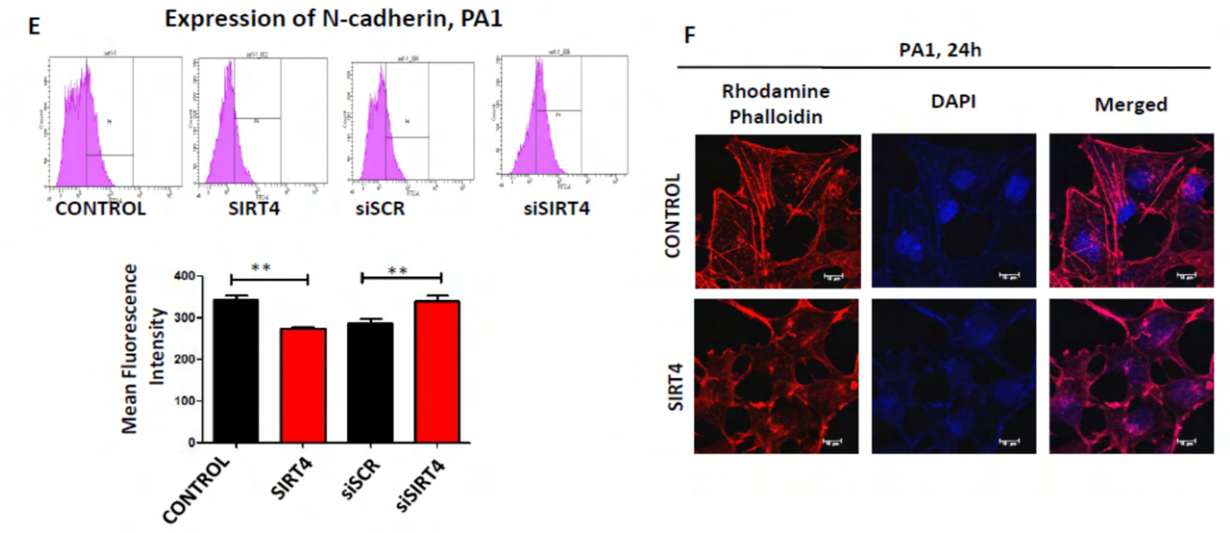

Figure 3: SIRT4 regulates EMT in OC. (A) Expression of SIRT4 in the human ovarian cancer tissue sample. (B) Transient transfection of SIRT4 leads to its overexpression and expression of Vimentin was observed through western blot analysis in PA1. (C, D) Expression of N-cadherin and E-cadherin were observed in PA1 through immunofluorescence microscopy. (E) Expression of N-cadherin was observed through flow cytometric analysis in PA1. (F) Phalloidin-stained F-actin was visualized through confocal microscopy in PA1. The statistical significance was analyzed and represented as NS for non-significant,*p<0.05, **p<0.01, ***p<0.001. Scale bar 100 µm (A), 10 µm (C, D, F).

Mitochondrial ROS regulates EMT via HIF1α expression upon SIRT4 overexpression in ovarian cancer

As SIRT4 is a mitochondrial resident protein, we, therefore, focused on the effect of SIRT4 on mitochondrial function and dynamics. We found that mitochondrial membrane potential decreased in SIRT4 overexpressed cells and increased during its silencing in PA1 **(Fig. 4A)**. SIRT4 inhibits GDH activity and therefore regulates cellular redox balance. Therefore, we investigated the mitochondrial ROS amount using mitosoxRed dye. It has been found that mitochondrial ROS was reduced upon SIRT4 overexpression and the opposite effect was observed upon its silencing **(Fig. 4B)**. Altogether, from these results, it was evident that SIRT4 regulates mitochondrial activity in ovarian cancer cells.

ROS is an important factor for promoting cell migration and EMT. ROS-mediated EMT occurs through the activation of HIF1α (Tam et al., 2020). To establish the pathway, we observed that HIF1α was decreased in SIRT4 overexpressed condition as observed through flow cytometry in PA1 **(Fig. 4C)**. Similar result was observed in confocal microscopic images **(Fig. 4D)**. Again inhibiting HIF1α, expression of N-cadherin was reduced compared to only SIRT4 overexpressed cells **(Fig. 4E).** In addition, the HIF1α inhibitor reduced the expression of Vimentin in the SIRT4 silenced condition in PA1 **(Fig. 4F)**. Therefore, SIRT4 attenuates EMT through repressing HIF1α expression in OC.

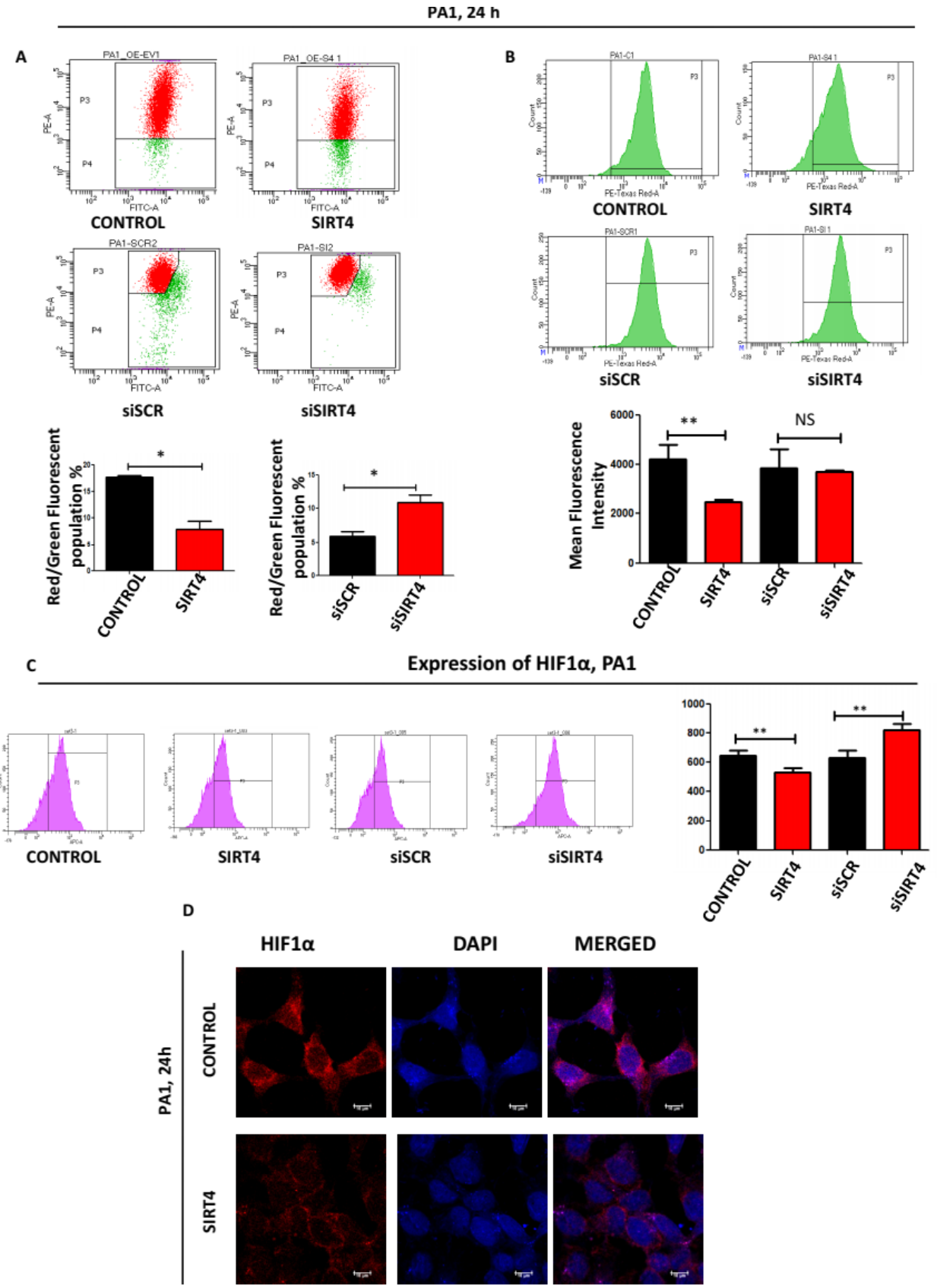
PA1, 24 h
A
CONTROL
SIRT4
siSCR
siSIRT4
Red/Green Fluorescent population %
B
Mean Fluorescence Intensity
**
NS
C
Expression of HIF1α, PA1
D
HIF1α
DAPI
MERGED
PA1, 24h
CONTROL
SIRT4

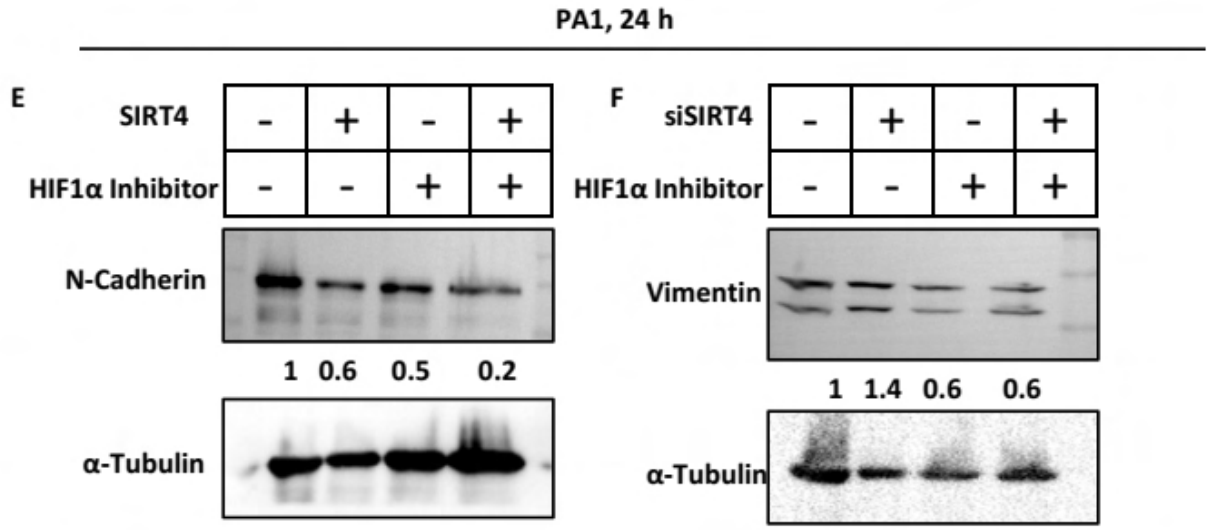

Figure 4: SIRT4 regulates mitochondrial function and EMT in cancer. (A) JC-1 dye was used to check membrane potential in PA1 upon SIRT4 overexpression and silencing. (B) The amount of mitochondrial ROS was measured using mitosox Red dye through flow cytometry in PA1 after overexpressing and silencing SIRT4. (C) Expression of HIF1α decreased upon SIRT4 overexpression as observed through flow cytometric analysis in PA1. (D) In confocal microscopy, nuclear translocation of HIF1α was not observed in PA1, however, treatment of HIF1α inhibitor reduces the expression of N-cadherin for the only SIRT4 transfected cells in PA1 (E). (F) Vimentin expression was checked in western blot analysis in PA1. The statistical significance was calculated and represented as NS for non-significant,*p<0.05, **p<0.01, ***p<0.001. Scale bar 10 µm (D).

Discussion:

Glutamine can promote EMT through the regulation of a transcription factor ETS1 in ovarian cancer. Under glutamine-deprived conditions, ETS1 was translocated into the nucleus through which it orchestrated signaling to promote the migration of OC cells (Prasad and Roy, 2021). However, we found that glutamine is not only responsible for EMT progression, but also the by-product of glutaminolysis is involved to promote EMT. Under the glutamine-deprived condition, EMT markers were reduced, but supplementation of glutamate and α-KG can rescue the cells and facilitate EMT in OC. It suggested that glutamine along with glutamate and α-KG are involved in promoting EMT in OC.

To find out the main regulator of glutaminolysis-induced EMT, we focused on the status of mTORC1 and its downstream effectors. It is reported that glutamine promotes proliferation through mTOR/S6K signaling in OC (Yuan et al., 2015). Additionally, glutamine deprivation also induced cancer cells proliferation by enhancing arginine uptake and enhancing mTORC1 signaling (Lowman et al., 2019). However, we found that glutamine deprivation downregulates phosphorylation of p70S6K at Thr389, which is a downstream target of mTORC1. Glutamate and α-KG can again abrogate the expression of p- p70S6K and inhibiting mTORC1 by rapamycin alter the expression of p- p70S6K.

Therefore, glutamine deprivation represses mTORC1 activation in OC whereas glutaminolysis stimulates its activation. Reports suggested that mTORC1 regulates GDH activity through SIRT4-associated ADP-ribosylation and promotes cancer cell proliferation through mTORC1 activation. We found that SIRT4 increased upon glutamine deprivation which suggested that as mTORC1 activation was hampered, therefore it cannot repress the expression of SIRT4. As SIRT4 regulates glutamine metabolism by inhibiting GDH activity, therefore under glutamine-deprived conditions, SIRT4 again reduces the utilization of glutamine in the TCA cycle. Therefore, it may be an adaptive feature of cancer cells in glutamine starved conditions.

To link glutaminolysis, SIRT4 and EMT, we focused on the role of SIRT4 in promoting EMT in OC. In most cancer cells, SIRT4 acts as a tumor suppresser. In ovarian cancer tissue, it is low expressive compared to the normal ovarian tissue. Therefore, ovarian cancer has a tumor-suppressive function. Under the glutamine-deprived condition, SIRT4 may enhance to reduce cancer cell proliferation, although we have not elucidated this function. SIRT4 attenuated EMT progression in PA1. The effect on PA1 has supported the result observed in human ovarian cancer tissue.

To find out the mechanism behind SIRT4 regulated EMT, we targeted mitochondrial function as SIRT4 is a mitochondrial protein. In non-small lung cancer, SIRT4 inhibits cancer progression by regulating mitochondrial dynamics (Fu et al., 2017). SIRT4 reduced the mitochondrial membrane potential and amount of ROS in PA1. There is a positive co-relation present between mitochondrial membrane potential and mitochondrial ROS generation which was revalidated by our results (Suski et al., 2012). ROS has a role in regulating EMT in various cancer (Wang et al., 2010). ROS regulates various transcription factors to promote EMT and HIF1α is one of them, which facilitate the expression of EMT markers in cancer (Tam et al., 2020). It was observed that ROS regulates HIF1α expression and mediates EMT upon silencing SIRT4 in OC.

Altogether, we suggested that under glutamine-deprived conditions, glutamine deprivation promotes SIRT4 expression and it reduces EMT in OC. Moreover, SIRT4 inhibits ROS production and inhibits ROS-mediated HIF1α expression. Therefore, SIRT4 overexpression hampers the ROS- HIF1α signaling axis to represse EMT in ovarian cancer. Therefore, this mechanism is important for controlling OC promotion.

GENERAL DISCUSSION

Tumor microenvironment (TME) formed with extracellular matrix (ECM), stromal cells (including fibroblasts, adipocyte, mesenchymal, endothelial, and immune cells) (Bighetti-Trevisan et al., 2019). These cells secrete growth factors and metabolites which promote cancer cell proliferation. Chemoresistance property is imparted in the cancer cells through the signaling of various growth factors and metabolites. CSCs acquired some strategies to get rid of the therapeutic condition. Normally, chemotherapeutics reach their target organelle, mostly the nucleus through the bloodstream and kill the cells. However, due to the low pH of the extracellular space of cancer cells, these drugs become charged and cannot enter through diffusion into the nucleus. Additionally, numerous drug-metabolizing enzymes such as cytochrome P450 system (CYP), glutathione-S-transferase (GSH) superfamily, or uridine diphospho-glucuronosyltransferase (UGT), aldehyde dehydrogenase (ALDH) inactivated the chemotherapeutic drugs. CSCs have a high expression of ATP binding cassette (ABC) transporters which efflux out drugs. Therefore, CSCs become chemoresistant (Yeldag and Alistair Rice, 2018).

Epidermal growth factor (EGF), fibroblast growth factor (FGF), platelet-derived growth factor (PDGF), transforming growth factor β (TGFβ) are the main growth factors abundant in the TME and they facilitate cancer progression. EGF promotes chemoresistance to gefitinib through activation of the AKT pathway (Jeannot et al., 2014). Likewise, FGF signaling induces resistance to cytarabine in acute myeloid leukemia cells (Karajannis et al., 2006). Among these growth factors, TGFβ plays a dual role as in some cancer. It acts as a pro-survival factor whereas in several cases it is pro-apoptotic. Its functional activity depends upon the activated signaling pathway, type of cancer cell, and various other factors in TME. In pancreatic cancer, TGF-βRII induces sensitivity to the chemotherapeutic drug, gemcitabine (Xelwa et al., 2021). It also suppresses the early stage of cancer progression. In contrast, TGFβ promotes chemoresistance through activation of pyruvate dehydrogenase kinase 4 (PDK4) in colorectal cancer (Yeldag and Alistair Rice, 2018).

Cancer-associated fibroblasts (CAF) are the main source of TGFβ1, which mediates stemness and chemoresistance. Cancer-associated mesothelial cells also have a role in regulating chemoresistance properties through TGFβ1 signaling in ovarian cancer (Qian et al., 2021). In this cancer, TGFβ1 augments stem-like characteristics through ZEB1-mediated EMT and by regulating the expression of transglutaminase (TG2) (Cao et al., 2012; Mitra et al., 2018). TGFβ promoter hypermethylation also promotes resistance to paclitaxel (Wang et al., 2012). Besides its role in cancer, TGFβ signaling and sonic hedgehog induces PITX2 expression in left-right asymmetry during embryonic development of vertebrate (Shiratori and Hamada, 2014). We have first deciphered the connection between TGFβ1 signaling and PITX2 expression in ovarian cancer and also investigated the mechanism through which PITX2 induces stemness and

chemoresistance. We observed that prolonged incubation with TGFβ1 enhanced the expression of PITX2A/B and to decipher the molecular signaling, we observed that knocking down of SMAD2 downregulates PITX2A/B signaling in TGFβ1-induced condition. Additionally, ERK inhibitors also attenuate TGFβ1 induced PITX2A/B signaling in ovarian cancer. Therefore, TGFβ1-mediated PITX2A/B signaling occurs through SMAD-dependent and ERK-dependent pathways.

Among various bicoid-like homeodomain transcription factors, PITX2A/B is involved both in embryonic development and cancer progression. It plays a significant role in gonadal development in a sexually dimorphic manner (Nandi et al., 2011). It links between asymmetric organ morphogenesis and transient nodal signaling in the left lateral plate mesoderm (l-LPM) (Schweickert et al., 2000). Through the Wnt/β-catenin pathway, PITX2 promotes cancer progression and chemoresistance in different cancer (Hirose et al., 2011; Lee and Thévenod, 2019; Luo et al., 2019). PITX2 also promotes resistance to letrozole via IFNα signaling in breast cancer and it becomes a prognostic marker for breast cancer progression (Aubele et al., 2017; Xu et al., 2019).

In our study, we observed that PITX2 overexpression upregulated the stemness markers and drug efflux transporter such as ABCG2, ABCB1 in OC. It is reported that PITX2 enhances ABCB1, ABCG2 activity through its binding to ABCB1 promoter in colon and kidney cancer cells (Lee and Thévenod, 2019). We depicted that, PITX2A/B also binds to the ABCB1 promoter and augmented its activity in ovarian cancer. We have also focused on metabolic alteration upon PITX2 induction in these cells and found that cells become metabolically less active. Therefore, we suggested that the PITX2 induced change in the metabolic phenomenon may depend upon its stem-like properties in ovarian cancer. Altogether, we highlighted that TGFβ1 induces PITX2 expression via SMAD and ERK-dependent signaling pathways and thereby promotes stemness and chemoresistance properties in ovarian cancer.

Besides deciphering the role of the growth factor to impart stemness and chemoresistance properties, we further studied the role of metabolites in promoting these features in cancer. Among the various metabolic alterations, glutamine dependency is a prominent feature in most cancer cells. Depending upon these features, 18F-FGln is used to diagnose different types of cancer and showed glutamine avidity varies with the differential mutation status (Dunphy et al., 2018). However, there is some limitation in using 18F-FGln due to its availability to targeted organs and the small size of the sample (Venneti et al., 2015). In addition, glutamine metabolism is therapeutically targeted to combat the burden of cancer cells. There are various small molecule inhibitors such as 6-Diazo-5-oxo-L-norleucine (L-DON), Bis-2-(5-phenylacetamido-1,2,4-thiadiazol-2-yl)ethyl sulfide (BPTES), glutaminase inhibitor compound 968, CB-839 which block glutaminolysis (Grinde et al., 2019; Jin et al., 2016).

Tumor cells choose an adaptive mechanism to sustain glutamine limiting conditions. The adaptive mechanism includes *de novo* glutamine synthesis, utilization of other nutrients, signal-mediated cell fate decision, and proteolytic scavenging. Glutamine deprivation in pancreatic ductal adenocarcinoma (PDAC) enhances expression of GOT2 and branched-chain amino acid transaminase (BCAT) which supply other amino acids and nucleotides. Altered amino acid metabolism and nucleotide synthesis are coupled with mTORC1 activation and stabilize GLUL in glutamine limiting conditions (Pei-Yun Tsai et al., 2021). Targeting glutamine metabolism can block both glycolytic and oxidative metabolism in tumor cells, but the effector T cells show high oxidative metabolism. These T cells have enhanced acetate metabolism which fuels the TCA cycle and channel glucose into the PPP pathway and maintain NADPH homeostasis (Leone et al., 2019). Upon glutamine deprivation, p53 is activated by phosphorylation at Ser18, and activated p53 binds to the promoter of the SLC7A3 gene, which is an arginine transporter. p53 induces arginine uptake in glutamine limiting condition and thereby maintain the mTORC1 signaling pathway (Lowman et al., 2019). Asparagine is another amino acid that helps the cancer cell to survive in glutamine-restricted conditions (Jiang et al., 2018). IκB kinase β (IKKβ) is a master regulator of the NF-kβ signaling pathway in cell survival and inflammatory response. In absence of glutamine, IKKβ is activated independently of NF-kβ signaling. It suppresses aerobic glycolysis and lactate production by phosphorylation of 6-phosphofructo-2-kinase/fructose-2,6-biphosphatase isoform 3 (PFKFB3) at Ser269 in glutamine deprived conditions (Reid et al., 2016). PDAC cells uptake extracellular protein by macropinocytosis and degrade by phagocytosis in the lysosome, producing glutamine and other essential amino acids (Kamphorst et al., 2015). The glutamine produced in lysosome is supplied by SNAT7 to cancer to sustain in glutamine deprived conditions (Verdon et al., 2017).

In the tumor core region, there is a deficiency of glutamine and it is reported that regional glutamine deficiency promotes dedifferentiation of cancer (Pan et al., 2016). In our study, we investigated the mechanism through which stemness and chemoresistance properties imparted in glutamine deprived conditions in cancer. We found that glutamine deficiency attenuates cancer cell proliferation and induces stem-like traits and chemoresistance. To find out the mechanism behind these phenomena, we observed that DRP1 is phosphorylated at S616 and this leads to mitochondrial fragmentation in glutamine deprived condition. It is reported that DRP1 phosphorylation promotes chemoresistance properties in cancer (Cai et al., 2016; Peiris-Pagès et al., 2018). Therefore, inhibiting DRP1 by its inhibitor and knocking down by siDRP1, the stem-like properties and drug effluxing capability were decreased in our case also. The perinuclear localization of mitochondria was observed which was one of the features of CSCs. By blocking mitochondrial movement by using microtubule inhibitors, nocodazole, the expression of drug efflux transporter ABCG2 was decreased in glutamine-deprived conditions.

Therefore, we suggest mitochondrial fragmentation and its localization is important to regulate stem-like features in cancer.

ROS play a major role in cancer progression and stemness and also regulate mitochondrial fragmentation in various cancer (Chatterjee and Chatterjee, 2020; Hu et al., 2019) Glutathione is responsible for scavenging intracellular ROS and xCT is responsible for glutathione synthesis as it transports cysteine into the cell. Therefore, xCT is linked with cellular ROS and its colocalization is observed with CD44 (Guo et al., 2011). We observed that colocalization of CD44 and xCT enhanced glutamine deprivation in cancer. However, total cellular and mitochondrial ROS remain unchanged upon silencing xCT in glutamine-deprived conditions. In contrast, ROS accumulated in the nucleus in glutamine limiting conditions. This nuclear ROS accumulation occurred due to the perinuclear localization of mitochondria. Nuclear ROS can activate various transcription factors through guanidine oxidation (Al-Mehdi et al., 2012). One of the transcription factors, NRF2 is responsible for regulating ROS and is enhanced in the nucleus in glutamine starved conditions. NRF2 has also a role in promoting chemoresistance via upregulating the expression of ABCG2 (No et al., 2014). We have also found that the expression of ABCG2 and the drug effluxing population were reduced upon silencing NRF2 in glutamine-limiting conditions. Therefore, we can conclude that DRP1 driven mitochondrial fragmentation and localization promote stemness and chemoresistance. In addition, NRF2 also play role in promoting stemness and chemoresistance upon glutamine deprivation.

We then focused on the strategy to reduce these stem cell populations generated in the glutamine-deprived condition. As monotherapy is not enough to combat cancer cells, dual targeting or combinatorial therapy is gaining interest that includes the metabolic pathway modulators. Alone CB-839 can reduce OXPHOS and has a synergistic effect with the BCL2 inhibitor ABT-199, showing high anti-proliferative activity in acute myeloid leukemia (Jacque et al., 2015). Combination therapy of BPTES and NOTCH1 inhibitor can impair the growth of T-cell acute lymphoblastic leukemia cells (Herranz et al., 2015). Similarly, BPTES along with metformin can significantly suppress tumor growth compared to monotherapy of BPTES or metformin (Elgogary et al., 2016). In the mouse non-small cell lung carcinoma (NSCLC) xenograft model, dual targeting using CB-839 and erlotinib induces autophagy to suppress cancer proliferation (Momcilovic et al., 2017). Similarly, CB-839 along with paclitaxel exhibit higher antiproliferative activity in xenograft models of triple-negative breast cancer (TNBC) cell lines. Metformin has GLS1 inhibiting activity and accumulates ammonium in hepatic encephalopathy in type 2 diabetic patients. The efficacy of the neo-adjuvant chemotherapeutic drug, cisplatin can be increased with the association of metformin in cancer (Matés et al., 2020).

We investigated that glutaminase inhibitor, L-DON imitated glutamine deprived condition in cancer cell line and mice tumor model. Though it kills cancer cells in *in vitro* system, in mice tumor model it inhibits tumor growth without altering cell survival. However, L-DON increased the expression of stemness markers SOX2, OCT4, NANOG in the tumor which is significantly reduced by the combination treatment of L-DON and MDiVi-1. It is already reported that MDiVi-1 has been used to reduce CSCs population (Peiris-Pagès et al., 2018). Therefore, dual treatment of L-DON and MDiVi-1 can reduce CSCs burden and halt tumor growth, which can be a promising approach for diagnostic purposes.

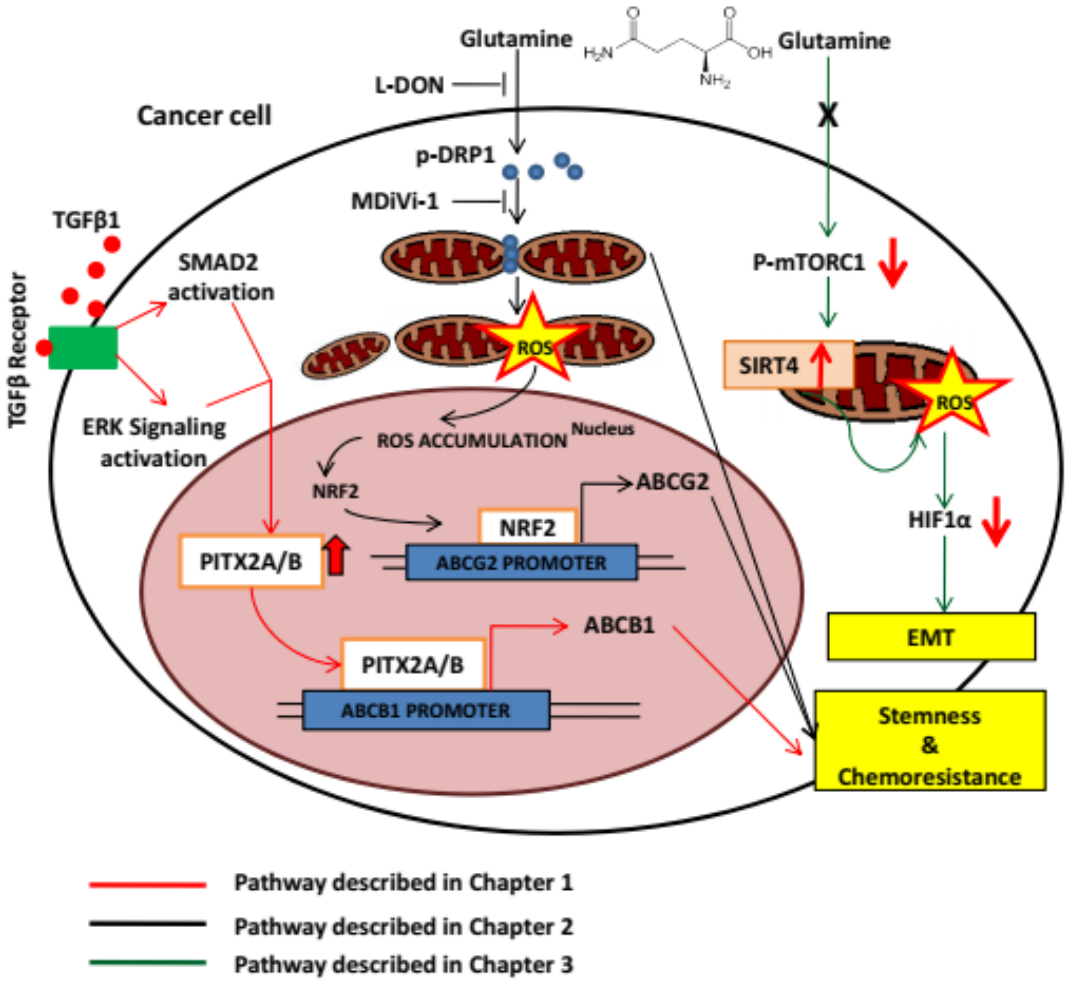

Figure 1: Schematic diagram depicted the three mechanistic pathways which regulate EMT, stemness and chemoresistance in cancer.

Along with the development of stemness and chemoresistance, glutamine deprivation also inhibits EMT and cancer metastasis (Prasad and Roy, 2021). Glutaminolysis is required for EMT in OC cells. As glutaminolysis is regulated by various factors such as c-MYC, KRAS, HIF1α, p53, SIRT4 in cancer. We observed that EMT was attenuated under glutamine depleted conditions and the addition of glutamate and α-KG can counteract the inhibition. Therefore we wanted to

decipher the mechanism and relation between glutaminolysis and EMT in OC. Upon glutamine deprivation, phosphorylation of mTORC1 at S2448 was hampered which in turn enhances the expression of SIRT4. As it is already reported that mTORC1 represses SIRT4 function, followed by enhanced GDH activity. Therefore, our study revalidated that glutamine deprivation suppresses EMT by regulating mTORC1 mediated SIRT4 expression. Moreover, we have investigated the sole function of SIRT4 in regulating EMT in ovarian cancer. Silencing of SIRT4 promotes mitochondrial ROS in OC. It is reported that ROS regulates HIF1α to promote EMT and by inhibiting HIF1α in SIRT4 silenced condition stalls EMT progression in OC. Therefore, we deciphered that glutamine deprivation inhibits EMT progression through regulating mTORC1 and SIRT4 expression in OC. Moreover, SIRT4 attenuates EMT through ROS-dependent regulation of HIF1α in OC.

Therefore, we concluded that two pathways were identified through which stemness and chemoresistance induce cancer cells. One of the pathways is TGFβ1-induced PITX2 signaling that enhances ABCB1 expression, followed by chemoresistance in the ovarian cancer cell. In the second pathway, we showed that chemoresistance was driven by glutamine depletion in the tumor cell. Glutamine deficiency enhances DRP1 phosphorylation through which fragmented mitochondria are localized in a perinuclear fashion. This mitochondrial localization enhances nuclear ROS that activates NRF2 which induces chemoresistance in cancer. Further, glutamine metabolism is regulated through SIRT4 which inhibits GDH activity. SIRT4 regulates EMT through maintaining redox balance and metabolism in ovarian cancer.

The major problem of ovarian cancers is the recurrence where the acquisition of chemoresistance by the tumor cells. In the present study, the role of various factors of the TME is associated with metabolic alteration in cancer cells and the mechanism of stemness/ chemoresistance induction has been investigated. We have highlighted the association of metabolic alteration by different factors with the induction of stemness properties in tumor cells. Considering the importance of the issues, the present study would help in understanding the disease and the information might help in identifying metabolic modulators as therapeutics in the future.

SUMMARY

The major problem associated with cancer is chemoresistance and metastasis; and we have focused on the molecular mechanism behind these problems. Therefore, the key findings associated with our study are:

1. TGFβ1 promotes PITX2A/B expression in ovarian cancer cells, besides their role in embryonic development.

2. The TGFβ1-PITX2 signaling axis occurs through SMAD and ERK activation in OC cells.

3. PITX2A/B enhances the expression of stemness markers and promotes chemoresistance in OC.

4. PITX2A/B overexpression downregulates glycolysis and oxidative phosphorylation, moreover cells become metabolically inactive.

5. TGFβ1-PITX2 promotes chemoresistance by binding of PITX2A/B to the ABCB1 promoter and enhances its expression in OC.

6. Tumor core regions are deprived of glutamine and stem cells are abundant in this region. We have found that glutamine deprivation promotes stemness and chemoresistance in OC cells and colorectal cancer cells.

7. Under glutamine deprived condition, p-DRP1 (S616) is responsible for mitochondrial fragmentation and fragmented mitochondria localized around nucleaus. The perinuclear localization is observed in cancer stem cells.

8. Perinuclear localization of fragmented mitochondria induces nuclear ROS accumulation in glutamine-deprived conditions. Though, total cellular and mitochondrial ROS remain unaltered in this condition. This ROS may be responsible for promoting stemness and chemoresistance in cancer.

9. NRF2 is enriched in the nucleus and enhances the expression of ABCG2 and drug effluxing capacity upon glutamine deprivation. Altogether, glutamine deprivation promotes stem-like features and chemoresistance through DRP1 phosphorylation at Ser616 and NRF2 activation in cancer.

10. Glutaminease inhibitor, L-DON treatment blocks cancer cell proliferation, but enhances the stem-like properties. It mimics the glutamine-deprived condition in cancer.

11. To reduce both tumor proliferation and stem-like properties, combined treatment of L-DON and DRP1 Inhibitor, MDiVi-1 effectively function in this scenario *in vivo* mice model. Therefore,

targeting both glutaminolysis and DRP1 phosphorylation can reduce the burden of cancer stem cells in the tumor.

12. Glutaminolysis also regulates EMT and cell migration in ovarian cancer. EMT markers are reduced upon glutamine deprivation; however, the addition of the product of glutaminolysis can restore this phenomenon in OC.

13. Glutamine deprivation leads to reduce mTORC1 which represses SIRT4 expression . Therefore, SIRT4 was enhanced in glutamine limiting condition.

14. SIRT4 reduces mitochondrial membrane potential and mitochondrial ROS in PA1. By regulating ROS production, SIRT4 represses EMT progression through ROS-HIF1α signaling in OC.

Altogether, we identified glutamine as a regulator of cancer stemness and attenuated EMT in ovarian cancer. In addition, the TGFβ-PITX2 signaling axis is also involved in the regulation of stem-like features and chemoresistance. Moreover, we proposed a therapeutic strategy to rescue cancer cell proliferation and reduce the stem cell population.

BIBLIOGRAPHY

A

Akhurst, R.J., and Hata, A. (2012). Targeting the TGF β signaling pathway in disease. Nat. Rev. Drug Discov. *11*.

Al-Mehdi, A.B., Pastukh, V.M., Swiger, B.M., Reed, D.J., Patel, M.R., Bardwell, G.C., Pastukh, V. V., Alexeyev, M.F., and Gillespie, M.N. (2012). Perinuclear mitochondrial clustering creates an oxidant-rich nuclear domain required for hypoxia-induced transcription. Sci. Signal. *5*, 1–10

Altman, B.J., Stine, Z.E., and Dang, C. V. (2016). From Krebs to clinic: Glutamine metabolism to cancer therapy. Nat. Rev. Cancer *16*, 619–634.

Aponte, P.M., and Caicedo, A. (2017). Stemness in cancer: Stem cells, cancer stem cells, and their microenvironment. Stem Cells Int. *2017*.

Aubele, M., Schmitt, M., Napieralski, R., Paepke, S., Ettl, J., Absmaier, M., Magdolen, V., Martens, J., Foekens, J.A., Wilhelm, O.G., et al. (2017). The Predictive Value of PITX2 DNA Methylation for High-Risk Breast Cancer Therapy : Current Guidelines, Medical Needs, and Challenges. Hindawi Dis. Markers *2017*.

B

Basu, M., and Roy, S.S. (2013). Wnt/β-catenin pathway is regulated by PITX2 homeodomain protein and thus contributes to the proliferation of human ovarian adenocarcinoma cell, SKOV-3. J. Biol. Chem. *288*, 4355–4367.

Basu, M., Bhattacharya, R., Ray, U., Mukhopadhyay, S., Chatterjee, U., and Roy, S.S. (2015). Invasion of ovarian cancer cells is induced byPITX2-mediated activation of TGF-β and Activin-A. Mol. Cancer *14*, 1–15.

Bellomo, C., Caja, L., and Moustakas, A. (2016). Transforming growth factor β as regulator of cancer stemness and metastasis. Br. J. Cancer *115*, 761–769.

Bhutia, Y.D., and Ganapathy, V. (2016). Glutamine transporters in mammalian cells and their functions in physiology and cancer. Biochim. Biophys. Acta - Mol. Cell Res. *1863*, 2531–2539.

Bhattacharya, R., Ray Chaudhuri, S., and Roy, S.S. (2018). FGF9-induced ovarian cancer cell invasion involves VEGF-A/VEGFR2 augmentation by virtue of ETS1 upregulation and metabolic reprogramming. J. Cell. Biochem. *119*, 8174–8189.

Bighetti-Trevisan, R.L., Sousa, L.O., Castilho, R.M., and Almeida, L.O. (2019). Cancer Stem Cells: Powerful Targets to Improve Current Anticancer Therapeutics. Stem Cells Int. *2019*.

Bosenko, D. V, and Semina, E. V (2005). Characterization of New Isoforms of Human PITX2 Gene and Expression of PITX Genes in Human Tissues . Invest. Ophthalmol. Vis. Sci. *46*, 43.

Brandon Faubert, Ashley Solmonson, R.J.D. (2020). Metabolic reprogramming and cancer progression. *152*, 1–10.

Burgos-ojeda, D., Rueda, B.R., and Buckanovich, R.J. (2012). Ovarian Cancer Stem Cell Markers: Prognostic and Therapeutic Implications. Cancer Lett. *322*, 1–7.

C

Cacace, A., Sboarina, M., Vazeille, T., and Sonveaux, P. (2017). Glutamine activates STAT3 to control cancer cell proliferation independently of glutamine metabolism. Oncogene *36*, 2074–2084.

Cai, J., Wang, J., Huang, Y., Wu, H., Xia, T., Xiao, J., Chen, X., Li, H., Qiu, Y., Wang, Y., et al. (2016). ERK / Drp1-dependent mitochondrial fission is involved in the MSC-induced drug resistance of T-cell acute lymphoblastic leukemia cells. Cell Death Dis. *e2459*, 1–11.

Cao, Y., Lin, S.H., Wang, Y., Chin, Y.E., Kang, L., and Mi, J. (2017). Glutamic pyruvate transaminase GPT2 promotes tumorigenesis of breast cancer cells by activating sonic hedgehog signaling. Theranostics *7*, 3021–3033.

Cao, L., Shao, M., Schilder, J., Guise, T., Mohammad, K.S., and Matei, D. (2012). Tissue transglutaminase links TGF-B, epithelial to mesenchymal transition and a stem cell phenotype in ovarian cancer. Oncogene *31*, 2521–2534.

Carafa, V., Altucci, L., and Nebbioso, A. (2019). Dual Tumor Suppressor and Tumor Promoter Action of Sirtuins in Determining Malignant Phenotype. Front. Pharmacol. *10*, 1–14.

Chae, Y.C., and Kim, J.H. (2018). Cancer stem cell metabolism: Target for cancer therapy. BMB Rep. *51*, 319–326.

Chatterjee, R., and Chatterjee, J. (2020).ROS and oncogenesis with special reference to EMT and stemness. Eur. J. Cell Biol. *99*, 151073.

Chen, K., Huang, Y., and Chen, J. (2013). Understanding and targeting cancer stem cells : therapeutic implications and challenges. Acta Pharmacol. Sin. *34*, 732–740.

Chen, W., Wu, J., Shi, W., Zhang, G., Chen, X., Ji, A., Wang, Z., Wu, J., and Jiang, C. (2021). PRRX1 deficiency induces mesenchymal- epithelial transition dependent SLUG / CTNNB1 regulation in hepatocellular carcinoma. Cancer Sci. *112*, 2158–2172.

Chen, Z., Lin, J., Feng, S., and Wang, C. (2019). SIRT4 inhibits the proliferation , migration , and invasion abilities of thyroid cancer cells by inhibiting glutamine metabolism. Onco. Targets. Ther. *12*, 2397–2408.

Craze, M.L., Cheung, H., Jewa, N., Coimbra, N.D.M., Soria, D., El-Ansari, R., Aleskandarany, M.A., Wai Cheng, K., Diez-Rodriguez, M., Nolan, C.C., et al. (2018). MYC regulation of glutamine-

proline regulatory axis is key in luminal B breast cancer. Br. J. Cancer *118*, 258–265.

Csibi, A., Fendt, S.M., Li, C., Poulogiannis, G., Choo, A.Y., Chapski, D.J., Jeong, S.M., Dempsey, J.M., Parkhitko, A., Morrison, T., et al. (2013). The mTORC1 pathway stimulates glutamine metabolism and cell proliferation by repressing SIRT4. Cell *153*, 840–854.

Cui, T.X., Kryczek, I., Zhao, L., Zhao, E., Kuick, R., Roh, M.H., Vatan, L., Szeliga, W., Mao, Y., Thomas, D.G., et al. (2013). Myeloid-derived suppressor cells enhance stemness of cancer cells by inducing microRNA101 and suppressing the corepressor CTBP2. Immunity *39*, 611–621.

D

Demas, D.M., Demo, S., Fallah, Y., Clarke, R., Nephew, K.P., Althouse, S., Sandusky, G., He, W., and Shajahan-Haq, A.N. (2019). Glutamine Metabolism Drives Growth in Advanced Hormone Receptor Positive Breast Cancer. Front. Oncol. *9*, 1–13.

De Francesco, E.M., Sotgia, F., and Lisanti, M.P. (2018). Cancer stem cells (CSCs): Metabolic strategies for their identification and eradication. Biochem. J. *475*, 1611–1634.

Dornier, E., Rabas, N., Mitchell, L., Novo, D., Dhayade, S., Marco, S., MacKay, G., Sumpton, D., Pallares, M., Nixon, C., et al. (2017). Glutaminolysis drives membrane trafficking to promote invasiveness of breast cancer cells. Nat. Commun. *8*, 1–14.

Du, L., Liu, X., Ren, Y., Li, J., Li, P., Jiao, Q., Meng, P., and Wang, F. (2020). Loss of SIRT4 promotes the self-renewal of Breast Cancer Stem Cells. Theranostics *10*, 9458–9476.

Dunphy, M.P.S., Harding, J.J., Venneti, S., Zhang, H., Burnazi, E.M., Bromberg, J., Omuro, A.M., Hsieh, J.J., Mellinghoff, I.K., Staton, K., et al. (2018). In vivo PET assay of tumor glutamine flux and metabolism: In-human trial of 18f-(2S,4R)-4-fluoroglutamine. Radiology 287, 667–675.

E

El Hout, M., Cosialls, E., Mehrpour, M., and Hamaï, A. (2020). Crosstalk between autophagy and metabolic regulation of cancer stem cells. Mol. Cancer *19*, 1–17.

Elgogary, A., Xu, Q., Poore, B., Alt, J., Zimmermann, S.C., Zhao, L., Fu, J., Chen, B., Xia, S., Liu, Y., et al. (2016). Combination therapy with BPTES nanoparticles and metformin targets the metabolic heterogeneity of pancreatic cancer. Proc. Natl. Acad. Sci. *113*, E5328 LP-E5336.

Essner, J.J., Branford, W.W., Zhang, J., and Yost, H.J. (2000). Mesendoderm and left-right brain , heart and gut development are differentially regulated by PITX2 isoforms. Development *127*, 1081–1093.

F

Faguet, G.B. (2015). A brief history of cancer: Age-old milestones underlying our current knowledge database. Int. J. Cancer *136*, 2022–2036.

Fu, L., Dong, Q., He, J., Wang, X., Xing, J., Wang, E., Qiu, X., and Li, Q. (2017). SIRT4 inhibits malignancy progression of NSCLCs , through mitochondrial dynamics mediated by the ERK-Drp1 pathway. Oncogene *36*, 2724–2736.

G

Gaglio, D., Metallo, C.M., Gameiro, P.A., Hiller, K., Danna, L.S., Balestrieri, C., Alberghina, L., Stephanopoulos, G., and Chiaradonna, F. (2011). Oncogenic K-Ras decouples glucose and glutamine metabolism to support cancer cell growth. Mol. Syst. Biol. *7*, 1–15.

Gao, J., Zhu, Y., Nilsson, M., and Sundfeldt, K. (2014). TGF-β isoforms induce EMT independent migration of ovarian cancer cells. Cancer Cell Int. *14*, 1–10.

Georgakopoulos-Soares, I., Chartoumpekis, D. V, Kyriazopoulou, V., and Zaravinos, A. (2020). EMT Factors and Metabolic Pathways in Cancer . Front. Oncol. *10*, 499.

Grinde, M.T., Hilmarsdottir, B., Tunset, H.M., Henriksen, I.M., Kim, J., Haugen, M.H., Rye, M.B., Mælandsmo, G.M., and Moestue, S.A. (2019). Glutamine to proline conversion is associated with response to glutaminase inhibition in breast cancer. Breast Cancer Res. 21, 1–13.

Guo, W., Zhao, Y., Zhang, Z., Tan, N., Zhao, F., Ge, C., Liang, L., Jia, D., Chen, T., Yao, M., et al. (2011). Disruption of xCT inhibits cell growth via the ROS/autophagy pathway in hepatocellular carcinoma. Cancer Lett. *312*, 55–61.

H

Haigis, M.C., Mostoslavsky, R., Haigis, K.M., Fahie, K., Christodoulou, D.C., Murphy, A.J.J., Valenzuela, D.M., Yancopoulos, G.D., Karow, M., Blander, G., et al. (2006). SIRT4 Inhibits Glutamate Dehydrogenase and Opposes the Effects of Calorie Restriction in Pancreatic β Cells. Cell *126*, 941–954.

Han, Y., Zhou, S., Coetzee, S., and Chen, A. (2019). SIRT4 and Its Roles in Energy and Redox Metabolism in Health, Disease and During Exercise . Front. Physiol. *10*, 1006.

Hanahan, D., and Weinberg, R.A. (2011). Hallmarks of cancer: the next generation. Cell *144*, 646–674.

Harris, K.S., Shi, L., Foster, B.M., Mobley, M.E., Elliott, P.L., Song, C.J., Watabe, K., Langefeld,

C.D., and Kerr, B.A. (2021). CD117 / c-kit defines a prostate CSC - like subpopulation driving progression and TKI resistance. Sci. Rep. 1–13.

Hay, N. (2016). Reprogramming glucose metabolism in cancer: can it be exploited for cancer therapy? Nat. Rev. Cancer *16*, 635–649.

Herranz, D., Ambesi-Impiombato, A., Sudderth, J., Sánchez-Martín, M., Belver, L., Tosello, V., Xu, L., Wendorff, A.A., Castillo, M., Haydu, J.E., et al. (2015). Metabolic reprogramming induces resistance to anti-NOTCH1 therapies in T cell acute lymphoblastic leukemia. Nat. Med. *21*, 1182–1189.

Hirose, H., Ishii, H., Mimori, K., Tanaka, F., Takemasa, I., Mizushima, T., Ikeda, M., Yamamoto, H., Sekimoto, M., Doki, Y., et al. (2011). The Significance of PITX2 Overexpression in Human Colorectal Cancer. Ann. Surg. Oncol. *18*, 3005–3012.

Honoré, A.L., Ouimette, J., Lavertu-jolin, M., and Drouin, J. (2010). Pitx2 defines alternate pathways acting through MyoD during limb and somitic myogenesis. Development *137*, 3847–3856.

https://stanfordhealthcare.org/medical-conditions/cancer/cancer/cancer-types.html Cancer Types | Stanford Health Care.

https://www.cancer.net/navigating-cancer-care/diagnosing-cancer/stages-cancer (2021). Stages of Cancer | Cancer.Net.

Https://www.proteinatlas.org/ENSG00000079215-SLC1A3/pathology Expression of SLC1A3 in cancer - Summary - The Human Protein Atlas.

Hu, Q., Qin, Y., Ji, S., Xu, W., Liu, W., Sun, Q., Zhang, Z., Liu, M., Ni, Q., Yu, X., et al. (2019). UHRF1 promotes aerobic glycolysis and proliferation via suppression of SIRT4 in pancreatic cancer. Cancer Lett. *452*, 226–236.

Hu, J., Zhang, Y., Jiang, X., Zhang, H., Gao, Z., Li, Y., Fu, R., and Li, L. (2019). ROS-mediated activation and mitochondrial translocation of CaMKII contributes to Drp1-dependent mitochondrial fission and apoptosis in triple-negative breast cancer cells by isorhamnetin and chloroquine. J. Exp. Clin. Cancer Res. *38*, 1–16.

Huang, Y., and Zhu, G. (2008). PITX2 is overexpressed in human thyroid cancer and functions in cell proliferation. Cancer Res. *68*, LB-166 LP-LB-166.

Hudson, C.D., Savadelis, A., Nagaraj, A.B., Joseph, P., Avril, S., DiFeo, A., and Avril, N. (2016). Altered glutamine metabolism in platinum resistant ovarian cancer. Oncotarget *7*, 41637–41649.

I

Issaq, S.H., Mendoza, A., Fox, S.D., and Helman, L.J. (2019). Glutamine synthetase is necessary for sarcoma adaptation to glutamine deprivation and tumor growth. Oncogenesis *8*, 1–20.

J

Jagust, P., De Luxán-Delgado, B., Parejo-Alonso, B., and Sancho, P. (2019). Metabolism-based therapeutic strategies targeting cancer stem cells. Front. Pharmacol. *10*, 1–26.

Jacque, N., Ronchetti, A.M., Larrue, C., Meunier, G., Birsen, R., Willems, L., Saland, E., Decroocq, J., Maciel, T.T., Lambert, M., et al. (2015). Targeting glutaminolysis has antileukemic activity in acute myeloid leukemia and synergizes with BCL-2 inhibition. Blood *126*, 1346–1356.

Jeannot, V., Busser, B., Brambilla, E., Wislez, M., Robin, B., Cadranel, J., Coll, J.-L., and Hurbin, A. (2014). The PI3K/AKT pathway promotes gefitinib resistance in mutant KRAS lung adenocarcinoma by a deacetylase-dependent mechanism. Int. J. Cancer 134, 2560–2571.

Jeong, S.M., Xiao, C., Finley, L.W.S., Lahusen, T., Souza, A.L., Pierce, K., Li, Y., German, N.J., Xu, X., Li, C., et al. (2013). SIRT4 Has Tumor-Suppressive Activity and Regulates the Cellular Metabolic Response to DNA Damage by Inhibiting Mitochondrial Glutamine Metabolism. 450–463.

Jin, L., Li, D., Alesi, G.N., Fan, J., Kang, H., Lu, Z., Boggon, T.J., Jin, P., and Yi, H. (2015). Glutamate Dehydrogenase 1 Signals through Antioxidant Glutathione Peroxidase 1 to Regulate Redox Homeostasis and Tumor Growth. Cancer Cell *27*, 257–270.

Jin, L., Alesi, G.N., and Kang, S. (2016). Glutaminolysis as a target for cancer therapy. Oncogene *35*, 3619–3625.

Jiang, J., Pavlova, N.N., and Zhang, J. (2018). Asparagine, a critical limiting metabolite during glutamine starvation. Mol. Cell. Oncol. 5, 1–2.

John, B.T. (2003). Interorgan Amino Acid Transport and its Regulation. Am. Soc. Nutr. Sci. 2nd Amin. Acid Work. *133*, 2068–2072.

K

Kamarajan, P., Rajendiran, T.M., Kinchen, J., Bermúdez, M., Danciu, T., and Kapila, Y.L. (2017). Head and Neck Squamous Cell Carcinoma Metabolism Draws on Glutaminolysis, and Stemness Is Specifically Regulated by Glutaminolysis via Aldehyde Dehydrogenase. J. Proteome Res. *16*, 1315–1326.

Kaowinn, S., Seo, E.J., Heo, W., Bae, J.H., Park, E.J., Lee, S., Kim, Y.J., Koh, S.S., Jang, I.H., Shin, D.H., et al. (2019). Cancer upregulated gene 2 (CUG2), a novel oncogene, promotes stemness-like properties via the NPM1-TGF-β signaling axis. Biochem. Biophys. Res. Commun. *514*, 1278–1284.

Kamphorst, J.J., Nofal, M., Commisso, C., Hackett, S.R., Lu, W., Grabocka, E., Vander Heiden,

M.G., Miller, G., Drebin, J.A., Bar-Sagi, D., et al. (2015). Human pancreatic cancer tumors are nutrient poor and tumor cells actively scavenge extracellular protein. Cancer Res. 75, 544–553.

Karajannis, M.A., Vincent, L., DiRenzo, R., Shmelkov, S. V., Zhang, F., Feldman, E.J., Bohlen, P., Zhu, Z., Sun, H., Kussie, P., et al. (2006). Activation of FGFR1β signaling pathway promotes survival, migration and resistance to chemotherapy in acute myeloid leukemia cells. Leukemia 20, 979–986.

Kim, B.N., Ahn, D.H., Kang, N., Yeo, C.D., Kim, Y.K., Lee, K.Y., Kim, T.J., Lee, S.H., Park, M.S., Yim, H.W., et al. (2020). OPEN TGF - β induced EMT and stemness characteristics are associated with epigenetic regulation in lung cancer. Sci. Rep. 1–11.

Klonisch, T., Wiechec, E., Hombach-klonisch, S., Ande, S.R., Wesselborg, S., Schulze-osthoff, K., and Los, M. (2008). Cancer stem cell markers in common cancers – therapeutic implications. Trends Mol. Med. *30*, 1–11.

L

Lee, W., and Chakraborty, P.K. (2013). Pituitary homeobox 2 (PITX2) protects renal cancer cell lines against doxorubicin toxicity by transcriptional activation of the multidrug transporter ABCB1. Int. J. Cancer *133*, 556–568.

Lee, W.K., and Thévenod, F. (2019). Oncogenic PITX2 facilitates tumor cell drug resistance by inverse regulation of hOCT3/SLC22A3 and ABC drug transporters in colon and kidney cancers. Cancer Lett. *449*, 237–251.

Lee, S.Y., Jeon, H.M., Ju, M.K., Jeong, E.K., Kim, C.H., Park, H.G., Han, S.I., and Kang, H.S. (2016). Dlx-2 and glutaminase upregulate epithelial-mesenchymal transition and glycolytic switch. Oncotarget *7*, 7925–7939.

Leone, R.D., Zhao, L., Englert, J.M., Sun, I.M., Oh, M.H., Sun, I.H., Arwood, M.L., Bettencourt, I.A., Patel, C.H., Wen, J., et al. (2019). Glutamine blockade induces divergent metabolic programs to overcome tumor immune evasion. Science (80-.). 366, 1013–1021.

Li, B., Cao, Y., Meng, G., Qian, L., Xu, T., Yan, C., Luo, O., Wang, S., Wei, J., Ding, Y., et al. (2019). Targeting glutaminase 1 attenuates stemness properties in hepatocellular carcinoma by increasing reactive oxygen species and suppressing Wnt/beta-catenin pathway. EBioMedicine *39*, 239–254.

Li, D., Fu, Z., Chen, R., Zhao, X., Zhou, Y., Zeng, B., Yu, M., Zhou, Q., Lin, Q., Gao, W., et al. (2015). Inhibition of glutamine metabolism counteracts pancreatic cancer stem cell features and sensitizes cells to radiotherapy. Oncotarget *6*, 31151–31163.

Liao, J., Liu, P.P., Hou, G., Shao, J., Yang, J., Liu, K., Lu, W., Wen, S., Hu, Y., and Huang, P. (2017). Regulation of stem-like cancer cells by glutamine through β-catenin pathway mediated by

redox signaling. Mol. Cancer *16*, 1–13.

Lowman, X.H., Hanse, E.A., Yang, Y., Ishak Gabra, M.B., Tran, T.Q., Li, H., and Kong, M. (2019). p53 Promotes Cancer Cell Adaptation to Glutamine Deprivation by Upregulating Slc7a3 to Increase Arginine Uptake. Cell Rep. *26*, 3051-3060.e4.

Lu, Z., Tang, Y., Luo, J., Zhang, S., Zhou, X., and Fu, L. (2017). Advances in targeting the transforming growth factor β1 signaling pathway in lung cancer radiotherapy. Oncol. Lett. *14*, 5681–5687.

Luo, J., Yao, Y., Ji, S., Sun, Q., Xu, Y., Liu, K., Diao, Q., Qiang, Y., and Shen, Y. (2019). PITX2 enhances progression of lung adenocarcinoma by transcriptionally regulating WNT3A and activating Wnt/β-catenin signaling pathway. Cancer Cell Int. *19*, 1–15.

M

Ma, Y., Wang, L., and Jia, R. (2020). The role of mitochondrial dynamics in human cancers. Am J Cancer Res *10*, 1278–1293.

Magi, S., Piccirillo, S., Amoroso, S., and Lariccia, V. (2019). Excitatory Amino Acid Transporters (EAATs): Glutamate Transport and Beyond. Int. J. Mol. Sci. *20*, 5674.

Matés, J.M., Di Paola, F.J., Campos-Sandoval, J.A., Mazurek, S., and Márquez, J. (2020). Therapeutic targeting of glutaminolysis as an essential strategy to combat cancer. Semin. Cell Dev. Biol. *98*, 34–43.

Maier, S., Nimmrich, I., Koenig, T., Eppenberger-castori, S., Thomssen, C., Bohlmann, I., Paradiso, A., Mueller, V., Schwope, I., Kluth, A., et al. (2007). DNA-methylation of the homeodomain transcription factor PITX2 reliably predicts risk of distant disease recurrence in tamoxifen-treated, node-negative breast cancer patients – Technical and clinical validation in a multi-centre setting in collaboration wi. Eur. J. Cancer *43*, 1679–1686.

Maycotte, P., Marín-hernández, A., Goyri-aguirre, M., Anaya-ruiz, M., Reyes-leyva, J., and Cortés-hernández, P. (2017). Mitochondrial dynamics and cancer. Tumor Biol. 1–16.

Menendez, J.A., and Alarco´n, T. (2014). Metabostemness: A new cancer hallmark. Front. Oncol. *4*, 1–21.

Mitra, T., Prasad, P., Mukherjee, P., Chaudhuri, S.R., Chatterji, U., and Roy, S.S. (2018). Stemness and chemoresistance are imparted to the OC cells through TGFβ1 driven EMT. J. Cell. Biochem. *119*, 5775–5787.

Mitra, T., and Roy, S.S. (2017). Co-activation of TGFβ and Wnt signalling pathways abrogates EMT in ovarian cancer cells. Cell. Physiol. Biochem. *41*, 1336–1345.

Miyo, M., Yamamoto, H., Konno, M., Colvin, H., Nishida, N., Koseki, J., Kawamoto, K., and Ogawa, H. (2015). Tumour-suppressive function of SIRT4 in human colorectal cancer. Br. J. Cancer *113*, 492–499.

Momcilovic, M., Bailey, S.T., Lee, J.T., Fishbein, M.C., Magyar, C., Braas, D., Graeber, T., Jackson, N.J., Czernin, J., Emberley, E., et al. (2017). Targeted Inhibition of EGFR and Glutaminase Induces Metabolic Crisis in EGFR Mutant Lung Cancer. Cell Rep. *18*, 601–610.

Morandi, A., Taddei, M.L., Chiarugi, P., and Giannoni, E. (2017). Targeting the Metabolic Reprogramming That Controls Epithelial-to-Mesenchymal Transition in Aggressive Tumors . Front. Oncol. *7*, 40.

Morotti, M., Bridges, E., Valli, A., Choudhry, H., Sheldon, H., Wigfield, S., Gray, N., Zois, C.E., Grimm, F., Jones, D., et al. (2019). Hypoxia-induced switch in SNAT2/SLC38A2 regulation generates endocrine resistance in breast cancer. Proc. Natl. Acad. Sci. U. S. A. *116*, 12452–12461.

Muncke, N., Niesler, B., Roeth, R., Schön, K., Rüdiger, H.-J., Goldmuntz, E., Goodship, J., and Rappold, G. (2005). Mutational analysis of the PITX2 coding region revealed no common cause for transposition of the great arteries (dTGA). BMC Med. Genet. *6*, 20.

N

Nallanthighal, S., Heiserman, J.P., and Cheon, D.-J. (2019). The Role of the Extracellular Matrix in Cancer Stemness. Front. Cell Dev. Biol. *7*, 1–14.

Nandi, S.S., Ghosh, P., and Roy, S.S. (2011). Expression of PITX2 Homeodomain Transcription Factor during Rat Gonadal Development in a Sexually Dimorphic Manner. Cell. Physiol. Biochem. *27*, 159–170.

Nguyen TL, Durán RV (2018). Glutamine metabolism in cancer therapy. *Cancer Drug Resist* ;1:126-38 .

Newsholme, P. (2001). Why Is L-Glutamine Metabolism Important to Cells of the Immune System in Health, Postinjury, Surgery or Infection? Am. Soc. Nutr. Sci. *131*, 2515–2522.

Newsholme, P., Procopio, J., Maria, M., Lima, R., and Pithon-curi, T.C. (2003). Glutamine and glutamate—their central role in cell metabolism and function. Cell Biochem. Funct. *21*, 1–9.

No, J.H., Kim, Y., and Song, Y.S. (2014). Targeting Nrf2 Signaling to Combat Chemoresistance. J. CANCER Prev. *19*, 111–117.

P

Pan, M., Reid, M.A., Lowman, X.H., Kulkarni, R.P., Tran, T.Q., Liu, X., Yang, Y., Hernandez-Davies, J.E., Rosales, K.K., Li, H., et al. (2016). Regional glutamine deficiency in tumours promotes dedifferentiation through inhibition of histone demethylation. Nat. Cell Biol. *18*, 1090–1101.

Pavlova, N.N., and Thompson, C.B. (2016). The Emerging Hallmarks of Cancer Metabolism. Cell Metab. *23*, 27–47.

Pavlova, N.N., Hui, S., Ghergurovich, J.M., Fan, J., Intlekofer, A.M., White, R.M., Rabinowitz, J.D., Thompson, C.B., and Zhang, J. (2018). As Extracellular Glutamine Levels Decline, Asparagine Becomes an Essential Amino Acid. Cell Metab. *27*, 428-438.e5.

Pei-Yun Tsai, Min-Sik Lee, Unmesh Jadhav, Insia Naqvi, Shariq Madha, Ashley Adler, Meeta Mistry, Caroline A. Lewis, Daniel S. Hitchcock, Frederick R. Roberts, Peter DelNero Thomas Hank, Kim C. Honselmann, Vicente Morales Oyarvide, Mari Mino-Kenudson, Clar, and N.Y.K. (2021). Adaptation of pancreatic cancer cells to nutrient deprivation is reversible and requires glutamine synthetase stabilization by mTORC1. PNAS 118, 1–11.

Peiris-Pagès, M., Bonuccelli, G., Sotgia, F., and Lisanti, M.P. (2018). Mitochondrial fission as a driver of stemness in tumor cells: mDIVI1 inhibits mitochondrial function, cell migration and cancer stem cell (CSC) signalling. Oncotarget *9*, 13254–13275.

Pérez-Escuredo, J., Dadhich, R.K., Dhup, S., Cacace, A., Van Hée, V.F., De Saedeleer, C.J., Sboarina, M., Rodriguez, F., Fontenille, M.J., Brisson, L., et al. (2016). Lactate promotes glutamine uptake and metabolism in oxidative cancer cells. Cell Cycle *15*, 72–83.

Prasad, P., and Roy, S.S. (2021). Glutamine regulates ovarian cancer cell migration and invasion through ETS1. Heliyon 7, e07064.

Q

Qian, J., Lesavage, B.L., Hubka, K.M., Ma, C., Natarajan, S., Eggold, J.T., Xiao, Y., Fuh, K.C., Krishnan, V., Enejder, A., et al. (2021). Cancer-associated mesothelial cells promote ovarian cancer chemoresistance through paracrine osteopontin signaling. J. Clin. Invest. 131, 1–16.

R

Ray, U., Roy Chowdhury, S., Vasudevan, M., Bankar, K., Roychoudhury, S., and Roy, S.S. (2017). Gene regulatory networking reveals the molecular cue to lysophosphatidic acid-induced metabolic adaptations in ovarian cancer cells. Mol. Oncol. *11*, 491–516.

Reid, M.A., Lowman, X.H., Pan, M., Tran, T.Q., Warmoes, M.O., Ishak Gabra, M.B., Yang, Y., Locasale, J.W., and Kong, M. (2016). IKKβ promotes metabolic adaptation to glutamine

deprivation via phosphorylation and inhibition of PFKFB3. Genes Dev. 30, 1837–1851.

Ribatti, D., Tamma, R., and Annese, T. (2020). Translational Oncology Epithelial-Mesenchymal Transition in Cancer : A Historical Overview. Transl. Oncol. *13*, 100773.

S

Schweickert, A., Campione, M., Steinbeisser, H., and Blum, M. (2000). Pitx2 isoforms : involvement of Pitx2c but not Pitx2a or Pitx2b in vertebrate left - right asymmetry. Mech. Dev. *90*, 41–51.

Senbanjo, L.T., and Chellaiah, M.A. (2017). CD44 : A Multifunctional Cell Surface Adhesion Receptor Is a Regulator of Progression and Metastasis of Cancer Cells. Front. Cell Dev. Biol. *5*, 1–6.

Shaheen, S., Ahmed, M., Lorenzi, F., and Nateri, A.S. (2016). Spheroid-Formation (Colonosphere) Assay for in Vitro Assessment and Expansion of Stem Cells in Colon Cancer. Stem Cell Rev. Reports 492–499.

Shiratori, H., and Hamada, H. (2014). TGFβ signaling in establishing left-right asymmetry. Semin. Cell Dev. Biol. *32*, 80–84.

Son, J., Lyssiotis, C.A., Ying, H., Wang, X., Hua, S., Ligorio, M., Perera, R.M., Ferrone, C.R., Mullarky, E., Shyh-Chang, N., et al. (2013). Glutamine supports pancreatic cancer growth through a KRAS-regulated metabolic pathway. Nature *496*, 101–105.

Sung, H., Ferlay, J., Siegel, R.L., Laversanne, M., Soerjomataram, I., Jemal, A., and Bray, F. (2021). Global Cancer Statistics 2020 : GLOBOCAN Estimates of Incidence and Mortality Worldwide for 36 Cancers in 185 Countries. CA. Cancer J. Clin. *71*, 209–249.

Suski, J.M., Lebiedzinska, M., Bonora, M., Pinton, P., Duszynski, J., and Wieckowski, M.R. (2012). Relation between mitochondrial membrane potential and ROS formation. Methods Mol. Biol. *810*, 183–205.

T

Tam, S.Y., Wu, V.W.C., and Law, H.K.W. (2020). Hypoxia-Induced Epithelial-Mesenchymal Transition in Cancers: HIF-1α and Beyond . Front. Oncol. *10*, 486.

Tilokani, L., Nagashima, S., Paupe, V., and Prudent, J. (2018). Mitochondrial dynamics : overview of molecular mechanisms. Essays Biochem. *62*, 341–360.

Tomaselli, D., Steegborn, C., Mai, A., and Rotili, D. (2020). Sirt4: A Multifaceted Enzyme at the Crossroads of Mitochondrial Metabolism and Cancer . Front. Oncol. *10*, 474.

Tran, T.Q., Hanse, E.A., Habowski, A.N., Li, H., Ishak Gabra, M.B., Yang, Y., Lowman, X.H., Ooi,

A.M., Liao, S.Y., Edwards, R.A., et al. (2020). α-Ketoglutarate attenuates Wnt signaling and drives differentiation in colorectal cancer. Nat. Cancer *1*, 345–358.

V

Valastyan, S., and Weinberg, R.A. (2011). Tumor Metastasis: Molecular Insights and Evolving Paradigms. Cell *147*, 275–292.

Vaupel, P., Kallinowski, F., and Okunieff, P. (1989). Blood Flow, Oxygen and Nutrient Supply, and Metabolic Microenvironment of Human Tumors: A Review. Cancer Res. *49*, 6449–6465.

Vaquero, L.B.-P. and A. (2011). The Dual Role of Sirtuins in Cancer. Genes Cancer *2*, 648–662.

Verdon, Q., Boonen, M., Ribes, C., Jadot, M., Gasnier, B., and Sagné, C. (2017). SNAT7 is the primary lysosomal glutamine exporter required for extracellular protein-dependent growth of cancer cells. Proc. Natl. Acad. Sci. U. S. A. 114, E3602–E3611.

Vinarskaja, A., Schulz, W.A., Ph, D., Ingenwerth, M., Hader, C., and Arsov, C. (2013). Association of PITX2 mRNA down-regulation in prostate cancer with promoter hypermethylation and poor prognosis ̊. Urol. Oncol. *31*, 622–627.

Venneti, S., Dunphy, M.P., Zhang, H., Pitter, K.L., Zanzonico, P., Campos, C., Carlin, S.D., La Rocca, G., Lyashchenko, S., Ploessl, K., et al. (2015). Glutamine-based PET imaging facilitates enhanced metabolic evaluation of gliomas in vivo. Sci. Transl. Med. *7*, 1–10.

Vučetić, M., Cormerais, Y., Parks, S.K., and Pouysségur, J. (2017). The Central Role of Amino Acids in Cancer Redox Homeostasis: Vulnerability Points of the Cancer Redox Code . Front. Oncol. *7*, 319.

W

Wang, Z., Li, Y., and Sarkar, F.H. (2010). Signaling mechanism(s) of reactive oxygen species in Epithelial-Mesenchymal Transition reminiscent of cancer stem cells in tumor progression. Curr. Stem Cell Res. Ther. *5*, 74–80.

Wang, C., Liu, Y., Zhu, Y., and Kong, C. (2020). Functions of mammalian SIRT4 in cellular metabolism and research progress in human cancer (Review). Oncol Lett *20*, 11.

Wang, L., Zhou, H., Wang, Y., Cui, G., and Di, L.J. (2015). CtBP maintains cancer cell growth and metabolic homeostasis via regulating SIRT4. Cell Death Dis. *6*, 1–10.

Wang, L., Li, J., Guo, L., Li, P., Zhao, Z., Zhou, H., and Di, L. (2018). Molecular link between glucose and glutamine consumption in cancer cells mediated by CtBP and SIRT4. Oncogenesis *7*.

Wang, Y.P., Zhou, W., Wang, J., Huang, X., Zuo, Y., Wang, T.S., Gao, X., Xu, Y.Y., Zou, S.W., Liu, Y. Bin, et al. (2016). Arginine Methylation of MDH1 by CARM1 Inhibits Glutamine Metabolism and Suppresses Pancreatic Cancer. Mol. Cell *64*, 673–687.

Wang, N., Zhang, H., Yao, Q., Wang, Y., Dai, S., and Yang, X. (2012). TGFBI promoter hypermethylation correlating with paclitaxel chemoresistance in ovarian cancer. J. Exp. Clin. Cancer Res. 31, 6.

Wappler, J., Arts, M., Röth, A., Heeren, R.M.A., Peter Neumann, U., Olde Damink, S.W., Soons, Z., and Cramer, T. (2020). Glutamine deprivation counteracts hypoxia-induced chemoresistance. Neoplasia (United States) *22*, 22–32.

Weeks, L., and Melton, D.A. (1987). A Maternal mRNA Localized to the Vegetal Hemisphere in Xenopus Eggs Codes for a Growth Factor Related to TGF-B. Cell *51*, 861–867.

Wise, D.R., and Thompson, C.B. (2010). Glutamine addiction: a new therapeutic target in cancer. Trends Biochem. Sci. *35*, 427–433.

Witsch, E., Sela, M., and Yarden, Y. (2010). Roles for Growth Factors in Cancer Progression. Physiol. *25*, 85–101.

Wu, W.C., Sun, H.W., Chen, J., OuYang, H.Y., Yu, X.J., Chen, H.T., Shuang, Z.Y., Shi, M., Wang, Z., and Zheng, L. (2019). Immunosuppressive immature myeloid cell generation is controlled by glutamine metabolism in human cancer. Cancer Immunol. Res. *7*, 1605–1618.

X

Xelwa, N., Candy, G.P., Devar, J., Omoshoro-Jones, J., Smith, M., and Nweke, E.E. (2021). Targeting Growth Factor Signaling Pathways in Pancreatic Cancer: Towards Inhibiting Chemoresistance . Front. Oncol. 11, 2206.

Xiang, L., Mou, J., Shao, B., Wei, Y., Liang, H., Takano, N., Semenza, G.L., and Xie, G. (2019). Glutaminase 1 expression in colorectal cancer cells is induced by hypoxia and required for tumor growth, invasion, and metastatic colonization. Cell Death Dis. *10*, 1–15.

Xu, X., Chai, S., Wang, P., Zhang, C., Yang, Y., Yang, Y., and Wang, K. (2015). Aldehyde dehydrogenases and cancer stem cells. Cancer Lett. 1–8.

Xu, X., Zhang, L., He, X., Zhang, P., Sun, C., and Xu, X. (2018). Biochemical and Biophysical Research Communications TGF- b plays a vital role in triple-negative breast cancer (TNBC) drug- resistance through regulating stemness , EMT and apoptosis. Biochem. Biophys. Res. Commun. *1*, 6–11.

Xu, Y., Cui, M., Li, J., Li, C., and Zhang, Q. (2019). Upregulation of PITX2 Promotes Letrozole Resistance Via Transcriptional Activation of IFITM1 Signaling in Breast Cancer Cells. Cancer Res. &Treatment. *51*, 576–592.

Y

Yadav, A.K., and Desai, N.S. (2019a). Cancer Stem Cells: Acquisition, Characteristics, Therapeutic Implications, Targeting Strategies and Future Prospects. Stem Cell Rev. Reports *15*, 331–355.

Yadav, A.K., and Desai, N.S. (2019b). Cancer Stem Cells: Acquisition, Characteristics, Therapeutic Implications, Targeting Strategies and Future Prospects. Stem Cell Rev. Reports *15*, 331–355.

Yang, L., Moss, T., Mangala, L.S., Marini, J., Zhao, H., Wahlig, S., Armaiz-Pena, G., Jiang, D., Achreja, A., Win, J., et al. (2014). Metabolic shifts toward glutamine regulate tumor growth, invasion and bioenergetics in ovarian cancer. Mol. Syst. Biol. *10*, 1–23.

Yeldag, G., and Alistair Rice, and A. del R.H. (2018). Chemoresistance and the Self-Maintaining Tumor Microenvironment. Cancers (Basel). 10, 1–33.

Yeh, H.-W., Lee, S.-S., Chang, C.-Y., Lang, Y.-D., and Jou, Y.-S. (2019a). A New Switch for TGFβ in Cancer. Cancer Res. *79*, 3797 - 3805.

Yeh, H., Lee, S., Chang, C., and Lang, Y. (2019b). A New Switch for TGF b in Cancer. 1–9.

Yeung TL, Leung CS, Wong KK, S.G. et al. (2013). TGF-β modulates ovarian cancer invasion by upregulating CAF- derived. Cancer Res. *23*, 1–7.

Yoo, H.C., Park, S.J., Nam, M., Kang, J., Kim, K., Yeo, J.H., Kim, J.K., Heo, Y., Lee, H.S., Lee, M.Y., et al. (2020). A Variant of SLC1A5 Is a Mitochondrial Glutamine Transporter for Metabolic Reprogramming in Cancer Cells. Cell Metab. *31*, 267-283.e12.

Yuan, L., Sheng, X., Willson, A.K., Roque, D.R., Stine, J.E., Guo, H., Jones, H.M., Zhou, C., and Bae-Jump, V.L. (2015). Glutamine promotes ovarian cancer cell proliferation through the mTOR/S6 pathway. Endocr. Relat. Cancer *22*, 577–591.

Yuan, Y., Jiang, Y.C., Sun, C.K., and Chen, Q.M. (2016). Role of the tumor microenvironment in tumor progression and the clinical applications (Review). Oncol. Rep. *35*, 2499–2515.

Z

Zacharias, N.M., McCullough, C., Shanmugavelandy, S., Lee, J., Lee, Y., Dutta, P., McHenry, J., Nguyen, L., Norton, W., Jones, L.W., et al. (2017). Metabolic Differences in Glutamine Utilization Lead to Metabolic Vulnerabilities in Prostate Cancer. Sci. Rep. *7*, 1–11.

Zhang, J., Chen, Z., Xu, Y., Chen, J., Weng, H., Yun, M., Zheng, Z., Chen, C., Wu, B., Li, E., et al. (2017). Downregulation of MicroRNA-644a Promotes Esophageal Squamous Cell Carcinoma Aggressiveness and Stem Cell – like Phenotype via Dysregulation of PITX2. Clin Cancer Res. *23*, 298–311.

Zhang, Y.E. (2017). Non-Smad signaling pathways of the TGF-β family. Cold Spring Harb. Perspect. Biol. *9*, 1–18.

PUBLICATION

1. Prasad, P*, **Ghosh, S***. & Roy, S.S. Glutamine deficiency promotes stemness and chemoresistance in tumor cells through DRP1-induced mitochondrial fragmentation. Cell. Mol. Life Sci. (2021). https://doi.org/10.1007/s00018-021-03818-6. (* Both authors contribute equally)

2. **Ghosh, S**, Mitra, T. & Roy, S.S. Roy. Stem-like features and chemoresistance in ovarian cancer cells are induced through TGFβ1-PITX2A/B signaling axis (Communicated)

Cellular and Molecular Life Sciences
https://doi.org/10.1007/s00018-021-03818-6

ORIGINAL ARTICLE

Glutamine deficiency promotes stemness and chemoresistance in tumor cells through DRP1-induced mitochondrial fragmentation

Parash Prasad[1] · **Sampurna Ghosh**[1] · **Sib Sankar Roy**[1,2]

Received: 30 October 2020 / Revised: 11 February 2021 / Accepted: 20 March 2021
© The Author(s), under exclusive licence to Springer Nature Switzerland AG 2021

Abstract

Glutamine is essential for maintaining the TCA cycle in cancer cells yet they undergo glutamine starvation in the core of tumors. Cancer stem cells (CSCs), responsible for tumor recurrence are often found in the nutrient limiting cores. Our study uncovers the molecular basis and cellular links between glutamine deprivation and stemness in the cancer cells. We showed that glutamine is dispensable for the survival of ovarian and colon cancer cells while it is required for their proliferation. Glutamine starvation leads to the metabolic reprogramming in tumor cells with enhanced glycolysis and unaltered oxidative phosphorylation. Production of reactive oxygen species (ROS) in glutamine limiting condition induces MAPK-ERK1/2 signaling pathway to phosphorylate dynamin-related protein-1(DRP1) at Ser616. Moreover, p-DRP1 promotes mitochondrial fragmentation and enhances numbers of CD44 and CD117/CD45 positive CSCs. Besides the established features of cancer stem cells, glutamine deprivation induces perinuclear localization of fragmented mitochondria and reduction in proliferation rate which are usually observed in CSCs. Treatment with glutaminase inhibitor (L-DON) mimics the effects of glutamine starvation without altering cell survival in in vitro as well as in in vivo model. Interestingly, the combinatorial treatment of L-DON with DRP1 inhibitor (MDiVi-1) reduces the stem cell population in tumor tissue in mouse model. Collectively our data suggest that glutamine deficiency in the core of tumors can increase the cancer stem cell population and the combination therapy with MDiVi-1 and L-DON is a useful approach to reduce CSCs population in tumor.

Keywords Glutaminase · Glutamine metabolism · ROS · Tumor growth · Mitochondrial fission

Introduction

The most prominent feature of cancer is the rapid proliferation of abnormal cells that grow beyond their usual boundaries and metastasize to other parts of the body. In the current scenario, cancer metastasis and its recurrence are the main clinical problems for the scientific community. The recurrence occurs after a short break of treatment due to the chemoresistance property acquired in the tumor cells. A tiny population of CSCs within the tumor is responsible for this chemoresistance [1].

One of the emerging hallmarks of cancer is metabolic reprogramming or plasticity, which is generated in the cancer cells to acclimatize in the nutrient-deprived and hypoxic environment. For their survival and proliferation, cancer cells depend upon two important nutrients glucose and glutamine. In tumor cells, glucose can supply rapid energy and produce lactate from pyruvate under the aerobic condition, known as the "Warburg effect" [2]. This pyruvate cannot enter into the TCA cycle as pyruvate dehydrogenase (PDH) remains inactive due to its phosphorylation by pyruvate dehydrogenase kinase (PDK). In such cells, glutamine plays a crucial role to fuel the TCA cycle and act as an anaplerotics agent to synthesize lipids, nucleotides, and hexosamines [3]. The normal physiological concentration of glutamine in blood is 0.6–0.9 mM and the level may reach up to 20 mM in some tissues [4]; however, in tumor tissue the glutamine level is reduced drastically. This is due to the fact that the tumor cells are highly glutamine-dependent and they utilize

Parash Prasad and Sampurna Ghosh contributed equally to this work.

✉ Sib Sankar Roy
sibsankar@iicb.res.in

[1] Cell Biology and Physiology Division, CSIR-Indian Institute of Chemical Biology, 4 Raja S. C. Mullick Road, Kolkata 700032, India

[2] Academy of Scientific and Innovative Research, CSIR-Indian Institute of Chemical Biology Campus, 4 Raja S. C. Mullick Road, Kolkata 700032, India

the glutamine rigorously leading to its reduction in the tumor microenvironment (TME). To meet the high demand for glutamine in tumor cells, its synthesis increases in cancer-associated fibroblasts (CAF) in TME [5]. In mammalian cell, de novo glutamine synthesis occurs through the glutamine synthetase (GS). However, GS does not express significantly in all tumor cells and hence they mostly depend on the extracellular sources [6]. In addition, glutamine transporters, such as ASCT2 (SLC1A5), LAT1 (SLC7A5), $ATB^{0,+}$ (SLC6A14), are overexpressed in tumor cells which help in glutamine uptake [7].

Glutaminase (GLS) is involved in the conversion of glutamine to glutamate and ammonium [8] and the glutamate is converted into α-ketoglutarate by glutamate dehydrogenase (GDH), which acts as a substrate for TCA cycle. Glutamine is also a constituent of the tripeptide glutathione (GSH), an antioxidant and there by maintains oxidative stress within the cell. Glutamine derived glutamate is exported out of the cell in exchange for cysteine through xCT(SLC7A11), where cysteine is the rate-limiting amino acid for GSH [3].

Mitochondria are the prime site for TCA cycle and glutamine metabolism. ROS also has been reported to be beneficial for cancer progression [9]. Moreover, mitochondrial dynamics and their specific localization inside the cell play an important role in oncogenesis. Recent reports suggest that mitochondrial fragmentation is increased in cancer cells to support actin polymerization and cell migration [10]. In some cells, after fragmentation, perinuclear localization of mitochondria increases regional ROS level in the vicinity of the nucleus and induces stem-like properties [11]. The cellular requirement of glutamine varies extensively among different cancer types as some are glutamine-dependent, whereas some cells can survive and proliferate in its absence [12]. Glutamine itself acts as a signaling molecule to activate STAT3 and mTORC1 for cancer proliferation, which is independent of glutamine metabolism. Some reports suggest that glutamine dependency increases with their aggressiveness [12–14]. Hence, the modulation of glutamine metabolism is associated with tumor progression, and regulation of this might be important from the therapeutic point of view. Various small molecules such as BPTES, compound 968, CB-839 that target GLS are presently in clinical trial. Though BPTES specifically targets GLS, it happens to be a poor drug candidate owing to its solubility and bioavailability. EGCG and R162, inhibitors of GDH have been shown to attenuate tumor growth in preclinical trial [15]. It is evident that the tumor core contains a population of CSCs and has limited nutrient supply. This regional glutamine deprivation leads to the de-differentiation of the cancer cells followed by chemoresistance [16, 31]. These stem-like cells can be identified by the expression of various cell surface antigens (CDs) and pluripotent stemness markers like Sox2, Oct4, Nanog, and high aldehyde dehydrogenase (ALDH) activity [1].

Considering this background information, we aimed to study the mechanism of survival of cancer cells in glutamine-deprived environment. We have mainly used epithelial ovarian cancer cell line, PA1 and OAW42 and the colorectal cancer cell line HCT116. Our study indicated that glutamine deprivation promotes mitochondrial fragmentation, which in turn enhances stem-like characteristics and chemoresistance. We also found that GLS1 inhibition enhances the expression of the stemness markers. Therefore, inhibitors of both GLS1 and DRP1 might be effective as promising therapeutic agent to treat the tumor growth and disease recurrence.

Materials and methods

Cell culture and glutamine deprivation

Human ovarian cancer cell lines PA1 (ATCC;Manassas, Virginia, United State; Cat# CRL-1572, RRID:CVCL_0479) and OAW42 (SIGMA-ALDRICH;St. Louis, Missouri, United States; Cat# 85073102, RRID:CVCL_1615) were grown in Minimal essential media alpha (MEM α, Gibco) and Dulbecco's modified Eagle's medium (DMEM, Gibco), respectively. Another ovarian carcinoma cell line OVCAR3 (RRID:CVCL_0465, a gift from Dr. Asima Mukhopadhyay, CNCI, Kolkata, India) was grown in RPMI-1640 media (Gibco). Human colorectal carcinoma cell line HCT116 (ATCC Cat# CCL-247, RRID:CVCL_0291), ID8 (MERCK Cat# SCC145,RRID:CVCL_IU14) and human non-small cell lung carcinoma H1299 (RRID: CVCL_0060, a gift from Prof. Samit Chattopadhyay, CSIR-IICB, Kolkata, India) were cultured in DMEM. Human cervical carcinoma cell lines, HeLa (RRID:CVCL_0058) and SiHa (RRID:CVCL_0032) (were gifts from Dr. Chinmay Kumar Panda, CNCI, Kolkata, India) were maintained in DMEM and MEM α respectively. All the media were supplemented with 10% FBS (Cat #16000–044, Gibco) and the cells were grown at 37 °C in a humified 5% CO_2 incubator. Glutamine deprivation studies were performed in glutamine-free medium (MEM α, Cat#AL080, DMEM, Cat#AL066, RPMI-1640, Cat#AL060, HIMEDIA) for respective cell lines with 10% FBS reconstitution. The cells were starved for at least 6 h prior to the glutamine deprivation.

Treatments of cells and siRNA transfection

The cells were starved for at least 6 h and the respective treatments were given. As mentioned, the cells were treated with 14 μM of MDiVi-1(Cat#M0199, Sigma-Aldrich), 2 mM of glutathione reduced ethyl ester (GSH,

Cat#G1404, Sigma-Aldrich), 0.5 mM, 1 mM, 3 mM and 5 mM of N-acetyl cysteine (NAC, Cat#A7250, Sigma-Aldrich), 10 µM of ERK inhibitor (Cat#328006, Calbiochem), 10 µM of U0126 (Cat#662005, Calbiochem), 30 µM of H_2O_2 (Cat#107209, Merck), 20 µM, 40 µM, 100 µM of L-DON (Cat#D2141, 6-Diazo-5-oxo-L-norleucine, Sigma-Aldrich), 250 µM of SSZ (Sulphasalazine, Cat#S0883, Sigma-Aldrich). The siRNA against DRP1 (Cat#sc-43732), xCT (Cat#sc-76933) and PDHE1α (Cat#sc-91064) (Santa Cruz Biotechnology; Dallas, Texas,United State) were used at 20 nM concentration along with lipofectamine 2000 (Cat#11668019, Invitrogen) in the cell lines. Scrambled (SCR) siRNA (Cat#sc-37007, Santa Cruz Biotechnology) was used as control for knockdown studies. The transfection was done at 50–60% confluency and the transfection reagents were added in Opti-MEM (Cat#31985062, Gibco) medium and after 4 h of transfection the media was changed to respective media of treatment (either glutamine containing or glutamine free medium).

Quantitative real-time PCR

Total RNA was isolated from the cells using RNAiso Plus reagent (Cat#9109, Takarabio; Kyoto, Japan) following the standard protocol. iScript cDNA synthesis kit (Cat#1708891, Bio-Rad; Hercules, California, United States) was used for synthesizing cDNA. Quantitative real time-PCR (Q-PCR) was performed with iTaq universal SYBR green supermix (Cat#1725120, Bio-Rad) on the ABI 7500 Fast Real-Time PCR system (Applied Biosystems; Waltham, Massachusetts, USA; 7500 Real-Time PCR Software, RRID:SCR_014596). Fold change in gene expression was calculated against 60S ribosomal protein L19 mRNA expression (considered as endogenous control). The primers were designed using Primer Express software (Primer Express Software, RRID:SCR_017376) and verified using Primer-Blast (Primer-BLAST, RRID:SCR_003095). Custom oligos were obtained from IDT (Integrated Technology Enterprise Inc, RRID:SCR_012186) and the sequences are given in Table 1.

Western blot analysis

The cells were lysed using radioimmunoprecipitation assay (RIPA) buffer and the protein was extracted. All the proteins were then subjected to western blot analysis using the standard protocol [17]. Each blot was stripped with stripping buffer (Cat#T7135A, TAKARA) and re-probed for checking corresponding α-tubulin as endogenous control (Cell signaling Technology (CST); Danvers, Massachusetts; Cat# 2125, RRID:AB_2619646). The primary antibodies such as p-DRP1 (Ser616) (CST Cat# 3455, RRID:AB_2085352), DRP1 (CST Cat# 8570, RRID:AB_10950498), HK2 (CST Cat# 2867, RRID:AB_2232946), SDHA (CST Cat# 5839, RRID:AB_10707493), VDAC (CST Cat# 4661, RRID:AB_10557420), MFN1 (CST Cat# 14739BC), MFN2 (CST Cat# 9482), p-AKT (CST Cat# 4060, RRID:AB_2315049), AKT (CST Cat# 4691, RRID:AB_915783), p38MAPK (CST Cat# 9218, RRID:AB_10694846), p-p38MAPK (T180/Y182) (CST Cat# 4631, RRID:AB_331765), p-p44/42MAPK (CST Cat# 9101, RRID:AB_331646), OCT4 (CST Cat# 2750, RRID:AB_823583), SOX2 (CST Cat# 3579, RRID:AB_2195767), xCT/SLC7A11 (CST Cat# 12691, RRID:AB_2687474), α-tubulin (CST Cat# 2125) were purchased from CST and used at 1:2000 dilution. Antibodies of PDHE1α (Santa Cruz Biotechnology Cat# sc-377092, RRID:AB_2716767), ABCG2 (Santa Cruz Biotechnology Cat# sc-58222, RRID:AB_630828) were obtained from Santa Cruz Technology and used at 1:1000 dilution. Antibodies against p-PDHE1α (Ser2193) (Millipore; Burlington, Massachusetts, United States; Cat# ABS204, RRID:AB_11213668) and total OXPHOS (Abcam; Cambridge, United Kingdom; Cat# ab110411, RRID:AB_2756818) complex were procured from Merck (1:10,000 dilution) and Abcam (1:3000 dilution), respectively. The chemiluminescent bands were detected in the blot using ECL detection reagent (Cat# 1705062, Bio-Rad).

Table 1 Primer details used for checking the respective mRNA expression

Gene name	Forward primer (5′–3′)	Reverse primer (5′–3′)	Amplicon size
OCT4	GCAGCTTAGCTTCAAGAACATGTG	TCAGCTTCCTCCACCCACTT	66
SOX2	TGCGAGCGCTGCACAT	GCAGCGTGTACTTATCCTTCTTCA	93
NANOG	GCATCCGACTGTAAAGAATCTTCA	CATCTCAGCAGAAGACATTTGCA	90
ABCG2	GATGTCTAAGCAGGGACGAACAA	GGTGAGGCTATCAAACAACTTGAA	82
CD44s	TCCAACACCTCCCAGTATGACA	GGCAGGTCTGTGACTGATGTACA	83
CD44 epithelial	GAAAGGAGCAGCACTTCAGG	GAGGTCCTGTCCTGTCCAAA	202
L19	GCGGATTCTCATGGAACACA	GGTCAGCCAGGAGCTTCTTG	68

Extracellular flux analysis

Extracellular acidification rate (ECAR) was measured using Agilent seahorse extracellular flux analyzer (XF^e24) as described earlier [17]. Briefly, PA1 and HCT116 cells were seeded at 3000 cells/well and 10,000 cells/well were plated for OAW42. Each treatment was given in triplicates. Primarily basal oxygen consumption rate (OCR) and ECAR were measured under glucose-free condition. After that, ECAR was measured using Glycostress assay kit with three consecutive injections of glucose, oligomycin and 2-deoxyglucose (2-DG) (Agilent; Santa Clara, CA; Cat#103344-100). Mitostress assay kit (Agilent, Cat# 103015-100) was used for analyzing mitochondrial bioenergetics using three consecutive injections of oligomycin, FCCP (Carbonyl cyanide 4-(trifluoromethoxy) phenylhydrazone) and antimycin/rotenone. The ECAR and OCR values were normalized by estimating protein concentration and cell concentration in each well. Analysis was done by WAVE (Seahorse Wave, RRID:SCR_014526) software.

Lactate assay

Amount of lactate was measured in both the condition media of glutamine-deprived condition and control media using lactate assay kit (Sigma-Aldrich, Cat# MAK064) following manufacturer's protocol. Lactate production was normalized using cell numbers and represented as 'fold change' with respect to control.

Analysis of metabolites using NMR

After completion of the treatment the media was aspirated, centrifuged in 12000 g for 5 min at 4 °C for the isolation of cell debris. From here, 1 ml media was withdrawn and mixed thoroughly with 300 µl of methanol-chloroform mixture (2:1) and centrifuged at 12000*g* for 10 min at 4 °C. Then the upper aqueous layer was extracted, mixed with five times of HPLC grade water and freezed at − 80 °C. Then it was lyophilized and re-suspended in 600 µl of D_2O (Sigma-Aldrich, Cat#151882) mixture (10% D_2O, 90% H_2O). TSP (Cat #269913, Sigma-Aldrich) was used as a control for reference peak. The samples were analyzed in 600 MHz proton NMR instrument (Brucker; Billerica, Massachusetts, US). The.fid file was uploaded in MetaboAnalyst 3 (MetaboAnalyst, RRID:SCR_015539) web application and output data was exported in.xlsx format. ClustVis (ClustVis, RRID:SCR_017133) was used to create a heatmap of the acquired metabolites after PCA analysis.

Confocal microscopy and live-cell video microscopy

To visualize the mitochondrial morphology and the fission, MitoTracker Red CMXRos (50 nM, Invitrogen; Waltham, Massachusetts, USA; Cat#M7512) was used for 20 min at 37 °C. Immunofluorescence microscopy was performed with DRP1 Antibody (CST Cat# 8570, RRID:AB_10950498), followed by Alexa flour 488 conjugated secondary antibody (Thermo Fisher Scientific; Waltham, Massachusetts, US; Cat# A32731, RRID:AB_2633280) as described previously [18]. The nuclei were stained with DAPI (0.25 µg/ml) for 5 min. The images were visualized and acquired by Leica confocal microscope SP8 (Leica Microsystems; Wetzlar, Germany; RRID:SCR_008960) with 63X oil immersion objective lens, Zeiss LSM 800 microscope (Zeiss; acquisition software: LAS X; Oberkochen, Germany) with 63X oil immersion objective lens (NA 1.4) and Olympus BX51 microscope (Olympus; acquisition software: cellSens; Shinjuku, Tokyo, Japan; RRID:SCR_017564) with 40X (NA 0.75) objective lens. 3D reconstruction of the images was done by LAS X software (LAS X, RRID:SCR_013673). Images were taken in room temperature.

For time-lapse video microscopy, the cells were grown in 35 mm cover glass-bottom dish (SPL Lifesciences; Korea), and the treatment was done for glutamine-deprived conditions. After completion of the treatment, the cells were incubated with MitoTracker Red (50 nM, Invitrogen, Cat#M7512) and Hoechst stain (5 µg/ml, Sigma-Aldrich, cat#14533) for 20 min at 37 °C in 5% CO_2 incubator. Then the images were taken in every 13.75 s for 7 min 6 s in case of control cells. The images were taken in every 5.061 s for 3 min 7.25 s for the cells grown in glutamine-deprived condition with 63X objective lens (NA 1.4). The video reconstruction was done by LAS X software (LAS X, RRID:SCR_013673).

Cellular ROS localization study using DCFDA and Mitotracker Red

The cells were grown in 35 mm cover glass-bottom dish and treated with respective glutamine-containing media and glutamine-deprived media. At 24 h the cells were stained with 2 µM DCFDA (CM-H2DCFDA, Invitrogen, Cat# C6827) and MitoTracker Red CMXRos (50 nM, Invitrogen, Cat#M7512) in the respective culture medium for 30 min in humified 37 °C incubator (5% CO_2). After that, the cells were washed with PBS and observed under Leica SP8 microscope (Leica Microsystems, RRID:SCR_008960) under 63X oil immersion objective [11].

Intracellular and extracellular antigen staining and measurement by flow cytometry

For intracellular antigen staining, the cells were grown in 60 mm dish. After the completion of the treatment, the media was discarded and cells were scraped with phosphate buffered saline (PBS). Then the cells were fixed with 4% formaldehyde, which was added drop-wise with vigorous mixing in vortex and kept at 37 °C for 10 min followed by a brief incubation in ice for 1 min. Then the cells were centrifuged at 3000*g* for 5 min and the supernatant was discarded. The cells were then resuspended in PBS and permeabilized by adding drop-wise 90% chilled methanol under stirring condition and incubated in ice and then kept it overnight at − 20 °C. Next day, the cells were washed with PBS and incubated with anti–GSH antibody (Cloud clone Corp. Cat# PAA294Ge01) at 37 °C for 2 h followed by washing with PBS and then incubated with FITC-tagged secondary antibody (Thermo Fisher Scientific Cat# A32731, RRID:AB_2633280) for 1 h. Flow cytometric analysis was performed using LSR Fortessa cell analyzer (BD Biosciences, RRID:SCR_013311).

Extracellular antigen staining was done in live cells. Cells from 60 mm dish were scrapped with PBS and incubated with Fluorophore tagged primary antibody CD44-PE (BD Biosciences Cat# 555479, RRID:AB_395871), CD117-APC (BD Biosciences; Franklin Lakes, New Jersey, U.S.; Cat# 550412, RRID:AB_398461), CD31-FITC (BD Biosciences Cat# 555445, RRID:AB_395838) and CD45-PE-Cy7 (BD Biosciences Cat# 557748, RRID:AB_396854) (used in 1:400 dilution) at 37 °C for 30 min followed by washing and analysis by flowcytometry [1]. Unstained control cells were used as experimental control.

Aldehyde dehydrogenase (ALDH) activity assay

Aldehyde dehydrogenase (ALDH) assay was done using the ALDEFLUOR kit (Stem Cell Technologies; Vancouver, British Columbia, Canada; Cat# 01700) following the manufacturer's protocol. Fluorescence intensity was measured by flow cytometer using FACSDiva (BD FACSDiva Software, RRID:SCR_001456). In the dot plot, gating was done on stained 'CONTROL + DEAB' tube keeping 1% cells in P3 gate.

Spheroid formation

Initially cells were culture in 35 mm dish and treated as mentioned. From these dishes, cells were trypsinized and 5×10^3 cells/well were seeded in low attachment 6-well plates (Cat#CLS3471, Corning, New York, NY). They were allowed to grow in serum-free media (SFM) supplemented with B27 supplement (Cat#17504044, Invitrogen), rhEGF (Cat# F0291, Sigma-Aldrich) and insulin (Cat#I0320000, Sigma-Aldrich) up to 4 days following the previous standard protocol [1]. The spheroids were visualized, counted, and their images were acquired using a phase-contrast microscope with 20X objective (EVOS, Invitrogen). The ImageJ (ImageJ, RRID:SCR_003070) software was used for measuring the size of the spheroids. The scale length of acquired images was fed to the software and after thresholding the image, the volume of every spheroid was acquired.

Rhodamine efflux assay

Cells were grown in 6-well plate. After treatment is over, Rh123 (200 ng/ml, Cat# R302, Invitrogen), a substrate for efflux transporter, was given in the medium and incubated in 37 °C CO_2 incubator for 1 h [1]. Then the cells were washed and again replenished with respective media under the optimum condition for 24 h. The cells that refluxed or retained drug, were measured through FACS analysis on the basis of unstained control cells.

Cell cycle analysis

The cells were grown in 6-well plate and after completion of the treatment, cells were trypsinized and washed with PBS. Fixation was done with 70% ethanol with gentle vortexing and were kept overnight at − 20 °C. Next day, after centrifugation, the cells were washed again with PBS and re-suspended in PBS containing Propidium Iodide (PI) (1.5 mM, Cat# P1304MP, Invitrogen), RNaseA (1 mg/ml, Cat# EN0531, Fermentas; Waltham, Massachusetts, USA). They were incubated for 15 min at room temperature and analyzed by flow cytometer with BD FACSDiva Software, (RRID:SCR_001456) (493/636 nm). Gating of flow cytometric data were done using unstained control cells. Histogram overlay were prepared using FlowJo software (FlowJo, RRID:SCR_008520).

Cell proliferation study

3000 cells were seeded per well in a 12-well plate. The cell count was taken at 24 h, 48 h, and 72 h of glutamine deprivation. The media was discarded and then the cells were trypsinized with 100 µl of trypsin-ETDA and mixed with 100 µl of complete medium. From this cell solution, 10 µl was added to the TC-10 cell counting slide and cell concentration was measured using TC-10 automated cell counter (Bio-Rad, USA).

Annexin-V-FITC/PI apoptosis assay

Annexin-V-FITC/PI assay was done to check the apoptosis in glutamine-deprived condition by flow cytometric

analysis following the manufacturer's protocol (Invitrogen). The results have been represented as dot plot using BD FACSDiva Software (RRID: SCR_001456) [18]. Using unstained control cells, gating was done in dot plot data of flow cytometry.

Estimation of mitochondrial ROS generation

$1X10^6$ cells were scraped and washed with PBS. To determine the mitochondrial ROS generation, cells were resuspended with 100 µl of PBS containing Mitosox^{TM}red (5 µM) mitochondrial superoxide indicator (Invitrogen, Cat#M36008) and incubated for 20 min at 37 °C. Then the cells were washed with PBS and the amount of ROS generation was determined using flow cytometer (510/580 nm) (BD FACSDiva Software, RRID:SCR_001456) [17].

Estimation of mitochondrial membrane potential

Approximately, 1×10^6 cells were scraped and washed with PBS. They were resuspended in PBS containing JC-1 (5 µg/ml, Invitrogen) followed by incubation for 15 min at 37 °C. The ratio of cells showing red/green (485/535 nm)/(514/529 nm) fluorescence was calculated from the dot plot of the flow cytometric data using BD FACSDiva Software (RRID:SCR_001456) [18].

Glucose oxidation

The cells were kept in serum-starved condition for 2 h prior to the addition of 0.5 µCi of U-C^{14}-glucose (BRIT) to the media and incubated at 37 °C for 2 h. During incubation, Whatman chromatography paper soaked with 3 M NaOH was placed on the lid of the plate, such that each well is covered. After incubation, 500 µL of perchloric acid was added to release the dissolved CO_2, which was then trapped in Whatman paper for 1 h. The filter paper was dried overnight and then put in the cocktail-T solution. The levels of C^{14} were measured using the scintillation counter (Tri-Carb 2810TR, Perkin Elmer) and the CPM value was normalized with the cell numbers [19].

Glucose uptake assay

0.5 µCi of 2-DG (C^{14}, BRIT; Navi Mumbai, India) was added to each well of a 6-well plate following 30 min of incubation in 37 °C. Then the media was discarded and the cells were trypsinized with 200 µl of trypsin–EDTA solution (0.25%). 10 µl cell solution was used to count the cells and the rest was pelleted down. After discarding the supernatant, the pellet was re-suspended and incubated for 20 min at room temperature in 10% NP40 for cell lysis. This lysed cell solution was then mixed with 5 ml of cocktail-T solution and the scintillation count was taken in Tri-Carb 2810TR counter (Perkin Elmer; Waltham, Massachusetts, US).

Determination of mitochondrial load using MitoTracker green and nonyle acridine orange

MitoTracker green (100 nM, Invitrogen, Cat# M7514) was added in the cell suspension in 1X PBS and incubated at 37 °C for 10–15 min. The green fluorescence (490/516 nm) intensity of the cells was determined using flow cytometer using BD FACSDiva Software (RRID:SCR_001456). Similarly 1 µM NOA (Nonyle acridine orange, Invitrogen, Cat# A1372) staining was performed where the incubation period is 30 min [20].

Analysis of mitochondrial morphology using Atomic force microscope (AFM)

Mitochondria were isolated from the treated cells using mitochondrial isolation kit (QIAGEN; Venlo, Netherlands; Cat#37612) following the manufacturer's protocol. The mitochondrial pellet was washed with PBS for two times and the suspension in PBS was fixed with 4% paraformaldehyde with gentle shaking. The fixed cells were washed twice with 1×PBS and then with deionized water and the pellet was resuspended in deionized water. 5 µl of the mitochondrial sample was deposited onto Ruby mica sheet (ASTM V1 Grade Ruby Mica from MICAFAB; Chennai, India) or coverslips for 5–10 min. Then the sample was gently washed with 0.5 ml Milli-Q water to remove the loosely attached molecule.

Contact mode AFM was performed using a Pico plus 5500 AFM (Agilent Technologies USA) with a piezo scanner having a maximum range of 100 µm. Image processing has been done through Pico Image Advanced version software (Agilent Technologies, USA).

Pyruvate dehydrogenase (PDH) activity assay

PDH activity was measured using the PDH assay kit (Sigma-Aldrich, Cat#MAK183) as instructed in the manufacturer's protocol. Briefly, mitochondria were isolated from both control and glutamine-deprived cells using mitochondria isolation kit (QIAGEN, Cat#37612) and the protein concentration was estimated in each sample. Using the NADH standard, the PDH activity of the unknown sample was measured.

Immunohistochemistry

Primary ovarian tumor tissue samples were collected from the Saroj Gupta Cancer Centre & Research Institute, Kolkata after appropriate approval from the Institutional Ethics Committee (approval number-IEC SGCCRI REF NO.-16/2/2018/

Non-Reg/SSR/3) and informed written consent from the patients in accordance with the 1964 Helsinki declaration. The nature of the tissue and stage of the disease was validated by the concerned clinician and respective histology experts of the source institute. Tissue sections were processed and fluorescently stained against CD44 (PE tagged) (BD Biosciences Cat# 555479, RRID:AB_395871) and p-DRP1 (S616) (CST Cat# 3455,RRID:AB_2085352) (stained with Alexa-fluor 488 secondary antibody, Thermo Fisher Scientific Cat# A32731, RRID:AB_2633280). Mouse tumor tissue sections of 5 µm thickness were stained with Cleaved Caspase 3 (Cell Signaling Technology Cat# 9661, RRID:AB_2341188), Ki67 (Abcam Cat# ab15580, RRID:AB_443209), ABCG2 antibody, p-DRP1 (Ser616), OCT4 (CST Cat# 2750, RRID:AB_823583), SOX2 (CST Cat# 3579, RRID:AB_2195767), and PE tagged CD44 antibody. Anti-mouse AF555 tagged antibody (Thermo Fisher Scientific Cat# A28180, RRID:AB_2536164) was used against ABCG2 antibody and AF488 tagged anti rabbit antibody was used to counterstain other primary antibodies. All the tissue sections were counter-stained with DAPI (0.25 µg/ml) for staining the nucleus. The images were acquired with Leica confocal microscope SP8 (Leica Microsystems, RRID:SCR_008960) with 20× objective lens (NA 0.4) in room temperature.

Co-immunoprecipitation assay

Proteins were extracted from whole cell lysate using immunoprecipitation lysis buffer and the protein concentration was estimated. Then 200 µg of protein was incubated with CD44 (BD Biosciences Cat# 555479, RRID:AB_395871) primary antibody for the formation of protein-antibody conjugation complex, which was then pulled down using ProteinA magnetic beads (Bio-Rad, Cat# 1614013). This protein-antibody conjugation complex was released from the beads by boiling in the SDS-electrophoresis sample buffer (1X), which was then subjected to SDS-PAGE followed by western blot using xCT antibody (CST Cat# 12691, RRID:AB_2687474) [17].

Image analysis

Image analysis was done with ImageJ software (ImageJ, RRID:SCR_003070). For measuring the mitochondrial distance from the nucleus, the red channel (MitoTracker red) images were first converted into 8-bit images, and then a straight line is drawn from the center of the nucleus up to the region of mitochondrial fluorescence within the cell boundary. The fluorescent intensity throughout the line was extracted.

For 'line scan' analysis, first, a freehand line was drawn over the mitochondrial length in the red channel image after converting them into 8-bit image and the intensity profile was extracted with the "Plot profile" option. Then the ROI was copied from that image of MitoTracker channel to green channel (8-bit image of the Drp-1) of the same image and the Drp-1 intensity throughout the ROI was plotted with "Plot Profile" option.

The relative mean fluorescence intensity was measured with ImageJ software after selecting the region of interest.

The mitochondrial length analysis and co-localization analysis were done with LAS X software (LAS X, RRID:SCR_013673) as done previously [21] and the co-localization was analyzed with ImageJ (ImageJ, RRID:SCR_003070) software.

TUNEL assay

The tissues were deparaffinized using xylene and then hydrated using serial ethanol gradation. After hydrating, the tissue sections were washed with 0.9% NaCl and digested with Proteinase-K. For positive control, the tissue was incubated with DNase1 (Invitrogen, Cat#AM2224) and TUNEL assay was performed according to the manufacturer's protocol (Invitrogen, Cat#A35125). DAPI was used for counterstaining the nucleus. The images were acquired using Leica SP8 confocal microscope.

Animal model

All animal procedures were approved by institutional animal ethics committee following the guidelines of CPCSEA, Govt. of India. The ID8 cells were cultured in DMEM supplemented with 10% FBS. About 3×10^7 cells/ml in PBS was mixed with Matrigel (19 mg/ml) (BD, Cat no. 356234) solution in 1:1 ratio prior to injection C57BL/6 female mice (3–4 weeks old) were injected subcutaneously with 300 µl cell-matrigel suspension at the lower right quadrant using a 1 ml insulin syringe (30G 5/16 in). After 4 days of injection, the animals which have detectable tumors were included in the study. When the tumors reached about 100 mm^3 size, they were randomly grouped in control and treatment set. Control mice were injected with 125 µl PBS and treated mice were injected with 125 µl L-DON solution (0.6 mg/kg body weight), 125 µl MDiVi-1 (5 mg/kg body weight) and 125 µl of MDiVi-1 + L-DON (5 mg/kg and 0.6 mg/kg of body weight), respectively, through tail vein for three consecutive days. Each day body weight and the tumor size were measured and after completion of the treatment the tumors were isolated and weighed. The tumors were then fixed with 10% formalin and paraffin blocks were prepared for histological analysis. Bright field images of Hematoxylin and Eosin stained histological sections were acquired under EVOS microscope (Applied Biosystems) with 20× objective lens (NA 0.45).

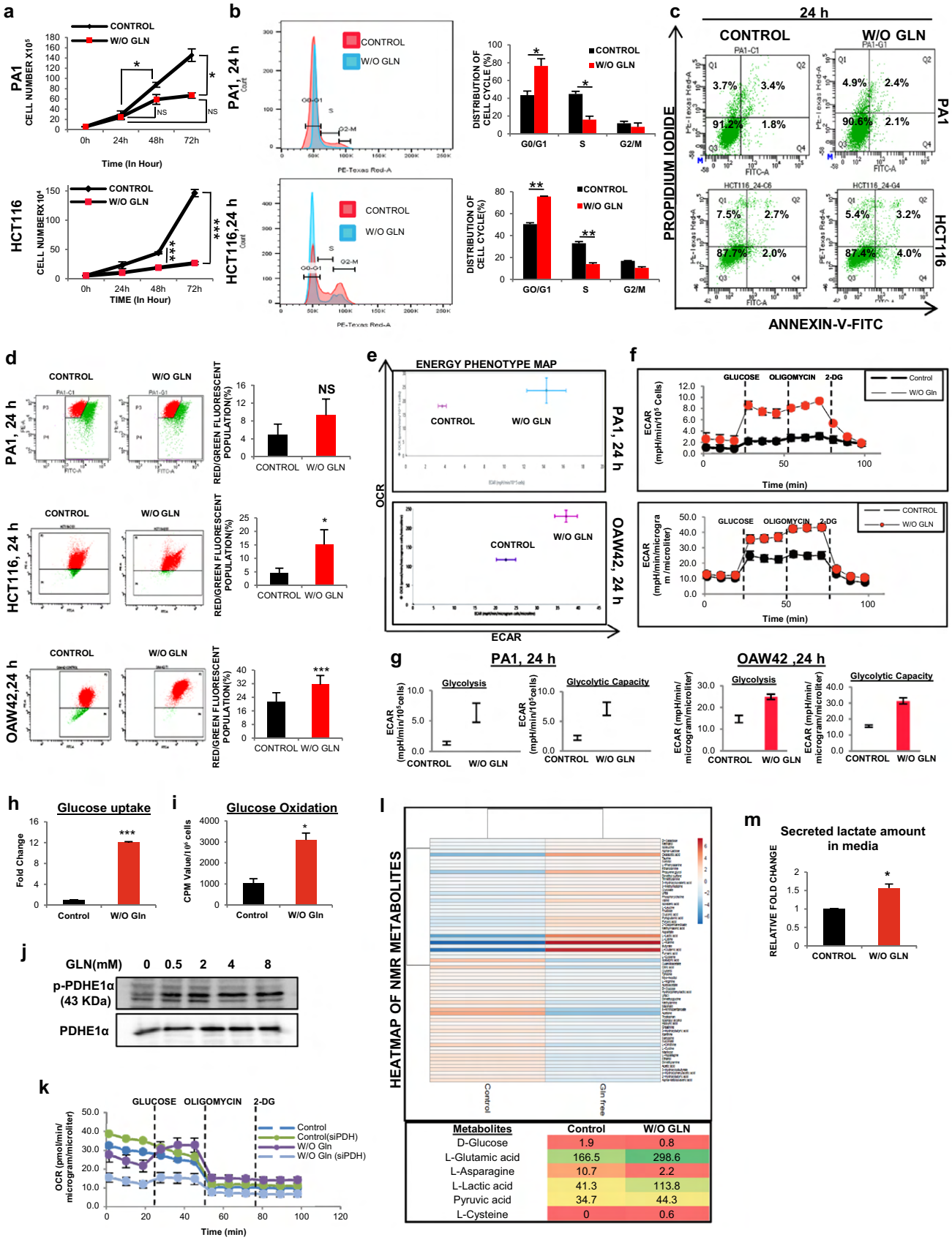

Metabolites	Control	W/O GLN
D-Glucose	1.9	0.8
L-Glutamic acid	166.5	298.6
L-Asparagine	10.7	2.2
L-Lactic acid	41.3	113.8
Pyruvic acid	34.7	44.3
L-Cysteine	0	0.6

◂**Fig. 1** Cancer cells can survive and rearrange their metabolic phenotype in absence of glutamine. **a** Cell proliferation assay was done by counting cell number in 3 consecutive time point (24 h, 48 h, and 72 h) in glutamine-deprived condition (indicated as W/O GLN) in PA1 ($n=3$) and HCT116 ($n=2$) cells. **b** Histogram of cell cycle analysis and corresponding bar diagram of the histogram depicts that the cells were arrested in G0 phase upon glutamine deprivation in both PA1 and HCT116 ($n=3$). **c** Apoptosis assay conducted in glutamine-deprived condition (24 h) and did not find any change in the live-cell population of PA1, and HCT116 ($n=3$). **d** Red/green fluorescent population (%) was quantified for mitochondrial membrane potential using JC-1 dye in PA1, HCT116, and OAW42 upon 24 h of glutamine limiting condition, and presented in bar diagram ($n=3$). **e, f** Extracellular flux analysis dictates that the cells became more glycolytic in nature while OXPHOS remained unchanged at 24 h time point in PA1 and OAW42 cells. **g** At 24 h of glutamine deprivation, glycolysis rate and glycolytic capacity increased in both PA1 and OAW42 cells. **h** Glucose uptake was increased in 24 h of glutamine deprivation in PA1 ($n=3$). **i** Glucose oxidation through TCA cycle was increased in absence of glutamine at 24 h in PA1 ($n=3$). **j** PDH phosphorylation increased in absence of glutamine at 24 h shown by Western blot in PA1 cells. **k** Glycostress assay kit was used to check the change in OCR after glucose injection in glutamine-deprived condition and silencing the PDHE1α in PA1 cells. **l** Heatmap of metabolites measured through NMR spectroscopy at 24 h of glutamine-starved condition in PA1. **m** Lactate level was increased in the medium when the cells are cultured in 24 h of glutamine limiting condition in PA1 ($n=3$). Data are expressed in ± SEM, and statistical significance was calculated using two-tailed Student's t-test (*$p<0.05$, **$p<0.01$, ***$p<0.001$). *NS* non-significant

Two-tailed paired *t* test was performed when the number of groups was two and the one-way ANOVA (followed by Bonferroni post-test analysis) was done, where the number of groups was more than two. *P* values < 0.05 were considered to be statistically significant.

Statistical analysis

All statistical analyses were performed using GraphPad Prism-5 (GraphPad Prism, RRID:SCR_002798) software. The data were represented as ± SEM. Two-tailed paired t test was performed when the number of groups was two and the one-way ANOVA (followed by Bonferroni post-test analysis) was done, where the number of groups was > 2. *P* values < 0.05 were considered to be statistically significant. All the experiments were performed thrice unless otherwise stated. Graphs were made with excel software (Microsoft Excel, RRID:SCR_016137).

Results

Tumor cells can survive in glutamine deficient condition

To understand whether glutamine harmonizes cell growth and proliferation in cancer, we first examined cellular proliferation of PA1 and HCT116 cells cultured with or without glutamine. Although cell number did not change significantly with time when grew in glutamine-starved condition (Fig. 1a), but cell population in S-phase was significantly reduced with concomitant enhancement of control as observed in the cell cycle (Fig. 1b**).** To test whether the reduced cell count was due to cell death upon glutamine deprivation, we performed annexin-V/PI apoptosis assay and observed that there was no significant change in the live cell population (Fig. 1c, Supplementary Fig. S1A).

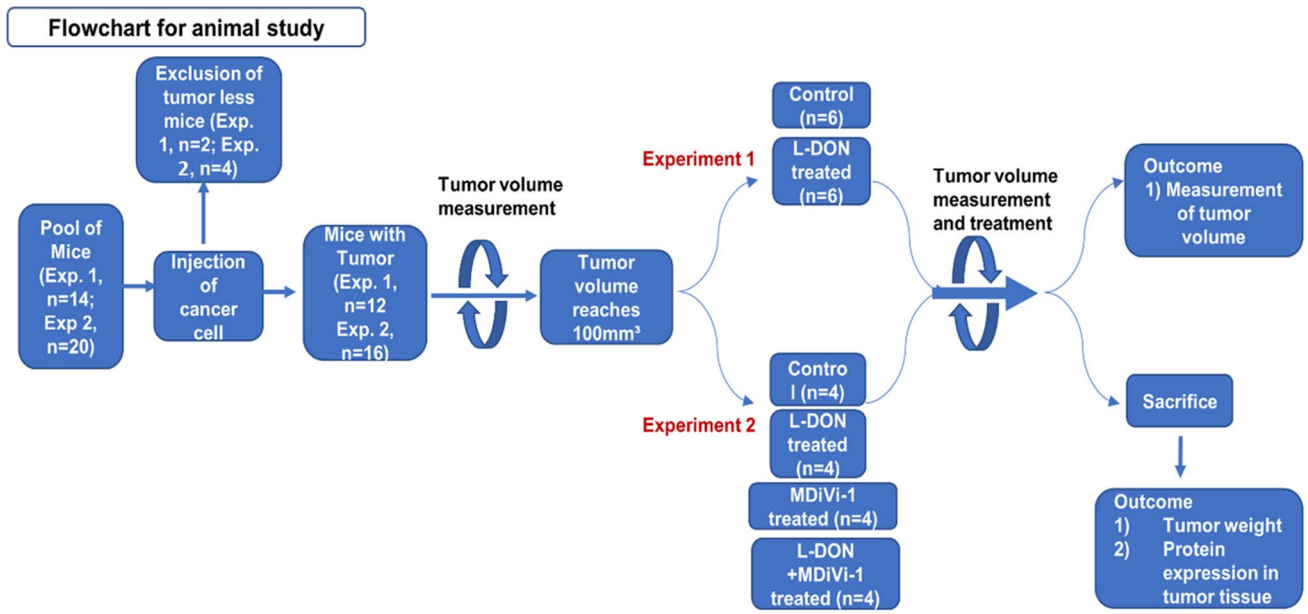

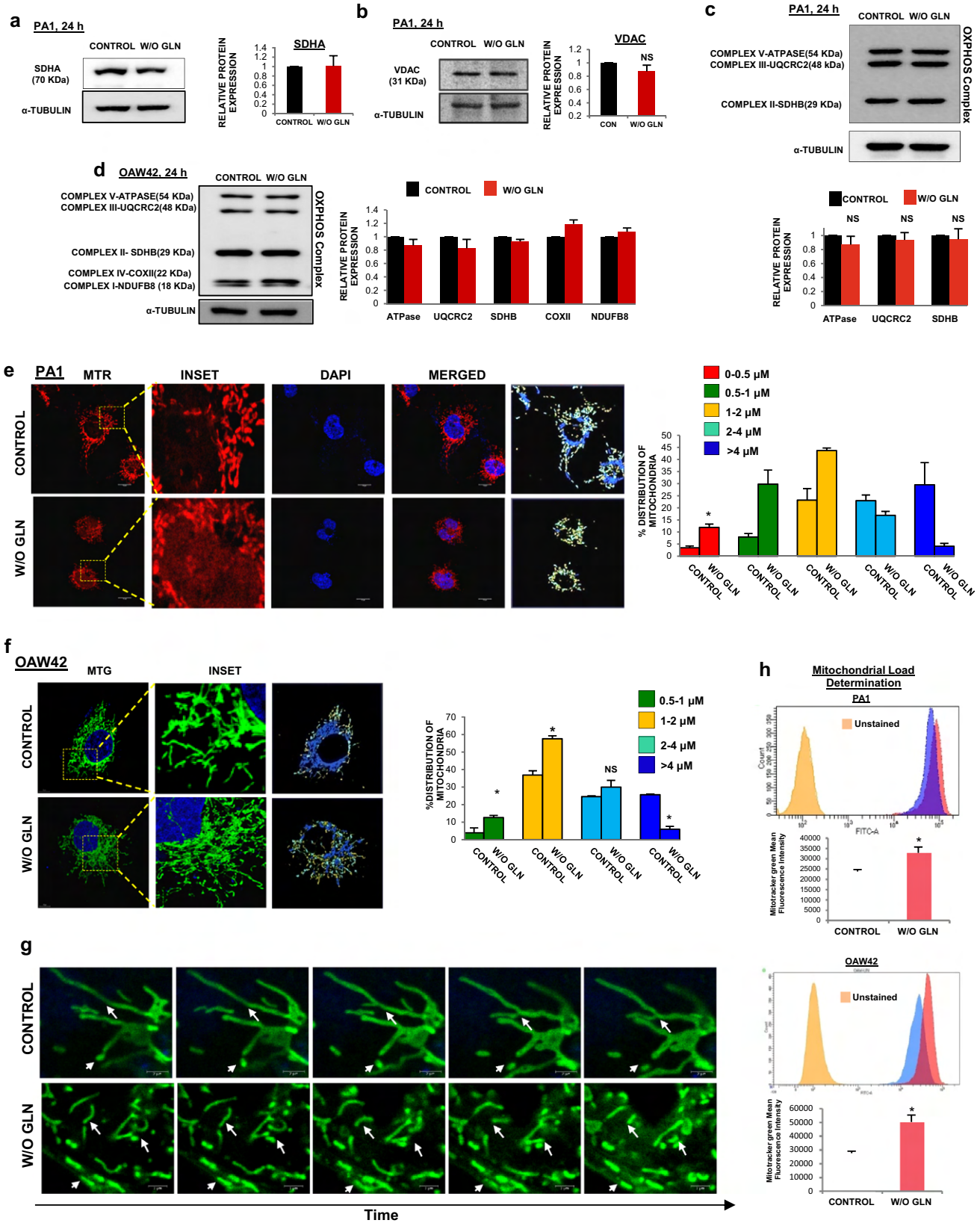
a
PA1, 24 h
CONTROL W/O GLN
SDHA (70 KDa)
α-TUBULIN
SDHA
RELATIVE PROTEIN EXPRESSION
CONTROL W/O GLN
b
PA1, 24 h
CONTROL W/O GLN
VDAC (31 KDa)
α-TUBULIN
VDAC
NS
CON W/O GLN
c
PA1, 24 h
CONTROL W/O GLN
COMPLEX V-ATPASE(54 KDa)
COMPLEX III-UQCRC2(48 kDa)
COMPLEX II-SDHB(29 KDa)
α-TUBULIN
OXPHOS Complex
CONTROL
W/O GLN
NS
ATPase UQCRC2 SDHB
d
OAW42, 24 h
CONTROL W/O GLN
COMPLEX V-ATPASE(54 KDa)
COMPLEX III-UQCRC2(48 KDa)
COMPLEX II- SDHB(29 KDa)
COMPLEX IV-COXII(22 KDa)
COMPLEX I-NDUFB8 (18 KDa)
α-TUBULIN
OXPHOS Complex
CONTROL
W/O GLN
ATPase UQCRC2 SDHB COXII NDUFB8
e
PA1
MTR INSET DAPI MERGED
CONTROL
W/O GLN
0-0.5 μM
0.5-1 μM
1-2 μM
2-4 μM
>4 μM
% DISTRIBUTION OF MITOCHONDRIA
f
OAW42
MTG INSET
CONTROL
W/O GLN
0.5-1 μM
1-2 μM
2-4 μM
>4 μM
%DISTRIBUTION OF MITOCHONDRIA
NS
g
CONTROL
W/O GLN
Time
h
Mitochondrial Load Determination
PA1
Unstained
FITC-A
Mitotracker green Mean Fluorescence Intensity
CONTROL W/O GLN
OAW42
Unstained
CONTROL W/O GLN

◂**Fig. 2** Glutamine starvation leads to the fragmentation of mitochondrion. **a–d** Western blot analysis of SDHA ($n=2$), VDAC, OXPHOS complex proteins (PA1 ($n=3$) and OAW42 ($n=2$) revealed that there was no change in the functional protein amount upon 24 h of glutamine starvation. The quantitative fold change of each protein is represented in the bar diagram along with the respective blot. Microscopic observation with Mitotracker red (MTR) and Mitotracker green (MTG) showing increased fragmentation of mitochondria upon 24 h of glutamine starvation in PA1 (**e**) and OAW42 (**f**) respectively (Being a 3D image, this image does not contain scale bar). Different sized mitochondria are indicated with different colour and their percentage was quantified and expressed in bar diagram for respective cell line **g** Sequential images of live (time lapse) videography of mitochondria undergoing fission and fusion at 24 h of glutamine limiting condition in PA1. The time interval between two consecutive frames for control was 13.75 s and for glutamine-starved cells was 7.25 s. **h** Mitochondrial load determination by Mitotracker Green (MTG) showed a significant increase in the mitochondrial amount upon 24 h of without glutamine condition in PA1 and OAW42 which represented in both histogram and bar diagram ($n=3$). Data are expressed in ± SEM, and statistical significance was calculated using two-tailed Student's t-test (*$p<0.05$). *NS* non-significant. Scale bars 10 µm (**e**), 2 µm (**g**)

Mitochondrial membrane potential known to be decreased in cells undergoing apoptosis [18], was also found to be increased whenever glutamine is depleted from the culture medium (Fig. 1d). Collectively, these data suggest that PA1 and HCT116 cells can sustain in glutamine-deprived condition, however, their proliferation is delayed.

Glutamine starvation leads to altered cellular bioenergetics

As cancer cells endure glutamine-restricted condition, we focused on bioenergetics profile to understand their survival strategy. Although the in vitro cellular oxygen consumption rate (OCR) was changed insignificantly at the basal condition at 24 h (Supplementary Fig. S1B), the extracellular acidification rate (ECAR) started increasing at 18 h and was increased at 24 h and 48 h in PA1 and OAW42 cells (Fig. 1e, f, Supplementary Fig. S1C-F). Similar result was obtained for HCT116 (Supplementary Fig. S5L). The glycolytic reserve, which is the level of full potential of the cell to perform glycolysis was also observed to be increased at 48 h, but not at 24 h of glutamine starvation (Supplementary Fig. S1F-G). Apart from the unaltered basal OCR, the coupling efficiency, which is the percentage of basal OCR used for the ATP synthesis remained unchanged and the glutamine-starved cells produced similar amounts of ATP compared to control cells (Supplementary Fig. S1B). Further, the enhancement of glycolysis and glycolytic capacity in glutamine starvation (Fig. 1g) correlated with the enhanced glucose uptake and glucose oxidation (Fig. 1h, i). In contrast, the protein level of Hexokinase 2 (HK2), a rate-limiting enzyme of glycolysis, remained unchanged (Supplementary Fig. S1H). Glucose is known to be converted into lactate in aerobic condition (Warburg effect) and glutamine can fuel TCA cycle in cancer cells [3]. To rescue the oxidative phosphorylation in glutamine-restricted condition, glucose can provide pyruvate to enter into the TCA cycle to maintain OCR. Therefore, we checked the PDH activity, which was modestly increased (Supplementary Fig. S1I) with a concomitant reduction of its phosphorylation in glutamine-starved condition (Fig. 1j). In addition, we observed that when glucose was injected during extracellular flux analysis, OCR was increased in absence of glutamine, but increment of OCR was reduced when PDHE1α (a subunit of PDH) was silenced (Fig. 1k). These data clearly indicated that in absence of glutamine, glucose takes part in TCA cycle and increases the OCR in PDH dependent manner. As shown by NMR spectroscopy data, glucose produces a higher amount of lactate apart from being the fuel of TCA cycle to maintain OCR (Fig. 1l). Similar result was obtained when extracellular lactate from the medium was quantified in glutamine-restricted condition (Fig. 1m, Supplementary Fig. S1J). Altogether, these first sets of data indicate that in glutamine-restricted condition, cancer cells maintain their cellular bioenergetics by utilizing glucose as the major fueling source for TCA cycle as well as for glycolysis.

Glutamine deprivation promotes mitochondrial fragmentation

Mitochondria are the major site for glutamine metabolism and OXPHOS. In glutamine-restricted condition the tumor cells adapt themselves to maintain an uninterrupted OXPHOS. Hence, we wanted to connect the mitochondrial dynamics and modulation of cellular bioenergetics in glutamine-deprived tumor cells. We did not find any significant change in the expression of mitochondrial proteins such as voltage-dependent anion channel (VDAC), succinate dehydrogenase A (SDHA), and total OXPHOS complex (complex I-V), which indicate unaltered mitochondrial mass (Fig. 2a-d). Surprisingly, we observed that mitochondria are fragmented in the glutamine-starved state. In PA1 and OAW42 cells, the relative number of short mitochondria (≤ 2 µm) was increased with a concomitant depletion of long mitochondria (>4 µm) (Fig. 2e, f, Supplementary Vid. S1-4). Similar results have been obtained for HCT116 cell line (Supplementary Fig. S2A-B). In live-cell videography of PA1 under glutamine limiting condition, shorter mitochondria were observed due to the rapid occurrence of 'kiss-n-run' phenomenon. In contrast, elongated mitochondria were present in the untreated cells with ubiquitous fission and fusion phenomenon (Fig. 2g, Supplementary Vid. S5-6). Interestingly, mitochondria fragmentation was found to be time-dependent, which started appearing at 18 h post-starvation and increased at 24 h (Supplementary Fig. S2C-D). Fragmentation was also increased in non-small cell

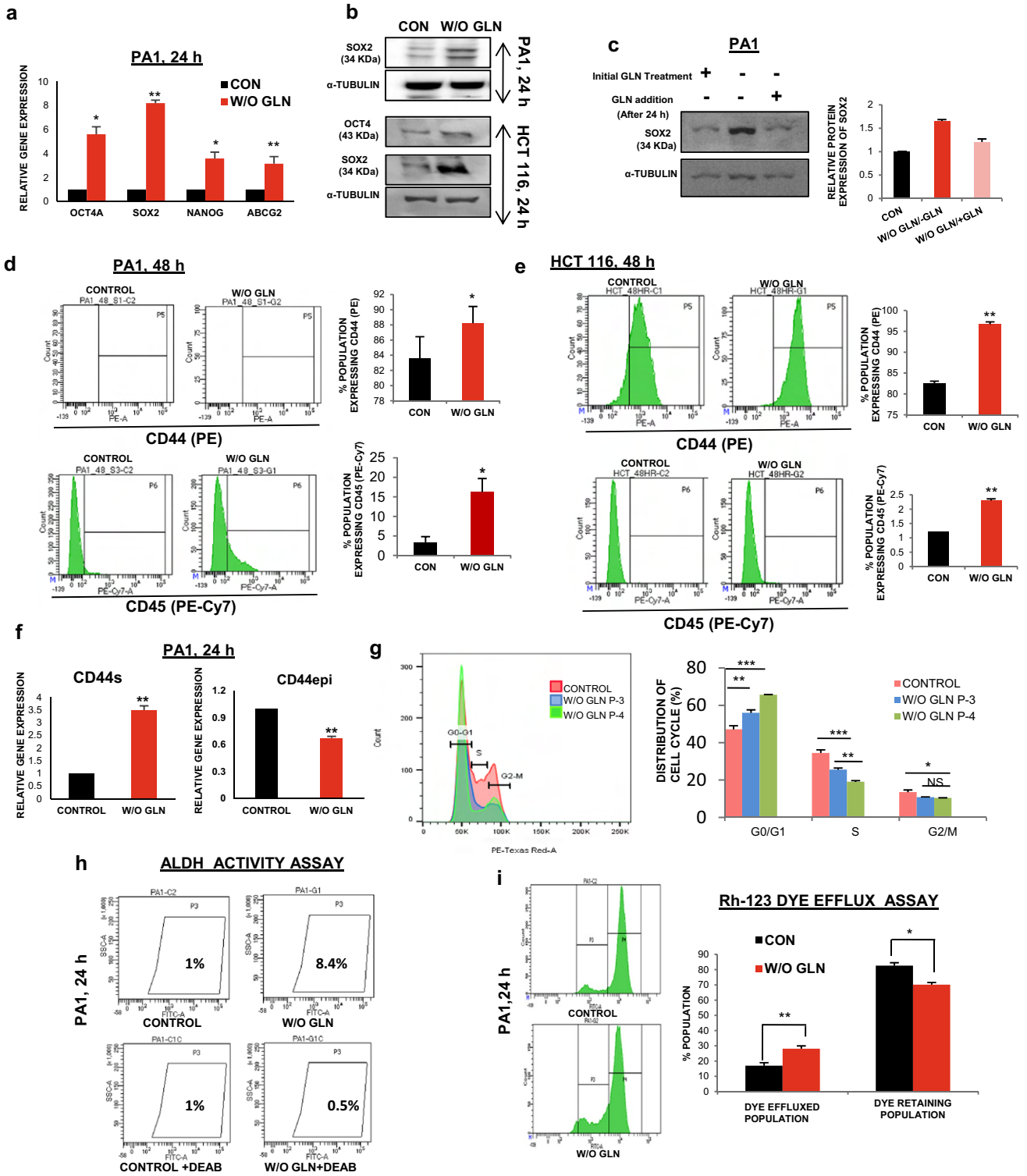

lung cancer cell H1299 and in another epithelial ovarian cancer cell line OVCAR3, at 24 h of glutamine starvation (Supplementary Fig. S2E-F). However, we did not find any difference in mitochondrial fragmentation in other cervical cancer cell line HeLa and SiHa (Supplementary Fig. S2G-H). Mitochondrial fragmentation has been reported to occur during apoptosis and mitophagy [18, 22]. Since the cells did not undergo apoptosis in glutamine limiting condition (Fig. 1c), we focused on the status of mitophagy using mitotracker green by flow cytometry. Mitochondrial amount is known to decrease due to mitophagy as well as mitochondrial degradation [23]. We found enhanced mitotracker

◂**Fig. 3** Glutamine deprivation promotes stemness. **a** The markers of stemness like OCT4, SOX2, NANOG, and ABCG2 mRNA expression was increased as shown by quantitative RT-PCR at 24 h glutamine-starved condition in PA1 ($n=3$). (CON indicates the control cell). **b** Protein expression of different stem markers (SOX2 and OCT4) was increased upon 24 h of glutamine deprivation in both PA1 and HCT116 cells. **c** Re-supplementation of glutamine after 24 h, in the glutamine-starved cell reduced the SOX2 protein level in PA1 and fold change is depicted in the bar diagram. Flow cytometry data reveals that expression of CD44 and CD45 increased in absence of glutamine at 48 h ($n=3$) in PA1 (**d**) and HCT116 (**e**) and % population of expressing cells represented in bar diagram. **f** Gene expression of CD44 variants (CD44epi) was decreased, whereas, CD44s expression was enhanced upon 24 h of glutamine deprivation in PA1 cells ($n=3$). **g** Continuous culture of cells without glutamine at passage 3 (P-3) and passage 4 (P-4) showed an increased population in G1 stage with a reduced population in S phase in PA1 ($n=3$) as shown by flowcytometry. These data are represented in both the histogram and bar diagram. **h** ALDH activity was increased in PA1 cells grew in glutamine-free medium for 24 h. **i** Drug efflux capacity was increased in glutamine-starved PA1 cells at 24 h. Data are expressed in ± SEM, and statistical significance was calculated using two-tailed Student's t test and one-way ANOVA (followed by Bonferroni post-hoc analysis) (*$p<0.05$, **$p<0.01$, ***$p<0.001$). *NS* non-significant

green intensity, suggesting increased mitochondrial load in glutamine starved condition both in PA1 and OAW42 cells (Fig. 2h). As mitotracker green intensity depends upon mitochondrial membrane potential and ROS, we further analyzed the mitochondrial amount by flow cytometry, using nonyl-acridine orange (NAO) which binds to cardiolipin present in inner mitochondrial membrane irrespective of mitochondrial metabolism through flow cytometric analysis [20]. No significant change was found in mitochondrial amount (Supplementary Fig. S2I) and hence we ruled out the possibility of mitophagy. Atomic force microscopic images also depicted that mitochondria were fragmented and their surface roughness remained unchanged in glutamine limiting condition (Supplementary Fig. S2J). Convincingly all these envisioned that glutamine restriction could promote mitochondrial fission in cancer cells.

Stemness and chemoresistance properties also promoted upon glutamine limitation in cancer cells

CSCs are a small population of cells within tumors with self-renewal capacity. They are quiescent in nature having reduced cell proliferation and prevalence of perinuclear localization of fragmented mitochondria [24]. We observed the perinuclear localization of fragmented mitochondria in glutamine limiting state (Supplementary Fig. S3A). The pluripotent stem cell markers like *SOX2, OCT4, NANOG* are highly expressed in CSCs along with the cell surface antigens, like CD44, CD117, CD45, CD31 [25, 26]. As expected, the expression of pluripotent cell markers was found to be upregulated both at the mRNA (Fig. 3a) and protein level (Fig. 3b, Supplementary Fig. S3B) in glutamine-deprived condition. Moreover, when glutamine was added to the medium at 24 h of glutamine starvation, the expression of SOX2 (as a representative marker for stemness) was reduced to the normal level after 24 h of glutamine supplementation (Fig. 3c). These results suggest that glutamine deprivation is responsible for promoting stem-like traits in cancer cells. When the status of different cell surface markers was observed at different hours of glutamine starvation, CD44 and CD117 were increased at 24 h in PA1 (Supplementary Fig. S3C), whereas the expression of CD44 and CD45 was elevated in PA1 and HCT116 at 48 h of glutamine deprivation (Fig. 3d-e). We did not find any significant change in the level of CD31 up to 48 h and similarly, CD45 remains unaltered at 24 h in PA1 cells (Supplementary Fig. S3C-D). However, CD117 was enhanced at 48 h in PA1 (Supplementary Fig. S3D). It was previously reported that deregulated alternative splicing of CD44 enhances CSC traits in tumor cells [27]. We observed increased gene expression of *CD44* standard (*CD44s*) isoform, whereas its epithelial variant (*CD44e*) was downregulated due to glutamine starvation in PA1 cells (Fig. 3f). To test the ultimate effect of glutamine deprivation, we made continuous culture of cells in glutamine-depleted media up to four passages. The cells were found to be arrested at the G0/G1 phase of the cell cycle irrespective of their passage number as evident from the flow cytometric analysis (Fig. 3g). Interestingly, the enhanced ALDH activity, a signature of CSCs, is also found in glutamine-starved PA1 cells (Fig. 3h).

Chemoresistance in CSCs is marked by the upregulation of efflux transporters of the ABC family, like ABCG2,which export drugs out of the cells [1]. Gene and protein expression analysis revealed that ABCG2 was elevated after glutamine deficiency (Fig. 3a, Supplementary Fig. S3B). Rhodamine-123 (Rh123) efflux assay was performed to study the efflux property of glutamine-deprived cells, which export out Rh123 more efficiently compared to the cells grown in glutamine-supplemented condition. There was also a significant reduction of cells that retain Rh123 in glutamine limiting condition as shown by flow cytometry (Fig. 3i, Supplementary Fig. S3E). Therefore, these results indicate that glutamine deprivation might promote stemness and chemoresistance in cancer cells.

Mitochondrial fragmentation is induced through enhanced DRP1 phosphorylation in glutamine-restricted condition

DRP1 is a cytosolic protein that shuttles between cytosol and mitochondrial outer membrane to promote mitochondrial fission. After phosphorylation of DRP1 at S616, it can bind to the mitochondrial outer membrane and constricts the

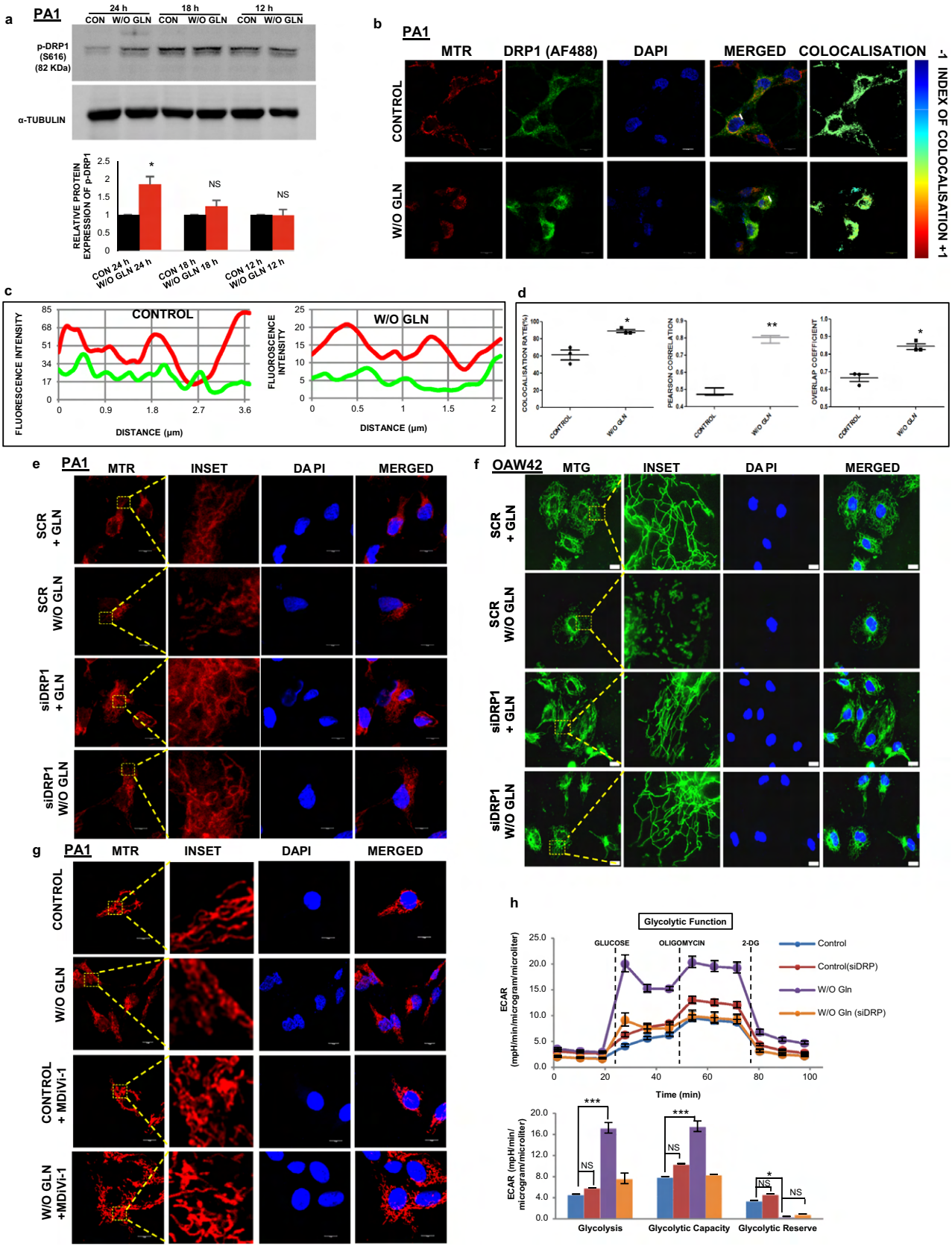
a
PA1
24 h
18 h
12 h
CON W/O GLN CON W/O GLN CON W/O GLN
p-DRP1 (S616) (82 KDa)
α-TUBULIN
RELATIVE PROTEIN EXPRESSION OF p-DRP1
CON 24 h
W/O GLN 24 h
CON 18 h
W/O GLN 18 h
CON 12 h
W/O GLN 12 h
b
PA1
MTR
DRP1 (AF488)
DAPI
MERGED
COLOCALISATION
CONTROL
W/O GLN
INDEX OF COLOCALISATION
c
CONTROL
W/O GLN
FLUORESCENCE INTENSITY
DISTANCE (μm)
d
COLOCALISATION RATE(%)
PEARSON CORRELATION
OVERLAP COEFFICIENT
e
PA1
MTR
INSET
DAPI
MERGED
SCR + GLN
SCR W/O GLN
siDRP1 + GLN
siDRP1 W/O GLN
f
OAW42
MTG
INSET
DAPI
MERGED
g
PA1
MTR
INSET
DAPI
MERGED
CONTROL
W/O GLN
CONTROL + MDiVi-1
W/O GLN +MDiVi-1
h
Glycolytic Function
GLUCOSE
OLIGOMYCIN
2-DG
Control
Control(siDRP)
W/O Gln
W/O Gln (siDRP)
ECAR (mpH/min/microgram/microliter)
Time (min)
Glycolysis
Glycolytic Capacity
Glycolytic Reserve

◂**Fig. 4** DRP1 phosphorylation and localization promote mitochondrial fragmentation. **a** The cells were grown for 12 h, 18 h, and 24 h in glutamine-free medium and cellular protein was isolated followed by SDS-PAGE and western blotting. The phosphorylation of DRP1 (S616) was increased at 24 h ($n=3$), as shown by bar diagram. **b** Microscopy-based colocalization analysis in PA1 revealed the significant enhancement of association between DRP1 and mitochondria in absence of glutamine at 24 h ($n=3$). **c** Line scan analysis of colocalization microscopy depicted significant overlapping of mitochondrial (RED) and DRP1 (GREEN) increased in absence of glutamine. **d** Intensity correlation analysis of colocalization through fluorescence microscopy of mitochondria and DRP1 revealed that colocalization rate, Pearson's correlation, and overlap coefficient are enhanced upon glutamine deprivation. Knockdown of DRP1 protected the mitochondria from fragmentation in PA1 (**e**) and OAW42 (**f**) as depicted in confocal microscopy. **g** Similarly, inhibition of DRP1 with MDiVi-1 significantly inhibits mitochondrial fragmentation upon 24 h of glutamine starvation in PA1 as observed by confocal microscopy. **h** Extracellular Flux analysis revealed that DRP1 knockdown was capable of restoring the glycolysis, glycolytic capacity similar to the control cells of PA1 upon 24 h of glutamine starvation ($n=3$). Data are expressed in ± SEM, and statistical significance was calculated using two-tailed Student's t test and one-way ANOVA (followed by Bonferroni post hoc analysis) (*$p<0.05$, **$p<0.01$, ***$p<0.001$). *NS* non-significant. Scale bars 10 µm (**b**, **e**, **g**), 20 µm (**f**)

membrane using its GTPase activity [28]. We observed that S616 phosphorylation was elevated upon glutamine deprivation for 24 h in PA1 and HCT116, although there was no significant change of p-DRP1 till 18 h of starvation (Fig. 4a, Supplementary Fig. S4A). We did not observe any change of expression in the mitochondrial fusion protein such as Mitofusin-1 (MFN1) and Mitofusin-2 (MFN2) (Supplementary Fig. S4B). Glutamine deprivation showed mitochondria-specific localization of DRP1 in PA1 cells (Fig. 4b). The colocalization was established qualitatively using line-scan analysis and intensity correlation analysis (ICA). The line scan graph analysis suggested that the mitochondrial localization of DRP1 was very specific in glutamine-restricted condition (Fig. 4c). The ICA statistical data showed that the colocalization rate, Pearson's correlation, and overlap coefficient were enhanced in glutamine deficiency (Fig. 4d). Further, the silencing of DRP1 using siRNA inhibited mitochondrial fission in glutamine depleted PA1 and OAW42 cells (Fig. 4e, f). Similar results were observed when DRP1 inhibitor MDiVi-1 was used (Fig. 4g). In contrast, extracellular flux analysis indicates that ECAR, total glycolysis, glycolytic capacity as well as the glycolytic reserve were decreased after treating the cells with MDiVi-1 and siDRP1 individually in glutamine-deprived condition (Fig. 4h, Supplementary Fig. S4C-E). These results thus point DRP1 as the potential component for mitochondrial fragmentation in glutamine-restricted condition.

DRP1 has a role in stimulating stem-like characteristics and chemoresistance

To test the impact of inhibition of mitochondrial fission, we used MDiVi-1 as an inhibitor of fission in glutamine-deprived condition. We observed a significant reduction of CD44 (a stem cell marker) after silencing and inhibiting DRP1 in HCT116 and PA1, respectively, in glutamine limiting condition (Fig. 5a, Supplementary Fig. S4F-G). Another remarkable trait of CSCs is to form spheroid in non-adherent condition. Glutamine-starved cells gave rise to larger spheroids when cultured in non-adherent condition for 4 days and its volume became the same as that of untreated cells, when treated with MDiVi-1 in absence of glutamine (Fig. 5b). We have also performed this assay with the cells continuously cultured for seven passages in absence of glutamine. They formed larger spheroids and could able to generate a greater number of spheroids than the other sets. It also gave rise to new smaller spheroids even after 4 days of the assay, which suggests that continuous culture in absence of glutamine could significantly increase the stemness potential. To check if the cells maintain the fragmented mitochondrial phenotype in spheroids, we have used mitotracker red (MTR) for confocal microscopy and observed the presence of fragmented mitochondria in the spheroid (Fig. 5c). In human high-grade ovarian cancer tissue sample, colocalization of CD44 and p-DRP1 (S616) was increased as compared to the normal ovarian tissue section (Fig. 5d). Taken together, we can conclude that glutamine deprivation can enhance stem-like characteristics through DRP1 signaling in cancer.

We then wanted to determine whether DRP1 mediated stem-like characteristics are associated with chemoresistance. Both MDiVi-1 and siDRP1 independently can markedly enhanced the Rh123 dye retaining population, which was decreased in glutamine-starved condition, suggesting a role of DRP1 in chemoresistance (Fig. 5e, Supplementary Fig. S4H-I). These results suggest that DRP1 promotes stem-like characteristics coupled with chemoresistance in cancer cells in glutamine limiting condition.

Glutamine-restricted cells augment ERK1/2 induced DRP-1 phosphorylation through ROS

Glutamine also plays a role in synthesizing GSH via glutamate. GSH is a major endogenous antioxidant and linked with the ROS level [29]. As glutamine restriction was associated with reduced GSH synthesis, we focused on the status of mitochondrial ROS and tried to find a causal link between the ROS and DRP1 phosphorylation at S616. To validate this, we found that there was no significant difference in cellular GSH at 24 h of glutamine starvation (Fig. 6a). Next, we measured mitochondrial ROS generation at 3, 6, 12 and 24 h of glutamine deprivation (Fig. 6b) and found its significant

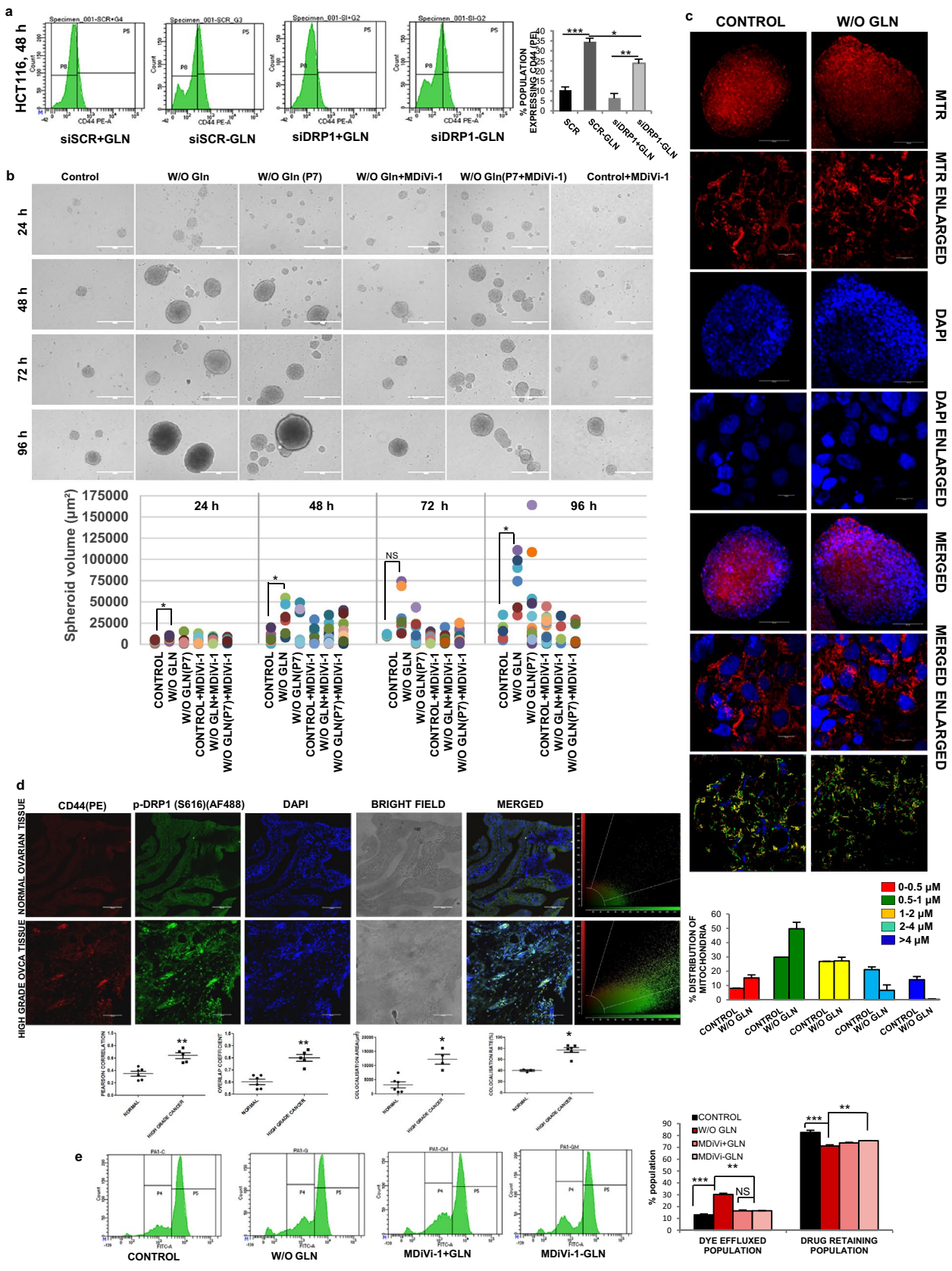
a
HCT116, 48 h
siSCR+GLN
siSCR-GLN
siDRP1+GLN
siDRP1-GLN
% POPULATION EXPRESSING CD44 (PE)
SCR
SCR-GLN
siDRP1+GLN
siDRP1-GLN
b
Control
W/O Gln
W/O Gln (P7)
W/O Gln+MDiVi-1
W/O Gln(P7+MDiVi-1)
Control+MDiVi-1
24 h
48 h
72 h
96 h
Spheroid volume (µm²)
CONTROL
W/O GLN
W/O GLN(P7)
CONTROL+MDiVi-1
W/O GLN+MDiVi-1
W/O GLN(P7)+MDiVi-1
c
CONTROL
W/O GLN
MTR
MTR ENLARGED
DAPI
DAPI ENLARGED
MERGED
MERGED ENLARGED
0-0.5 µM
0.5-1 µM
1-2 µM
2-4 µM
>4 µM
% DISTRIBUTION OF MITOCHONDRIA
d
CD44(PE)
p-DRP1 (S616)(AF488)
DAPI
BRIGHT FIELD
MERGED
NORMAL OVARIAN TISSUE
HIGH GRADE OVCA TISSUE
PEARSON CORRELATION
OVERLAP COEFFICIENT
COLOCALISATION AREA
COLOCALISATION RATE
NORMAL
HIGH GRADE CANCER
e
CONTROL
W/O GLN
MDiVi-1+GLN
MDiVi-1-GLN
CONTROL
W/O GLN
MDiVi+GLN
MDiVi-GLN
% population
DYE EFFLUXED POPULATION
DRUG RETAINING POPULATION

◂**Fig. 5** DRP1 inhibition reduced stem-like features. **a** Flow cytometric data showed that the reduced expression of CD44 in HCT116 cells upon DRP1 silencing when grown in glutamine-starved condition for 48 h. The % population of CD44 expressing cells are quantified and represented in the bar diagram ($n=2$). **b** MDiVi-1 treatment reduced spheroid size in absence of glutamine in PA1 as shown in bright field microscopy suggesting DRP1 dependency in spheroid formation. The number and volume of spheroid at different time points are shown in the bar diagram ($n=3$). **c** In the spheroid cultures of PA1, the cells retained their fragmented morphology of mitochondria as shown in confocal microscopy and quantified the percentage of different mitochondrial length ($n=2$). **d** CD44 expression and colocalization with p-DRP1 was high in high-grade ovarian cancer compared to normal ovarian tissue in IHC. Intensity correlation analysis of this colocalization was shown in the bar diagram in the form of co-localization rate, colocalization area, Pearson's correlation co-efficient, overlap co-efficient (**e**) MDiVi-1 treatment also reduced drug efflux capacity of cells at 24 h of glutamine starvation in PA1 ($n=2$). Data are expressed in ± SEM, and statistical significance was calculated using two-tailed Student's t test and one-way ANOVA (followed by Bonferroni post hoc analysis) (*$p<0.05$, **$p<0.01$, ***$p<0.001$). *NS* non-significant. Scale bars 400 µm (**b**), 100 µm (**c, d**), 10 µm (Enlarged images of **c**)

elevation only at 12 h. By H_2O_2 treatment, we have shown that ROS independently induces mitochondrial fragmentation which is reduced by NAC treatment, an exogenous ROS scavenger (Supplementary Fig. S5A-B). In glutamine-deprived condition, another exogenous ROS scavenger, cell-permeable glutathione (GSH) reduces ROS-induced mitochondrial fragmentation (Fig. 6c). Similarly, NAC also reduces the phosphorylation of DRP1 at S616 (Fig. 6d) and reduced mitochondrial fragmentation (Supplementary Fig. S5C) in glutamine-depleted situation. Thus, glutamine depletion generates ROS, which might be responsible for the phosphorylation of DRP1 followed by mitochondrial fragmentation.

To explore the pathways associated with mitochondrial fragmentation and DRP1 phosphorylation, we further checked the phosphorylation level of AKT (S473) and p38MAPK (T180/Y182) through Western blot analysis and found no alteration of their phospho- and total forms at 24 h of glutamine deprivation (Fig. 6e). The ERK1/2 phosphorylation on T202/204 was increased at 24 h of glutamine depletion (Fig. 6f). Moreover, DRP1 phosphorylation (S616) was found to be dependent on the ERK1/2 signaling pathway as ERK inhibitor prevented this phosphorylation (Fig. 6g). The number of longer mitochondria was significantly increased when U0126 (inhibitor of MEK, the upstream kinase of ERK) was added in the glutamine-depleted media (Fig. 6h). The above results convincingly show that DRP1 was phosphorylated through ROS-dependent activation of the ERK1/2 signaling pathway and promote mitochondrial fragmentation in tumor cells.

It is well known that xCT (antiporter of glutamate and cysteine) colocalizes with CD44 protein for maintaining the redox balance in the cell. Its expression also increased along with its enhanced colocalization with CD44 (Supplementary Fig. S5D-G). Since the ROS induced phosphorylation of DRP1, we checked the role of xCT in maintaining the ROS level in glutamine-deprived condition; however, no significant increase in the total cellular and mitochondrial ROS was observed upon inhibition of xCT by siRNA and its inhibitor sulfasalazine (Supplementary Fig. S5H-J). It suggested that xCT is not involved in the maintenance of ROS in glutamine-restricted condition. Perinuclear localization of mitochondria is known to increase nuclear ROS accumulation and activate various transcription factors for their downstream functioning. Therefore, we performed microscopy with DCFDA and MTR-stained cells and found that the perinuclear localization of mitochondria led to the accumulation of ROS in the nucleus in glutamine limiting condition (Supplementary Fig. S5K). Considering these results, we speculated that ROS accumulation within the nucleus is responsible for promoting stemness in glutamine-deprived condition.

Combinatorial treatment of glutaminase inhibitor (L-DON) and MDiVi-1inhibit tumor growth and reduce CSCs population

Glutamine metabolism is therapeutically targeted for killing aggressive cancer cells. GLS1 inhibition by L-DON can stop the usage of glutamine by the cancer cells and hence, it can mimic a situation of glutamine deprivation. We observed that L-DON treatment can significantly increase the level of p-DRP1 at S616 (Fig. 7a) and consequently, the number of fragmented mitochondria (Fig. 7b). Like glutamine-starved condition, L-DON treatment also increases ECAR (Fig. 7c, d, Supplementary Fig. S5L) and protein expression of SOX2 (Supplementary Fig. S5M). Further, to establish the results in in-vivo, we studied the parameters in syngeneic mouse model (C57BL/6) using ID8 (mouse ovarian epithelial cancer cell) cells. After the appearance of 100 mm^3 tumor volume, mice were injected intravenously with L-DON consecutively for 3 days, whereas the animals of the control set were injected with equal volume of PBS (Fig. 7e). We found that L-DON treatment significantly inhibited tumor growth and weight gain as compared to the control set (Fig. 7f–h). Histological analysis with hematoxylin and eosin staining demarcated the tumor core area with lower number of cells, implying that glutamine starvation in the tumor core could be responsible for lowered cell number (Fig. 7i). To check if there is any necrotic cell population in the core of those tumors, we performed TUNEL assay and found no significantly increased TUNEL positive cells (Supplementary Fig. S6A). There was reduced Ki67 protein in the nucleus of L-DON treated cells, depicting that L-DON treatment ceased cell proliferation (Fig. 7j). To further validate the effect of MDiVi-1 in glutamine-starved condition,

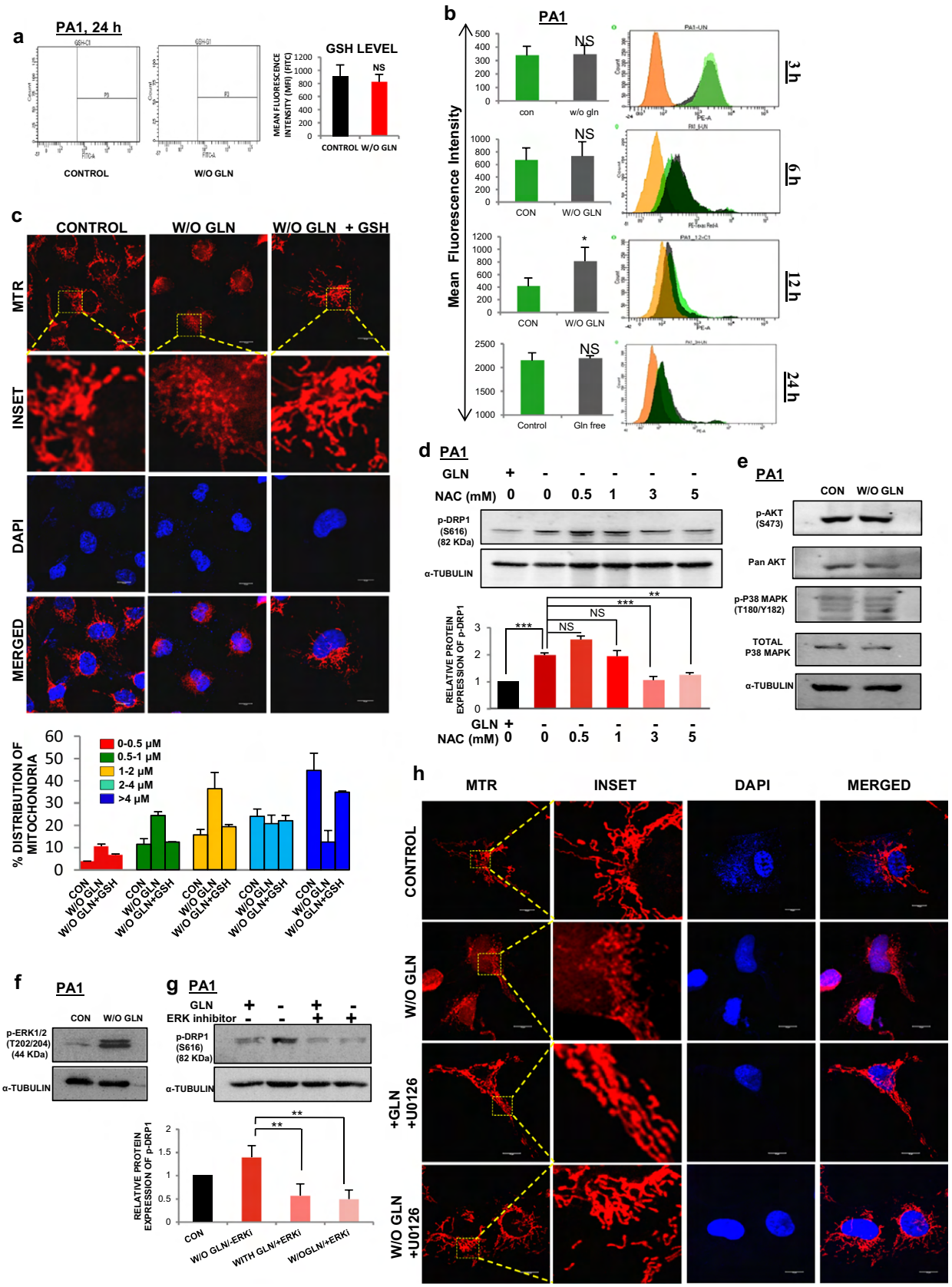
a
PA1, 24 h
CONTROL
W/O GLN
GSH LEVEL
MEAN FLUORESCENCE INTENSITY (MFI) (FITC)
NS
CONTROL W/O GLN
b
PA1
Mean Fluorescence Intensity
NS
con
w/o gln
3 h
CON
W/O GLN
6 h
*
12 h
Control
Gln free
24 h
c
CONTROL
W/O GLN
W/O GLN + GSH
MTR
INSET
DAPI
MERGED
% DISTRIBUTION OF MITOCHONDRIA
0-0.5 µM
0.5-1 µM
1-2 µM
2-4 µM
>4 µM
CON
W/O GLN
W/O GLN+GSH
d
PA1
GLN
NAC (mM)
p-DRP1 (S616) (82 KDa)
α-TUBULIN
RELATIVE PROTEIN EXPRESSION OF p-DRP1
***
NS
**
e
PA1
CON
W/O GLN
p-AKT (S473)
Pan AKT
p-P38 MAPK (T180/Y182)
TOTAL P38 MAPK
α-TUBULIN
f
PA1
p-ERK1/2 (T202/204) (44 KDa)
g
PA1
ERK inhibitor
W/O GLN/-ERKi
WITH GLN/+ERKi
W/OGLN/+ERKi
h
MTR
INSET
DAPI
MERGED
CONTROL
W/O GLN
+GLN +U0126
W/O GLN +U0126

◂**Fig. 6** DRP1 phosphorylation occurs through ROS driven ERK1/2 signaling pathway (**a**) Total internal GSH was measured through flow cytometry at 24 h of glutamine starvation in PA1 and MFI was quantified and represented in the bar diagram ($n=3$). **b** Mitochondrial ROS was measured upon glutamine deprivation at different time points (3 h,6 h,12 h, and 24 h) by flow cytometry in PA1. At 12 h only, there was a significant increment in the ROS level which decreased eventually ($n=3$). The results were represented as histograms along with the bar diagram. **c** GSH treatment in absence of glutamine at 24 h reduced mitochondrial fragmentation in PA1 as depicted by confocal microscopy. **d** NAC treatment for 24 h in glutamine depleted media significantly reduced the DRP1 phosphorylation in PA1, as observed in western blot analysis ($n=3$). Fold change was measured by densitometric analysis using ImageJ software and represented as bar diagram. **e** As shown by western blot analysis, there was no change in phosphorylation of AKT and p38 MAP kinase upon 24 h of glutamine starvation in PA1 cell. **f** There was a significant change in phosphorylated ERK1/2 at 24 h of glutamine starvation in PA1. **g** ERK inhibitor is sufficient to inhibit DRP1 phosphorylation at glutamine starvation in PA1 at 24 h. Densitometric analysis of this blot quantified the fold change of protein expression and represented in bar diagram. **h** Treatment of U0126 also inhibited mitochondrial fragmentation at 24 h of glutamine-starved condition in PA1 cell as shown in confocal microscopy. Data are expressed in ± SEM, and statistical significance was calculated using two-tailed Student's t test and one-way ANOVA (followed by Bonferroni post hoc analysis) (*$p<0.05$, **$p<0.01$, ***$p<0.001$). NS is for non-significant. Scale bars 10 µm (**c, h**)

we injected it with or without L-DON in tumor-bearing mice (Fig. 8a, b). We found no significant increase in cell death as shown by Cleaved caspase-3 staining (Fig. 8c, e). L-DON treatment even in presence of MDiVi-1 significantly inhibited tumor growth (Supplementary Fig. S6B). There was increased expression of ABCG2, SOX2 and OCT4 after L-DON treatment that was significantly reduced by MDiVi-1 in in vivo model (Fig. 8d, e, Supplementary Fig. S6C-D). L-DON-treated tumors showed increased DRP1 phosphorylation (S616) and CD44 expression along with increased co-localization of these proteins, while dual treatment of L-DON and MDiVi-1 significantly reduced the CD44 expression (Fig. 8f). These results point towards a possibility that simultaneous pharmacological inhibition of GLS1 and mitochondrial fission might inhibit tumor growth with reduction in CSC population.

Discussion

Growing tumors require and consume plenty of glutamine for their survival and this addiction for glutamine is used to diagnose the growing tumors through 18F-FGln based PET scanning systems [30]. It is well established that the core of a solid tumor is glutamine-deprived and cancer cells survive in this nutrient limiting condition [16]. Further, this regional glutamine deficiency is supposed to be a major contributor of chemoresistance property that tumor cells acquire subsequently [31]. In this report, we showed that glutamine deficiency generates stem-like characteristics to induce chemoresistance property in the tumor cells by inducing mitochondrial fragmentation.

Glutamine dependency is acquired by tumor cells and is a crucial phenotype for aggressive cancer cell. Glutamine is required for their survival, proliferation, and metastasis [32]. In contrast, our present findings suggest that glutamine is crucial for the proliferation of cancer cells, but is not essential for their survival (Fig. 1a–c, Supplementary Fig. S1A). However, in absence of glutamine, the cell division potency of cancer cells did not cease, but significantly reduced as they still continued to proliferate even after several passages of culture in glutamine-free medium (Fig. 1b, 3g). This addiction towards glutamine is varied in different cancer cell types and their metabolic phenotype changes with their glutamine dependency level [32, 33]. In some cervical and breast cancer cells, basal oxygen consumption rate and glycolytic efficiency decreased in the absence of glutamine independently of their metabolic phenotype [12]. However, we identified that upon glutamine starvation, glucose uptake and glucose oxidation is enhanced to maintain both glycolysis and TCA cycle (Fig. 1e–m, Supplementary Fig. S1B-G, I-J). In tumor core, there is a possibility of both glucose and glutamine scarcity. In that condition, it is interesting to understand how glutamine-starved cells maintain high glycolysis rate. The possible explanation could be addressed by two different mechanisms. Firstly, in the periphery of the tumor, the glucose consumption is less than the core, rendering high availability and consumption of glucose by the glutamine-starved cells in the core [34]. Second, when the cells in the core perform higher glycolysis, they produce extracellular lactate, which can relay signal to the peripheral cells to reduce their glucose uptake [35]. Thus, it ensures that the core cells get adequate glucose in absence of glutamine. To further confirm the effect of lactate, we have treated the PA1 cells with it in presence of glutamine and observed reduced glucose uptake and glycolysis. Further, by blocking the lactate receptor with 3-OBA (3-hydroxy-butyrate) and using its transporter (MCT1) blocker the lactate signaling was found inhibited in glutamine supplemented cells (data not shown).

Mitochondrial fragmentation is an essential phenotype for various types of tumors and in melanoma cells, it is found to increase glycolytic rate [36]. We convincingly showed that glutamine deficiency facilitates mitochondrial fragmentation through phosphorylation of DRP1 at S616 (Fig. 4). DRP1 level is directly linked to the mitochondrial network (length) as silencing or inhibiting DRP1 reduces the mitochondrial fragmentation in absence of glutamine (Fig. 4e-g) and this DRP1 phosphorylation also linked with cell metabolism as glycolytic function remain same as control when DRP1 was silenced or inhibited (Fig. 4h, Supplementary Fig. S4C–E). We did not find any difference in mitochondrial protein level (Fig. 2a–d) and the level of mitochondrial OXPHOS

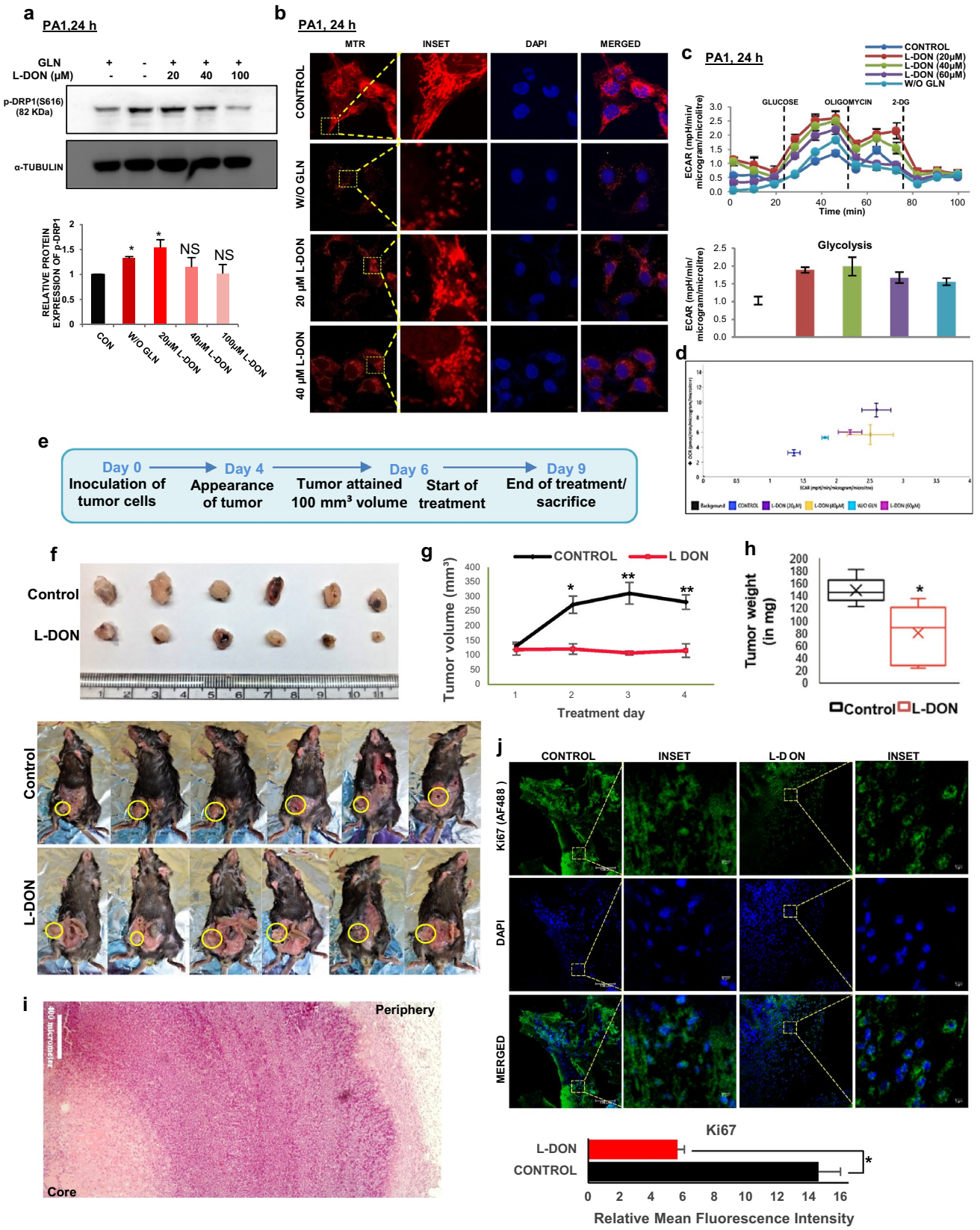
a
PA1,24 h
GLN
L-DON (μM)
p-DRP1(S616) (82 KDa)
α-TUBULIN
RELATIVE PROTEIN EXPRESSION OF p-DRP1
CON
W/O GLN
20μM L-DON
40μM L-DON
100μM L-DON
NS
b
PA1, 24 h
MTR
INSET
DAPI
MERGED
CONTROL
W/O GLN
20 μM L-DON
40 μM L-DON
c
PA1, 24 h
CONTROL
L-DON (20μM)
L-DON (40μM)
L-DON (60μM)
W/O GLN
GLUCOSE
OLIGOMYCIN
2-DG
ECAR (mpH/min/microgram/microlitre)
Time (min)
Glycolysis
d
e
Day 0
Inoculation of tumor cells
Day 4
Appearance of tumor
Day 6
Tumor attained 100 mm³ volume
Day 9
End of treatment/ sacrifice
Start of treatment
f
Control
L-DON
g
CONTROL
L DON
Tumor volume (mm³)
Treatment day
h
Tumor weight (in mg)
Control
L-DON
i
Periphery
Core
j
CONTROL
INSET
L-D ON
INSET
Ki67 (AF488)
DAPI
MERGED
Ki67
L-DON
CONTROL
Relative Mean Fluorescence Intensity

◂**Fig. 7** L-DON mimics glutamine starvation in tumor cells. **a** L-DON treatment increased DRP1 phosphorylation at the concentration of 20 µM in PA1 cell. Densitometric analysis was done using ImageJ software and the fold change is presented as bar diagram ($n=3$). **b** L-DON treatment increased mitochondrial fragmentation as observed in confocal microscopy. **c** L-DON treatment for 24 h also increased the ECAR value along with glycolysis like glutamine starvation in PA1. **d** The energy phenotype graph also showed increased ECAR after L-DON treatment in PA1. **e** Timeline of development of tumor in mouse model and L-DON treatment. **f** Representative images of tumors formed in C57BL/6 injected with PBS or L-DON. **g** Tumor volume measured during 3 days of L-DON treatment course and represented graphically ($n=6$) and **h** tumor weight was measured at the end of treatment course (Day-4) and represented in bar diagram. **i** Histological section stained with Hematoxylin and Eosin showed meagre amount of cell in the core of the tumor. **j** Fluorescence-immunohistochemistry depicted that amount of Ki67 in tumors was decreased in L-DON treated set ($n=5$). In the control tissue, Ki67 localized in the nucleus whereas extranuclear localization of Ki67 was observed in L-DON treated set. Data are expressed in ± SEM, and statistical significance was calculated using two-tailed Student's t test and one-way ANOVA (followed by Bonferroni post hoc analysis) (*$p<0.05$, **$p<0.01$). *NS* non-significant. Scale bars 10 µm (**b**), 400 µm (**i**), 100 µm (**j**) and 5 µm (INSET of **j**)

(Supplementary Fig. S1B) and hence, we have not linked mitochondrial function with DRP1 level upon glutamine starvation. Treatment with MDiVi-1 also inhibited the retrograde transport of the mitochondria, i.e., the perinuclear localization of the mitochondria, indicating that the retrograde movement is fission dependent as reported previously [37].

Mitochondrial ROS act as an important second messenger to drive intracellular signaling pathways [38] and it is associated with mitochondrial fragmentation in malignant cells through ROS-RAS-RAF-ERK1/2-DRP1 signaling axis [39, 40]. It is reported that high glucose treatment in primary liver cells increased ROS production with concomitant enhancement in the mitochondrial fragmentation followed by perinuclear localization [41]. According to this report, ROS was increased at 15 min of incubation and decreased after 60 min, but the mitochondrial fragmentation persisted. Similarly, in the present study, we have also found a very dynamic and variable pattern of ROS level, which increases at 12 h of glutamine deprivation and surprisingly reduced again at 24 h, but the mitochondria remain fragmented (Fig. 6b, 2e). Treatment with cell-permeable anti-oxidant GSH and NAC in glutamine-deprived conditions can rescue the mitochondria from fragmentation (Fig. 6c, Supplementary Fig. S5C). Therefore, the rise in the mitochondrial ROS may be responsible for the acute activation of ERK1/2 and DRP1. Then perinuclear accumulation of fragmented mitochondria increases the local ROS accumulation in the nucleus (Supplementary Fig. S3A, S5K). This local ROS accumulation in the nucleus has been reported as a regulatory factor of gene expression through guanidine oxidation [11]. Moreover, we also found nuclear accumulation of NRF2, which is a well-established transcriptional regulator of ABCG2 in glutamine limiting condition (data not given). We suggested that DRP1-driven mitochondrial fragmentation and its perinuclear localization may promote stemness via nuclear accumulation of NRF2 in glutamine-deprived condition. Therefore, it is an interesting area to follow-up in detail and future studies are needed to determine the actual cause of ROS generation that leads to mitochondrial fragmentation in glutamine-starved cells.

In gynecological cancer, DRP1 and mitochondrial dynamics play a vital role in promoting chemoresistance [42, 43]. According to recent evidence, mitochondrial fragmentation and clustering around the nucleus is an important feature associated with stem cells [11, 28, 44]. Some reports have demonstrated that this "mitochondrial flirtation" with the nucleus induces the ROS level in the nucleus and this micro milieu leads to the activation of various transcription factors that can regulate gene associated with stemness [11]. ROS also can regulate stemness by suppressing Wnt/β-catenin signaling pathway in glutamine-dependent pancreatic ductal carcinoma, hepatocellular carcinoma, and non-small cell lung carcinoma [45, 46]. In contrast, glutamine deprivation inhibits Wnt signaling pathway and induces stemness in colorectal cancer. This effect can be reversed by the addition of α-ketoglutarate which may take over the function of glutamine in the downstream signaling [47]. In this report, we show that glutamine starvation enhances perinuclear localization of fragmented mitochondria, which leads to the promotion of stem-like features and chemoresistance in cancer cells (Fig. 3, Supplementary Fig. S3). The CD44-xCT colocalization has been reported to maintain the redox balance in cancer cells. xCT is an antiporter for glutamate and cysteine and is involved in the synthesis of glutathione and thereby preserves the redox homeostasis within the cell. Therefore, the interaction between CD44 and xCT is important for maintaining the ROS balance in CSCs [48]. Glutamine starvation also leads to the enhanced expression as well as colocalization of xCT with CD44 (Supplementary Fig. S5D-G). However, we did not find any significant increase in the cellular or mitochondrial ROS level after inhibiting xCT, which indicates that it is not involved in reducing the mitochondrial ROS after 12 h of glutamine starvation (Supplementary Fig. S5H-J). In high-grade ovarian cancer patient samples, we found enhanced colocalization of p-DRP1 (S616) and CD44, which again suggests that mitochondrial fragmentation is associated with stem-like feature in cancer (Fig. 5d).

Targeting glutaminolysis has become one of the most emerging therapeutic strategies to reduce tumor growth [49]. In contrast, a recent report suggested that blocking of glutamine metabolism affects the glycolysis and OXPHOS of tumor cells, but enhances the oxidative metabolism of effector T cells, which helps the tumor cells to overcome

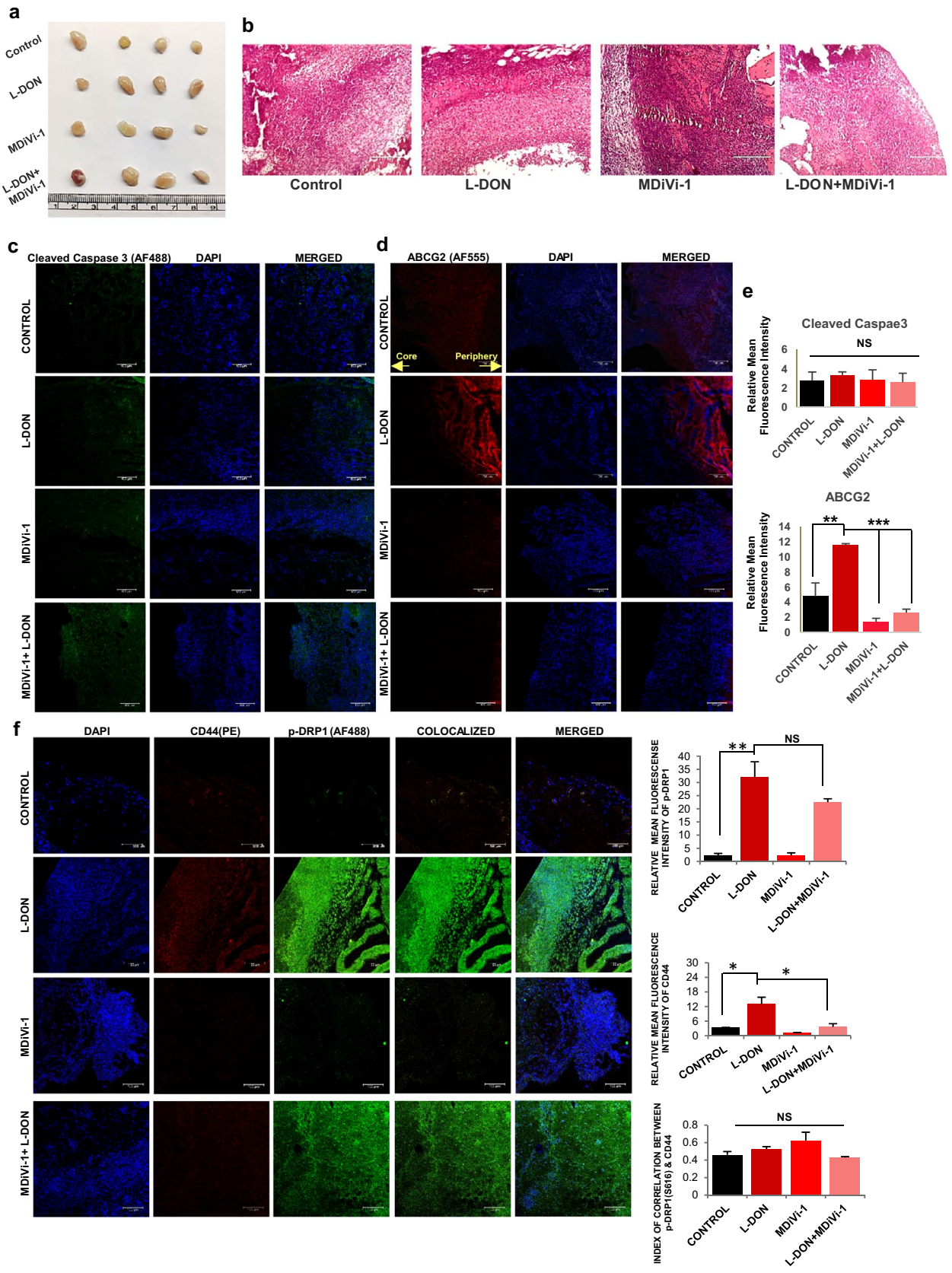
a
Control
L-DON
MDiVi-1
L-DON+ MDiVi-1
b
Control
L-DON
MDiVi-1
L-DON+MDiVi-1
c
Cleaved Caspase 3 (AF488)
DAPI
MERGED
CONTROL
L-DON
MDiVi-1
MDiVi-1+ L-DON
d
ABCG2 (AF555)
DAPI
MERGED
Core
Periphery
e
Cleaved Caspae3
NS
Relative Mean Fluorescence Intensity
ABCG2
**
***
f
DAPI
CD44(PE)
p-DRP1 (AF488)
COLOCALIZED
MERGED
RELATIVE MEAN FLUORESCENSE INTENSITY OF p-DRP1
RELATIVE MEAN FLUORESCENCE INTENSITY OF CD44
INDEX OF CORRELATION BETWEEN p-DRP1(S616) & CD44

◂**Fig. 8** Pharmacological inhibitor of glutaminase (L-DON) and DRP1 (MDiVi-1) can together reduce CSCs population in in-vivo mouse model. **a** Representative images of tumors formed in C57BL/6 injected with PBS, L-DON, MDiVi-1 and MDiVi-1 + L-DON. **b** Hematoxylin and eosin stained histology sections of the tumor. **c** There is minimal expression of cleaved caspase 3 showing no change in control and L-DON treated tumors whereas (**d**) ABCG2 expression was increased in tumors treated with L-DON. as depicted in immunofluorescence microscopy images. MDiVi-1 treatment significantly reduced the ABCG2 expression. **e** Relative fluorescence intensity of cleaved caspase 3 ($n=3$), Ki67 ($n=3$) and ABCG2 ($n=5$) were presented in bar diagram. **f** Both the expression and colocalization of CD44 with phosphorylated DRP1 (Ser616) was increased. Data are expressed in ± SEM, and statistical significance was calculated using two-tailed Student's t test and one-way ANOVA (followed by Bonferroni post hoc analysis) (*$p<0.05$, **$p<0.01$, ***$p<0.001$). NS is for non-significant. Scale bars 400 µm (**b**), 100 µm (**c, d, f**)

immune supervision [50]. Our observation suggests that glutaminase inhibitor L-DON is capable of mimicking glutamine-deprived conditions in the tumor as it enhances glycolysis and mitochondrial fragmentation (Fig. 7a–d, Supplementary Fig. S5L). L-DON treatment in mouse tumor model attenuated tumor growth without hampering the cell survival (Fig. 7f–h, 8c). It is interesting that, there was increased expression of ABCG2 in the core region than the periphery of the same tissue. This result indicated that glutamine starvation in the tumor core region may lead to increased expression of ABCG2. The MDiVi-1 treatment successfully reduced CD44 expression without affecting the p-DRP1 level. However, the co-treatment with L-DON and MDIVi-1 significantly reduced the expression of the stemness markers, like OCT4, SOX2, CD44 and ABCG2 (Supplementary Fig. S6C–D, Fig. 8d–f). Considering the importance of glutamine metabolism in cancer, it has been suggested that combinatorial therapy of glutaminase inhibitor along with the blocking of specific signaling pathway might have high anti-proliferative activity [51]. In addition, MDiVi-1-mediated blocking of mitochondrial fragmentation has also been used as therapeutics to combat cancer stem cells [52]. Altogether, this study shows a promising approach to inhibit tumor cell-specific growth and reduce CSCs population using a dual treatment of L-DON and MDiVi-1. Future studies including clinical investigation will strengthen the possibilities for the usage of a combination of such metabolic inhibitors as therapeutic agent.

Supplementary Information The online version contains supplementary material available at https://doi.org/10.1007/s00018-021-03818-6.

Acknowledgements We thankfully acknowledge Mr. Sounak Bhattacharya (confocal microscopy), Mr. Tanmoy Dalui, & Mrs. Debalina Chakraborty (flow cytometry), Dr. E. Padmanaban (NMR spectroscopy), and Mr. T. Muruganandan (AFM) of Central Instrumentation Facility of IICB. Prof. Pijush K. Das (CSIR-IICB) and Dr. Partha Chakrabarti (CSIR-IICB) are gratefully acknowledged for their valuable suggestions in preparing the manuscript. We are also thankful to Prof. Susanta Roychoudhury and Dr. Damayanti Das Ghosh (both from Saroj Gupta Cancer Centre & Research Institute, Kolkata, India) for providing human patient tissue samples and also for their valuable suggestions. Technical assistance of Mr. Prabir Kumar Dey is acknowledged. Other members of SSR laboratory are acknowledged for their co-operation.

Author contributions PP, SG and SSR conceptualized the study; PP and SG investigated, performed analysis and validation of the data and wrote the original draft. SSR provided the financial support, supervised the work, reviewed, and approved the final manuscript.

Funding This work was supported by grants from Science and Engineering Research Board (SERB) project GAP-360 (EMR/2016/002578) and the Council of Scientific and Industrial Research (CSIR) in house projects.

Availability of data Data are available on request from the corresponding author.

Declarations

Conflict of interest The authors declare that they have no conflict of interest.

Ethical approval for animal studies All animal experiments were approved by the institutional animal ethics committee (IAEC), CSIR-Indian Institute of Chemical Biology, India, (Registration no. 147/GO/ReBi/S/99/CPSCEA) following the guidelines of Committee for the Purpose of Control and Supervision of Experiments on Animals (CPCSEA), Govt. of India.

Ethical approval for human studies The human patients' tissue samples were collected from Saroj Gupta Cancer Centre and Research Institute (SGCCRI), Kolkata, India with proper human ethics clearance from the Institutional Ethics Committee (approval number -IEC SGCCRI REF NO.- 16/2/2018/Non-Reg/SSR/3).

Consent to participate Informed written consent was taken from the patients in accordance with the 1964 Helsinki declaration.

References

1. Mitra T, Prasad P, Mukherjee P et al (2018) Stemness and chemoresistance are imparted to the OC cells through TGFβ1 driven EMT. J Cell Biochem 119:5775–5787. https://doi.org/10.1002/jcb.26753
2. Hanahan D, Weinberg RA (2011) Hallmarks of cancer: the next generation. Cell 144:646–674. https://doi.org/10.1016/j.cell.2011.02.013
3. Pavlova NN, Thompson CB (2016) The Emerging hallmarks of cancer metabolism. Cell Metab 23:27–47. https://doi.org/10.1016/j.cmet.2015.12.006
4. Souba WW (1993) Glutamine and cancer. Ann Surg 218:715–728
5. Yang L, Achreja A, Yeung TL et al (2016) Targeting stromal glutamine synthetase in tumors disrupts tumor microenvironment-regulated cancer cell growth. Cell Metab 24:685–700. https://doi.org/10.1016/j.cmet.2016.10.011
6. Cluntun AA, Lukey MJ, Cerione RA, Locasale JW (2017) Glutamine metabolism in cancer: understanding the heterogeneity. Trends in Cancer 3:169–180. https://doi.org/10.1016/j.trecan.2017.01.005

7. Scalise M, Pochini L, Galluccio M et al (2017) Glutamine transport and mitochondrial metabolism in cancer cell growth. Front Oncol 7:1–9. https://doi.org/10.3389/fonc.2017.00306
8. Huang W, Choi W, Chen Y et al (2013) A proposed role for glutamine in cancer cell growth through acid resistance. Cell Res 23:724–727. https://doi.org/10.1038/cr.2013.15
9. Sabharwal SS, Schumacker PT (2014) Mitochondrial ROS in cancer: initiators, amplifiers or an Achilles' heel? Nat Rev Cancer 14:709–721. https://doi.org/10.1038/nrc3803
10. Zhao J, Zhang J, Yu M et al (2013) Mitochondrial dynamics regulates migration and invasion of breast cancer cells. Oncogene 32:4814–4824. https://doi.org/10.1038/onc.2012.494
11. Al-Mehdi AB, Pastukh VM, Swiger BM et al (2012) Perinuclear mitochondrial clustering creates an oxidant-rich nuclear domain required for hypoxia-induced transcription. Sci Signal 5:1–10. https://doi.org/10.1126/scisignal.2002712
12. Cacace A, Sboarina M, Vazeille T, Sonveaux P (2017) Glutamine activates STAT3 to control cancer cell proliferation independently of glutamine metabolism. Oncogene 36:2074–2084. https://doi.org/10.1038/onc.2016.364
13. Yang L, Moss T, Mangala LS et al (2014) Metabolic shifts toward glutamine regulate tumor growth, invasion and bioenergetics in ovarian cancer. Mol Syst Biol 10:1–23. https://doi.org/10.1002/msb.20134892
14. Yuan L, Sheng X, Willson AK et al (2015) Glutamine promotes ovarian cancer cell proliferation through the mTOR/S6 pathway. Endocr Relat Cancer 22:577–591. https://doi.org/10.1530/ERC-15-0192
15. Choi Y, Park K (2018) Targeting glutamine metabolism for cancer treatment. Biomol Ther 26:19–28
16. Vaupel P, Kallinowski F, Okunieff P (1989) Blood flow, oxygen and nutrient supply, and metabolic microenvironment of human tumors: a review. Cancer Res 49:6449–6465
17. Das N, Mandala A, Naaz S et al (2017) Melatonin protects against lipid-induced mitochondrial dysfunction in hepatocytes and inhibits stellate cell activation during hepatic fibrosis in mice. J Pineal Res 62:1–21. https://doi.org/10.1111/jpi.12404
18. Chowdhury SR, Ray U, Chatterjee BP, Roy SS (2017) Targeted apoptosis in ovarian cancer cells through mitochondrial dysfunction in response to Sambucus nigra agglutinin. Cell Death Dis 8:1–12. https://doi.org/10.1038/cddis.2017.77
19. Khan M, Biswas D, Ghosh M et al (2015) mTORC2 controls cancer cell survival by modulating gluconeogenesis. Cell Death Discov 1:1–12. https://doi.org/10.1038/cddiscovery.2015.16
20. Maftah A, Petit JM, Ratinaud MH, Julien R (1989) 10-N nonylacridine orange: a fluorescent probe which stains mitochondria independently of their energetic state. Biochem Biophys Res Commun 164:185–190. https://doi.org/10.1016/0006-291X(89)91700-2
21. De R, Sarkar S, Mazumder S et al (2018) Macrophage migration inhibitory factor regulates mitochondrial dynamics and cell growth of human cancer cell lines through CD74-NF-κB signaling. J Biol Chem 293:19740–19760. https://doi.org/10.1074/jbc.RA118.003935
22. Bordi M, Nazio F, Campello S (2017) The close interconnection between mitochondrial dynamics and mitophagy in cancer. Front Oncol 7:1–9. https://doi.org/10.3389/fonc.2017.00081
23. Xiao B, Deng X, Zhou W, Tan EK (2016) Flow cytometry-based assessment of mitophagy using mitotracker. Front Cell Neurosci 10:1–4. https://doi.org/10.3389/fncel.2016.00076
24. Song IS (2015) Mitochondria as therapeutic targets for cancer stem cells. World J Stem Cells 7:418. https://doi.org/10.4252/wjsc.v7.i2.418
25. Parte SC, Batra SK, Kakar SS (2018) Characterization of stem cell and cancer stem cell populations in ovary and ovarian tumors. J Ovarian Res 11:1–16. https://doi.org/10.1186/s13048-018-0439-3
26. Akhter Z, Sharawat SK, Kumar V et al (2018) Aggressive serous epithelial ovarian cancer is potentially propagated by EpCAM + CD45 + phenotype. Oncogene. https://doi.org/10.1038/s41388-017-0106-y
27. Bhattacharya R, Mitra T, Ray Chaudhuri S, Roy SS (2018) Mesenchymal splice isoform of CD44 (CD44s) promotes EMT/invasion and imparts stem-like properties to ovarian cancer cells. J Cell Biochem 119:3373–3383. https://doi.org/10.1002/jcb.26504
28. Chen H, Chan DC (2017) Mitochondrial dynamics in regulating the unique phenotypes of cancer and stem cells. Cell Metab 26:39–48. https://doi.org/10.1016/j.cmet.2017.05.016
29. Cetinbas NM, Sudderth J, Harris RC et al (2016) Glucose-dependent anaplerosis in cancer cells is required for cellular redox balance in the absence of glutamine. Sci Rep 6:1–12. https://doi.org/10.1038/srep32606
30. Venneti S, Dunphy MP, Zhang H et al (2015) Glutamine-based PET imaging facilitates enhanced metabolic evaluation of gliomas in vivo. Sci Transl Med 7:1–10. https://doi.org/10.1126/scitranslmed.aaa1009
31. Pan M, Reid MA, Lowman XH et al (2016) Regional glutamine deficiency in tumours promotes dedifferentiation through inhibition of histone demethylation. Nat Cell Biol 18:1090–1101. https://doi.org/10.1038/ncb3410
32. Wise DR, Thompson CB (2010) Glutamine addiction: a new therapeutic target in cancer. Trends Biochem Sci 35:427–433. https://doi.org/10.1016/j.tibs.2010.05.003
33. Zacharias NM, McCullough C, Shanmugavelandy S et al (2017) Metabolic differences in glutamine utilization lead to metabolic vulnerabilities in prostate cancer. Sci Rep 7:1–11. https://doi.org/10.1038/s41598-017-16327-z
34. Zhu L, Ploessl K, Zhou R et al (2017) Metabolic imaging of glutamine in cancer. J Nucl Med 58:533–537. https://doi.org/10.2967/jnumed.116.182345
35. Sonveaux P, Végran F, Schroeder T et al (2008) Targeting lactate-fueled respiration selectively kills hypoxic tumor cells in mice. J Clin Invest 118:3930–3942. https://doi.org/10.1172/JCI36843
36. Trotta AP, Chipuk JE (2017) Mitochondrial dynamics as regulators of cancer biology. Cell Mol Life Sci 74:1999–2017. https://doi.org/10.1007/s00018-016-2451-3
37. Campello S, Scorrano L (2010) Mitochondrial shape changes: Orchestrating cell pathophysiology. EMBO Rep 11:678–684. https://doi.org/10.1038/embor.2010.115
38. Zhao RZ, Jiang S, Zhang L, Bin YuZ (2019) Mitochondrial electron transport chain, ROS generation and uncoupling (review). Int J Mol Med 44:3–15. https://doi.org/10.3892/ijmm.2019.4188
39. Kashatus JA, Nascimento A, Myers LJ et al (2015) Erk2 phosphorylation of Drp1 promotes mitochondrial fission and MAPK-driven tumor growth. Mol Cell 57:537–551. https://doi.org/10.1016/j.molcel.2015.01.002
40. Afanas'ev I (2011) Reactive oxygen species signaling in cancer: comparison with aging. Aging Dis 2:219–230
41. Yu T, Robotham JL, Yoon Y (2006) Increased production of reactive oxygen species in hyperglycemic conditions requires dynamic change of mitochondrial morphology. Proc Natl Acad Sci U S A 103:2653–2658. https://doi.org/10.1073/pnas.0511154103
42. Kong B, Tsuyoshi H, Orisaka M et al (2015) Mitochondrial dynamics regulating chemoresistance in gynecological cancers. Ann N Y Acad Sci 1350:1–16. https://doi.org/10.1111/nyas.12883
43. Kingnate C, Charoenkwan K, Kumfu S et al (2018) Possible roles of mitochondrial dynamics and the effects of pharmacological interventions in chemoresistant ovarian cancer. EBioMedicine 34:256–266. https://doi.org/10.1016/j.ebiom.2018.07.026
44. Lonergan T, Bavister B, Brenner C (2007) Mitochondria in stem cells. Mitochondrion 7:289–296. https://doi.org/10.1016/j.mito.2007.05.002

45. Liao J, Liu PP, Hou G et al (2017) Regulation of stem-like cancer cells by glutamine through β-catenin pathway mediated by redox signaling. Mol Cancer 16:1–13. https://doi.org/10.1186/s12943-017-0623-x
46. Li B, Cao Y, Meng G et al (2019) Targeting glutaminase 1 attenuates stemness properties in hepatocellular carcinoma by increasing reactive oxygen species and suppressing Wnt/beta-catenin pathway. EBioMedicine 39:239–254. https://doi.org/10.1016/j.ebiom.2018.11.063
47. Tran TQ, Hanse EA, Habowski AN et al (2020) α-Ketoglutarate attenuates Wnt signaling and drives differentiation in colorectal cancer. Nat Cancer 1:345–358. https://doi.org/10.1038/s43018-020-0035-5
48. Ju HQ, Lu YX, Chen DL et al (2016) Redox regulation of stem-like cells though the CD44v-xCT axis in colorectal cancer: mechanisms and therapeutic implications. Theranostics 6:1160–1175. https://doi.org/10.7150/thno.14848
49. Jin L, Alesi GN, Kang S (2016) Glutaminolysis as a target for cancer therapy. Oncogene 35:3619–3625. https://doi.org/10.1038/onc.2015.447
50. Leone RD, Zhao L, Englert JM et al (2019) Glutamine blockade induces divergent metabolic programs to overcome tumor immune evasion. Science 366:1013–1021. https://doi.org/10.1126/science.aav2588
51. Matés JM, Di Paola FJ, Campos-Sandoval JA et al (2020) Therapeutic targeting of glutaminolysis as an essential strategy to combat cancer. Semin Cell Dev Biol 98:34–43. https://doi.org/10.1016/j.semcdb.2019.05.012
52. Peiris-Pagès M, Bonuccelli G, Sotgia F, Lisanti MP (2018) Mitochondrial fission as a driver of stemness in tumor cells: mDIVI1 inhibits mitochondrial function, cell migration and cancer stem cell (CSC) signalling. Oncotarget 9(17):13254–13275

Publisher's Note Springer Nature remains neutral with regard to jurisdictional claims in published maps and institutional affiliations.